CALCIUM(II)-SENSITIVE AND SILSESQUIOXANE-BASED CONTRAST AGENTS FOR MAGNETIC RESONANCE IMAGING

Synthesis, Characterisation and Mechanistic Studies

CALCIUM(II)-SENSITIVE UND SILSESQUIOXAN-BASIERTE KONTRASTMITTEL FÜR DIE MAGNETRESONANZTOMOGRAPHIE

Synthese, Charakterisierung und Mechanistische Untersuchungen

DISSERTATION

der Fakultät für Chemie und Pharmazie
der Eberhard Karls Universität Tübingen

zur Erlangung des Grades eines Doktors
der Naturwissenschaften

2010

vorgelegt von

Jörg Henig

Tag der mündlichen Prüfung: 28. April 2010

Dekan: Prof. Dr. Lars Wesemann

1. Berichterstatter: Prof. Dr. Hermann A. Mayer
2. Berichterstatter: Prof. Dr. Martin E. Maier
3. Berichterstatter: Prof. Dr. Franc Meyer

Die vorliegende Arbeit wurde am Institut für Anorganische Chemie der Eberhard Karls Universität Tübingen im Zeitraum von Mai 2007 bis Januar 2010 unter Anleitung von Herrn Prof. Dr. Hermann A. Mayer angefertigt.

Meinem Doktorvater,
Herrn Prof. Dr. Hermann A. Mayer,
danke ich herzlich für die die Überlassung des interessanten Themas,
die Bereitstellung der hervorragenden Arbeitsbedingungen,
die zahlreichen wertvollen Anregungen und Diskussionen,
sein stetes Interesse an meiner Arbeit,
das hervorragende Arbeitsklima,
sowie die Möglichkeit, meine Ergebnisse auf Tagungen zu präsentieren.

Dem Fonds der Chemischen Industrie gilt mein Dank für die Förderung durch ein Promotionsstipendium.

Mein herzlicher Dank gilt:

Herrn Prof. Dr. M.E. Maier für die guten Ratschläge und die freundliche Übernahme des Koreferats.

Herrn Prof. Dr. L. Wesemann für die Bereitstellung der sehr guten Arbeitsbedingungen.

Herrn Dr. I. Mamedov (Max-Planck-Institut für biologische Kybernetik, Tübingen) für das zur Verfügung stellen von Substanzen, die Durchführung der Lumineszenzmessungen sowie die gute Zusammenarbeit.

Frau Dr. É. Jakab Tóth (Le Centre de Biophysique Moléculaire**,** CNRS Orléans, Orléans) für die herzliche Aufnahme in Orléans, die Möglichkeit ^{17}O NMR- und NMRD-Untersuchungen durchführen zu können, sowie ihre Unterstützung bei der Auswertung der Daten.

Frau Dr. P. Fousková und Herrn Bohuslav Drahos (Le Centre de Biophysique Moléculaire**,** CNRS Orléans, Orléans) für die freundliche Einführung in die ^{17}O NMR-Spektroskopie sowie in die Tücken des SMARtracers.

Herrn Dr. K. Eichele für Rat und Tat bei allen NMR-spektroskopischen Problemen.

Frau A. Ehmann für die Pflege der NMR-Spektrometer und ihre Unterstützung bei allen Belangen, die die Spektrometer betreffen.

Herrn Dr. J. Engelmann und Herrn Dr. S. Gottschalk (Max-Planck-Institut für biologische Kybernetik, Tübingen) für die Durchführung der Relaxivitätsmessungen am 3 T MR Scanner.

Herrn Dr. G. Angelovski (Max-Planck-Institut für biologische Kybernetik, Tübingen) für viele fruchtbare Diskussionen.

Herrn Prof. Dr. N.K. Logothetis (Max-Planck-Institut für biologische Kybernetik, Tübingen) für die Bereitstellung der Infrastruktur seitens des Max-Planck-Instituts.

Herrn Dr. K. Möschel für die freundliche Aufnahme im IFIB und seine Hilfe in allen

gebäudetechnischen Belangen.

Allen Angestellten und Praktikanten für ihren Beitrag zum Gelingen dieser Arbeit und die durchgeführten Messungen.

Den Mitarbeitern des Arbeitskreises Mayer, allen voran Herrn Wolfgang Leis danke ich für viele gute Ratschläge und das freundschaftliche Klima.

Meinen Eltern, meinem Bruder und ganz besonders Elif, die mich während der gesamten Doktorarbeit uneingeschränkt unterstützt haben und auf die ich mich in allen Situationen stets verlassen konnte.

Parts of this work have been presented:

„Azamacrocyclic Ca^{2+} sensitive contrast agents for MR imaging", **COST D38 workshop**, Lisbon, Portugal, 2008

„Ca^{2+} sensitive contrast agents for MR imaging - Unexpected coordination behaviour of lanthanide complexes in the presence of Ca^{2+}", **38th International Conference on Coordination Chemistry**, Jerusalem, Israel, 2008

„The unexpected behaviour of potential calcium(II) sensitive contrast agents for MRI", **2nd EuCheMS Chemistry Congress**, Turin, Italy, 2008

Meinen Eltern

Table of Contents

Abbreviations V

1 Introduction 1

2 General Basics 2

2.1 Magnetic Resonance Imaging 2

2.2 Contrast Agents in Magnetic Resonance Imaging 3

2.3 Mechanistic Aspects of Gadolinium(III)-based Contrast Agents 4

2.3.1 Inner-Sphere Relaxivity 6

2.3.2 Outer-Sphere Relaxivity 9

2.4 Types of Gadolinium(III) Chelates for Magnetic Resonance Imaging 10

2.4.1 Gd-DTPA and Derivatives 10

2.4.2 Gd-DOTA-type Contrast Agents 13

3 Calcium(II)-sensitive MRI Contrast Agents 16

3.1 Introduction 16

3.1.1 Responsive or “Smart” Contrast Agents 17

3.1.1.1 Agents sensitive to enzyme activity 17

3.1.1.2 pH-dependent contrast agents 19

3.1.1.3 Metal ion sensitive contrast agents 20

3.1.2 Aim of this Project 23

3.2 Results and Discussion 24

3.2.1 Relaxivity *vs.* Calcium(II) Concentration 24

3.2.2 Relaxivity *vs.* Complex Concentration 25

3.2.3 PGSE Diffusion ^{1}H NMR Spectroscopy 26

3.2.4 ^{31}P{^{1}H} NMR Spectroscopy 29

3.2.5 Luminescence Spectroscopy 32

3.2.6 Determination of the Hydration Number *q* 33

3.2.7 ^{17}O NMR Spectroscopy 36
3.3 Conclusions 41
4 Silsesquioxane-based MRI Contrast Agents 43
4.1 Introduction 43
4.1.1 High Sensitivity MRI Contrast Agents 43
4.1.1.1 Macromolecular contrast agents 46
4.1.2 Silsesquioxanes 48
4.1.3 Aim of this project 49
4.2 Results and Discussion 51
4.2.1 Synthesis of T_8-Silsesquioxanes 51
4.2.1.1 Synthesis of an amino-functionalised T_8-silsesquioxane 51
4.2.1.2 Synthesis of a carboxylic acid-functionalised T_8-silsesquioxane 52
4.2.2 Introduction of Macrocyclic Ligands *via* their *tert*-Butyl protected Form 52
4.2.2.1 Synthesis of DOTA(^{t}Bu)$_3$ 53
4.2.2.2 Coupling of DOTA(^{t}Bu)$_3$ to octa(3-aminopropyl)silsesquioxane 54
4.2.2.3 Deprotection of the carboxylic acid functions 57
4.2.3 Introduction of Macrocyclic ligands *via* non *tert*-Butyl protected Forms 58
4.2.3.1 Synthesis of La-DO3A-hexylamine 58
4.2.3.2 Coupling of La-DO3A-hexylamine to the silsesquioxane 60
4.2.3.3 Synthesis of DOTA(Bn)$_3$ 63
4.2.3.4 Coupling of DOTA(Bn)$_3$ to octa(3-aminopropyl)silsesquioxane 64
4.2.3.5 Cleavage of the benzyl esters 66
4.2.4 Introduction of Charged Macrocyclic Complexes 67
4.2.4.1 Synthesis of DOTAGA 67
4.2.4.2 Synthesis of Gadoxane G 70
4.2.4.3 Synthesis of DOTAMA and DOTABA 72
4.2.4.4 Coupling of DOTAMA complexes to the silsesquioxane 76
4.2.4.5 Synthesis of Gadoxane B 77

4.2.5 The Molecular Size of Gadoxane G and B 80
4.2.6 The Stability of the Silsesquioxane Cage in Aqueous Media 81
4.2.6.1 Time-dependent ^{29}Si NMR measurements 81
4.2.6.2 Time-dependent PGSE diffusion ^{1}H NMR spectroscopy 83
4.2.6.3 Time-dependent ESI-MS measurements 84
4.2.6.4 Time-dependent relaxivity measurements 85
4.2.7 Physico-chemical Characterisation of Gadoxane G and B 87
4.3 Conclusions and Perspectives 95
5 Experimental Part 99
5.1 Calcium(II)-sensitive MRI Contrast Agents 99
5.1.1 General Remarks 99
5.1.2 Relaxivity *vs.* Calcium(II) Concentration 99
5.1.3 Relaxivity *vs.* Complex Concentration 100
5.1.4 PGSE Diffusion ^{1}H NMR Spectroscopy 102
5.1.5 ^{31}P{^{1}H} NMR Spectroscopy 102
5.1.6 Luminescence Spectroscopy 102
5.1.7 Luminescence Lifetime Measurements 103
5.1.8 ^{17}O NMR Spectroscopy 104
5.2 Silsesquioxane-based MRI Contrast Agents 108
5.2.1 Materials and General Remarks 108
5.2.2 Diafiltration 108
5.2.3 pH-metric Measurements 109
5.2.4 Mass Spectrometry 109
5.2.5 Elemental Analysis 109
5.2.6 Solid-State NMR Spectroscopy 109
5.2.7 Solution NMR Spectroscopy 109
5.2.7.1 NMR spectroscopy for structural analysis 109
5.2.7.2 Bulk magnetic susceptibility shift measurements 110

5.2.7.3 PGSE diffusion ^{1}H NMR spectroscopy 110
5.2.7.4 Relaxivity measurements 111
5.2.7.5 Variable temperature ^{17}O NMR and ^{1}H NMRD measurements 113
5.2.8 Syntheses 120
5.2.8.1 Synthesis of octa(3-chloroammoniumpropyl)silsesquioxane (29) 120
5.2.8.2 Synthesis of octa(3-(ethylmercapto)-propionic acid)silsesquioxane (33) 120
5.2.8.3 Synthesis of DOTA(^{t}Bu)$_3$ (36) 120
5.2.8.4 Synthesis of compound 46 121
5.2.8.5 Attempted deprotection of compound 46 121
5.2.8.6 Synthesis of compound 49 122
5.2.8.7 Synthesis of DOTA(Bn)$_3$ (53) 122
5.2.8.8 Synthesis of compound 54 124
5.2.8.9 Attempted deprotection of compound 54 124
5.2.8.10 Synthesis of DOTAGA (60) 125
5.2.8.11 Synthesis of Gadoxane G (GG) 128
5.2.8.12 Synthesis of DOTAMA (64) 129
5.2.8.13 Attempted synthesis of compound 77 131
5.2.8.14 Synthesis of DOTABA (65) 131
5.2.8.15 Synthesis of Gadoxane B (GB) 133
5.2.8.16 General procedure for the synthesis of complexes 63 and 78 134
6 References 136
Summary 143

Abbreviations

Abbreviation	Name
$1/T_{1r}$	reduced ^{17}O longitudinal relaxation rate
$1/T_{2r}$	reduced ^{17}O transverse relaxation rate
AIBN	azobisisobutyronitrile
$A/\hbar$	hyperfine coupling constant
B	magnetic field
BBB	blood–brain barrier
BOLD	blood-oxygen-level-dependency
BAPTA	1,2-bis(o-aminophenoxy)ethane-N,N,N′,N′-tetraacetic acid
BMS	bulk magnetic susceptibility
Bn	benzyl
BOPTA	benzyloxypropionictetraacetic acid
br	broad
BT-DO3A	10-(2,3-dihydroxy-1-hydroxymethylpropyl)-DO3A
Bu	butyl
CA	contrast agent
C_{OS}	outer-sphere contribution
COSY	correlation spectroscopy
CP	cross polarisation
CT	computer tomography
d	doublet
D	diffusion coefficient
DAB	diaminobutane
DCM	dichloromethane
DD	dipole-dipole
DIPEA	diisopropylethylamine
DMA	dimethylacetamide
DMF	dimethylformamide
DMSO	dimethylsulfoxide
DO3A	1,4,7,10-tetraazacyclododecane-1,4,7-triacetatic acid
DO3A-β-gal	l0-(2-β-galactopyranosylethoxy)-DO3A

DOTA	1,4,7,10-tetraazacyclo-dodecane-1,4,7,10-tetracetic acid
DOTABA	1,4,7,10-tetraazacyclododecane-1-(4-(carboxymethyl)benzoic)-4,7,10-triacetic acid
DOTAGA	1,4,7,10-tetraazacyclododecane-1-glutaric-4,7,10-triacetic acid
DOTAMA	1,4,7,10-tetraazacyclododecane-1-malonic-4,7,10-triacetic acid
DOTASA	1,4,7,10-tetraazacyclododecane-1-succinic-4,7,10-triacetic acid
DTPA	diethylenetriaminepentaacetic acid
DTPA-BMEA	DTPA-bis(methoxyethylamide)
DTPA-BMA	DTPA-bismethylamide
DTPA-FA	DTPA-fatty acids
EDTA	ethylenediaminetetraacetic acid
ENDOR	electron-nuclear double resonance
EOB-DTPA	ethoxybenzyl-DTPA
EPR	electron paramagnetic resonance
E_R	activation energy of τ_R
ESI	electrospray ionisation
Et	ethyl
FCS	fetal calf serum
FID	free induction decay
fMRI	functional magnetic resonance imaging
G	magnetic field gradient (strength)
GB	Gadoxane B
GG	Gadoxane G
g	Landé factor
HEPES	4-(2-hydroxyethyl)-1-piperazineethanesulfonic acid
HMBC	heteronuclear multiple bond coherence
HOBt	1-hydroybenzotrialzol
HP-DO3A	10-(2-hydroxypropyl)-DO3A
HR	high resolution
HSA	human serum albumin
HSQC	heteronuclear single quantum coherence
I	integral
IS	inner sphere
$^{n}J_{ij}$	coupling constant of nuclei i,j *via* n bonds

k_B	Boltzmann constant
k_{ex}	water exchange rate
K_{GdL}	thermodynamic stability constant
K^*_{GdL}	conditional stability constant
K_n	protonation constant
m	multiplet
M	molar mass
M	molarity
MAS	magic angle spinning
Me	methyl
MRI	magnetic resonance imaging
mRNA	messenger ribonucleic acid
MS	mass spectrometry
N_A	Avogadro number
NBS	N-bromosuccinimide
NSF	nephrogenic systemic fibrosis
NMR	nuclear magnetic resonance
NMRD	nuclear magnetic relaxation dispersion
OS	outer sphere
PAMAM	polyamidoamino
PEG	polyethylene glycol
PES	polyethersulfone
PGSE	pulsed gradient spin echo
P_m	mole fraction of bound water
POSS	polyhedral oligosilsesquioxane
ppm	parts per million
q	hydration number
r_1	longitudinal relaxivity
r_2	transverse relaxivity
r_H	hydrodynamic radius
r.t.	room temperature
s	singlet
S	total electron spin
S^2	spatial restriction parameter

SC	scalar
SPIO	superparamagnetic iron oxide
SS	second sphere
t	time
$t_{1/2}$	half-life
T	absolute temperature
T	T type silicon atom (three oxygen neighbours)
T_1	longitudinal relaxation time
T_2	transverse relaxation time
TAFI	thrombin-activatable fibrinolysis inhibitor
TBTA	*tert*-butyltrichloroacetimidate
TBTU	*O*-(benzotriazol-1-yl)-N,N,N',N'-tetramethyluronium tetrafluoroborate
tert	tertiary
TFA	trifluoroacetic acid
TMS	tetramethylsilane
TPEN	N,N,N',N'-tetrakis(2-pyridylmethyl)ethylenediamine
V_H	hydrodynamic Volume
ZFS	zero-field-splitting
γ	gyromagnetic ratio
δ	chemical shift
δ	gradient duration
Δ	delay between the midpoints of two gradients
Δ^2	mean-square zero-field-splitting energy
$\Delta H^{\ddagger}$	activation enthalpy
$\Delta S^{\ddagger}$	activation entropy
$\Delta\omega_r$	reduced ^{17}O chemical shift
Δ_χ	BMS chemical shift
η	viscosity
μ_B	Bohr magneton
ρ	spin density
τ_D	diffusional correlation time
τ_{H_2O}	luminescence lifetime in H_2O

τ_{D_2O}	luminescence lifetime in D_2O
τ_m	water residual time
τ_v	correlation time of the zero-field-splitting interaction
τ_R	rotational correlation time
ω_I	proton Larmor frequency
ω_S	electron Larmor frequency

1 Introduction

In the early 1980s, magnetic resonance imaging (MRI) caught the attention of clinicians by its ability to visualise abnormalities in the posterior fossa of the brain and in the upper cervical spine. Visualisation of lesions in these regions by computer tomography (CT), the only alternative imaging technique for such applications, had failed before due to the bony structures of these areas. While in the beginning MRI was mostly used only for such special problems, over the last two decades it has evolved into one of the most powerful tools in diagnostic clinical medicine and biomedical research. Today, MRI is not only on a par with CT - in many diagnostic areas, such as the detection and characterisation of brain tumors, MRI has outstripped CT.[1-3]

The strong expansion of medical MRI, however, was only possible due to the concomitant development of a new class of pharmacological products, named contrast agents (CAs). These compounds are designed in order to enhance the contrast between normal and diseased tissue or to indicate organ function or blood flow after administration of the CA to the patient. Nowadays, more than 30 % of all MRI investigations use a contrast medium, a number still set to increase.[1]

The CAs which are to date in clinical use, like Dotarem™ or Magnevist™, are mainly low molecular weight extracellular perfusion agents which distribute non-specifically throughout plasma and interstitial spaces and are rapidly excreted *via* the kidneys or, in the case of more lipophilic hepatobiliary CAs, *via* the liver.[4]

Current research is focused on a new generation of CAs. These novel CAs are designed in order to allow a more efficient and more specific imaging. So called targeted CAs are able to specifically locate certain types of cells and biomolecules within the body.[5] Responsive or “smart” CAs afford the detection of changes in the physiological environment of the CA, such as variations in the pH, concentrations of inorganic ions, the partial pressure of oxygen or enzyme activity. This enables the visualisation of the cellular function and the follow-up of the molecular process in living organisms without perturbing them.[4]

2 General Basics

2.1 Magnetic Resonance Imaging

Magnetic resonance imaging (MRI) is an imaging technique used primarily in medical settings to produce high quality images of the inside of the human body. MRI is based on the principles of nuclear magnetic resonance (NMR) spectroscopy. The human body consists of water to more than 55%. For this reason MRI primarily images the ^{1}H NMR signal from the hydrogen nuclei of the water molecules.

In order to generate images from an NMR measurement, it is necessary to encode spatial information into the NMR signal. This is accomplished by the use of time-dependent, linear magnetic field gradients $\boldsymbol{G}$ along the three directions in space. The magnetic field $B(x, t)$ in x-direction at a time t is thereby given by the following relationship:

$$B(x,t) = B_0 + G_x(t)x \tag{2.1}$$

where B_0 describes the external magnetic field, x is the spatial coordinate along the x-axis, measured from the magnet centre, and $G_x(t)$ is the gradient strength. The equation is valid analogously for the y- and z-directions. Altogether this results in a Larmor frequency $\boldsymbol{\omega}$ which depends on the spatial position $\boldsymbol{r}$ and the time t:

$$\boldsymbol{\omega}(\boldsymbol{r},t) = -\gamma \boldsymbol{B}(\boldsymbol{r},t), \boldsymbol{r} = \begin{bmatrix} x \\ y \\ z \end{bmatrix} \tag{2.2}$$

where γ is the gyromagnetic ratio.

With the gained position-dependency of the resonance frequency it is possible to excite only spins of water protons in certain parts of the body. The use of all three field gradients and combinations of them thereby allows the assignment of the signal intensity to a definite volume element (voxel). Furthermore, *via* the application of different pulse sequences it is possible to create a dependency of the signal intensity on the longitudinal relaxation time T_1, the transverse relaxation time T_2 or the spin density ρ of the water protons. Those factors are in turn influenced by the chemical environment and thus by the type of tissue in which the water molecules are located. The NMR signal intensity of each voxel is then transformed into the brightness of a gray-level scale. A matrix of these voxels makes up the final MR image.[1]

2.2 Contrast Agents in Magnetic Resonance Imaging

Spin-lattice relaxation times T_1 and spin-spin relaxation times T_2 of NMR active nuclei can be significantly shortened in the presence of unpaired electron spins. This effect is utilised in the application of CAs for MRI. All CAs which are used in MRI are metal based agents which possess unpaired electrons which influence T_1 and/or T_2 of the surrounding water protons.

CAs which mainly shorten the transverse relaxation times are called "T_2-agents". Those are typically iron oxide (Fe_3O_4) nanoparticles which are made up of several thousand magnetic ions and are said to have superparamagnetic properties if the magnetic ions are mutually aligned. By using certain pulse sequences the shortening of the T_2-relaxation time leads to a significantly reduced transverse magnetisation already before the free induction decay (FID) is recorded. This results in a weaker signal and therefore in darker regions in the MR image.

On the contrary, a brightening of the affected area can be achieved *via* the use of "T_1-agents" (Figure 1). Since any CA which reduces T_1 must also reduce T_2, this term might seem inaccurate. However, as $T_1 \gg T_2$ for most tissues, the relative effect of a T_1-agent on T_1 is much larger than the relative effect on T_2. With shorter T_1-relaxation times, a larger population of the hydrogen nuclei surrounding the CA relaxes back to the equilibrium state in a given delay time after the first pulse sequence. As this results in a higher longitudinal magnetisation before each repetition of the pulse sequence, the signal intensity and thus the image brightness increases. For most applications T_1-agents are favoured over T_2-agents, as a positive contrast enhancement is often more easily detectable as a negative one. Typical T_1-agents are based on paramagnetic metal ions.[1, 6]

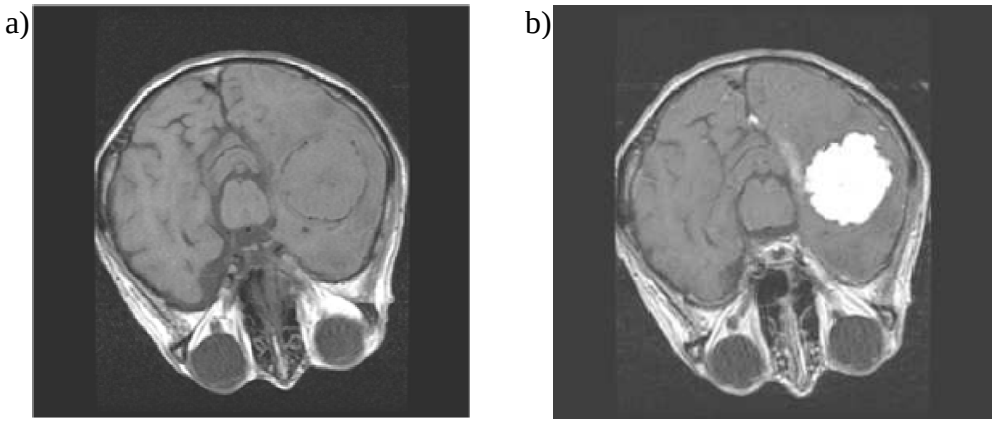

Figure 1. MR images of a brain tumor. a) without a CA, b) with a T_1-agent

In order to have a strong influence on the longitudinal relaxation time T_1 of the surrounding water protons the paramagnetic metal ions do not only have to possess a high number of unpaired electrons resulting in a large magnetic moment, they also need long electron spin

relaxation times T_{1e}. For example, dysprosium(III) and holmium(III) have the largest magnetic moments of all elements, but due to the asymmetry of their electronic states they show very rapid electron spin relaxation and thus water protons are hardly influenced by the effects of these ions.[6] On the contrary, in the transition metal ions manganese(II) and iron(III) as well as the lanthanide ion gadolinium(III), having half-filled d or f shells, the pathways for electronic relaxation are relatively inefficient. Hence their electron spin relaxation is more closely in tune with the proton's frequency.[6, 7] Gadolinium(III) is most commonly used in CAs, as with seven unpaired electrons it has in general the strongest effect on the longitudinal proton spin relaxation. Additionally favorable is the short residual time τ_m of the water molecules on the gadolinium aqua complex (τ_m = 0.94 ns), which allows thousands of water molecules to transiently coordinate to a single ion on the MRI time scale.[8]

The major drawback of gadolinium(III) based CAs is the high toxicity of free Gd^{3+} ions. With an ionic radius (107.8 pm) close to that of Ca^{2+} (114 pm), but a higher charge, gadolinium(III) is an inorganic blocker of many types of voltage-gated calcium(II) channels and several other calcium(II) regulated processes within the body.[9] To diminish the toxicity to clinically acceptable levels, gadolinium(III) needs to be complexed by multidentate ligands. Since the relaxation time shortening effect of the paramagnetic metal ion on the water protons vanishes rapidly with increasing metal-proton distance, it is desirable to have at least one remaining coordination site on the gadolinium(III) ion for water to coordinate. Examples are $[Gd(DOTA)H_2O]^-$ (Dotarem™ (**1**), Guerbet, France, DOTA = 1,4,7,10-tetraazacyclo-dodecane-1,4,7,10-tetracetic acid) or $[Gd(DTPA)H_2O]^{2-}$ (Magnevist™ (**2**), Bayer-Schering Pharma, Germany, DTPA = diethylenetriaminepentaacetic acid) (Figure 2).

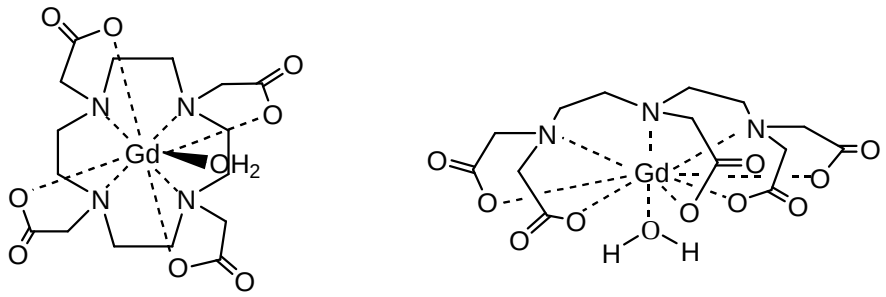

1 **2**

Figure 2. Structures of the commercially available CAs Dotarem™ (**1**) und Magnevist™ (**2**).

2.3 Mechanistic Aspects of Gadolinium(III)-based Contrast Agents

The general theory of the influence of paramagnetic substances on the nuclear relaxation of the surrounding solvent was developed by the groups of Solomon, Bloembergen and others.[10-12] Accordingly, the observed longitudinal or transverse relaxation rate $1/T_{1,2obs}$ of the water

protons consists of a diamagnetic term $1/T_{1,2d}$, describing the relaxation rate of the protons in the absence of a paramagnetic solute and an additional paramagnetic term $1/T_{1,2p}$ due to the presence of the paramagnetic compound:

$$\frac{1}{T_{1,2obs}} = \frac{1}{T_{1,2d}} + \frac{1}{T_{1,2p}} \tag{2.3}$$

The paramagnetic contribution is thereby directly proportional to the concentration [Gd] of the paramagnetic species:

$$\frac{1}{T_{1,2obs}} = \frac{1}{T_{1,2d}} + r_{1,2}[\mathrm{Gd}] \tag{2.4}$$

The concentration [Gd] is usually given in mmol/L, however for non-dilute systems, the linear relationship is valid only if [Gd] is expressed in mmol/kg of solvent. The proportionality constant $r_{1,2}$ is called relaxivity [$mM^{-1}s^{-1}$]. For a gadolinium complex in water, the relaxivity is a direct measure for the efficiency of the complex to act as a contrast agent.[1]

The paramagnetic relaxation of the water protons originates from the dipole-dipole interactions between the large and fluctuating local magnetic field caused by the unpaired electron spins and the nuclear spins of the water protons. Since the magnetic field around the paramagnetic centre falls off rapidly with distance, random translational diffusion of solvent molecules and the complex as well as specific chemical interactions that bring the solvent molecules close to the metal ion (e.g., within 5 Å) are important in transmitting the paramagnetic effect. Each type of chemical interaction can yield different relaxation efficiencies as governed by the distance and time scale of the interaction. The sum of these contributions and that due to translational diffusion gives the total relaxivity of the paramagnetic species.[7]

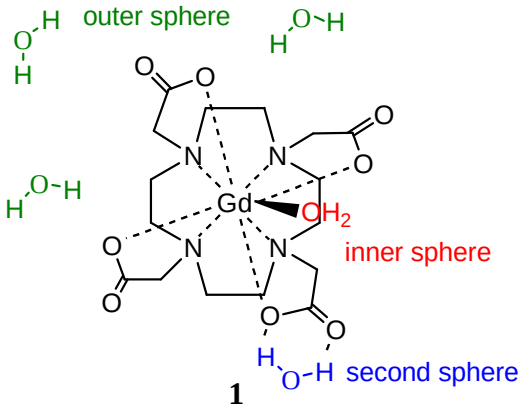

1

Figure 3. Different types of interactions of water molecules with a gadolinium(III) based CA.

The relevant contributions for water proton relaxivity can be classified in three distinct types of interactions (Figure 3). The effect on bulk water molecules which diffuse in the

surroundings of the paramagnetic complex is defined as outer-sphere (OS) relaxation. For gadolinium(III) complexes, the specific interaction is mainly the binding of water molecule(s) in the first coordination sphere of the metal ion. These inner-sphere (IS) water molecules exchange with the bulk solvent which propagates the paramagnetic influence into the bulk. This mechanism is depicted as the inner-sphere contribution to the overall relaxivity. In certain agents, solvent molecules that are not directly bound to the first coordination sphere can also remain in the proximity of the paramagnetic centre for a relatively long time, e.g. due to hydrogen bridges to carboxylate or phosphate groups of the ligand. The relaxivity contribution originating from these interactions is called second-sphere (SS) relaxivity, and to this contribution the same theory as for the inner-sphere term applies. However, as the involved parameters are hardly available, its effect is usually taken into account in the outer-sphere term.[1, 7] The total paramagnetic relaxation rate enhancement due to the paramagnetic agent is therefore generally given by equation 2.5, or expressed in relaxivities in equation 2.6:

$$\left(\frac{1}{T_{1,2p}}\right) = \left(\frac{1}{T_{1,2p}}\right)^{IS} + \left(\frac{1}{T_{1,2p}}\right)^{OS} \tag{2.5}$$

$$r_{1,2} = {r_{1,2}}^{IS} + {r_{1,2}}^{OS} \tag{2.6}$$

For the currently used low molecular weight gadolinium(III) based CAs, like $[Gd(DOTA)H_2O]^-$ (**1**) and $[Gd(DTPA)H_2O]^-$ (**2**) (Figure 2), the outer and inner-sphere relaxation mechanisms contribute approximately to the same extent to the observed relaxivity at magnetic field strength used in MRI.[1] However, it is the inner sphere term that can be considerably manipulated by chemists, whereas the outer-sphere contribution can hardly be modified. Since gadolinium(III) based CAs are T_1-agents, the following sections focus on the factors that determine the longitudinal inner-sphere and outer-sphere relaxation mechanisms.

2.3.1 Inner-Sphere Relaxivity

The longitudinal relaxation contribution from the inner-sphere mechanism results from a chemical change of the coordinated water molecules with the bulk, and thus represents a two-site exchange problem. The bulk site is much more populated than the site of coordinated water, and the observed signal corresponds to that of the free water. The longitudinal inner-sphere relaxation rate is therefore given by equation 2.7:

$$\left(\frac{1}{T_1}\right) = \left(\frac{P_m}{T_{1m} + \tau_m}\right) = \frac{[\mathrm{Gd}]q}{55.5}\left(\frac{1}{T_{1m} + \tau_m}\right) \tag{2.7}$$

where, P_m is the mole fraction of bound water nuclei, T_{1m} is the proton relaxation rate in the bound water, τ_m is the lifetime of a water molecule in the inner sphere of the complex (equal

to the reciprocal water exchange rate, $1/k_{ex}$), q is the number of bound water molecules per gadolinium ion (hydration number) and [Gd] is the molal concentration of gadolinium ions. A schematic representation of a gadolinium(III) chelate with the most important parameters of inner-sphere relaxivity is depicted in Figure 4.

The longitudinal relaxation time T_{1m} of the bound water protons is governed by a dipole-dipole (DD) ("through space") and a scalar (SC) ("through bonds") mechanisms. The dipolar interaction is modulated by the reorientation of the nuclear spin-electron spin vector, by changes in the orientation of the electron spin (electron spin relaxation $T_{1,2e}$) and the water (proton) exchange rate k_{ex}. The scalar interaction does not depend on the reorientation of the molecule, but is modulated by electron spin relaxation and water exchange.

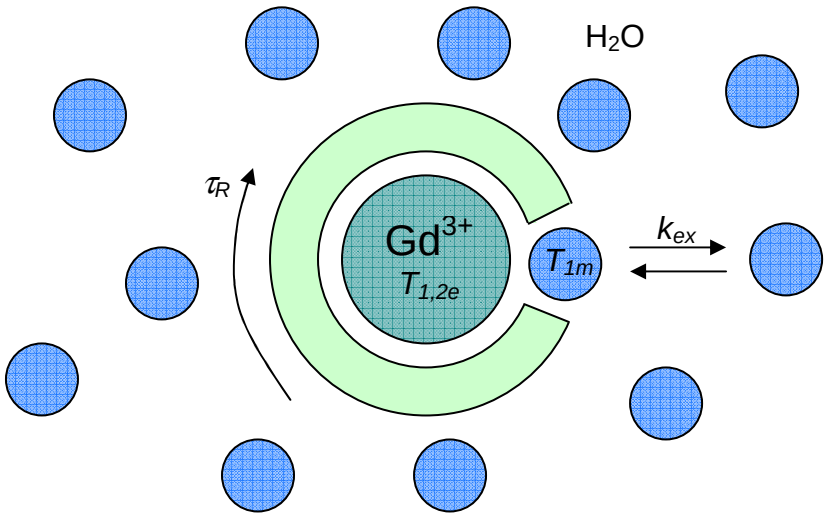

Figure 4. Schematic representation of a gadolinium(III) chelate having one inner-sphere water molecule. τ_R is the rotational correlation time of the complex, k_{ex} is the water (proton) exchange rate, T_{1m} is the longitudinal relaxation time of the bound water protons and $T_{1,2e}$ are the longitudinal and transverse relaxation times, respectively, of the gadolinium(III) electron spin.

The longitudinal relaxation rate $1/T_{1m}$ of the bound water protons and its depending parameters are expressed by the modified Solomon-Bloembergen equations:[13]

$$\frac{1}{T_{1m}} = \frac{1}{T_1^{DD}} + \frac{1}{T_1^{SC}} \tag{2.8}$$

$$\frac{1}{T_1^{DD}} = \frac{2}{15}\left(\frac{\gamma_I^2 g^2 \mu_B^2}{r_{GdH}^6}\right) S(S+1)\left(\frac{\mu_0}{4\pi}\right)^2 \left(7\frac{\tau_{c2}}{1+\omega_S^2\tau_{c2}^2} + 3\frac{\tau_{c1}}{1+\omega_I^2\tau_{c1}^2}\right) \tag{2.9}$$

$$\frac{1}{T_1^{SC}} = \frac{2S(S+1)}{3}\left(\frac{A}{\hbar}\right)^2 \left(\frac{\tau_{e2}}{1+\omega_S^2\tau_{e2}^2}\right) \tag{2.10}$$

where γ_I is the nuclear gyromagnetic ratio, g is the electron g-factor, μ_B is the Bohr magneton, r_{GdH} is the electron spin-proton distance, S is the total electron spin of the metal ion, ω_I and ω_S are the nuclear and electron Larmor precession frequencies, respectively ($\omega = \gamma B$), and $A/\hbar$ is the electron-nuclear hyperfine or scalar coupling constant. The dipolar and the scalar relaxation mechanisms are modulated by the correlation times $\tau_{c1,2}$ and τ_{e2} as the following:

$$\frac{1}{\tau_{c1,2}} = \frac{1}{\tau_R} + \frac{1}{T_{1,2e}} + \frac{1}{\tau_m} \tag{2.11}$$

$$\frac{1}{\tau_{e2}} = \frac{1}{T_{2e}} + \frac{1}{\tau_m} \tag{2.12}$$

where τ_R is the rotational correlation time or, more precisely, the reorientational correlation time of the metal-proton vector, and $T_{1,2e}$ are the longitudinal and transverse electron spin relaxation times, respectively, of the gadolinium(III) ion.

The field dependence of $T_{1,2e}$ can be described by the theory developed by Bloembergen and Morgan.[10] In this theory the paramagnetic electron spin relaxation is interpreted in terms of a zero-field-splitting (ZFS) interaction:

$$\left(\frac{1}{T_{1e}}\right)^{ZFS} = 2C\left(\frac{1}{1+\omega_S^2\tau_v^2} + \frac{4}{1+4\omega_S^2\tau_v^2}\right) \tag{2.13}$$

$$\left(\frac{1}{T_{2e}}\right)^{ZFS} = C\left(\frac{5}{1+\omega_S^2\tau_v^2} + \frac{2}{1+4\omega_S^2\tau_v^2} + 3\right) \tag{2.14}$$

$$C = \frac{1}{50}\Delta^2\tau_v[4S(S+1) - 3] \tag{2.15}$$

where Δ^2 is the mean-square zero-field-splitting energy and τ_v is the correlation time of the modulation of the zero-field-splitting interaction.

The inclusion of these equations into the modified Solomon-Bloembergen equations constitutes a complete theory for relating the observed paramagnetic relaxation rate enhancement to the microscopic properties, which is generally referred to as the Solomon-Bloembergen-Morgan theory. However, the theory is based on several assumptions.[1] First of all, they are valid only within the Redfield limit. This assumption, referred to as the so-called strong-narrowing condition, demands that the motions in the lattice must occur on a much faster time scale than the motions in the spin system, i.e. $\tau_R \ll T_{1,2e}$. Additionally, two main assumptions are involved, namely that the electron spin relaxation is uncorrelated with the molecular reorientation, and that the electron spin system is dominated by the electron Zeeman interaction and other interactions result only in electron spin relaxation.

The above equations point out that proton relaxivity is influenced by numerous parameters. In

any case the inner-sphere contribution to the relaxation rate depends linearly on the hydration number *q*. Just in one case, namely when the water (proton) exchange is very slow ($T_{1m} \ll \tau_m$), the exchange rate will be the only further determining factor (equation 2.7). Therefore a fast water exchange is appreciated. However, if τ_m becomes too small, no efficient interaction can take place. From equation 2.9 it is obvious, that a slightly longer Gd-H distance r_{GdH} results in a significant decrease in r_1 due to the sixth-power dependence. The influence of the other parameters is less evident to predict, as the influence of these parameters strongly depends on the magnetic field.

For the rotational correlation time τ_R, the water exchange rate k_{ex} and the longitudinal electron spin relaxation T_{1e}, the maximum relaxivity would be achieved when the correlation time τ_{c1} equals the inverse proton Larmor frequency ($1/\tau_{c1} = 1/\tau_R + k_{ex} + 1/T_{1e} = \omega_I$). It can be shown, that the reachable maximum decreases with increasing field strength. On the other hand, the use of higher magnetic fields allows a better resolution and sensitivity. T_{2e} is not important for optimisation purposes, as the "7-term" in equation 2.9 becomes negligible at field strength above 0.5 T (*B* of scanners today in clinical use: 1-3 T).[6]

Contrast agents that are currently in clinical use are far-off this optimum. The main reason is that their rotational correlation time (~ 10^{-10}s) is too short and their water (proton) exchange rate (~ $10^6 s^{-1}$) is too slow (~ $10^8 s^{-1}$ would be optimal).[1]

2.3.2 Outer-Sphere Relaxivity

As mentioned above, all contributions to the relaxivity from water molecules outside of the inner coordination sphere are usually summarised in the outer-sphere term (2.5), without distinguishing between second- and outer-sphere water molecules. The relaxivity of the outer-sphere arises from a dipolar intermolecular interaction between the nuclear spin *I* of the water protons and the total electron spin *S* of the gadolinium(III) ion, whose fluctuations are governed by the random translational diffusion of the water molecules near the gadolinium(III) complex. In the theory of outer-sphere relaxation, both the water molecules and the paramagnetic complex are treated as hard spheres. Thus, the outer-sphere relaxation rate can be described by equations 2.16 and 2.17:[1, 6]

$$\left(\frac{1}{T_1}\right)^{OS} = \frac{32\pi}{405}\gamma_I^2\gamma_S^2\hbar^2 S(S+1)\frac{N_A[\mathrm{Gd}]}{dD_{IS}}[7j(\omega_S) + 3j(\omega_I)] \tag{2.16}$$

$$j(\omega) = Re\left(\frac{1+\frac{z}{4}}{1+z+\frac{4}{9}z^2+\frac{1}{9}z^3}\right) \quad \text{with } z = \sqrt{i\omega\tau_D + \frac{\tau_D}{T_{1e}}} \tag{2.17}$$

where N_A is the Avogadro number, d is the closest distance of approach of a water molecule and gadolinium(III), D_{IS} is the sum of the diffusion coefficients D_I and D_S of water and the gadolinium(III) complex, respectively and τ_D is the diffusional correlation time ($\tau_D = d^2/D_{IS}$). A direct determination of the outer-sphere relaxivity is only possible for complexes with no water molecule in the inner-sphere ($q = 0$). The only possibility to approximate the inner-sphere relaxivity of a complex with $q > 0$ is the subtraction of the relaxivity of a chemically similar complex with $q = 0$ from the obtained overall relaxivity of the complex.[6] The different types of gadolinium(III) complexes used in MRI are highlighted in the following section.

2.4 Types of Gadolinium(III) Chelates for Magnetic Resonance Imaging

2.4.1 Gd-DTPA and Derivatives

Diethylenetriaminepentaacetic acid (DTPA) is a linear octadentate ligand, which is easily derivatised. Their gadolinium(III) complexes provide a widely used group of CAs (Figure 5).

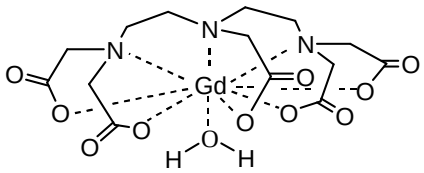

Gd-DTPA (Magnevist™)

2

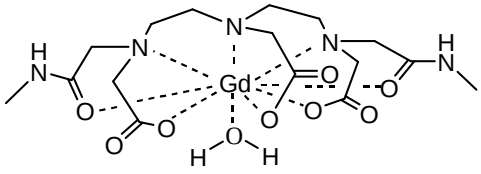

Gd-DTPA-BMA (Omniscan™)

3

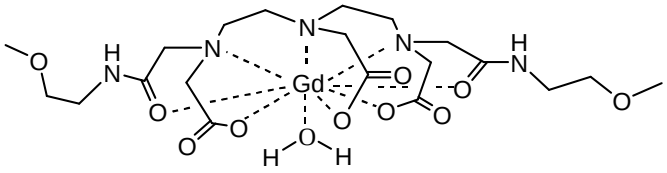

Gd-DTPA-BMEA (OptiMARK™)

4

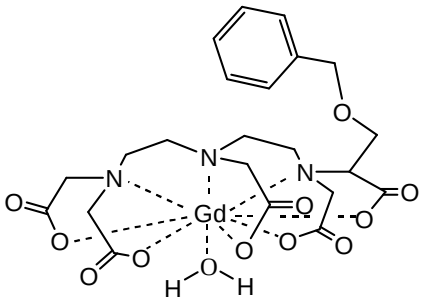

Gd-DTPA-BOPTA (MultiHance™)

5

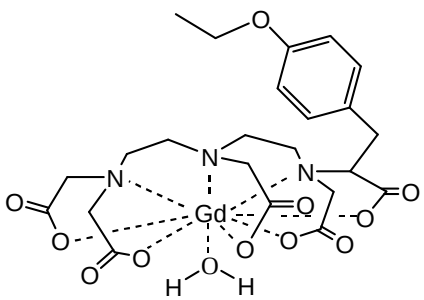

Gd-EOB-DTPA (Primovist™)

6

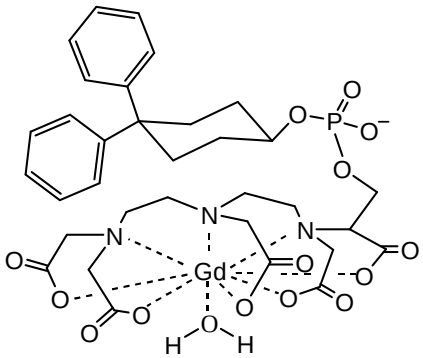

MS-325 (Vasovist™)

7

Figure 5. Commercial Gd-DTPA-based CAs.

Gd-DTPA (**2**) was marketed as Magnevist™ by Schering in 1988 and thereby was the first intravenous CA for MRI to become available for clinical use. The complex is two-times negatively charged and bears one inner-sphere water molecule. Due to its charge **2** is hyperosmolar with respect to body fluids. However, as the injected amounts are low (dosage about 0.1 mmol kg^{-1}), the increase in blood osmolality after intraveneous injection does not cause significant disturbance of the organism's osmotic balance.[2] Nevertheless neutral derivatives with lower osmolalities, like Gd-DTPA-BMA (Omniscan™) (**3**) and Gd-DTPA-BMEA (OptiMARK™) (**4**) were developed. The ligands of both complexes are amides of DTPA and are obtained by treating the dianhydride of DTPA with the corresponding amine.[2] All three complexes are freely soluble in water (usually to about 0.5-1.0 M). With relaxivities in water between 3.5 and 4.2 $mM^{-1}s^{-1}$ at 37°C and 0.47 T (Table 1), their efficiency as a contrast agent is comparably low. **2**-**4** are rapidly distributed in the extravascular space and excreted in unchanged form (no metabolism) exclusively *via* the kidneys by glomerular filtration (elimination half-lives are in the range of 1.5 hours in healthy volunteers, and almost all of the injected dose is recovered within 24 hours).[14] Since these CAs do not diffuse through plasma membranes and are therefore unable to cross the intact blood–brain barrier (BBB), they are very efficient tools for detecting any pathological abnormality of the BBB, e.g. in tumors of the central nervous system.[9]

Table 1. Clinically used DTPA-type gadolinium(III) complexes and their ionicity, relaxivity r_1, thermodynamic stability constant K_{GdL} and conditional stability constant K^*_{GdL} at pH 7.4.

Complex	**Trademark**	**Ionicity**	r_1 **[$mM^{-1}s^{-1}$]**	**log K_{GdL}**	**log K^*_{GdL}**
Gd-DTPA	Magnevist™	Di-ionic	3.9[a]	22.1[d]	17.7[d]
Gd-DTPA-BMA	Omniscan™	Neutral	3.5[a]	16.9[d]	14.9[d]
Gd-DTPA-BMEA	OptiMARK™	Neutral	4.2[a]	16.6[d]	15.0[d]
Gd-BOPTA	MultiHance™	Di-ionic	4.2[a] (6.7)[c]	22.6[d]	16.9[d]
Gd-EOB-DTPA	Primovist™	Di-ionic	5.3[a] (7.3)[c]	23.5[d]	N/A
MS-325	Vasovist™	Tri-ionic	5.8[b] (19)[c]	23.2[e]	N/A

[a]Ref. 9, water, 37°C, 20 MHz; [b]Ref. 15, water, 37°C, 20 MHz; [c]Ref. 15, blood, 37°C, 1.5 T; [d]Ref. 6; [e]Ref. 16.

In order to allow liver imaging the two CAs Gd-BOPTA (MultiHance™) (**5**) and Gd-EOB-DTPA (Primovist™) (**6**) were developed. Both are Gd-DTPA derivatives which have a lipophilic aromatic moiety in their structure. Thereby they can be taken up by hepatocytes and undergo partial hepatobiliary excretion (2 %-4 % and 50 % for **5** and **6**, respectively).[14, 17] The

aromatic ring in **5** and **6** leads to some weak plasma protein binding, although the protein-bound fraction is only about 10 %.[17] The protein binding leads to an increase in relaxivity of these compounds in blood compared to that in water (Table 1). However, the binding does not appear to impact plasma clearance. By contrast, MS-325 (**7**), being marketed as Vasovist™, binds reversibly to human serum albumin (HSA) *via* a lipophilic biphenylcyclohexyl group, which increases the elimination half-life in subjects with normal renal function to 18.5 h.[17] The concentration of albumin in plasma is high enough (600-700 μM) to reversibly bind most of the CA after injection, leading to a significant increase in relaxivity (Table 1).

All these CAs are usually well tolerated, show few side effects and were considered as generally safe.[18] However, since a correlation between gadolinium(III) and the development of a new severe disease named nephrogenic systemic fibrosis (NSF) was reported in early 2006,[19] the *in vivo* stability of the CAs regained attention. Up to now, NFS appeared exclusively in patients with severe impaired kidney function. In these patients the renal excretion half-life of the CAs is significantly increased (e.g. for Omniscan™ from ~90 min in healthy persons to ~ 2000 min in diseased persons).[20] Due to their eight-dentate ligands the thermodynamic stability K_{GdL} (defined by equation 2.18) of **2**-**7** is quite high (Table 1).

$$K_{GdL} = \frac{[GdL]}{[Gd][L]} \tag{2.18}$$

To describe the *in vivo* stability, the conditional stability constant K^*_{GdL} is more appropriate than K_{GdL} (Table 1). K^*_{GdL} is measured at pH 7.4 and takes into account all protonation constants of the ligand. The conditional stability constant is defined as:

$$K^*_{GdL} = \frac{K_{GdL}}{(1 + K_1[H^+] + K_1K_2[H^+]^2 + \cdots + K_1K_2K_n[H^+]^n)} \tag{2.19}$$

where K_1, K_2,…, K_n are the stepwise protonation constants of the ligand. Since also their K^*_{GdL} values are fairly large, **2**-**7** are generally considered as highly stable. However, blood and other body fluids are very complex milieus containing a large number of potential ligands and metal ions which can displace the gadolinium(III) from its complex. Hence, their kinetic inertia especially towards this so-called “transmetallation” must also be considered.

Numerous studies were carried out in order to investigate transmetallation under various conditions.[9, 14, 21-23] It could be shown that all linear, open-chained CAs release gadolinium(III) *via* transmetallation under physiological conditions whereby the neutral CAs **3** and **4** exhibited a significantly lower kinetic inertness then their ionic derivatives. Therefore it is no surprise that most of the reported cases of NSF could be attributed to these two CAs.[20] However, there are also reported cases of NSF triggered by Magnevist™ (**2**) in patients with

severe renal dysfunction, showing that **2** is also not inert enough to prevent the release of too high amounts of gadolinium(III) if the CA remains in the body for a prolonged period of time. The comparatively low kinetic inertia of these open-chained chelates has been modeled by rapid unwrapping of these molecules due to their conformational mobility.[24] The replacement of the two ionic carboxylate (COO^-) donor moieties by non-ionic amide groups in the case of **3** and **4** leads to a weaker binding of these moieties to gadolinium(III). This may introduce more flexibility and conformational mobility, which explains the significant loss in kinetic inertness of these systems. On the other hand, the introduction of an aromatic moiety in the case of **5-7** slightly improves kinetic inertia. This can be explained by the steric effect of the bulky substituents that hinders unwrapping of the ligand around gadolinium(III).[25]

2.4.2 Gd-DOTA-type Contrast Agents

Macrocyclic MRI CAs show a significantly higher kinetic inertia, which is attributed to their tight packing and their high conformational rigidity.[26, 27] All commercially available macrocyclic CAs are based on a 1,4,7,10-tetraazacyclododecane ring (cyclen), which forms an ideal cavity for the complexation of gadolinium(III) (Figure 6).

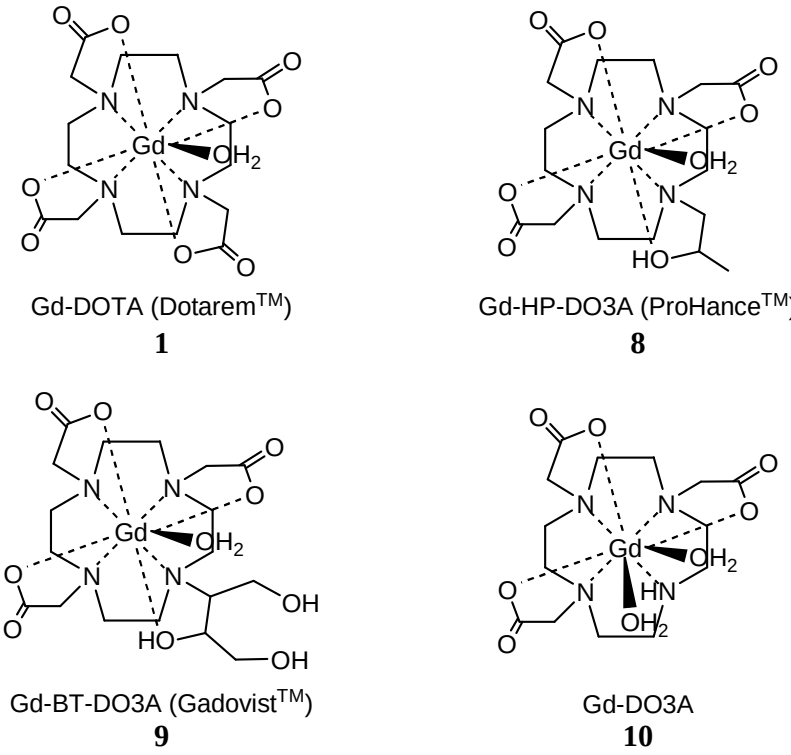

Figure 6. Gd-DOTA and derivatives.

Gd-DOTA (**1**) was the first macrocyclic MRI CA. It was marketed under the trademark Dotarem™ in 1989 by the Guerbet Company. Due to its higher kinetic and thermodynamic stability (Table 2) Gd-DOTA (**1**) is considered as the safer alternative towards Gd-DTPA (**2**).

Up to now, there is no reported case of NSF in the peer reviewed literature which can be related exclusively to the administration of **1**. Another advantage of **1** over **2** lies in its lower relative viscosity. This allows a faster injection for a given applied pressure, which minimises patient discomfort as a burning sensation due to hyperosmolality is felt otherwise.[18] However, also for the macrocyclic CAs neutral derivatives of Gd-DOTA, namely Gd-HP-DO3A (Prohance™) (**8**) and Gd-BT-DO3A (Gadovist™) (**9**) were developed to further reduce osmolality.

Table 2. Clinically used DOTA-type gadolinium(III) complexes and their ionicity, relaxivity r_1, thermodynamic stability constant K_{GdL} and conditional stability constant K^*_{GdL} at pH 7.4

Complex	**Trademark**	**Ionicity**	r_1 [$mM^{-1}s^{-1}$]	log K_{GdL}	log K^*_{GdL}
Gd-DOTA	Dotarem™	Ionic	3.4[a]	25.8[c]	18.8[c]
Gd-HP-DO3A	Prohance™	Neutral	3.1[a]	23.8[c]	17.1[c]
Gd-BT-DO3A	Gadovist™	Neutral	3.7[a]	21.8[c]	N/A
Gd-DO3A	-	Neutral	4.8[b]	21.0[c]	15.0[c]

[a]Ref. 9, water, 37°C, 20 MHz; [b]Ref. 28, water, 40°C, 20 MHz; [c]Ref. 6

Compound **8** shows a two orders of magnitude lower thermodynamic stability than **1** (Table 2). This is not unexpected since the hard Lewis acid gadolinium(III) binds more tightly to negatively charged atoms rather than neutral ones. The introduction of additional hydroxyl groups in the case of **9** decreases K_{GdL} even further. However, due to their excellent kinetic stability the lower thermodynamic stability has no impact on its use in patients. All three marketed macrocyclic CAs are extracellular fluid agents, which target no specific anatomical site or physiological function.[29] Their increased stability does not lead to a lack in other properties. They show similar pharmacokinetics as their unspecific open-chained counter parts and, with relaxivities between 3.1 and 3.7 $mM^{-1}s^{-1}$ at 37°C and 20 MHz, display also comparable efficiencies (Table 2). As mentioned in chapter 2.3.1 the reasons why these relaxivities are far-off the theoretically possible values are their too short rotational correlation times and too slow water exchange rates. A further reason is their low hydration number *q*. All commercial CAs consist of octadentate ligands and thereby possess only one free coordination site for the interaction with water. A system with a heptadentate ligand is Gd-DO3A (**10**). The hydration number of **10** was determined to be about two[30] However, a small fraction of monohydrated species was also observed.[31] Due to this coordination equilibrium the water exchange rate k_{ex} of Gd-DO3A (**10**) is as twice as high as that of Gd-DOTA (**1**). Hence, with 4.8 $mM^{-1}s^{-1}$ the relaxivity of **10** is about 40 % higher than that of **1**

(Table 2). Unfortunately a clinical use of **10** is prevented by its comparably low conditional stability constant (Table 2) and by the possibility of reversible oxy-anion binding under physiological conditions which can lead to the complete loss of inner sphere water.[32, 33]

3 Calcium(II)-sensitive MRI Contrast Agents

3.1 Introduction

In the field of neuroscience the so-called functional magnetic resonance imaging (fMRI) offers a possibility to locate brain activity *via* MRI. Today, fMRI in the brain is based on the increase in cerebral blood flow to the local vasculature, which is involved in the increase in oxygen level and glucose consumption that follows neural activity in the brain. The release of dioxygen from hemoglobin causes its iron to become paramagnetic by changing from a low spin state to a high spin state.[34] The so generated "internal CA" accelerates the relaxation rate of the surrounding water protons which in turn leads to a detectable blood-oxygen-level-dependent (BOLD) magnetic resonance signal.[35, 36] fMRI is currently the most widely used method for brain mapping and studying the neural basis of human cognition.[37-39] Indeed, more detailed investigations showed in first approximation a linear relationship between the BOLD signal and the neural response elicited by a short stimulus duration. However, the hemodynamic response seems to be better correlated with the local field potentials (input signals of a neural population), implying that activation in an area is often likely to reflect the incoming input and the local processing in a given area rather than the spiking activity. Even though it can be expected that local field potentials will usually correlate with neurotransmitter release, fMRI experiments based on the BOLD signal may reveal activation in areas in which no single-unit activity is found in physiological experiments.[35] Additionally, the indirect hemodynamic BOLD signal is associated with a time lag which broadens the response. All this can make BOLD fMRI insufficient for an accurate study of neural activity.

A way to detect neuronal activity in a more direct manner could be the use of CAs which are able to respond to changes in the physiological environment directly linked to the release of neurotransmitters.

Calcium(II) ions are a promising target for such CAs as they play a central role for the release of neurotransmitters into the synaptic cleft (Figure 7). When an action potential reaches the axon terminal, the electrical depolarisation of the synaptic membrane causes calcium channels to open. Calcium(II) ions flow through the presynapitic membrane which increases the calcium(II) concentration in the interior. This in turn causes vesicles to fuse with the membrane of the presynaptic cell, thereby opening the vesicles and releasing their neurotransmitter content into the synaptic cleft.[40, 41]

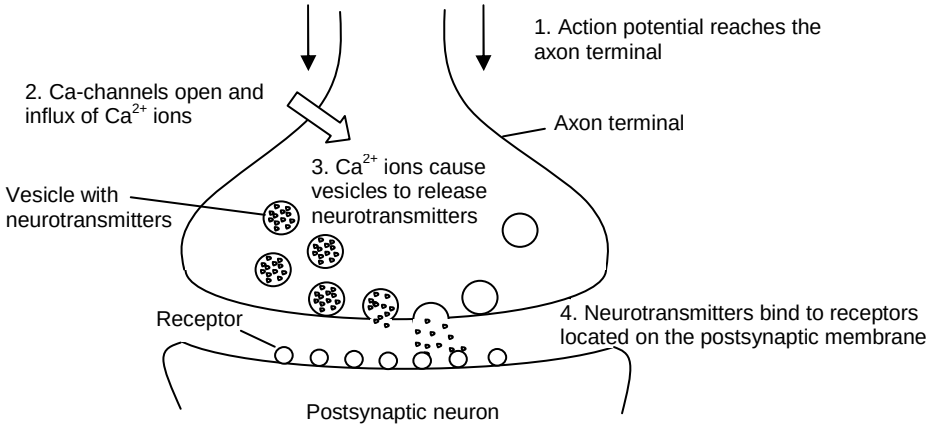

Figure 7. Schematic presentation of the synaptic signal transmission in a chemical synapse.

Measurements in the cerebellar cortex of the cat revealed a decrease in the calcium(II) concentration of the extracellular microenvironment of the active neuron from 1.2 mmol/L to 0.8 mmol/L.[42] This concentration change then needs to be detected by the responsive or "smart" CA.

3.1.1 Responsive or "Smart" Contrast Agents

In recent years an increasing number of CAs were described in the literature, which are able to convert changes in physico-chemical parameters that characterise their physiological environment into a change in relaxivity r_1 and hence in a contrast change. Typical parameters are enzyme activity, pH and metal ion concentrations.

3.1.1.1 Agents sensitive to enzyme activity

The first enzyme sensitive contrast agent was developed in response to the need to correlate biological events with gene expression during an imaging experiment. The Meade group thereto developed a CA (Gd-DO3A-β-gal (**11**)) whose relaxivity r_1 responds to β-galactosidase mRNA expression.[43, 44] Gd-DO3A-β-gal (**11**) is a derivative of Gd-DOTA (**1**) which bears a galactopyranose residue (Scheme 1). This residue is a substrate of the β-galactosidase enzyme and blocks the open coordination side of the gadolinium(III) ion. As no water molecule can therefore enter the inner coordination sphere, the relaxivity of **11** is diminished. Upon the production of the targeted enzyme the sugar moiety is cleaved irreversibly from the complex, allowing water to interact with the paramagnetic centre. The increase in inner sphere water then results in a 50 % higher r_1 of **12** as compared to **11**,[44] which allowed the successful use of **11** in the *in vivo* detection of β-galactosidase mRNA expression in living Xenopuslaevis embryos by MRI.[43]

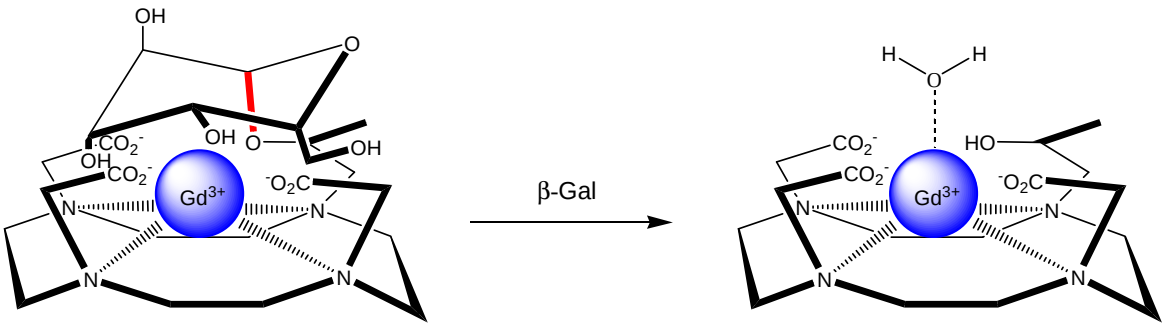

11 **12**

Scheme 1.

Himmelreich *et al.* recently developed a contrast agent for imaging of dendritic cells.[45] The contrast agent, called Gd-DTPA-FA is a Gd-DTPA (**2**) derivative which contains two long fatty acid chains ($COOC_{17}H_{35}$) connected to the ligand surface *via* an ester bond. These chains make the CA insoluble in water, resulting in inactive particles showing no relaxivity r_1. The particles are internalised into the dendritic cells by phagocytosis were they are solubilised by intracellular lipase activity through cleavage of the insolubilising moieties. Hence, the increase in intracellular relaxivity r_1 is a function of the enzyme activity. MR images of the so labelled cells implanted into the rat brain showed the suitability of this CA for functional cellular in *vivo* MRI.

A CA that is sensitive to the presence of the human carboxy peptidase B, thrombin-activatable fibrinolysis inhibitor (TAFI), was prepared by Nivorozhkin *et al.*.[46] The CA is a derivative of Gd-DTPA (**2**) exposing an aromatic group that has a high affinity for human serum albumin (HSA), like the biphenylcyclohexyl moiety of MS-325 (**7**) (see chapter 2.4.1). In contrast to **7** the aromatic function of this CA is masked by a trilysine group, preventing a HSA binding. TAFI, which has been implicated in thrombotic disease, cleaves the trilysine masking group, allowing the CA to bind to albumin. The resulting longer rotational correlation time τ_R then leads to an increase in r_1.

A further example of enzyme sensitive CAs was reported by Bogdanov *et al.*.[47] Their CA is a Gd-DOTA (**1**) derivative which bears a benzene-1,2-diol moiety. In the presence of a peroxidase and an excess of hydrogen peroxide the monomeric CA oligomerises, yielding a three-fold increase in relaxivity r_1 (0.47 T and 40°C) due to the accompanied increase in τ_R. This allows a detection of peroxidase concentration *in vitro* and has been used to detect E-selectin expression on human endothelial cells in culture.

3.1.1.2 pH-dependent contrast agents

pH-dependent CAs are of great interest especially in the detection of cancer, as the pH on the surface of tumors is about 0.4 units lower than in healthy tissue.[48]

One CA which shows a pH dependency due to changes in its second-sphere was reported by the Sherry group.[49] The CA, Gd-DOTA-4AmP, is a Gd-DOTA (**1**) derivative where the four carboxylic acid functions are replaced by amidomethylphosphonate groups. In this system the pH has no direct influence on the water exchange rate, however, the protonation/deprotonation of the phosphonates creates/destroys a hydrogen bonding network which provides a catalytic pathway for the exchange of protons from the bound water with protons of bulk water. The CA was applied in vivo for extracellular pH mapping by assessing the local concentration of the CA through the use of a pH-insensitive analogue, assuming the same biodistribution for the two systems.[50]

In other examples the pH-dependency of the relaxivity r_1 reflects changes in the hydration number *q*. Mamedov *et al.* developed a series of pH-sensitive CAs based on Gd-DO3A (**10**), where the forth cyclen nitrogen is alkylated with an ethyl or propylphosphonate moiety.[51] At low pH the phosphonate group is mostly protonated and therefore not coordinated to the gadolinium(III) ion (**13** in Scheme 2). This leaves two coordination sites free for water to coordinate. When the pH is increased the phosphonates become deprotonated which allows a coordination of the phosphonate moiety to the paramagnetic centre (**14** in Scheme 2). The decrease in *q* results in a reduction of the relaxivity r_1 to about 50-60 % of the starting value when increasing the pH from 4 to 7.

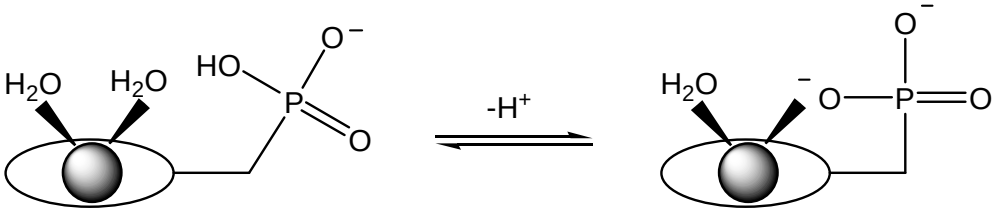

13 **14**

Scheme 2.

A similar approach was used by Lowe *at al.*[52] Instead of an alkylphosphonate moiety, an alkylsulfonamide function was introduced, whose nitrogen is protonated at low pH thus preventing a coordination. As at higher pH the coordination of the deprotonated sulfonamide nitrogen hinders the interaction of any water molecule with the gadolinium(III) the effect on r_1 is higher in this case.

Aime *et al.* prepared a macromolecular CA with 30 macrocyclic gadolinium(III) chelates and 114 ornithine residues, which turned out to have a pH dependent relaxivity.[53] The gadolinium(III) complexes are conjugated to the amino acid chain *via* squaric esters. The pH-dependency arises from an interaction of the, at higher pH, deprotonated amide side chains with the squaric esters. This interaction increases the rigidity of the polymer, causing an increase in the rotational correlation time τ_R and therefore an increase in relaxivity r_1.

3.1.1.3 Metal ion sensitive contrast agents

The first MRI CA which showed a change in its relaxivity r_1 in the presence of a metal ion was reported by Aime *et al.* in 1993.[54] However, it was not developed in order to respond *in vivo* to changes in the surrounding metal ion concentration, but to obtain a high relaxivity CA. The CA is a Gd-DTPA (**2**) derivative functionalised with salicylate moieties. Upon addition of iron(III), the Gd-DTPA–salicylate complexes bind to the iron(III) ions *via* the salicylate functional groups, thereby increasing τ_R and r_1.

A similar, but much more efficient approach to increase the relaxivity r_1 was recently reported by Livramento *et al.*.[55] They developed a heterotritopic ligand named $[bpy(DTTA)_2]^{8-}$ which has two diethylenediamine-tetraacetate units for gadolinium(III) binding and a 2,2'-bipyridine function for selective iron(II) coordination. In aqueous solution and in the presence of these metals, the ligand is capable of self-assembly to form a rigid supramolecular metallostar structure with six efficiently relaxing gadolinium(III) centres confined to a small molecular space. The metallostar has a remarkable high relaxivity r_1 particularly at very high magnetic fields (r_1 = 15.8 $mM^{-1}s^{-1}$ at 200 MHz and 37°C in H_2O) and has already shown its potential *in vivo*.[56]

Hanaoka *et al.* developed a CA which is capable to respond to changes in the surrounding zinc(II) ion concentration.[57] This Gd-DTPA-bisamide complex (**15**) (Scheme 3) was designed on the basis that N,N,N',N'-tetrakis(2-pyridylmethyl)ethylenediamine (TPEN) readily complexes with Zn^{2+} ions but hardly complexes Ca^{2+} and Mg^{2+} ions. In the absence of zinc(II), water is bound to the gadolinium(III) ion. Upon the addition of Zn^{2+} ions, the pyridine moieties coordinate to zinc(II) thus restricting the access of water to the gadolinium(III) ion (Scheme 3). This decrease in q results in a decrease in r_1. However, when the Zn^{2+}-CA molar ratio exceeds 1:1 the relaxivity increases again as **15** is capable to form the 2:1 complex **17** (Scheme 3). In terms of application this is problematic as one cannot distinguish for example the r_1 values of solutions containing 0.3 and 1.5 equivalents of zinc(II). This problem could be circumvented by replacing one of the pyridine moieties on each of the amide functions of **15** by a carboxylate group.[58] This CA showed a similar zinc(II)

sensitivity without the limitation of an increasing relaxivity above a 1:1 ratio.

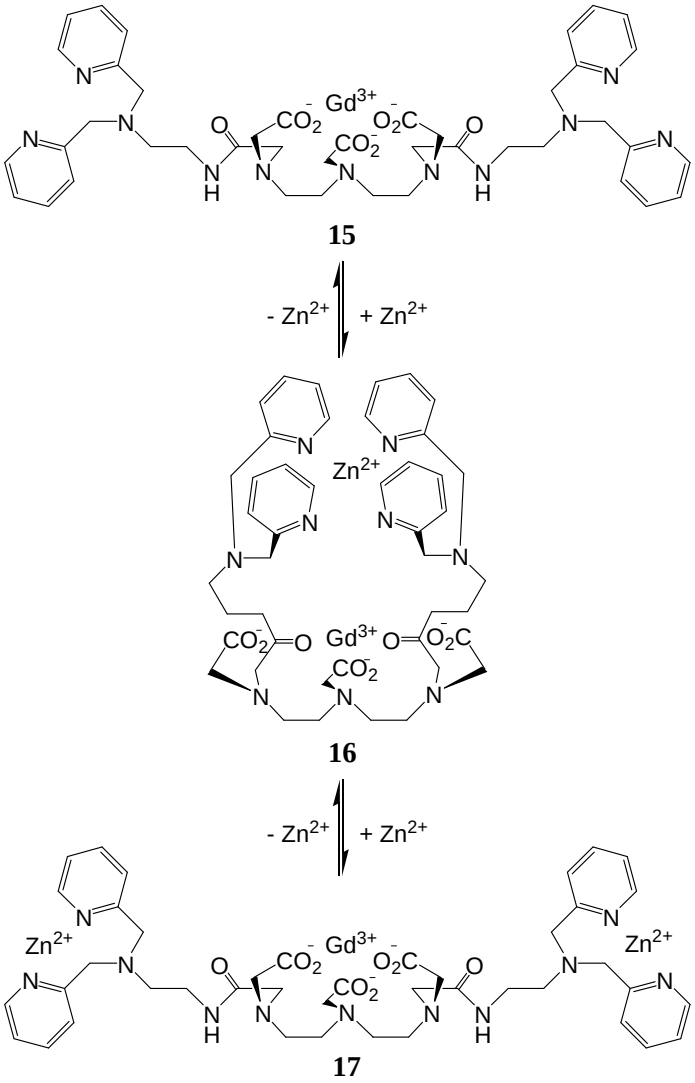

Scheme 3.

The first calcium(II) sensitive MRI CA, called Gd-DOPTA (**18**) (Scheme 4) was invented by Li *et al*..[59] It consists of two Gd-DO3A chelates attached to a 1,2-bis(o-aminophenoxy)ethane-N,N,N′,N′-tetraacetic acid (BAPTA) moiety for selective calcium(II) coordination. As the zinc(II) sensitive CAs of Hanaoka *et al.*, **18** is designed in order to change the hydration state of gadolinium(III) in the presence of the metal ion. However, the mechanism works in an opposite manner (Scheme 4). It is assumed that in the absence of calcium(II) the aromatic iminoacetates shield the gadolinium(III) ion from water resulting in a low longitudinal relaxivity (3.26 $mM^{-1}s^{-1}$ at 500 MHz and 25°C). With increasing calcium(II) concentration the BAPTA groups begin to coordinate the Ca^{2+} ions. This reorganisation of the complex exposes the gadolinium ion to bulk water, thereby increasing the relaxivity (plateau at 5.76 $mM^{-1}s^{-1}$ at 500 MHz and 25°C after the addition of about one equivalent of calcium(II)). The assumption

rests on an observed change in the hydration number *q* from 0.5 for **18** to 1.0 for **19**.[60]

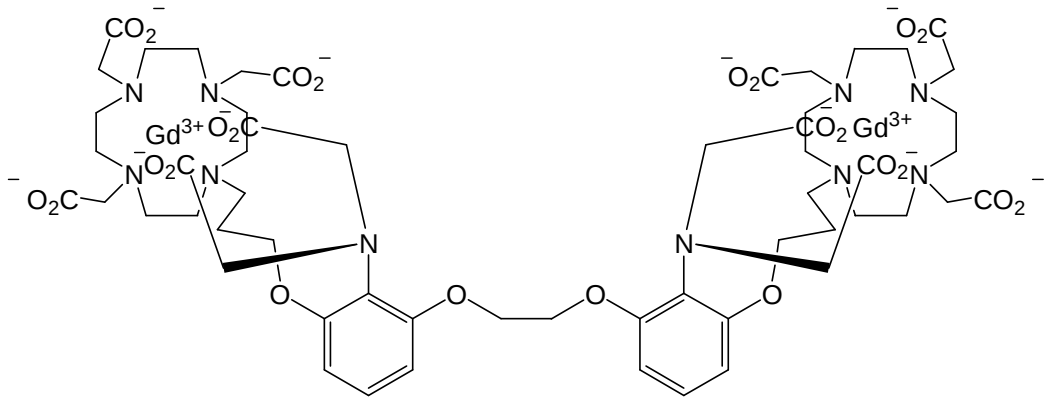

18

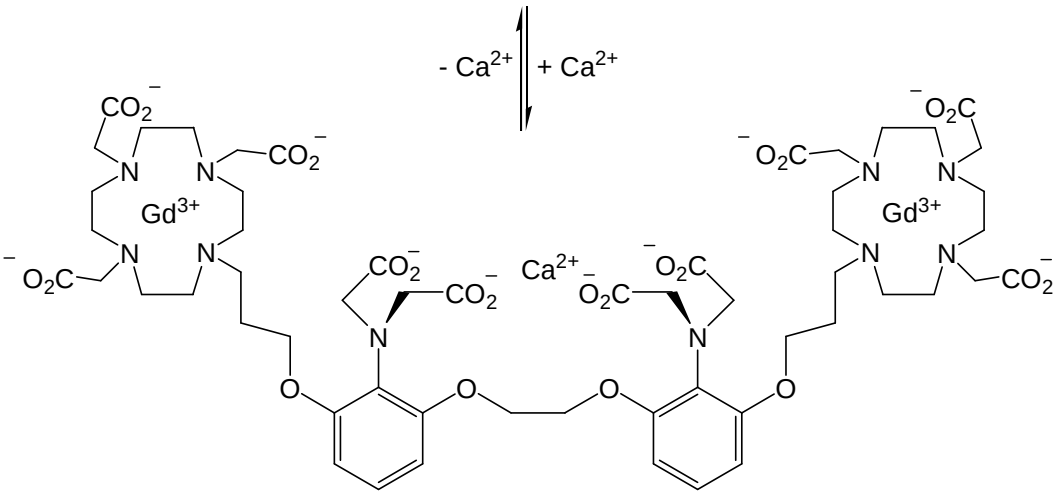

19

Scheme 4.

Since then several approaches to further optimise the selectivity and efficiency of calcium(II) sensitive CAs were undertaken in particular by the Logothetis group.[61-64] So far the strongest increase in relaxivity (98 % at 400 MHz and 27°C) upon the addition of calcium(II) was observed for Gd-DOPTRA (**20**) (Figure 8).[63]

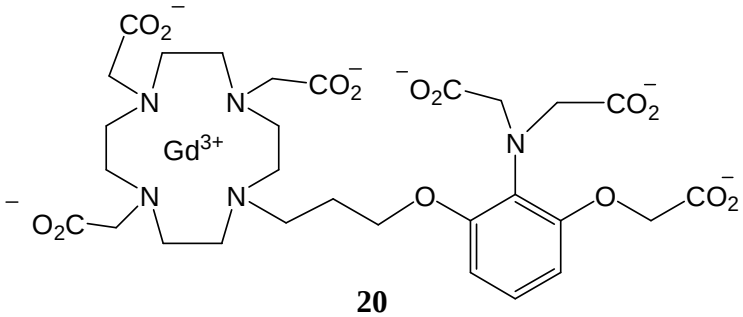

20

Figure 8. Gd-DOPTRA

However, still not one of them proved its suitability to detect neuronal activity in the brain.

3.1.2 Aim of this Project

An alternative to the systems with aminocarboxylate moieties for calcium(II)-sensing was developed by I. Mamedov[65] in our research group. He synthesised a series of potential gadolium(III)-based calcium(II)-sensitive CAs bearing an alkylaminobis(methylene-phosphonate) group as the calcium(II) sensor (Figure 9). Four different ligands with propyl (**L**^{1}), butyl (**L**^{2}), pentyl (**L**^{3}) or hexyl (**L**^{4}) linkers between the aminobis-(methylenephosphonates) and DO3A were prepared in order to allow an optimisation of the calcium(II)-sensitivity.

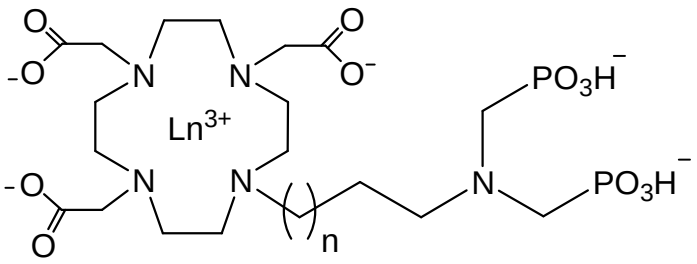

LnL^{1}-LnL^{4}, n = 1-4

Figure 9. Structures of the aminobis(methylenephosphonates)-based potential calcium(II) sensitive CAs; **L**^{1}, n= 1; **L**^{2}, n= 2; **L**^{3}, n= 3; **L**^{4}, n= 4; Ln^{3+} = Gd^{3+}, Y^{3+}, Eu^{3+}

The aminobis(methylenephosphonate) unit was chosen since the introduction of negatively charged phosphonate groups into common Gd^{3+}-based CAs increases their relaxivity r_1 due to an acceleration of the water exchange rate k_{ex} and their ability to form a second sphere water network around the Gd^{3+} complexes. Both factors are important to improve the MR signal, especially in high magnetic fields.[16, 66, 67] The use of bis(phosphonates) attached to the DO3A core or to superparamagnetic iron oxide (SPIO) particles was already proposed for potential bone targeted CAs.[68, 69] Most important, aminopolyphosphonic acids are well-known chelators for transition metal ions,[70, 71] but also exhibit high complexation efficiency towards biologically important metal ions such as Ca^{2+}, Mg^{2+} and Zn^{2+}.[72]

In a preliminary investigation Mamedov observed a calcium(II)-dependent relaxivity change for two systems. However, r_1 decreased with increasing calcium(II) concentration which is inconsistent with the mechanism (Scheme 4) proposed for the other calcium(II)-sensitive CAs.

The aim of this project was a more detailed investigation of the calcium(II)-sensitivity of these potiential MRI CAs in order to understand the mechanistic aspects leading to the decrease in r_1. This should allow conclusions about the suitability of the novel type of calcium(II) sensor for biomedical applications.

3.2 Results and Discussion

3.2.1 Relaxivity *vs.* Calcium(II) Concentration

Initially, the paramagnetic response of the gadolinium(III) complexes **GdL^1**-**GdL^4** to changes in the concentration of surrounding calcium(II) ions was studied by means of relaxometric titrations at complex concentrations of 2.5 mM (9.4 T, 25 ^{o}C). It could be shown that, already in the absence of calcium(II), the length of the pendant arm has an influence on the relaxivity of the complexes. r_1 values of 6.92, 7.43, 6.70 and 5.76 $mM^{-1}s^{-1}$ were determined for **GdL^1**, **GdL^2**, **GdL^3**, and **GdL^4**, respectively.

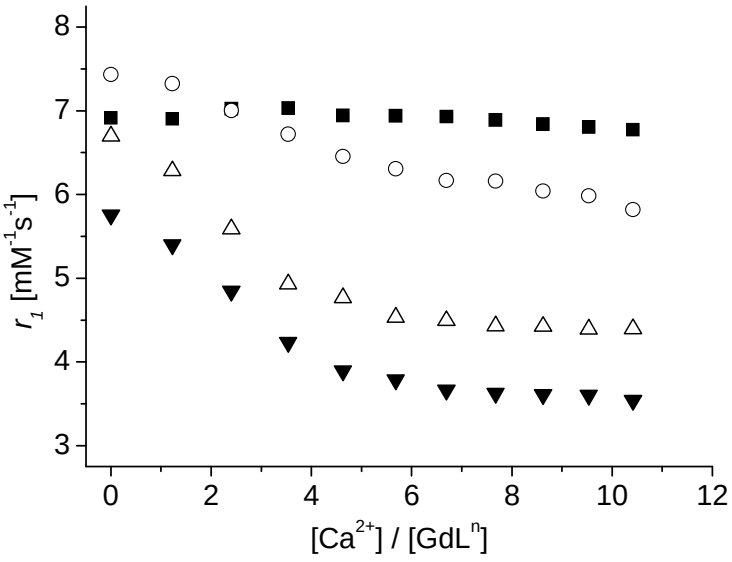

Figure 10. Relaxometric Ca^{2+} titration curves of **GdL^1** (■), **GdL^2** (○), **GdL^3** (Δ) and **GdL^4** (▼) at [GdL^n] = 2.5 mM, 9.4 T, 25 °C, pH 7.3 (HEPES buffer)

Even more considerable were the differences between the complexes **GdL^1**-**GdL^4** in their r_1 response to the addition of Ca^{2+} ions (Figure 10), namely, the sensitivity of the complexes towards calcium(II) increases with the extension of the aliphatic side chain. No changes in r_1 of **GdL^1** were found over the whole span of calcium(II) concentration. In the case of **GdL^2**, a moderate decrease of r_1 was observed on addition of calcium(II), whereas the r_1 of the **GdL^3** and **GdL^4** solutions showed a strong dependence on the calcium concentration resulting in the decrease to 66% and 61% of the initial r_1 values, respectively. Upon addition of equimolar amounts of EDTA (ethylenediaminetetraacetic acid) after the titration of **GdL^3** and **GdL^4** with calcium(II), the relaxivity of both complexes returned to the values in calcium(II)-free solutions, indicating that r_1 changes are reversible and exclusively induced by calcium(II).

3.2.2 Relaxivity *vs.* Complex Concentration

As already mentioned in chapter 3.1.2 the relaxivity decrease observed for **GdL^2**-**GdL^4** upon the addition of calcium(II) ions is not explicable with the mechanism assumed for the previously reported calcium(II)-sensitive CAs (Scheme 4, chapter 3.1.1.3). Since **GdL^2**-**GdL^4** all bear only one amino(bismethylenephosphonate) function, a monomeric "blocking"-mechanism as described for the zinc(II)-sensitive systems in chapter 3.1.1.3 (Scheme 3) is also very unlikely. However, phosphonates, diphosphonates and aminobis-(methylenephosphonates) are able to form aggregates in solution, either hydrogen bonded (units with two or more molecules) or metal-assisted,[72, 73] which might have an influence on the relaxivity. As the ratio between aggregated and non aggregated complexes should be concentration dependent, r_1 was studied as a function of the **GdL^1**-**GdL^4** concentration itself, in absence and presence of Ca^{2+} ions (Figure 11a and Figure 11b, respectively).

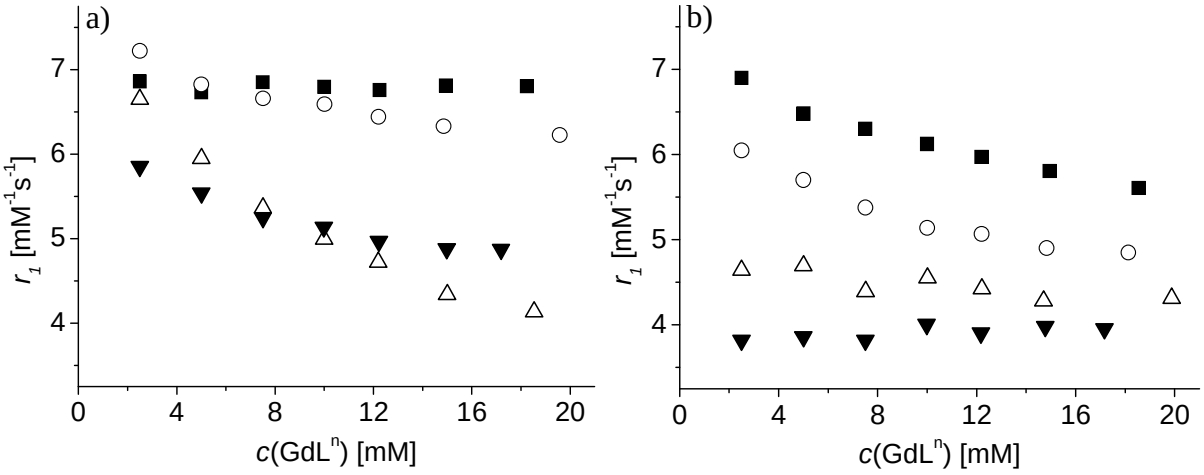

Figure 11. Concentration-dependence of r_1 for **GdL^1** (■), **GdL^2** (○), **GdL^3** (Δ) and **GdL^4** (▼) in (a) the absence of Ca^{2+} and (b) the presence of three equiv. of calcium(II) at 9.4 T, 25 °C, pH 7.3 (HEPES buffer).

In Ca^{2+}-free solutions, only **GdL^1** has concentration independent relaxivities, while for **GdL^2**-**GdL^4**, the r_1 values have been found to be concentration dependent. The relaxivity of **GdL^2**, **GdL^3** and **GdL^4** dropped by 14, 38 and 17 %, respectively, when the concentration was increased from 2.5 to 20 mM. However, when the same experiment was performed in the presence of three equivalents of calcium(II), the change in r_1 for **GdL^3** and **GdL^4** was low, while r_1 decreased by 19 and 20% for **GdL^1** and **GdL^2**, respectively. This shows that also **GdL^1** has a calcium(II)-dependent r_1, however only at higher complex concentrations than used in the initial r_1 measurements ([**GdL^1**] = 2.5 mM in Figure 10). If the same experiment would have been performed at a complex CA concentration of about 18.5 mM the addition of three equivalents would have resulted in a decrease in r_1 of 18 % (cf. Figure 11). The

observed concentration dependences of the relaxivity give strong evidence for the presence of aggregates with and/or without the involvement of calcium(II), depending on the system.

3.2.3 PGSE Diffusion ^{1}H NMR Spectroscopy

Pulsed gradient spin echo (PGSE) diffusion ^{1}H NMR measurements were performed in order to confirm that the changes in relaxivity are the result of an aggregation / disaggregation process. Over the last years, this method has shown to be a powerful tool in the elucidation of aggregation processes[74-77] as well as for the determination of rotational correlation times τ_R.[78] As the paramagnetic gadolinium(III) is not suitable for such measurements, the diamagnetic yttrium(III) analogue was used. Yttrium(III) is an appropriate substitute for gadolinium(III) in such systems as it has an almost identical ion radius and all involved interactions are almost exclusively electrostatic. The diffusion coefficients D of the complexes **YL^1** and **YL^4** were determined in the same range of concentration as the concentration dependent relaxivity measurements, both in the absence and presence of Ca^{2+} ions at 25°C (Figure 12).

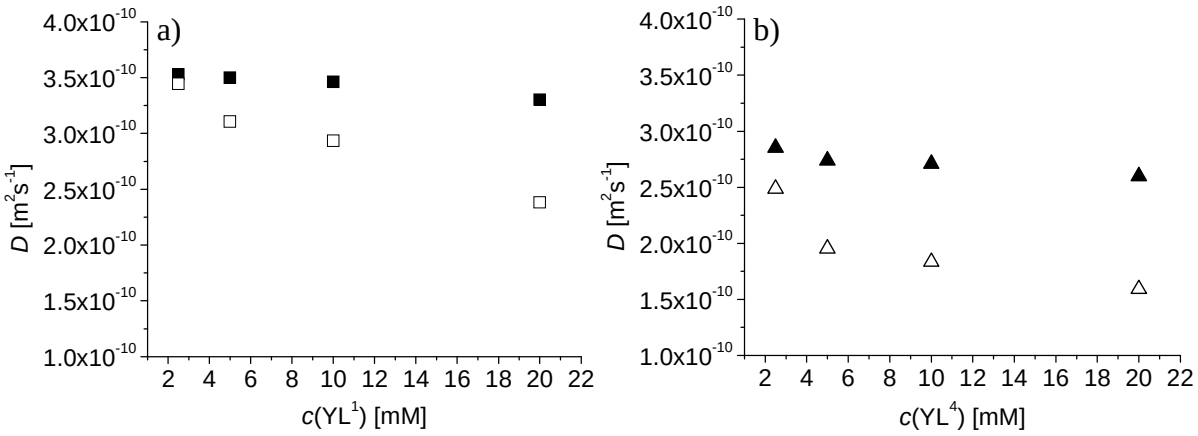

Figure 12. Concentration-dependence of the diffusion coefficient D of **YL^1** (a) and **YL^4** (b) in the absence of Ca^{2+} (full symbols) and the presence of three equiv. Ca^{2+} (empty symbols) at 11.75 T, 25 °C, pH 7.3 (HEPES buffer).

As mentioned above, aggregation is a concentration dependent process. This means that for an infinitely diluted sample the determined diffusion coefficient D is that of the monomer, whereas in highly concentrated samples D corresponds to that of the aggregate. In samples with concentrations between those two extremes only an average D is determined, corresponding to mixtures of aggregated, partly aggregated and monomeric species. For the quantification of aggregation processes usually the viscosity independent hydrodynamic volume V_H is used.[76] V_H can be calculated from the hydrodynamic radius r_H which is, for spherical molecules, related to the diffusion coefficient D *via* the Stokes-Einstein equation (equation 3.1), where k_B is the Boltzmann constant, T is the absolute temperature, η is the

viscosity, and r_H is the hydrodynamic radius. Additionally, the rotational correlation time τ_R can be calculated from r_H using equation 3.2.

$$D = \frac{k_B T}{6\pi\eta r_H} \tag{3.1}$$

$$\tau_R = \frac{4\pi\eta r_H^3}{3k_B T} \tag{3.2}$$

Assuming dilute solutions where $\eta_{solution} = \eta_{solvent}$, values for r_H, τ_R and V_H were calculated from the obtained diffusion constants (Table 3). For comparison, D and the related values of compound **21** (Figure 13), where no aggregation is expected, were also ascertained.

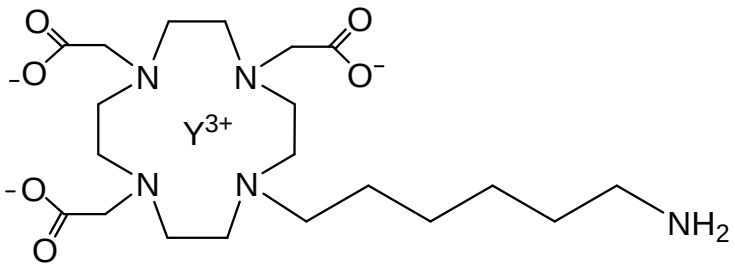

21

Figure 13. Y-DO3A-hexylamine

In this study, the calculated values of r_H, τ_R and V_H should only be regarded as approximations and serve mainly for visualization purposes, as not all complexes and possible aggregates can be considered as spherical, making equation 3.1 valid only within certain limits. However, it is unambiguous that in the absence of Ca^{2+} ions the diffusion constants of **YL^1** are significantly higher than those of **YL^4**. The calculated hydrodynamic volume V_H of **YL^4** is about two-times the volume of **YL^1**, whereas V_H of **YL^1** is only slightly higher than that of the monomeric compound **21**. This confirms the presence of aggregates for **LnL^4** already in the absence of calcium(II). D of **YL^4** and all related values are therefore only average values over all forms of **YL^4** in solution. The aggregation process is also shown by the increase in V_H of **YL^4** with higher complex concentrations, at which the equilibrium between aggregated and monomeric species is shifted towards the aggregate. As, on the other hand, the relaxivity of **GdL^4** is decreasing with increasing complex concentration (Figure 11a), r_1 of these aggregates must be smaller than r_1 of the monomeric complex.

The tendency of **LnL^1** to form aggregates is much lower resulting in the significantly smaller hydrodynamic volume. However, in contrast to the relaxivity measurements, V_H of **YL^1** shows a small dependence on complex concentration, especially at higher concentrations. Therefore it might be possible that a certain amount of weak aggregates is formed at higher

concentrations of **LnL^1** but they do not seem to influence the relaxivity.

Table 3. Diffusion coefficient *D*, hydrodynamic radius r_H, hydrodynamic volume V_H, and rotational correlation time τ_R at 25°C of **21** as well as of **YL^1** and **YL^4** in the absence and presence of three equivalents of calcium(II) as a function of the complex concentration.

		Concentration			
	Complex	2.5 mM	5 mM	10 mM	20 mM
D [m^{2}s^1]	**21**	3.85 x 10^{-10}	3.85 x 10^{-10}	3.85 x 10^{-10}	3.85 x 10^{-10}
	YL^1	3.53 x 10^{-10}	3.50 x 10^{-10}	3.46 x 10^{-10}	3.30 x 10^{-10}
	YL^1 + 3 equiv. Ca^{2+}	3.45 x 10^{-10}	3.11 x 10^{-10}	2.93 x 10^{-10}	2.38 x 10^{-10}
	YL^4	2.85 x 10^{-10}	2.74 x 10^{-10}	2.71 x 10^{-10}	2.60 x 10^{-10}
	YL^4 + 3 equiv. Ca^{2+}	2.49 x 10^{-10}	1.95 x 10^{-10}	1.84 x 10^{-10}	1.59 x 10^{-10}
r_H [Å][a]	**21**	5.01	5.01	5.01	5.01
	YL^1	5.47	5.52	5.57	5.84
	YL^1 + 3 equiv. Ca^{2+}	5.60	6.21	6.58	8.10
	YL^4	6.76	7.05	7.12	7.42
	YL^4 + 3 equiv. Ca^{2+}	7.75	9.87	10.51	12.12
V_H [Å^3][b]	**21**	528	528	528	528
	YL^1	684	702	725	835
	YL^1 + 3 equiv. Ca^{2+}	736	1003	1192	2228
	YL^4	1295	1465	1511	1711
	YL^4 + 3 equiv. Ca^{2+}	1953	4031	4867	7454
τ_R [ps][a)]	**21**	145	145	145	145
	YL^1	188	193	199	230
	YL^1 + 3 equiv. Ca^{2+}	202	276	328	613
	YL^4	356	403	416	471
	YL^4 + 3 equiv. Ca^{2+}	537	1109	1339	2050

[a]Calculated from equations 3.1 and 3.2 using η = 1.13 × 10^{-3} Pa × s for D_2O. [b]Calculated from r_H with $V_H = \frac{4}{3}\pi r_H^3$

The addition of three equivalents of calcium(II) to **LnL^1** then clearly induces aggregation. V_H of **YL^1** at c = 20 mM in the presence of Ca^{2+} ions (three equivalents) is about three-times higher than V_H of **YL^1** in the absence of calcium(II). However, at c = 2.5 mM the hydrodynamic volume of **YL^1** with calcium(II) is only slightly larger than without calcium(II). This implies that calcium(II) does not significantly increase the amount of aggregates at this concentration, which is an explanation for the independence of r_1 on the

calcium(II) concentration in the initial r_1 measurements at a gadolinium(III) complex concentration of 2.5 mM. The ratio of the aggregated to non-aggregated complexes increases at higher concentrations of calcium(II) which in turn results in the observed decrease in relaxivity at [GdL^1] = 18.5 mM (cf. Figure 11).

In the case of **YL^4**, the addition of Ca^{2+} ions increases the hydrodynamic volume even more than in the case of **YL^1**. The V_H of **YL^4** at c = 2.5 mM in the presence of Ca^{2+} is 1.5 times bigger than in its absence. As for **LnL^1**, the increased formation of aggregates seems to be responsible for the decrease in relaxivity of **LnL^4**. With increasing complex concentration the average size of the species in solution seems to further increase. However, no influence on the r_1 was observed for **GdL^4** in the concentration dependent experiments (Figure 11b).

The results indicate that calcium(II) generally amplifies the formation of aggregates of these systems. Up to a certain point, the formation of bigger aggregates results in the observed decrease in relaxivity. The formation of aggregates leads to a slower rotation (see τ_R in Table 3). However, the relaxivity enhancing effect of the increased τ_R should not be strong at the applied high magnetic field (9.4 T)[56] and in the cases where r_1 decreases an opposite effect must be also operative.

3.2.4 $^{31}P\{^1H\}$ NMR Spectroscopy

In order to understand whether the different tendencies to form aggregates are related to differences in the interaction of the phosphonate-containing side arms with the paramagnetic centre, $^{31}P\{^1H\}$ NMR experiments on **EuL^1** and **EuL^4** solutions (50 mM in D_2O, pD 7.4) were performed. The complexes of europium(III) are usually used to obtain information on the coordination behaviour of the gadolinium(III) analogues by NMR spectroscopy due to their favourable ratio between paramagnetic induced shift and line broadening. The $^{31}P\{^1H\}$ NMR spectrum of **EuL^4** measured at 298 K (Figure 14a) shows only one signal at 6.8 ppm. As this is nearly at the same position as the ^{31}P signal of the free ligand (6.6 ppm at pD 7.4), the phosphonate groups of **LnL^4** are most likely not coordinated to the lanthanide ion. When the $^{31}P\{^1H\}$ NMR spectrum is measured at 273°K (Figure 14b) the signal becomes more narrow and is split into two resonances (7.0 ppm and 6.3 ppm), indicating inequivalent phosphonates. However, as a coordination to the lanthanide should have a more significant influence on the chemical shift, the inequivalency most likely arises from aggregation where the phosphonates become chemically inequvalent. This cannot be observed at higher temperatures due to an increased dynamic or a stronger paramagnetic influence on the transverse relaxation time from the europium(III) ion.

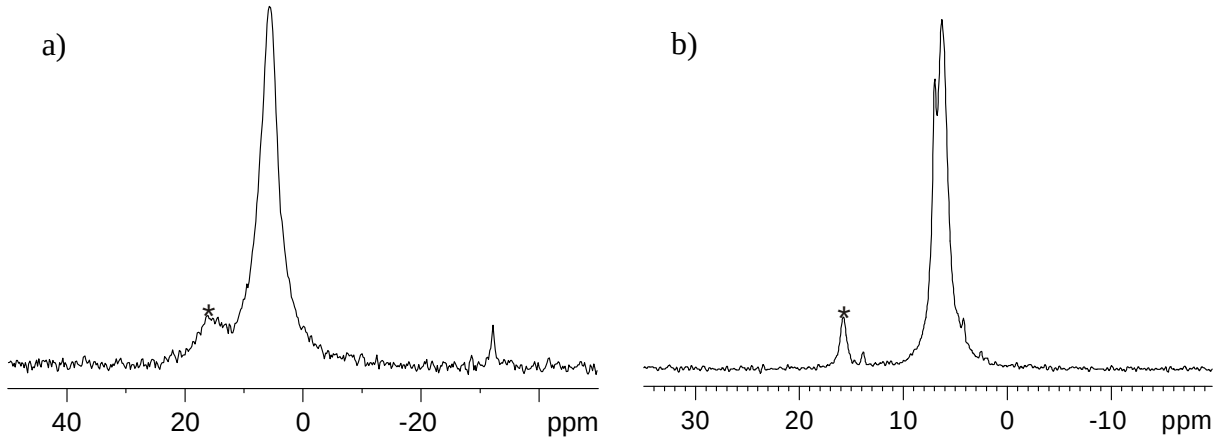

Figure 14. $^{31}P\{^{1}H\}$ NMR spectra of **EuL^{4}** at 298 K (a) and 273 K (b). *Impurity from the ligand synthesis, being hardly visible in solutions of the free ligand, but more intense in these spectra as it experiences only a weak paramagnetic influence.

The addition of calcium(II) then results in a broadening of the signal but not in a change of the chemical shift. As for **LnL^{4}** neither of the phosphonate groups binds to the lanthanide(III) ion, both groups can interact with calcium(II).

In the case of **EuL^{1}**, the $^{31}P\{^{1}H\}$ NMR spectrum measured at 298 K (Figure 15) shows three resonances. The signal at 3.1 ppm matches to the chemical shift of the free ligand indicating the presence of phosphonate species which are not coordinated to the paramagnetic center. However, the observation of two strongly upfield shifted resonances at -102.3 and -109.6 ppm, respectively, suggests an interaction of phosphonate groups with the paramagnetic Eu^{3+} ion, as well.[79]

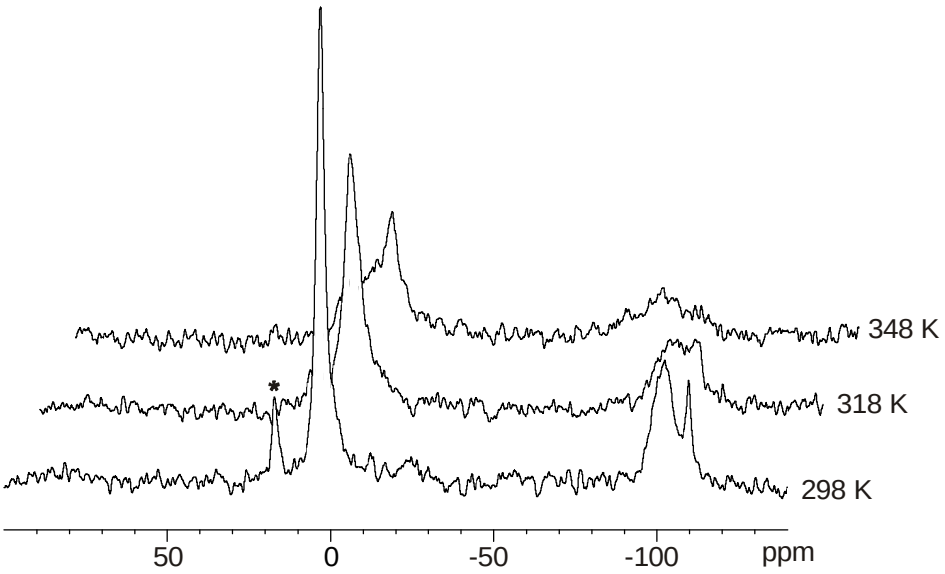

Figure 15. $^{31}P\{^{1}H\}$ NMR spectra of **EuL^{1}** at different temperatures. *Impurity from the ligand synthesis (see above).

The two upfield shifted signals of **EuL^1** merge into one broadened peak when the temperature is increased to 318 K, which can be explained by the existence of two different coordination isomers at lower temperatures.[69, 80] Moreover, when the temperature is further increased, the signals of the free and the coordinated phosphonates keep broadening and move closer to each other indicating an equilibrium between coordinated and non-coordinated phosphonates.

The integration ratio between the signal at 3.1 ppm and the two upfield shifted signals is not 1:1, but rather 3:2. Therefore, it is possible that the solution contains a mixture of species where in two cases one of the two phosphonates is coordinated and the other one is not coordinated resulting each in an upfield shifted signal and a signal in the range of the free ligand, and a small fraction where both phosphonates are non-coordinated which results only in a signal in the range of the free ligand. Since the diffusion measurements indicated a weak tendency to form aggregates at higher complex concentrations, as are necessary for the $^{31}P\{^1H\}$ NMR measurements, an intermolecular interaction cannot be excluded, as well. Nevertheless, it is possible that both signals belong to the same complex with one coordinated and one non-coordinated phosponate group. The discrepancy between a therefore expected 1:1 integration ratio and the observed 3:2 can be explained by the difficulty of correct integration in these paramagnetic systems as the paramagnetic influence can also determine the signal intensity. This is most obvious for the signal at about 16 ppm which belongs to a small impurity being already visible in the $^{31}P\{^1H\}$ NMR spectrum of the free ligand. Though there the signal is negligible, the ratio between the signal of the impurity and the signals of the complex is significantly increased in the spectra of the paramagnetic europium(III) complex.

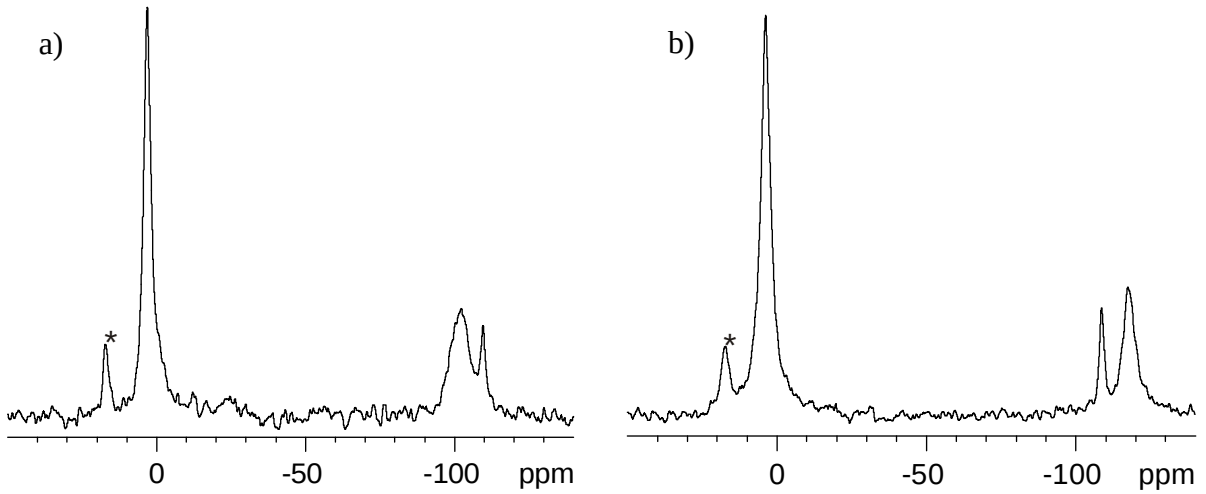

Figure 16. $^{31}P\{^1H\}$ NMR spectra of **EuL^1** at 298 K in the absence of calcium(II) (a) and in the presence of three equiv. calcium(II) (b). *Impurity from the ligand synthesis.

After the addition of three equivalents of calcium(II), the $^{31}P\{^1H\}$ NMR spectrum of **EuL^1**

(Figure 16b) shows a signal at 3.9 ppm and still two upfield shifted signals, now at -104.3 and -131.6 ppm, respectively. The addition of Ca^{2+} ions affects the chemical shift of the signals corresponding to coordinated phosphonate groups, which means that the aminobis(methylenephosphonate) group of **LnL^1** can interact with Ca^{2+} ions while one phosphonate group is still coordinated. In this case only one of the phosphonates is free to interact with calcium(II) resulting in smaller and less stable aggregates and explaining the lower affinity to form aggregates, as was observed in the diffusion measurements (see Table 3 in chapter 3.2.3). By contrast, in the case of **LnL^4** where only species with two free phosphonate groups exist, the formation of more stable and larger aggregates involving one or even more Ca^{2+} ions is possible.

3.2.5 Luminescence Spectroscopy

Luminescence emission spectra of **EuL^1-EuL^4** in aqueous media give further details about their coordination environment. An advantage of this technique is that it requires a much lower concentration of the complex than for $^{31}P\{^1H\}$ NMR spectroscopy, thereby giving the opportunity to observe concentration dependent changes. For **EuL^1**, the coordination of a phosphonate group in the absence and presence of calcium(II), already observed in the $^{31}P\{^1H\}$ NMR spectra for a complex concentration of 50 mM, could be confirmed for all measured complex concentrations (5 mM – 50 mM). The appearance of a distinctive band at 625 nm and the form and splitting of the $\Delta J = 1$ manifold in the luminescence emission spectrum of **EuL^1** (Figure 17a) is a clear evidence for the coordination of a phosphonate group to the europium(III) centre.[79, 81]

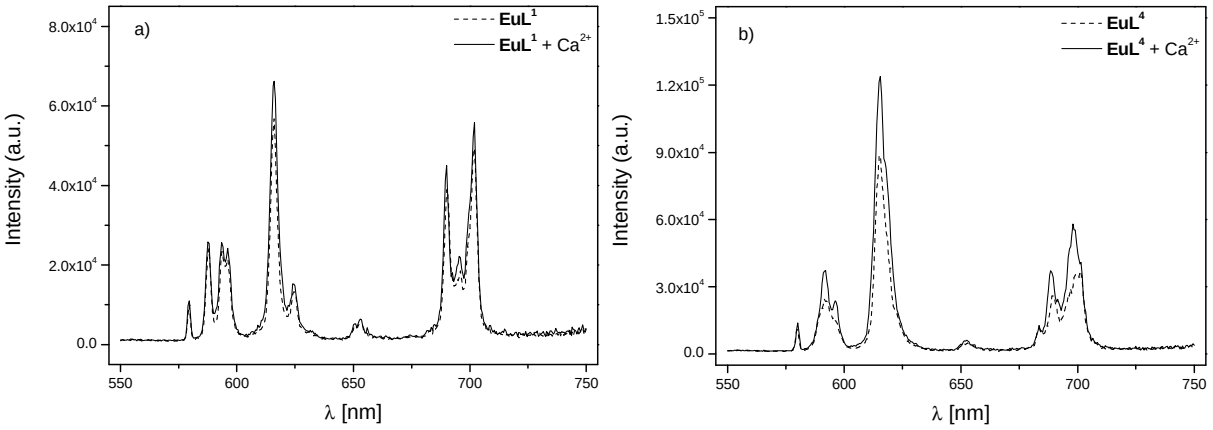

Figure 17. Luminescence emission spectra of **EuL^1** (a) and **EuL^4** (b) in the presence and absence of three equiv. calcium(II) (5 mM, λ_{ex}=395 nm, 25 °C, pH 7.3, HEPES).

Since the coordination can be observed also at low complex concentrations where the diffusion measurements indicated no significant aggregation, it is much more likely that the

coordination to the lanthanide(III) ion is an intramolecular rather than an intermolecular process. This results in complexes, where one phosphonate is coordinated and the other one is free to interact with calcium(II). None of the luminescence emission spectra of **EuL^2-EuL^4** exhibit the characteristic pattern for a phosphonate coordination, neither in the absence nor in the presence of calcium (II). This confirms that the phosphonate groups of these complexes are not coordinated to the lanthanide(III) ion over the whole range of complex concentration. The spectrum of **EuL^4** is shown in Figure 17b as an example.

3.2.6 Determination of the Hydration Number *q*

The differences in the coordination behaviour of **LnL^1** and the other three complexes **LnL^2-LnL^4** can explain the differences in the tendency to form aggregates in the absence and presence of calcium(II), but do not give an explanation for the decrease in relaxivity. A possible reason for a lower r_1 could be a reduction in the number of inner-sphere water molecules, *q*, accompanied with aggregation. This could overcompensate the positive effect of an increase in the rotational correlation time τ_R on the relaxivity and therefore lead to an overall drop in r_1 (see equations 2.7 - 2.12 in chapter 2.3.1).

The measurement of luminescence lifetimes in H_2O and D_2O solutions of the complexes offers a possibility to estimate the hydration number *q*. The method is based on the difference in the effectivity of O-H and O-D oscillators to act as a quencher of the excited state. O-H oscillators close to the europium(III) ion are about 200 times more efficient for non-radiative desactivation than O-D oscillators. *q* can then be calculated by using the empirical equation 3.3.[82]

$$q = 1.2 \times (\tau_{H_2O}^{-1} - \tau_{D_2O}^{-1} - 0.25) \qquad (3.3)$$

where τ_{H_2O} and τ_{D_2O} are the luminescence lifetimes in H_2O and D_2O, respectively.

Using this equation, the hydration number *q* of **EuL^1-EuL^4** was determined in the absence and presence of calcium(II) (Table 4).

Table 4. Luminescence emission lifetimes and estimated *q* values of **EuL^1-EuL^4** (4-5 mM) in the absence and presence of Ca^{2+} ions (three equiv.).

Complex	τ_{H_2O}[ms]	τ_{D_2O}[ms]	*q*	Complex + Ca^{2+}	τ_{H_2O}[ms]	τ_{D_2O}[ms]	*q*
EuL^1	0.42	1.37	1.7	**EuL^1** + Ca^{2+}	0.54	1.75	1.2
EuL^2	0.58	1.55	1.0	**EuL^2** + Ca^{2+}	0.68	1.65	0.7
EuL^3	0.50	1.63	1.4	**EuL^3** + Ca^{2+}	0.84	1.60	0.4
EuL^4	0.65	1.66	0.8	**EuL^4** + Ca^{2+}	0.89	1.75	0.4

For **EuL^1**, the only complex with a coordinated phosphonate group, a *q* value of 1.7 is obtained at 5 mM complex concentration in the absence of Ca^{2+} ions, suggesting the presence of dihydrated species. Since a coordination number of ten is unlikely for europium(III) complexes, this is only possible if the solution contains a fraction of species with non-coordinated phosphonate groups allowing two inner-sphere water molecules. As mentioned in chapter 3.2.4, the presence of such species would not generally be in contradiction to the results of the phosphorous NMR study and can also not be excluded from the luminescence spectra. However, equation 3.3 is an empirical equation, working already for systems with no second sphere only with an error of ±0.5. Furthermore, it has been shown previously,[83] that the non-consideration of additional oscillator(s) brought into the proximity of the europium(III) ion as in our case by the coordination of the aminobis(methylenephosphonate) group (Figure 18a) might increase the obtained *q* value, thereby suggesting two hydrated species where only monohydrated species exist. By contrast, for **EuL^2**-**EuL^4**, the *q* values are rather one than two in the absence of Ca^{2+} ions. This still agrees with the fact that no experimental evidence of the coordination of phosphonates to the paramagnetic centre is found, as it is known that non-polar moieties attached to the fourth cyclen nitrogen can reduce the overall coordination number in water (Figure 18b).

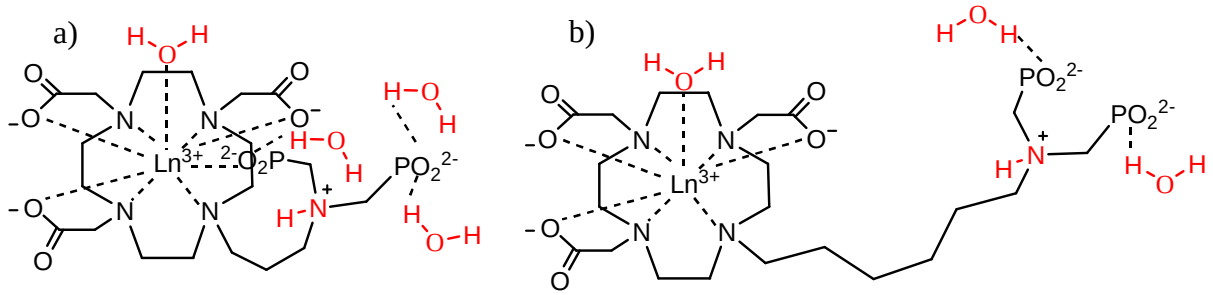

LnL^1 **LnL^4**

Figure 18. Solution structures of **LnL^1** and **LnL^4** with possible oscillators (red) influencing the luminescence lifetimes of the europium complexes.

The addition of three equivalents of calcium(II) to solutions of **EuL^1**-**EuL^4** reduced *q* for all four complexes (Table 4). As Matczak-Jon *et al.*[72] have shown that the coordination of calcium(II) by an aminobis(methylenephosphonate) does not involve the amino nitrogen, the N-H or N-D oscillator (see Figure 18) remains unchanged upon the addition of calcium(II) and has therefore no influence on the decrease in *q*. On the other hand, this means that even though the apparent *q* value might not represent the exact number of coordinated water molecules in the inner-sphere, in all cases the reduction of the apparent *q* values must be related to a decreasing number of water O-H and O-D oscillators, respectively. This can arise

from a lower number of inner-sphere water molecules, as well as from a reduction of second sphere water on the aminobis(methylenephosphonate) groups (see Figure 18). In both cases the observed reduction in the obtained q values explains the observed decrease in r_1 for **GdL^2**-**GdL^4** at low CA concentrations, although the relation between q and r_1 is not linear. This is most obvious in the case of **LnL^1** where a decrease of in q 0.5 results in hardly any r_1 change at a complex concentration of 5 mM. By contrast, for **EuL^4** q decreases by only 0.4 whereas r_1 of **GdL^4** for the same concentration decreases from 5.54 $mM^{-1}s^{-1}$ to 3.86 $mM^{-1}s^{-1}$(-30%).
The hydration number q was also determined as a function of the complex concentration in the absence and presence of three equivalents of calcium(II) (Figure 19a and Figure 19b, respectively). Similar trends were observed as for the concentration-dependence of the relaxivities (see Figure 11 in chapter 3.2.2).

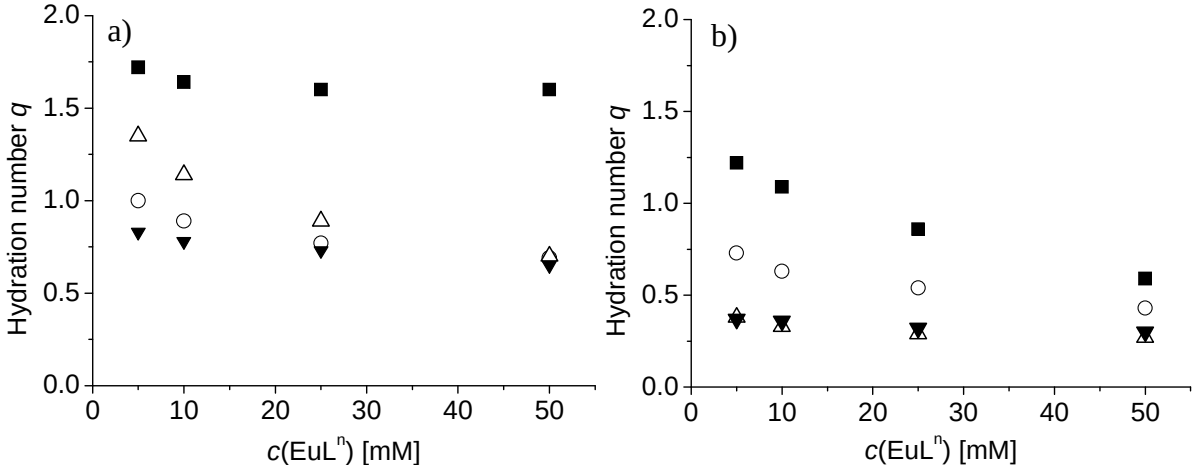

Figure 19. Concentration-dependence of q for **EuL^1** (■), **EuL^2** (○), **EuL^3** (Δ) and **EuL^4** (▼) in (a) the absence of Ca^{2+} and (b) the presence of three equiv. of calcium(II) at 25 °C, pH 7.3 (HEPES buffer).

In the systems where r_1 was independent of the gadolinium(III)-complex concentration, q also remained unchanged. However, in all cases where r_1 decreased with increasing complex concentration, the hydration number also dropped for the respective europium(III) complexes. It could be shown in chapter 3.2.3 that the decrease in relaxivity is accompanied with the formation of aggregates, thus the aggregation must lead to structures in which the water access to the inner and/or second sphere of the lanthanide ion is significantly hindered. The lower number of water molecules being able to interact with the paramagnetic centre, is then reflected in the reduced relaxivity. Similarly, Rojas-Quijano *et al.* reported a decrease of q with increasing complex concentration for the phosphonate containing Ln-PCTA-(ampOBu)$_3$ which was related to oligomer formation.[84]

3.2.7 ^{17}O NMR Spectroscopy

In order to assess parameters characterising the water exchange and rotational dynamics on the gadolinium(III) complexes, variable temperature transverse and longitudinal ^{17}O NMR relaxation rates and chemical shifts were measured at 11.7 T in aqueous solutions of **GdL^1-GdL^4** at concentrations of about 50 mM. A detailed discussion of this method can be found in ref. 1. A short summary involving all important equations is given in the experimental part (chapter 5.1.8) of this thesis. Therein the reduced ^{17}O relaxation rates ($1/T_{1,2r}$) and the reduced ^{17}O chemical shifts $\Delta\omega_r$ are defined as the following:

$$\left(\frac{1}{T_{1,2r}}\right) = \frac{1}{P_m}\left(\frac{1}{T_{1,2}} - \frac{1}{T_{1,2A}}\right) \tag{3.4}$$

$$\Delta\omega_r = \frac{1}{P_m}\left(\omega_p - \omega_A\right) \tag{3.5}$$

where P_m is the molar fraction of bound water molecules, $1/T_{1,2}$ is the longitudinal or transverse ^{17}O NMR relaxation rate of the paramagnetic solution, $1/T_{1,2A}$ is the longitudinal or transverse ^{17}O relaxation rate of a reference and ω_p and ω_A are the ^{17}O chemical shifts of the paramagnetic solution and the reference, respectively.

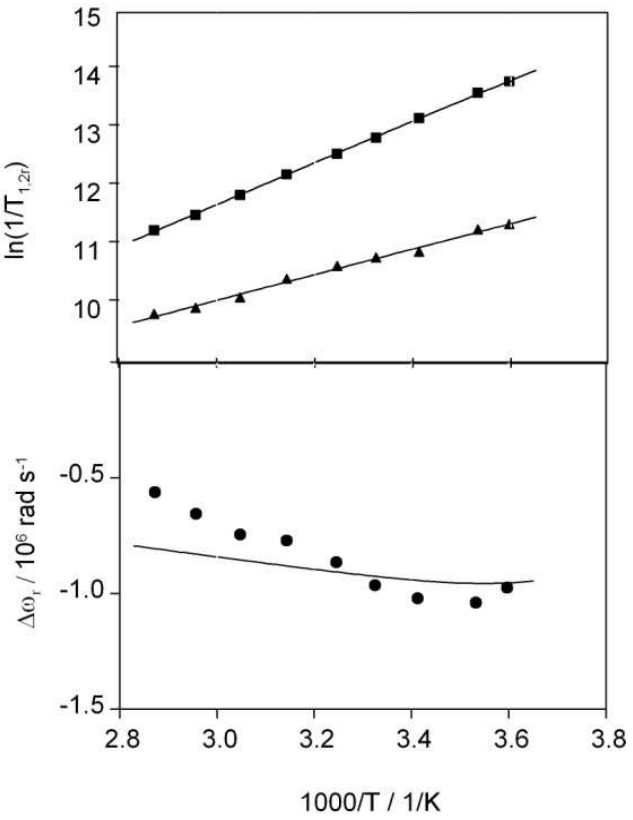

Figure 20. Variable temperature reduced ^{17}O transverse (■) and longitudinal (▲) relaxation rates and chemical shifts (●) for **GdL^1**. B = 11.75 T. The lines correspond to the least-squares fit as explained in the text.

For complexes **GdL^1** (Figure 20), **GdL^2** and **GdL^3** (Figure 21), the reduced ^{17}O transverse relaxation rates ($1/T_{2r}$) decrease with increasing temperature in the whole temperature range investigated, indicating that they are in the fast exchange region. In the fast exchange regime, the reduced transverse relaxation rate is defined by the transverse relaxation rate of the bound water oxygen $1/T_{2m}$, which is in turn influenced by the water exchange rate k_{ex}, the longitudinal electronic relaxation rate $1/T_{1e}$, and the scalar coupling constant $A/\hbar$. The reduced ^{17}O chemical shifts $\Delta\omega_r$ are determined by $A/\hbar$. Transverse ^{17}O relaxation is governed by the scalar relaxation mechanism, thus contains no information on the rotational motion of the system. In contrast to $1/T_{2r}$, the longitudinal ^{17}O relaxation rates $1/T_{1r,}$ are determined by dipole-dipole and quadrupolar relaxation mechanisms, both related to rotation. The dipolar term depends on the gadolinium(III)-water oxygen distance r_{GdO}, while the quadrupolar term is influenced by the quadrupolar coupling constant $\chi(1+\eta^2/3)^{1/2}$. For **GdL^2** and **GdL^3**, the experimentally measured paramagnetic ^{17}O chemical shifts were considerably smaller than what would be expected for a gadolinium(III) complex with the given q value, which is why they have not been included in the final fitting. A diminution of the chemical shifts has been previously reported in systems with a significant second sphere contribution.[85, 86]

The behaviour of **GdL^4** is unusual, as the $1/T_{2r}$ values at high temperature start to increase (Figure 22). On the other hand, the $1/T_{1r}$ values show only small temperature dependences. This can be related to the presence of the relatively large amount of aggregates even in the absence of Ca^{2+} ions, being observed in the PGSE NMR diffusion experiments (see Figure 12b in chapter 3.2.3). The formation of such aggregates is likely temperature dependent. Therefore no further analysis of the ^{17}O NMR data on **GdL^4** was performed.

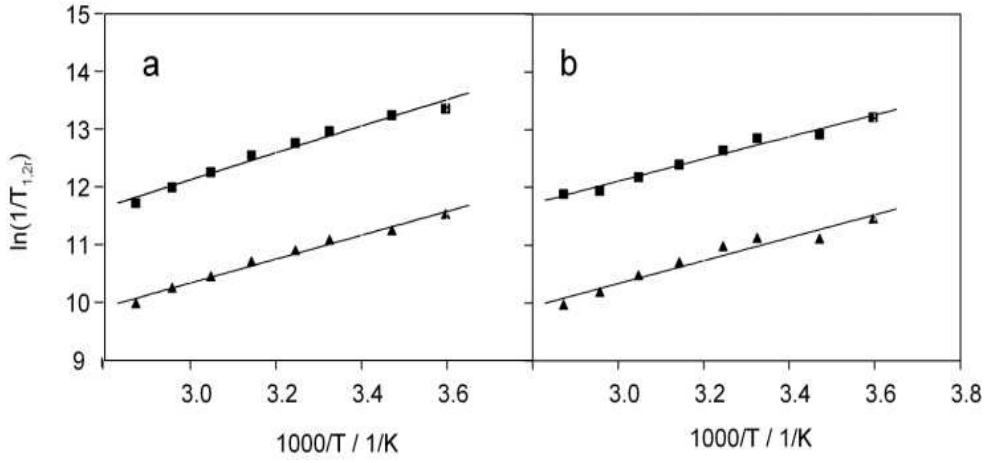

Figure 21. Variable temperature reduced ^{17}O transverse (■) and longitudinal (▲) relaxation rates for **GdL^2** (a) and **GdL^3** (b). B = 11.75 T. The lines correspond to the least-squares fit as explained in the text. q = 1

At the concentration used for the ^{17}O NMR measurements, some aggregation is expected in the absence of calcium(II) for **GdL^1**, based on the slight concentration-dependence of the diffusion NMR data on **YL^1** (see Figure 12a in chapter 3.2.3). However, the relaxivities of **GdL^1** (see Figure 11a in chapter 3.2.2) and the q values of **EuL^1** (Figure 19a in chapter 3.2.6) showed no dependence on the concentration. In the case of **GdL^2** and **GdL^3** stronger aggregation is expected, though, no unusual behaviour was observed for $1/T_{2r}$ and $1/T_{1r}$. It was therefore decided to further analyse the three systems. Nevertheless, one should be aware that changing the temperature might change the aggregation state and thereby the size and also the hydration number of the systems, which should be considered in the judgement of the obtained data.

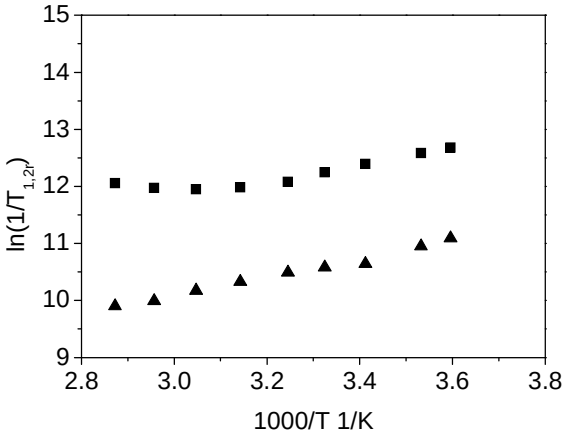

Figure 22. Variable temperature reduced ^{17}O transverse (■) and longitudinal (▲) relaxation rates for **GdL^4**. B = 11.75 T.

Even though a higher q value has been obtained for **EuL^1** from the luminescence lifetime measurements (Figure 19 in chapter 3.2.6) and the possibility of the existence of some dehydrated species with uncoordinated phosphonate groups cannot be excluded from the luminescence and ^{31}P NMR data, the hydration number of **GdL^1** was fixed to one in this analysis, as q = 1 correlates better with the obtained values of the reduced chemical shifts $\Delta\omega_r$ than q = 1.7. This indicates that it is more likely that the luminescence data pretend an increased q value rather than the existence of dehydrated species. For **GdL^2** and **GdL^3** the increased formation of aggregates at 50 mM concentration might lead to a reduction of inner sphere water, which was indicated by a reduction in q to 0.7 in the concentration-dependent q measurements (Figure 19a in chapter 3.2.6). However, as the equation used in these measurements is not optimised for this system, the reduction can also only be due to a change in the second sphere and the number of inner sphere water molecules might still be one. Therefore, for **GdL^2** and **GdL^3** two fits of the ^{17}O data were performed by assuming q = 0.7 or q = 0.7 (Figure 21 shows the fit with q = 1).

The experimental data for **GdL^1-GdL^3** were fitted according to the Solomon-Bloembergen-Morgan theory of paramagnetic relaxation (see chapter 2.3) using the equations presented in the experimental part (chapter 5.1.8). In the fitting procedure, r_{GdO} has been fixed to the common value of 2.50 Å.[87] The quadrupolar coupling constant $\chi(1+\eta^2/3)^{1/2}$ was set to the value for pure water, 7.58 MHz. For **GdL^2** and **GdL^3**, the scalar coupling constant $A/\hbar$, was fixed to -3.6 MHz, the value obtained for **GdL^1**. The electron spin relaxation rate $1/T_{1e}$, was fitted to a simple exponential function. Since it makes a negligible contribution to the transverse relaxation rates, the fit of parameters related to the zero-field splitting mechanism, as usually done, has very low confidence. The following parameters were adjusted: the water exchange rate k_{ex}^{298}, or the activation entropy $\Delta S^{\ddagger}$, the activation enthalpy for water exchange $\Delta H^{\ddagger}$, the rotational correlation time τ_{RO}^{298}, and its activation energy E_R, and the electron spin relaxation rate at 298 K $1/T_{1e}^{298}$ as well as its activation energy E_T. The values obtained for these parameters are presented in Table 5.

Table 5. Parameters obtained from the fitting of the ^{17}O NMR data at 11.75 T.

	GdL^1	**GdL^2**		**GdL^3**		Gd-DOTA[b]
q[a]	1	1	0.7	1	0.7	1
k_{ex}^{298} [10^6 s^{-1}]	170±13	160±15	120±15	190±15	130±10	4.1
$\Delta H^{\ddagger}$ [kJ mol^{-1}]	27.2±0.5	16.8±0.4	16.3±0.4	13.4±0.5	13.4±0.5	49.8
$\Delta S^{\ddagger}$ [J mol^{-1} K^{-1}]	0±2	-32±2	-36±2	-42±2	-44±2	+48.5
$A/\hbar$ [10^6 rad s^{-1}]	-3.6±0.3	-3.6[a]	-3.6[a]	-3.6[a]	-3.6[a]	-3.7
τ_{RO}^{298} [ps]	290±10	390±10	540±10	380±10	550±20	90
E_R [kJ mol^{-1}]	17.8±0.9	17.1±0.7	16.3±0.7	16.5±0.9	16.6±1.0	17

[a] fixed in the fit. [b]Ref. 88

For $1/T_{1e}^{298}$, for all three **GdL^1-GdL^3** complexes values between (1.1-1.3)×10^7 s^{-1} were obtained, while E_T was fixed to 1 kJ/mol, otherwise small negative values were obtained. It is noticeable that the electron spin relaxation $1/T_{1e}$ makes a limited contribution in any of the three systems, representing maximum 10 % in the correlation time τ_c governing the relaxation rate of the bound water oxygen, $1/T_{2m}$ ($1/\tau_c = k_{ex} + 1/T_{1e}$). Therefore, the water exchange rate can be obtained with a very good certitude.

The second sphere water molecules that are present around the phosphonate groups might affect the ^{17}O longitudinal relaxation rates, governed by dipolar and quadrupolar interactions. However, this effect is difficult to describe quantitatively, which is why no second sphere effect was included in the fit. On the other hand, ^{17}O T_2 relaxation is mainly driven by the

scalar contribution, thus it is not sensitive to rotation and consequently to the presence of a second hydration shell. Consequently, the water exchange rates calculated are not influenced by second sphere effects.

The water exchange rate is very high on all the three gadolinium(III) complexes. It is in the same order of magnitude as for the $[Gd(H_2O)_8]^{3+}$ aqua ion (k_{ex}^{298} = 8×10^8 s^{-1}), and this dependents only to a very small extent on the q value assumed for **GdL²** and **GdL³**. As already mentioned in chapter 2.3.1, DOTA- or DO3A-type complexes have in general much slower water exchange (k_{ex}^{298} = (4-10)x10^6 s^{-1}) though one example of a very fast water exchange has been reported on the gadolinium(III) complex of a Gd-DO3A complex bearing an N-linked CH_2CH_2NHCO–pyridyl moiety (k_{ex}^{298} = 1.1×10^8 s^{-1}).[89] For **GdL²** and **GdL³**, the fast water exchange can be likely related to the associative nature of the exchange mechanism. Indeed, the strong negative values of the activation entropy obtained for **GdL²** and **GdL³** are clearly indicative of an associative activation mode, in contrast to the large positive value reported for Gd-DOTA (**1**), with a dissociatively activated water exchange. As mentioned above, for **GdL²** and **GdL³**, an overall coordination number of eight with the participation of seven donor groups of the ligand and one inner sphere water molecule (cf. Figure 18b in chapter 3.2.6) is assumed for q = 1 or even partly seven-fold coordination in the case of q = 0.7. Since the common coordination numbers for gadolinium(III) are eight or nine, eight- and seven-coordinate gadolinium(III) complexes typically undergo associative water exchange. The associative character, as indicated by the activation entropy of zero, is less important for **GdL¹**. A plausible explanation for this difference between **GdL¹** and **GdL²**/**GdL³** is the existence of an overall coordination number of nine in the case of **LnL¹** due to the coordination of one phosphonate group to the lanthanide(III) ion and one inner-sphere water molecule. In this case, the fast exchange can be rather related to the presence of the coordinated phosphonate group. Indeed, the phosphonate coordinating group has been often recognized to induce fast water exchange on the Gd^{3+} complexes.[16] One should note that even if the hypothesis of q = 1 was not correct for **GdL¹**, the water exchange would be fast (if we assume q = 2, we calculate k_{ex}^{298} = 3.4×10^8 s^{-1}). However, for a dehydrated complex where no phosphonate group is coordinated to the gadolinium(III) ion the observed fast water exchange is hard to explain.

The rotational correlation time of the gadolinium(III)-water oxygen vector, τ_{RO}^{298}, as obtained from the analysis of the longitudinal ^{17}O relaxation rates for **GdL¹**, is similar to that calculated from the NMR diffusion experiments for the y analogue (see Table 3 in chapter 3.2.3). It is longer than τ_{RO}^{298} of Gd-DOTA (**1**) which can be explained in terms of a less

compact structure brought by the side-chain and the high number of water molecules hydrogen-bound to the bisphosphonate group which will considerably increase the hydrodynamic radius of the complex and the existence of a small fraction of aggregated species at this concentration. The rotational correlation times of **GdL^2** and **GdL^3** depend on the *q* assumed, but in any case, they are longer than that for **GdL^1**, indicative of stronger aggregation. For **GdL^1**, the longitudinal ^{17}O relaxation rates were also measured in the presence of three equivalents of calcium(II). The $1/T_{1r}$ values were higher than in the absence of Ca^{2+} ions, being in accordance with a longer rotational correlation time and indicating again the calcium(II)-induced aggregation.

3.3 Conclusions

A series of novel DO3A-type gadolinium(III) complexes, having alkylaminobis(methylene-phosphonate) moieties were extensively investigated towards their relaxivity response to the presence of calcium(II). At low complex concentrations (2.5 mM), the longitudinal relaxivity of **GdL^2**-**GdL^4** decreased after addition of calcium(II), whereas **GdL^1** had no calcium(II) dependence. Concentration-dependent relaxivity and PGSE ^{1}H diffusion measurements showed that calcium(II)-induced aggregation is responsible for the observed changes in relaxivity. **GdL^1** has a lower tendency to form aggregates in the presence of calcium(II) than **GdL^2**-**GdL^4**, resulting in a calcium(II) dependent relaxivity change only at high complex concentrations. This is attributed to a different coordination behaviour of the phosphonate groups in **GdL^1** as compared to **GdL^2**-**GdL^4**. ^{31}P{^{1}H} NMR spectroscopy and luminescence measurements on the europium(III) analogues indicated coordination of a phosphonate group to the lanthanide(III) ion for **GdL^1**, but not for **GdL^2**-**GdL^4**. Since the coordination in the case of **GdL^1** can be observed also at low complex concentrations where the diffusion measurements indicated no significant aggregation, it is much more likely that the coordination to the lanthanide(III) ion is an intramolecular rather than an intermolecular process. Form the obtained ^{31}P{^{1}H} NMR and luminescence data, it cannot be clarified whether exclusively complexes with one coordinated and one uncoordinated phosphonate group exist in solution or also a certain amount of species exists with no coordinated phosphonate group at all. However, according to the integration ratio of the ^{31}P{^{1}H} NMR spectrum, this amount is maximum 20 % and due to the problems with integration in the paramagnetic solutions it is likely even less. Therefore most or perhaps all **GdL^1** complexes have one coordinated and one free phosphonate group. Since the ^{31}P{^{1}H} NMR spectra show that the phosphonate group remains coordinated to the lanthanide(III) ion even after the interaction of the aminobis(methylenephosphonate) group with calcium(II), only one of the

phosphonates is free to interact with calcium(II). This results in smaller and less stable aggregates and is the reason for the lower affinity of **GdL^1** to form aggregates. In contrast, for **GdL^2**-**GdL^4**, where no coordination of a phosphonate group to the lanthanide(III) ion is observed, both phosphonate groups can be involved in the calcium(II)-induced aggregate formation, resulting in larger and more stable aggregates. In these aggregates, the water access to the inner and/or the second sphere is significantly hindered, shown by a reduction in the apparent hydration number *q*, which therewith explains the observed decrease in relaxivity. A still remaining question is the high apparent hydration number *q* of **GdL^1** in the absence of calcium(II). The luminescence lifetime measurements resulted in *q* values between 1.7 and 1.6 for complex concentrations between 5 and 50 mM. If one assumes a mixture of monohydrated complexes with one coordinated phosphonate group and dihydrated complexes with two uncoordinated phosphonate groups, a *q* value of 1.7 would refer to a mixture of 30 % monohydrated and 70 % dehydrated complexes (40 to 60 % for $q = 1.6$). However, this is in contradiction to the results from the $^{31}P\{^1H\}$ NMR measurements which allowed maximum 20 % dehydrated species. Therefore it is very likely that the used equation is not valid for this system due to the additional oscillators brought in the proximity of the lanthanide(III) ion and a *q* value of about one is a more realistic reflection of the hydration state in a solution of **GdL^1** than a *q* of 1.7. This is also supported by the better correlation of $q = 1$ with the obtained values of the reduced chemical shifts $\Delta\omega_r$ in the variable temperature ^{17}O NMR measurements as compared to $q = 1.7$.

Furthermore, the ^{17}O NMR measurements revealed an extremely high water exchange rate k_{ex}^{298} for these complexes, being in the same order of magnitude as that of the $[Gd(H_2O)_8]^{3+}$ aqua ion. All these physico-chemical data show that structurally relatively simple lanthanide complexes might have unexpected and complicated solution chemistry behaviour.

In terms of potential MRI applications, both **GdL^3** and **GdL^4** show a relaxivity increase upon decrease in calcium(II) concentration (at low **GdL^n** concentration), thus the drop in extracellular calcium(II) associated to brain activity would result in increased image intensity. However, the complexity of their solution behaviour would prevent any practical use: the MR signal intensity and the calcium response would be also influenced by their aggregation state thereby making data analysis extremely complicated. Nevertheless, the obtained results demonstrate that the quest for responsive CAs can be enriched with novel approaches.

4 Silsesquioxane-based MRI Contrast Agents

4.1 Introduction

4.1.1 High Sensitivity MRI Contrast Agents

Since the development of the first gadolinium(III)-based CA for MRI, there has been a quest for improving the efficiency e.g. the longitudinal relaxivity r_1 of the agents. Two reasons are mainly responsible for this ambition. The first reason is that due to their low relaxivity, most commercial CAs are only effective at high concentrations. The smallest change in the observed relaxation rate $1/T_{1obs}$ necessary to be detected as a change in contrast is about 0.15 s^{-1}.[90] For Dotarem™ (**1**), having the typical low relaxivity of 3.4 $mM^{-1}s^{-1}$ at 37°C and a proton Larmor frequency of 20 MHz,[9] this means a CA concentration of at least 0.044 mM (cf. equation 2.4 in chapter 2.3). To achieve a satisfying contrast enhancement usually concentrations of more than 0.1 mM are applied.[91] For certain applications like MR angiography, which is the visualisation of blood vessels, even double and triple this dose is sometimes used. The high dose, but also the related longer exposure of the body to the CA, increase the risk of a release of free gadolinium(III).[17] Compounds with high relaxivity can be detected at lower doses, or provide greater contrast at equivalent doses as compared to compounds with lower relaxivity. The second reason to develop high sensitivity CA is the desire to detect molecular targets by MRI. This so called molecular imaging has the aim to locate certain types of cells or biomolecules within the body in order to visualise molecular events occurring at cellular levels. This would represent a breakthrough in clinical settings as, in addition to provide early diagnosis, it would allow the assessment of the underlying therapy. The early knowledge of processes on the molecular level will largely anticipate the time currently required for assessment based on anatomical changes and thereby reduce the time required to decide whether a chosen therapy is going to provide the expected effects or another approach might be more promising. However, to locate such biomarkers they must coordinate or at least interact with an appropriate CA and in order to visualise this event *via* MRI, the concentration of the respective cell or biomolecule must be in the range of the CA. As outlined above, this would require a biomarker concentration of at least 0.044 mM, better 0.1 mM or more for the typical commercially available CAs, which strongly limits the number of potential biological targets.

The parameters mainly determining the relaxivity were introduced in chapter 2.3 and are namely the number of coordinated water molecules q, the water exchange rate k_{ex}, the

rotational correlation time τ_R, the electronic properties of the gadolinium(III) ion $1/T_{1e}$ and the external field expressed by the proton Larmor frequency ω_I. It was already mentioned in chapter 2.4.2 that an increase in the hydration number q can provide a significant increase in relaxivity independently from the other parameters. However, as this involves a reduction in ligand denticity, it is often accompanied with an unwanted decrease in complex stability. Furthermore, the existence of more than one free coordination site can allow reversible oxy-anion binding under physiological conditions which in turn can lead to the complete loss of inner sphere water.[32, 33] As described in chapter 2.3.1 the dependence of the relaxivity on the other parameters is more complicated. For an optimal relaxivity, equation 4.1 needs to be fulfilled, which would require the simultaneous optimisation of all three parameters depending on the magnetic field desired for the particular application.

$$\frac{1}{\tau_{c1}} = \frac{1}{\tau_R} + \frac{1}{T_{1e}} + k_{ex} = \omega_I \tag{4.1}$$

However, it could be shown, that k_{ex} and τ_R of the currently used CAs are generally too slow and too short, respectively at any field strengh. Some useful empirical relationships have emerged which influence water exchange rates of CAs. Replacing an acetate oxygen donor with an amide oxygen donor will result in a slower water exchange rate. As most of the studied complexes undergo dissociative water exchange, increasing the steric bulk will increase the water exchange rate. For example replacing an acetate oxygen donor with the larger phosphonate oxygen donor increases the exchange rate (see also chapter 3.2.7).[92] However, the development of CAs with faster water exchange rates is not straight forward, and changes in the coordination sphere can be accompanied with a loss in stability. Furthermore, at the mostly used field strength of 1.5 T the short rotational correlation time τ_R is the most limiting factor of current CAs and k_{ex} becomes only important when rotational motion is slowed down.[91]

The influence of the applied magnetic field on the optimal values of the parameters determining the relaxivity of a CA can be identified from the equations of the Solomon-Bloembergen-Morgen theory in chapter 2.3. A bit more graphical is the measurement of so called ^{1}H nuclear magnetic relaxation dispersion (NMRD) profiles. In a ^{1}H NMRD profile the relaxivity of a CA is measured as a function of the magnetic field expressed by the proton Larmor frequency. The ^{1}H NMRD profile of Gd-DOTA (Dotarem™) (**1**) together with the range of magnetic fields currently used in clinical MR scanners is shown in Figure 23. By using the Solomon-Bloembergen-Morgan equations in a simultaneous fitting of this profile together with ^{17}O NMR (cf. chapter 3.2.7) and electron paramagnetic resonance (EPR) data

Powell *et al.* determined the values of the relevant parameters described above.[88]

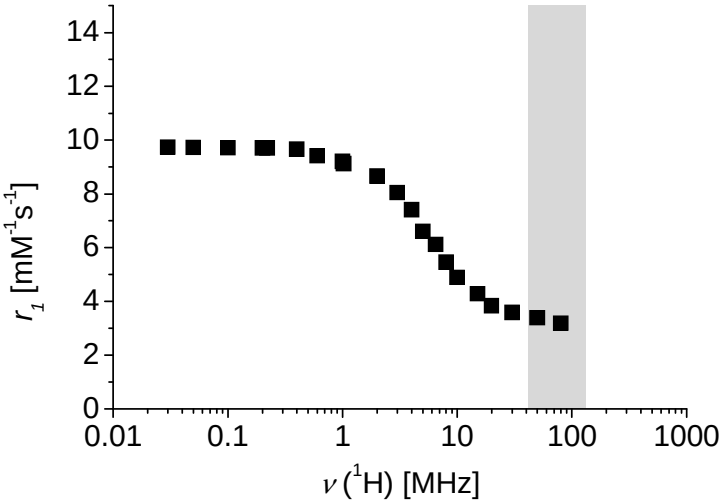

Figure 23. ^{1}H NMRD profile (black squares) of Gd-DOTA (**1**) at 312 K (39°C) (data from Ref. 88). Range of magnetic fields (grey area) currently used in clinical MR scanners (1-3 T).

In order to visualise the effect of a slower rotational motion, the so obtained values can be used in simulated ^{1}H NMRD profiles where only the value of the rotational correlation time τ_R is varied and all other parameters remain fixed (Figure 24).

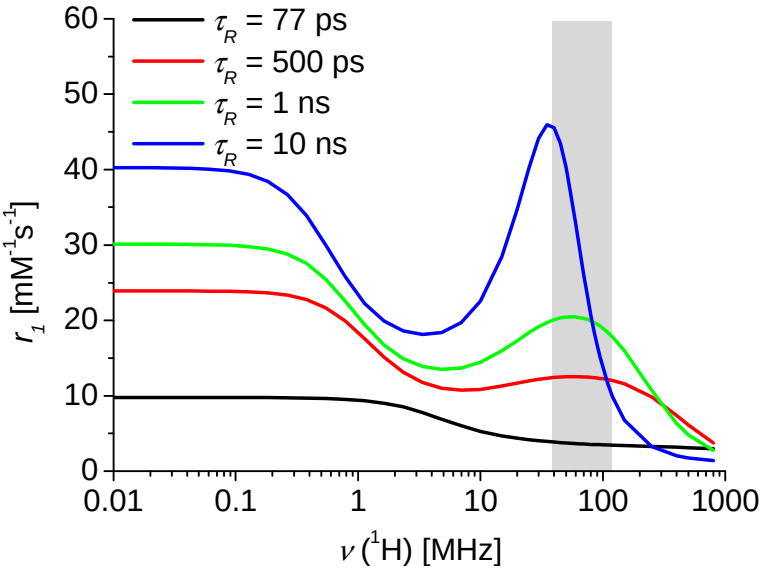

Figure 24. Simulated ^{1}H NMRD profiles (for 37°C) on the basis of the parameter values obtained for Gd-DOTA (**1**) and varying only τ_R.

From Figure 24 it is obvious, that τ_R of Gd-DOTA (**1**) is with only 77 ps far too short. A prolongation of τ_R results generally in an increase in r_1, but most interesting is the appearance of a so called “high field peak” being especially effective in the magnetic field range of interest for clinical use. All these aspects make the prolongation of the rotational correlation time τ_R the prior aim in the development of high sensitivity CAs for MRI.

4.1.1.1 Macromolecular contrast agents

Several approaches have been reported in order to optimise the rotational motion. The Guerbet group developed a molecule called gadomelitol (also called P792 or Vistarem™) that can be described as Gd-DOTA (**1**) with large hydrophilic groups appended to each of the α-carbons on the acetate arms.[93] Although there is flexibility within the hydrophilic arms, the Gd-H_{water} vector cannot rotate independently of the entire molecule, which results in a remarkably high relaxivity (r_1 = 39.0 $mM^{-1}s^{-1}$ at 37°C, 0.47 T). Fulton *et al.* showed that the rotational effect can be modulated by adjusting the size of the hydrophilic "arms".[94]

The approach of Livramento *et al.* to slow down the rotational motion by self-assembly of 2,2'-bipyridine functionalised gadolinium(III) complexes binding around an iron(II) ion was outlined already in chapter 3.1.1.3. Another promising type of self-assembled macromolecular CAs are amphiphilic gadolinium(III) chelates which form micelles in aqueous media.[95, 96] Additional to the increase in τ_R, the self-assembly of functionalised gadolinium(III) complexes to a micelle results in a higher local gadolinium(III) concentration, which multiplies the efficiency when used as a target specific CA. Furthermore, the increased size can prevent a leakage of the CAs into the interstitium and slows down the renal clearance from the body, thus allowing more efficient blood pool and tumor angiogenesis imaging.[97, 98] However, for micellar aggregates it is essential to maintain the monomer concentration in the body above the critical micelle concentration, which might prevent the application of lower concentrations of the CA in certain cases.[99]

The grafting of many low molecular weight gadolinium(III) complexes to one macromolecule would be a concentration independent way to obtain higher local gadolinium(III) concentration and slower rotational motion. Numerous approaches have been reported in this direction. The noncovalently binding of MS-325 (**7**) to HSA as an example for increasing τ_R by conjugation to biomolecules was already described in chapter 2.4.1. Linear polymeric CAs from the conjugation of Gd-DTPA (**2**) to poly-*L*-lysine chains were reported by Spanoghe *et al.*.[100] Other examples of this type of CA include alternating copolymers of DTPA-class gadolinium(III) conjugates, linked by α,ω-alkyldiamides[101, 102] or a modified dextran polymer with DO3A-monoamide chelates with a total molecular weight of 52 kDa.[103] However, the increase in relaxivity of these linear polymers is usually much smaller than expected. The lower relaxivity can be attributed to anisotropic local rotational motions of the bound paramagnetic moiety with components rapid as compared to the overall motion of the macromolecule itself. The local motion may be rapid because the linkage between the gadolinium(III) complex and the macromolecule is highly flexible or because of rapid local

motion of the macromolecule itself, particularly if the gadolinium(III) complex is bound to a highly flexible linear polymer.[91, 101] Furthermore, their random morphology can lead to inconsistent and unpredictable pharmacokinetics, which may limit experimental repeatability.

Dendrimers are large molecules with well-defined chemical structures, with a regular and highly branched three-dimensional scaffold. Their structure can be separated in three major components, namely the core, the branches and the end groups. The synthesis of dendrimers is a process using a series of repetitive steps starting with the central initiator core. Each subsequent step represents a new "generation" of the dendrimer with a larger molecular diameter, doubles in general the number of reactive surface sites, and approximately doubles the molecular weight from that of the preceding generation. Unlike classical polymers, dendrimers therefore have a high degree of molecular uniformity, narrow molecular weight distribution, specific size characteristics, and a highly functionalised surface. Numerous types of dendrimeric CAs with various types of gadolinium(III) complexes, dendrimeric cores, branches and generations were reported over the last 15 years. The most often used type of dendrimer for the development of macromolecular CAs are so called polyamidoamino (PAMAM) dendrimers (G2-PAMAM dendrimer (**22**) is depicted in Figure 25).[86, 104-109]

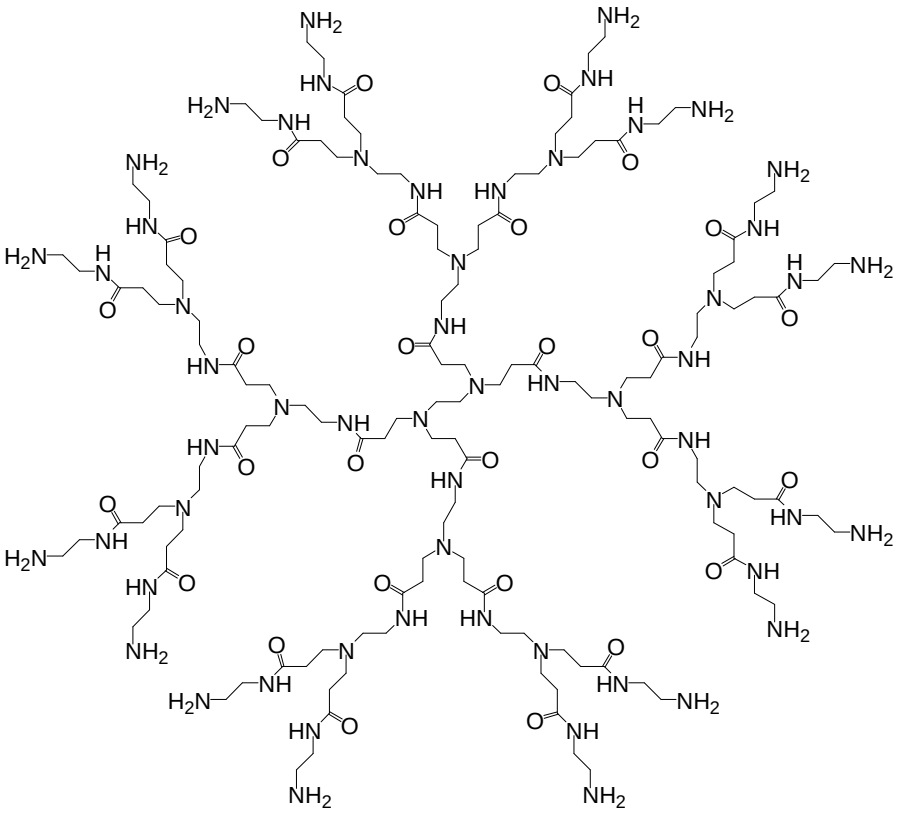

22

Figure 25. G2-polyamidoamino (G2-PAMAM) dendrimer.

The high-generation versions of these water soluble dendrimers are generally accepted to be globular molecules, with the core and interior being almost completely shielded owing to the numerous terminal surface groups.

Other examples of dendrimers being used for MRI CAs, are diaminobutane (DAB)-based dendrimers,[106] and dendrimers having poly-*L*-lysine branches on a polyethylene glycol (PEG) core[110] or a trimesoyl triamide core.[111] In contrast to linear polymeric CAs, in these dendrimeric CAs the effect of the increased molecular weight on relaxivity is more realised as the dendritic structure imposes a more isotropic rotational dynamic allowing higher relaxivities.[91] Nevertheless, the large systems are often relatively flexible and medium-sized dendrimeric contrast agents may no longer have a well defined three-dimensional spherical structure. To minimize nonspecific interactions with healthy tissues and lower systemic accumulation, however, a compact and globular shaped CA would be preferred.

An important drawback of very large CAs is also their slow excretion from the body, which increases the possibility to release toxic gadolinium(III) from the complexes, e.g. by transmetallation.[9, 14, 17, 20] The kidneys, being the exclusive excretion organ of most MRI CAs, possess a filtration system, called glomerulus, which has small pores with an effective radius of 3-5 nm.[112, 113] Everything that is small enough can freely diffuse through those pores and is rapidly cleared from the body. However, most of the large macromolecular CAs have sizes in the range of these pores or even higher and therefore need to diffuse through so called “shunt pathways” being significantly lower in number than small pores,[113] which slows down the excretion rate.

4.1.2 Silsesquioxanes

Silsesquioxanes are all structures with the formula $[RSiO_{1.5}]_n$, where R is hydrogen or any alkyl, alkylene, aryl, arylene, or organofunctional derivative of alkyl, alkylene, aryl, or arylene groups. They were first discovered by D.W. Scott in 1946 when he was investigating the thermal rearrangement of the co-hydrolysis product of dimethyldichlorosilane and silicon tetrachloride.[114] Since then silsesquioxanes have found an ever increasing number of applications. Most of these applications are in the field of materials science where differently functionalised silsesquioxanes are used as additives, polymers and precursors for inorganic/organic hybrid materials.[115-118] The silsesquioxanes used in these applications include random polymeric structures (**23**), ladder structures (**24**) and cage structures (**25**-**27**) (see Figure 26).[115, 117, 119] The cage structures are called polyhedral oligosilsesquioxanes (POSS) and their nomenclature T_n refers to the number of Si-OR’ functions (T: three oxygens attached to the silicon)[120] and to the number of silicons *n* involved in the cage. POSS

compounds embody a truly hybrid (inorganic–organic) architecture, which contains an inner inorganic framework made up of silicon and oxygen that is externally covered by organic substituents. By functionalisation of these substituents, especially the symmetric T_8-POSS (**26**) has already shown its potential as dendrimeric core.[121, 122] Owing to its three-dimensional structure and the generally accepted nontoxic properties of silica compounds,[123] T_8-POSS cubes could therefore be ideal building blocks for the development of dendrimeric CAs which possess already a compact globular shape at low numbers of generations.

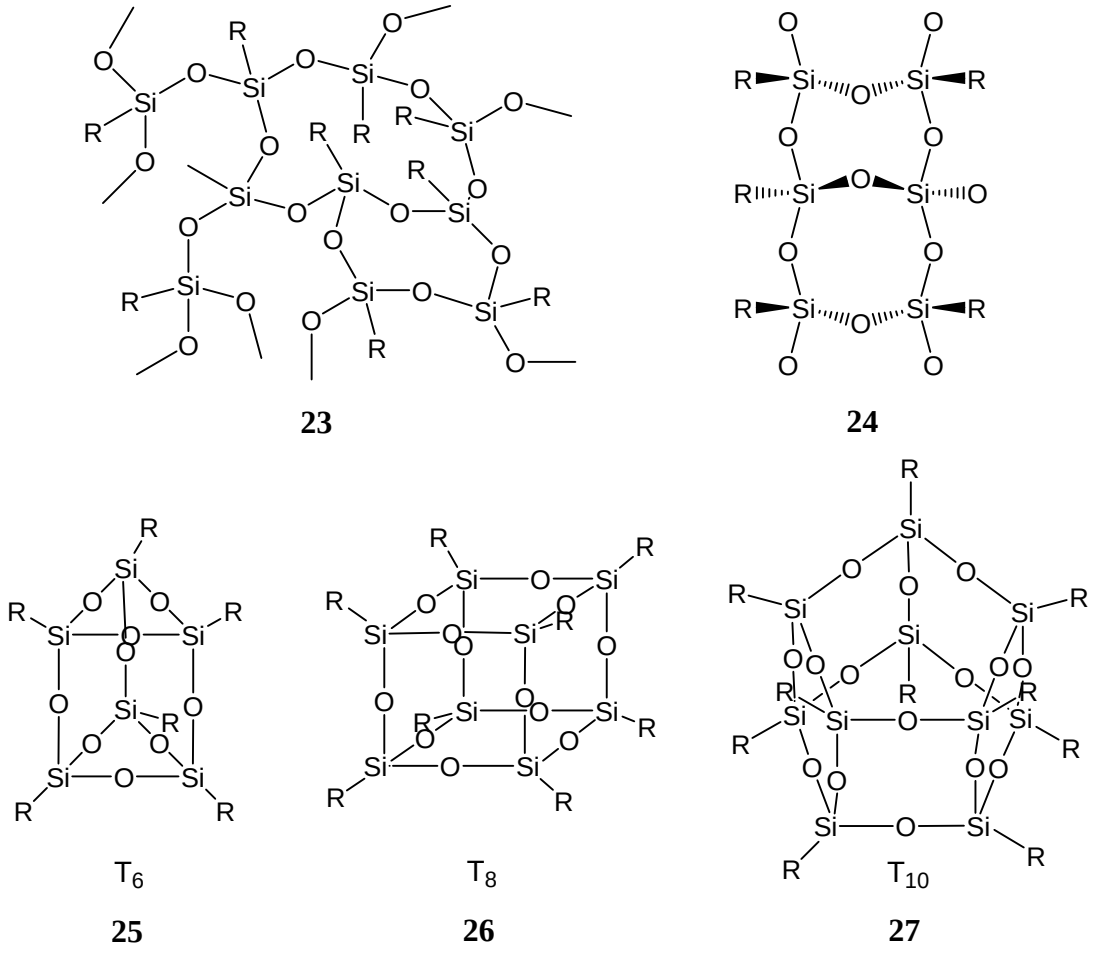

Figure 26. Structures of various silsesquioxanes.

4.1.3 Aim of this project

From Figure 24 in chapter 4.1.1 it is obvious that the maximum achievable relaxivity r_1 increases with increasing τ_R, however, the maximum of the resulting high field peak shifts towards lower field strength. This is easily understandable from equation 2.9 in chapter 2.3.1. Once $\omega_I^2 \tau_{c1}^2$ in the "3-term" becomes larger than one, the relaxation rate becomes slower and disperses with increasing frequency (field). An increased τ_R, increases τ_{c1} and therefore $\omega_I^2 \tau_{c1}^2 > 1$ is already fulfilled at a lower proton Larmor frequency. To achieve a high

relaxivity at field strength currently used in clinical MRI, novel macromolecular CAs should therefore be only of moderate size. Due to the Debye-Stokes equation (equation 3.2 in chapter 3.2.3) for example a rotational correlation time τ_R of 10 ns, being the longest τ_R used in Figure 24, belongs to a hydrodynamic radius r_H of about 2 nm in water.

As outlined in chapter 4.1.1.1, for an acceptable excretion rate of the CA from the body it is also essential to keep the hydrodynamic radius of the CA below the effective radius of the small pores of the glomerular filtration system.

On the other hand, for the development of target specific CAs, large CAs with a high number of gadolinium(III) ions are favourable, as each paramagnetic centre on the CA which locates a biomolecule in the body serves as a multiplier, allowing the detection of lower concentrated biomarkers.

CAs based on T_8-polyhedral oligosilsesquioxanes could be the ideal compromise, as T_8-POSS cubes form a precast three-dimensional platform for the synthesis of compact globular CAs, loaded with a high number of gadolinium(III) complexes already at the lowest possible number of dendrimeric generations.

The aim of this project is therefore the development of synthetic strategies to functionalise T_8-silsesquioxanes with eight appropriate gadolinium(III) complexes each. Once a working protocol is established, novel potential CAs shall be synthesised and fully characterised. All aspects of their solution behaviour shall be investigated by means of various analytical techniques in order to optimise their properties as a CA.

4.2 Results and Discussion

4.2.1 Synthesis of T_8-Silsesquioxanes

Two differently functionalised T_8-silsesquioxanes were prepared to serve as the building block for macromolecular silsesquioxane-based CAs, an amino-functionalised one for the coupling of carboxylic acid-functionalised ligand systems and a carboxylic acid-functionalised silsesquioxane for the binding of amino-functionalised ligand systems.

4.2.1.1 Synthesis of an amino-functionalised T_8-silsesquioxane

Aminopropyl-functionalised T_8-silsesquioxanes can be directly obtained by hydrolytic condensation of γ-aminopropyltriethoxysilane in methanol-conc. hydrochloric acid (Scheme 5).[124]

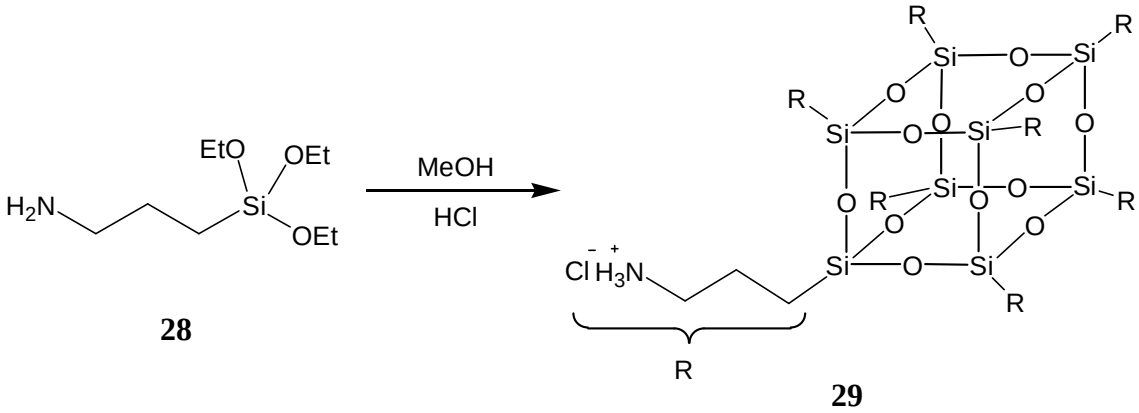

28 **29**

Scheme 5.

Following the literature procedure, octa(3-chloroammoniumpropyl)silsesquioxane (**29**) could be synthesised in 39 % yield. All analytical data were in agreement with those reported in the literature.[124] **29** needs to be isolated as the octaammonium chloride salt, since the octaamine species is marginally stable in solution and decomposes rapidly when the solvent is removed. At least two different pathways for the decomposition of the silsesquioxane cage of the octaamine species were proposed. The most rapid one probably involves the formation of hydroxide ions *via* reaction of water with the free amine. Support for this pathway was given from the observation that other silsesquioxane frameworks are slowly decomposed by exposure to amine bases (e.g. Et_3N) in wet solvents and the fact that decomposition is much slower in anhydrous solvents (e.g. MeOH over 3 Å sieves). However, as decomposition still occurs when solutions of the octaamine species are prepared in dimethylsulfoxide (DMSO) and stored over molecular sieves a second mechanism must be operative that does not require water. It is believed that this mechanism involves the nucleophilic attack of the amino nitrogen on the silicon on which it is bound to.[124]

4.2.1.2 Synthesis of a carboxylic acid-functionalised T_8-silsesquioxane

So far, there is no method for direct hydrolytic condensation of acid-functionalised T-silicon monomers. Therefore a two step route, developed in our group by D. Ruiz-Abad,[125] was used for the synthesis of carboxylic acid-functionalised T_8-silsesquioxanes. In the first step, octavinylsilsesquioxane (**31**) was synthesised by the hydrolytic condensation of $CH_2CHSiCl_3$ (**30**) in an excess of methanol containing acidic Amberlite IR-120, following the method reported by Dare *et al.* (Scheme 6).[126] The synthesis of pure product **31** in 15 % yield was confirmed by the agreement of the analytical data with those reported in the literature. In the second step the so obtained octavinylsilsesquioxane (**31**) was treated with mercaptopropionic acid (**32**) in the presence of azobisisobutyronitrile (AIBN) as a radical initiator in toluene (Scheme 7). This radical addition yielded selectively the octa(3-(ethylmercapto)propionic acid) silsesquioxane (**33**) as the *anti*-Markovnikov product in an excellent yield of 98 %. All analytical data were in full accordance with those reported in the literature.[125]

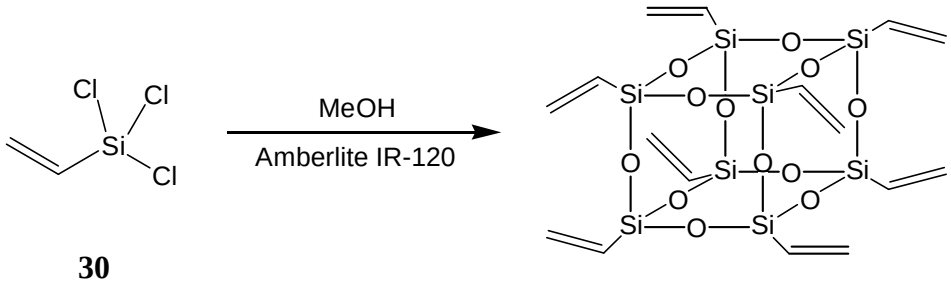

30 **31**

Scheme 6.

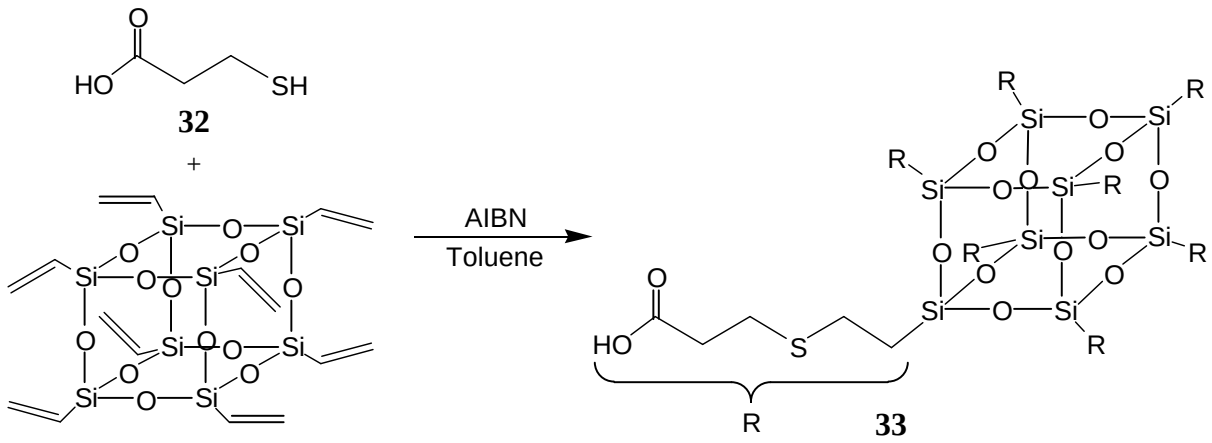

32 **31** **33**

Scheme 7.

4.2.2 Introduction of Macrocyclic Ligands *via* their *tert*-Butyl protected Form

It was discussed in detail in chapter 2.4.2, that CAs based on macrocyclic DOTA-type ligand

systems are a much safer alternative as compared to the open chained linear systems, as their higher inertness significantly slows down the leaking of toxic free gadolinium(III) ions from the ligand systems. As was reinvestigated recently in the context of the gadolinium(III)-related decease NSF,[9, 14, 17, 20] this can be essential for the development of macromoleclar CAs being designed to remain longer in the body than their low molecular derivatives. It was therefore decided to use macrocyclic DOTA-type ligand systems for the development of silsesquioxane-based CAs.

4.2.2.1 Synthesis of DOTA(^{t}Bu)$_3$

The most common way to introduce DOTA-type ligands into macromolecular systems is to use the monoreactive prochelator DOTA(^{t}Bu)$_3$ (4,7,10-tricarboxymethyl-*tert*-butyl ester 1,4,7,10-tetraazacyclododecane-1-acetic acid (**36**), Scheme 9), which can be coupled to e.g. amino-functionalised systems *via* its free carboxylic acid group. Furthermore, Feher *et al.* already demonstrated the octafunctionalisation of octa(3-chloroammoniumpropyl)-silsesquioxane (**29**) with *N*-protected amino acids and *N*-protected di- and tri-peptides under standard peptide coupling conditions.[127]

Divergent from the literature method which starts with the monoalkylation of cyclen,[128] DOTA(^{t}Bu)$_3$ (**36**) was synthesised in two steps from tri-*tert*-butyl 1,4,7,10-tetraazacyclododecane-1,4,7-triacetate (DO3A(^{t}Bu)$_3$ (**34**)). In the first step the secondary nitrogen of **34** was alkylated by benzyl bromoacetate (Scheme 8).

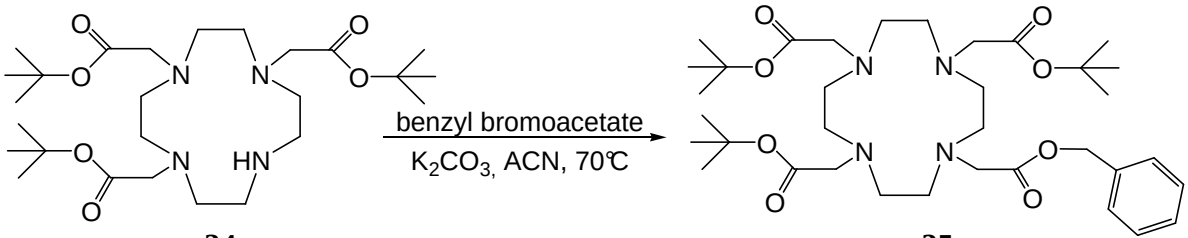

34 **35**

Scheme 8.

The successful synthesis of 4,7,10-tri-*tert*-butyl-1-benzyl-1,4,7,10-tetraazacyclododecane-1,4,7,10-tetraacetate (DOTA(^{t}Bu)$_3$Bn (**35**)) in 87 % yield could be shown by the appearance of new signals in the aromatic region of the ^{1}H NMR spectrum in the correct ratio of integrals and the agreement of the analytical data with those reported in the literature.[128] Deprotection of the benzyl ester was accomplished by catalytic hydrogenation using palladium on charcoal (Scheme 9). **36** was isolated in 87 % yield and the obtained analytical data agreed with that reported in the literature.[128] Due to their hygroscopic properties no elemental analysis was carried out for the macrocyclic ligands.

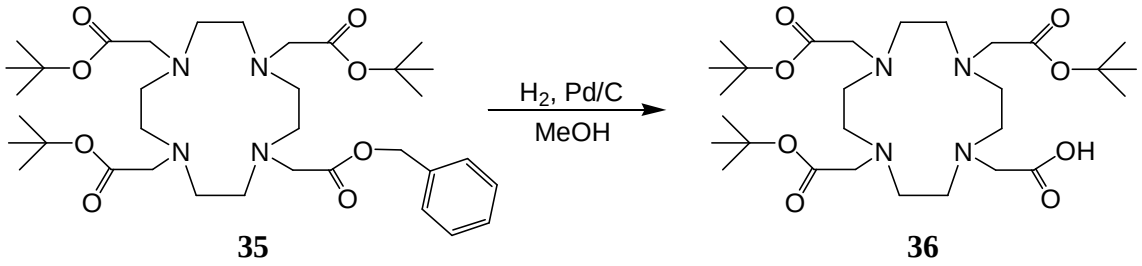

35 **36**

Scheme 9.

4.2.2.2 Coupling of DOTA(^{t}Bu)$_3$ to octa(3-aminopropyl)silsesquioxane

Following the procedure reported by Feher *et al.*[127] for the attachment of *N*-protected amino acids, octa(3-aminopropyl)silsesquioxane (**29**) was treated with an excess of ligand **36** in the presence of classical peptide coupling reagents and a base. Analogous to Feher *et al.* *O*-(benzotriazol-1-yl)-N,N,N',N'-tetramethyluronium tetrafluoroborate (TBTU)[129] (**38**) and 1-hydroybenzotrialzol (HOBt) (**44**) were used as coupling reagents and diisopropylethylamine (DIPEA) was used as base. The proposed mechanism for such reactions is depicited in Scheme 10.[130] It involves the *in situ* formation of the highly reactive hydroxybenzotriazol ester **42**, which reacts with the amino component **43** to yield the amide **45**.

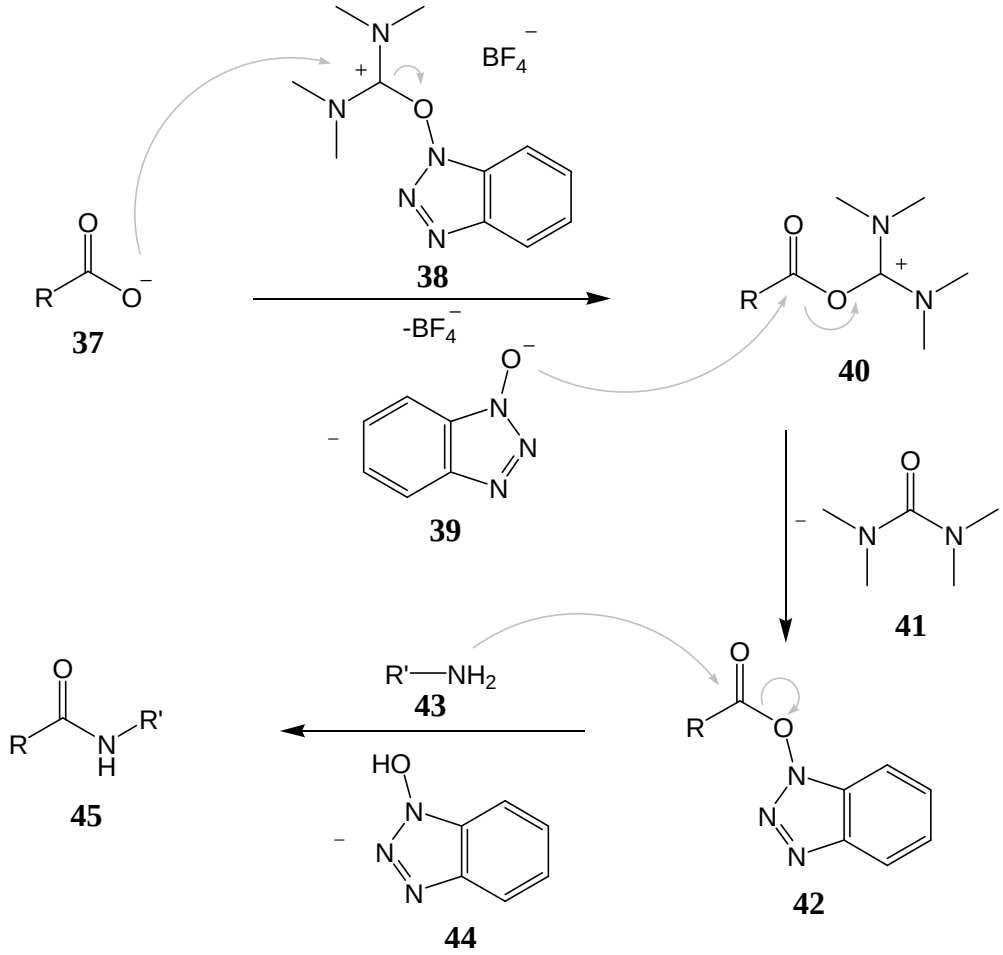

Scheme 10.

Feher *et al.* carried out their syntheses in dimethylformamide (DMF) or DMSO and allowed the solutions to stir for one day at room temperature. As **29** needs to be available in its deprotonated form a large excess of DIPEA was used. When DOTA(^{t}Bu)$_3$ (**36**) was reacted with **29** under the conditions decribed by Feher *et al.* in both dry DMF and dry DMSO, a yellowish crude product could be isolated. The ^{1}H and ^{13}C{^{1}H} NMR spectra of the crude products measured in DMSO-d6 showed the signals corresponding to the *tert*-butyl protected DOTA-type ligand systems and also the signals of the propyl groups attached to the silsesquioxane core. Furthermore, the ^{1}H NMR spectra showed the changes in chemical shift of the resonances of the propyl groups (SiC*H*$_2$: δ 0.71 → 0.59 ppm, SiCH$_2$C*H*$_2$: δ 1.71 → 1.60 ppm, NC*H*$_2$: δ 2.75 → 3.19 ppm), being characteristic for the amide formation on **29**.[127] The deprotonation of the ammonium group as the source for the observed changes in the chemical shift could be excluded, as the ^{1}H NMR spectrum of **29** in DMSO-d6 did not show such changes after the addition of excess DIPEA. This clearly shows the successful attachment of **36**. However, no resonance could be observed in the ^{29}Si{^{1}H} NMR spectra of the crude products. A possibility why no signal was observed could be the broadness of the signal due to hindered rotation, leading to a low signal intensity. Moreover, it is also possible that the silsesquioxane cage partly decomposes during the long reaction time. As was already mentioned in chapter 4.2.1.1, silsesquioxane frameworks can slowly decompose by exposure to amine bases in wet solvents. Even though dry solvents were used for the attachment of **36** to **29**, HOBt was added as its monohydrate, allowing the formation of hydroxide ions which in turn can destroy the cage.

In order to investigate the stability of the silsesquioxane cage under the used conditions and to exclude that the loss of the silicon signal is due to hindered rotation accompanying the successful reaction, octa(3-aminopropyl)silsesquioxane (**29**) was dissolved in dry DMSO-d6 and transferred in an screw capped NMR tube under argon atmosphere and ^{29}Si{^{1}H} NMR spectra were recorded (Figure 27). Due to the cubic symmetry of **29**, the spectrum shows only one resonance at -66.5 ppm which is in the typical range of T^3 groups.[120] After 145 minutes the equivalent amount of DIPEA as used in the coupling reactions was added and another spectrum was recorded. After further 240 minutes and 20 h additional spectra were recorded. As was mentioned earlier, it was reported, that the deprotonation of the ammonium groups of **29** leads to the decomposition of the silsesquioxane cage, however, in this study no decrease in signal intensity was observed. Only the addition of a small amount of water (about five times the amount that would have been included in HOBt·H$_2$O) to the solution resulted in a fast decrease in signal intensity with an almost complete disappearance of the signal already

after 110 minutes. For comparison the same investigation was carried out with the carboxylic acid functionalised octa(3-(ethylmercapto)propionic acid) silsesquioxane (**33**). In this case the signal also decreased only after the addition of water. However, the loss in signal intensity was significantly slower than for **29** resulting in a noticeable decrease only after 27 hours. The longer alkyl chain in the case of **33** might hinder the approach of the hydroxide ions. The reason why no new signals appear in the spectra is probably the reduced symmetry of the partly degraded cages, which generates numerous magnetically inequivalent ^{29}Si nuclei in poor concentrations circumventing their detection in a reasonable time.

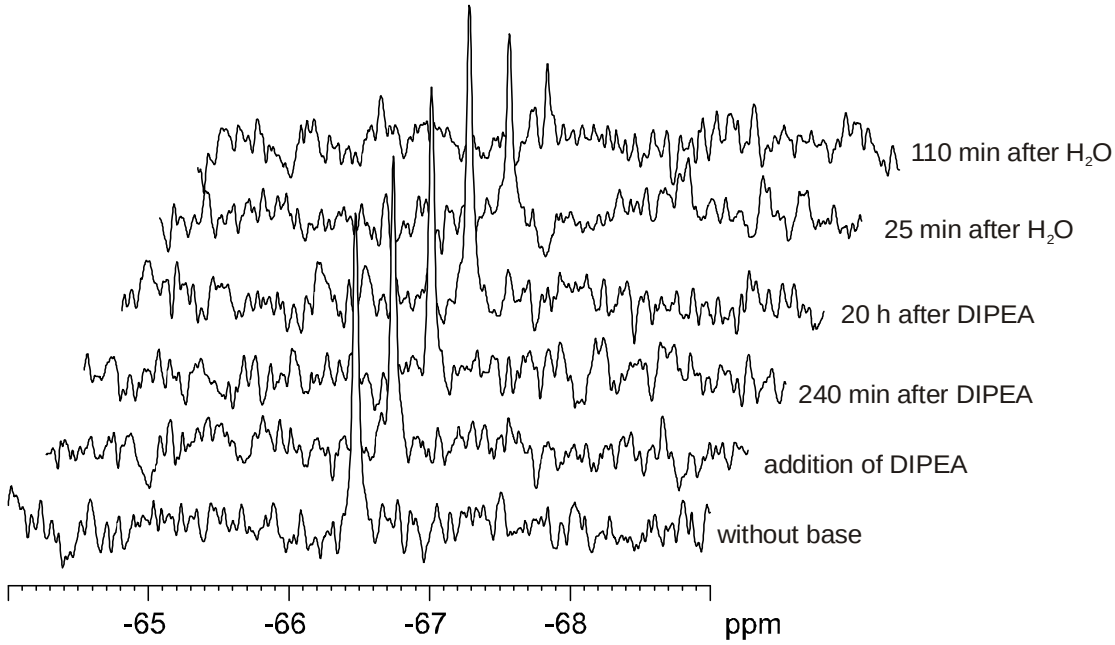

Figure 27. ^{29}Si{^{1}H} NMR spectra of **29** in dry DMSO-d6, without base, directly after the addition of DIPEA, 240 min and 20 h after the addition of DIPEA and 25 and 110 min after additional addition of water.

HOBt (**44**) is usually added in peptide coupling reactions as it improves the stereocontrol by preventing racemisation. However, in the coupling of **36** to **29** racemisation is not an issue and therefore it was omitted in further reactions. Moreover, the reaction was reset in a screw capped NMR tube under argon atmosphere and monitored by ^{1}H NMR spectroscopy to optimise the reaction time. It could be shown, that almost immediately after the addition of DIPEA, which was the last component added, the resonances became broad and were shifted in the characteristic way. Completeness of the reaction was indicated after about 20 minutes. This shows that a reaction time as long as used in the initial attempts is not required to achieve octafunctionalisation of the silsesquioxane.

In a new attempt the octaammonium silsesquioxane **29** was therefore treated with an excess of DOTA(^{t}Bu)$_3$ (**36**), TBTU (**38**) and DIPEA in dry DMSO under argon atmosphere and the

mixture was stirred for only 30 minutes at room temperature (Scheme 11). Workup resulted in the desired product **46** in excellent yield. The ^{1}H NMR spectrum of the obtained yellowish solid dissolved in $CDCl_3$ showed the signals of the product in the correct ratio of integrals indicating a complete octafunctionalisation. Furthermore, according to the spectrum the yellowish solid contained mostly the product, however, a small amount of TBTU byproducts was also observed. This time the ^{29}Si{^{1}H} NMR spectrum revealed a single resonance at -66.9 ppm suggesting the intactness of the silsesquioxane core.

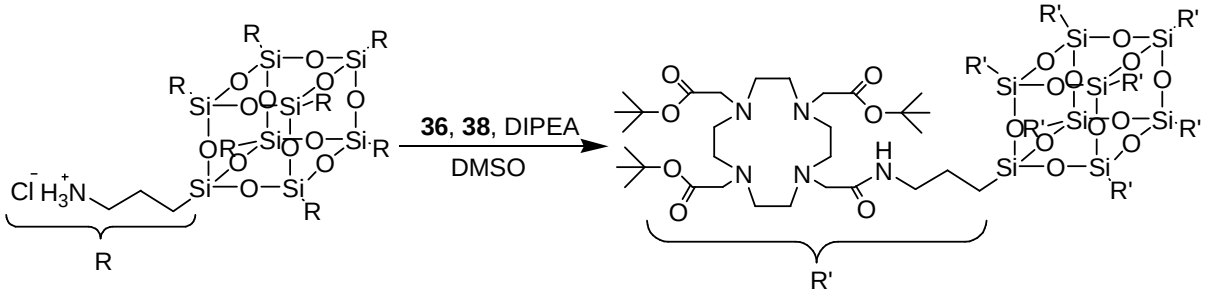

29 **46**

Scheme 11.

4.2.2.3 Deprotection of the carboxylic acid functions

A typical way to cleave *tert*-butyl esters is their hydrolysis under acidic conditions, using formic acid or trifluoroacetic acid (TFA) in dichloromethane (DCM). Furthermore, Feher *et al.* used TFA in DCM to remove their Boc (*tert*-butoxycarbonyl) protecting groups without decomposition of the silsesquioxane cage under these acidic conditions.[127]

Thus, **46** was stirred in TFA:DCM (1:2) for about eight hours, after which the volatile matter was removed under reduced pressure. The residue was precipitated from acetone after the addition of diethyl ether. The ^{1}H NMR spectrum (Figure 28b) of the obtained crude product in D_2O showed an almost complete disappearance of the resonance at about 1.4 ppm, belonging to the *tert*-butyl hydrogens. Unfortunately, the two signals of the methylene groups $SiCH_2CH_2$ and $SiCH_2$ of **46** at 1.6 and 0.6 ppm, respectively, also changed. The signal of the $SiCH_2$ methylene group, being adjacent to the silicon atom, split in several resonances. Due to the also measured ^{1}H-^{13}C HSQC NMR spectrum, at least three distinct resonances could be assigned. Together with the disappearance of the signal in the ^{29}Si{^{1}H} NMR spectrum, this indicated the decomposition of the silsesquioxane cage under the used conditions. The cleavage was therefore attempted using milder conditions. **46** was stirred in formic acid:DCM (1:1) for 16 hours at room temperature. In this case, the obtained product remained soluble in DCM and its ^{1}H NMR spectrum revealed that the protecting groups had only partly been removed. However, also in this case the resonance at 0.6 ppm split, indicating again the

decomposition of the cage.

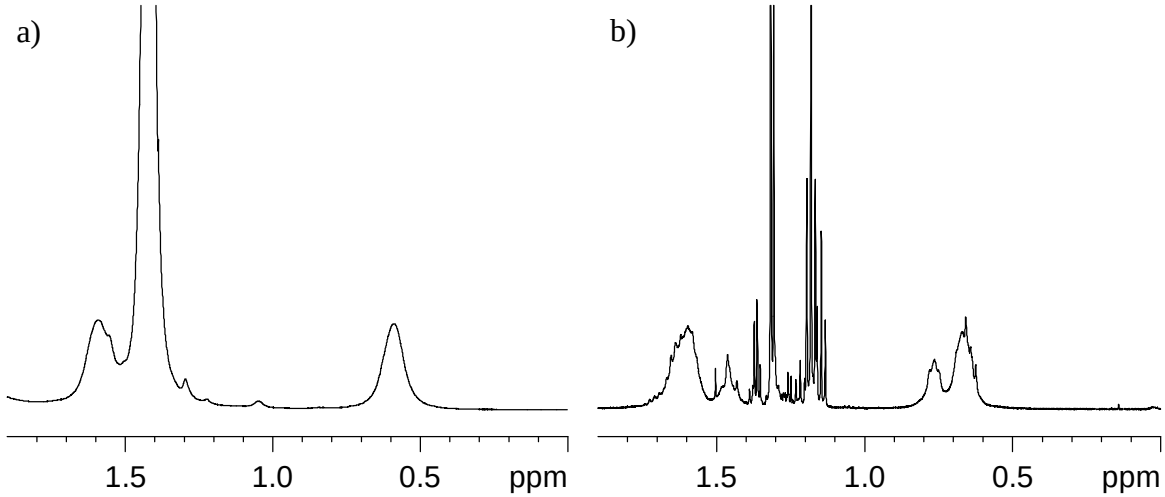

Figure 28. ^{1}H NMR spectra of (a) **46** in DMSO-d6 and (b) the crude product of the reaction of **46** with TFA:DCM, measured in D_2O.

As in the case of the coupling reaction, it is hard to explain why under the chosen conditions decomposition of the silsesquioxane cage takes place for these systems, but not for the systems described by Feher *et al.*. It is known that strong acids can break Si-O-Si bonds, even in the absence of water. Acids like HBF_4/BF_3, CF_3SO_3H or CH_3SO_3H are used for the selective cleavage of one corner from T_8-silsesquioxanes.[119, 131] Furthermore, it is possible that due to the hygroscopic nature of the DOTA moiety, water is introduced into the systems leading to acid catalysed hydrolysis.

4.2.3 Introduction of Macrocyclic ligands *via* non *tert*-Butyl protected Forms

As the deprotection of the *tert*-butyl protected carboxylic acids proved unsuccessful, two alternative ways to introduce macrocyclic ligands into silsesquioxane systems were explored contemporaneously.

4.2.3.1 Synthesis of La-DO3A-hexylamine

André *et al.* have shown that it is possible to directly couple functionalised gadolinium(III) DOTA-complexes to a designated molecule without using protecting groups, since the four DOTA-carboxylate groups are protected by the coordination to the gadolinium(III) ion.[95] This would make a later deprotection and complexation unnecessary. For this approach initially the lanthanum(III) complex (**48**) of the in our lab available 1-aminohexyl-1,4,7,10-tetraazacyclododecane-1,4,7-triacetic acid (DO3A-hexylamine) ligand[65] (**47**) was prepared (Scheme 12). The successful coordination was confirmed by electrospray ionisation mass spectrometry (ESI-MS) (m/z: 582.4 ($[M+H]^+$), 604,2 ($[M+Na]^+$)). Lanthanum(III) was chosen

as ^{139}La is an NMR active nucleus whose chemical shift allows conclusions about the number of coordinated carboxyl and amino functions.[132] This should indicate whether the hexylamino moiety is coordinated to the lanthanide(III) ion or not and hence is free to be coupled to the carboxylic acid functionalised silsesquioxane **33** or not.

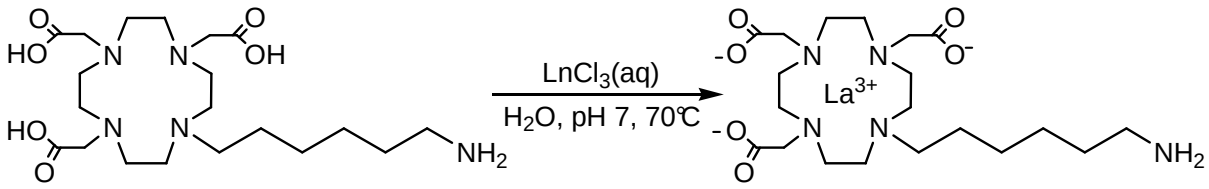

47 **48**

Scheme 12.

Contrary to the ^{139}La NMR spectrum (Figure 29) of La-DO3A (cf. compound **10** in chapter 2.4.2), which showed a broad resonance at about 295 ppm corresponding to four coordinated nitrogen atoms and three negatively charged oxygen ions,[132] the ^{139}La NMR spectrum of **48** did not show a signal corresponding to a coordinated lanthanide(III) ion. Due to the comparably large quadrupolar moment of ^{139}La and the reduced symmetry as compared to the La^{3+}_{aq} ion, the signal of La-DO3A already has a line-width of about 8600 Hz. As no signal is observed for **48**, the amino function terminating the hexyl chain is most likely not permanently coordinated to the lanthanum(III) ion. In solution the flexibility of the hexyl moiety rather allows the amino group to tumble, thereby sometimes approaching the lanthanum(III) ion. This increased dynamics can further broaden the ^{139}La NMR signal leading to the non-observability of the resonance.

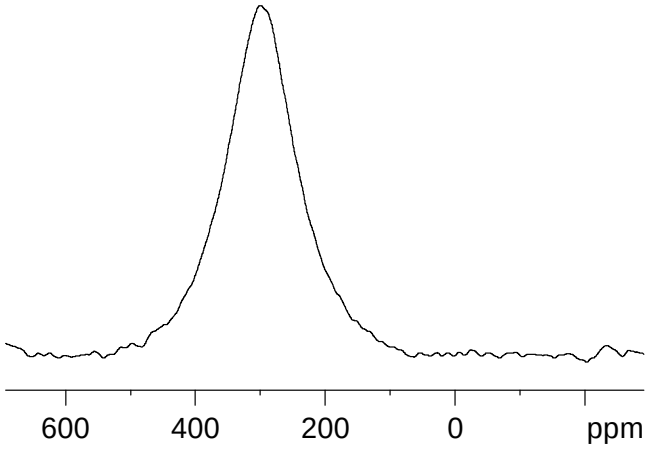

Figure 29. ^{139}La NMR spectrum of La-DO3A in D_2O, pD 7.0, 65°C.

Further evidence for the non-coordination of the hexylamine function comes from the ^{1}H NMR spectrum of **48** (Figure 30). Due to the quadrupolar moment of the lanthanum nucleus and the hindered motion, the signals belonging to hydrogens on the DO3A moiety are

extremely broad. The further apart the nuclei are located from the lanthanum(III) and the higher the flexibility of the respective group is, the sharper is the line-width of the corresponding NMR signal. As the signals become narrower from 1 to 5 in Figure 30, the methylene group 5 is further apart from the lanthanum(III) ion than methylene group 1. This suggests a free amino group and enables the amino function to react with a carboxylic acid. Furthermore, when the amino group is not coordinated, it should be protonated under the used conditions and needs to be deprotonated prior the coupling.

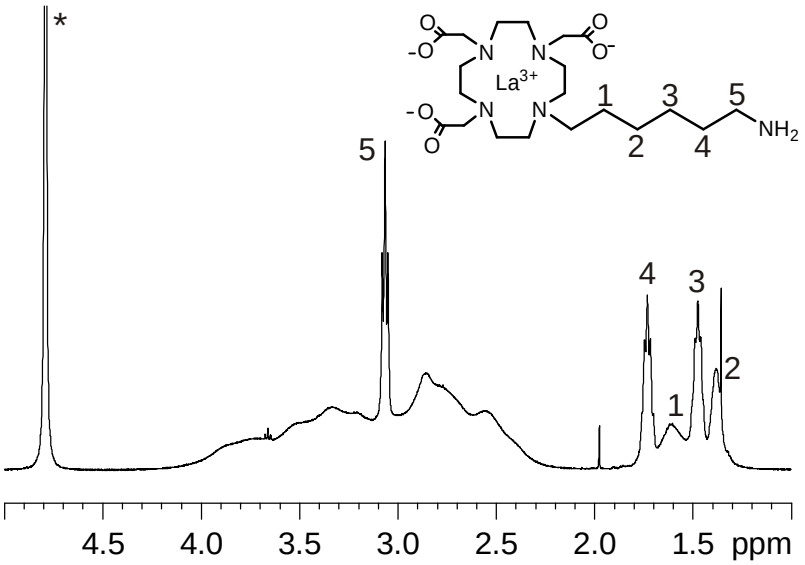

Figure 30. ^{1}H NMR spectrum of **48** in D_2O (pD 7.0). 1-5 are the resonances of the methylene groups of the alkylchain as shown. * is the solvent residual peak.

4.2.3.2 Coupling of La-DO3A-hexylamine to the silsesquioxane

The water was removed from complex **48** and the solid residue was dried at 50°C under reduced pressure over night in order to minimise the amount of remaining water in the systems. **48** was then coupled to the carboxylic acid functionalised octa(3-(ethylmercapto)propionic acid) silsesquioxane (**33**) in dry DMSO using TBTU and DIPEA and stirring only for 30 minutes at room temperature. The mixture was then added drop-wise to a diluted acetic acid/sodium acetate buffer (pH 5.5) in order to purify the solution *via* diafiltration. Unexpectedly, an off-white solid precipitated during the addition. The precipitate was isolated by centrifugation. It turned out to be insoluble in acetone, chloroform, diethyl ether and DMF and could hardly be redissolved in DMSO. In solution, only a poor ^{1}H NMR spectrum of the precipitate could be obtained using DMSO-d6 (Figure 31). Nevertheless, the spectrum contains signals corresponding to structural elements of the lanthanum(III) complex **48** and of the silsesquioxane **33**, indicating that the formed precipitate is the desired octalanthanum(III)-functionalised silsesquioxane **49** (Figure 32).

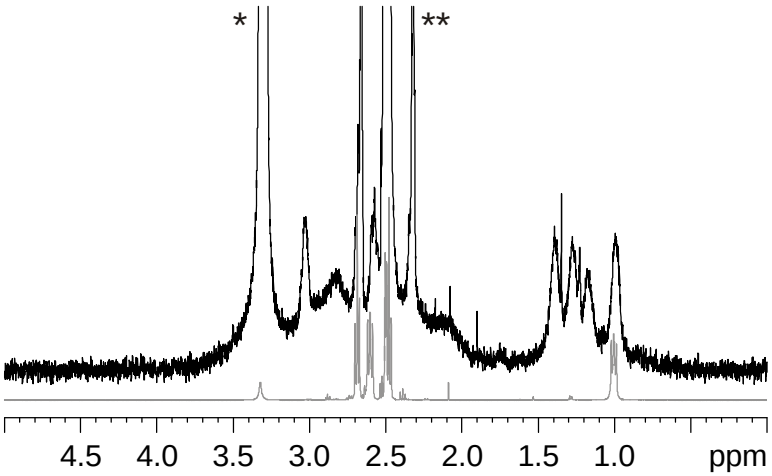

Figure 31. ^{1}H NMR spectra of **49** (black) and **33** (grey) in DMSO-d6. * H_2O, ** DMSO with satellite signals due to coupling to ^{13}C.

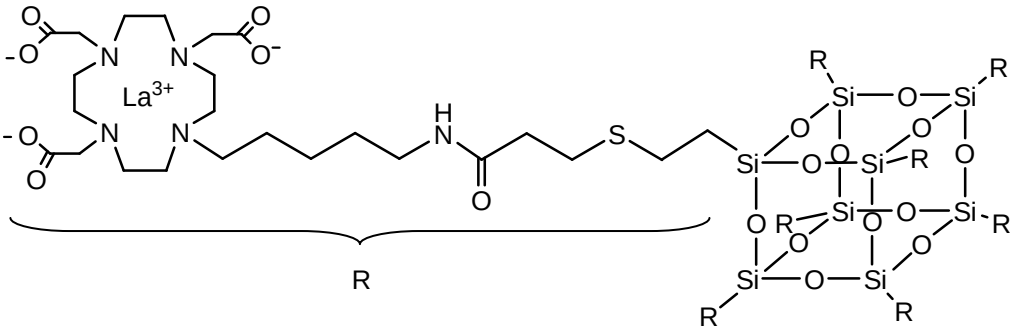

49

Figure 32. Structure of compound **49**.

As compound **49** was not sufficiently soluble in any tested solvent, solid state ^{13}C and ^{29}Si CP/MAS NMR spectra were recorded (Figure 33a and b, respectively).

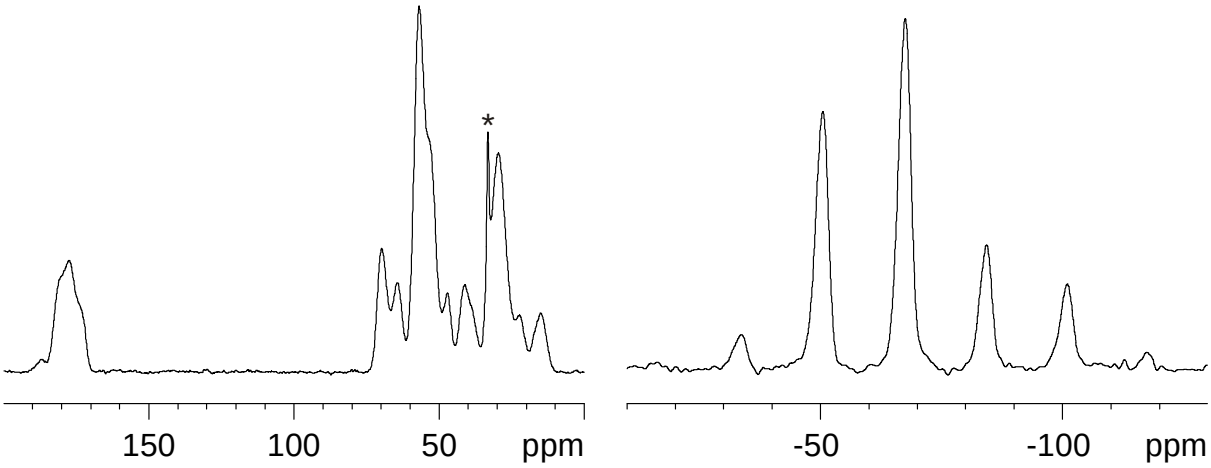

Figure 33. (a) ^{13}C and (b) ^{29}Si CP/MAS NMR spectra of compound **49**. The rotation frequency was (a) 10000 Hz and (b) 1000 Hz. * residual acetone.

Due to the broadness and therefore overlapping of the signals in the ^{13}C CP/MAS NMR spectrum (Figure 33a), not all signals corresponding to the former octa(3-(ethylmercapto)propionic acid) silsesquioxane moiety and the hexylamine chain can be assigned unambiguously. However, the signal at 14 ppm clearly corresponds to the CH_2Si group whereas the signals between 70 and 42 ppm belong to the La-DO3A moiety. The signals between 183 and 167 ppm can be assigned to the carboxylate and amide carbons. The ^{29}Si CP/MAS NMR spectrum (Figure 33b) of **49** shows a singlet at -67.5 ppm. This indicates again the octafunctionalisation and points out the intactness of the cage. However, as the signal is broad and the spectrum shows side-bands due to the low rotation frequency, this cannot finally be ascertained.

Since compound **49** is insoluble in aqueous media at moderate pH, it is not suitable as a CA in MRI. When compound **49** was placed in D_2O and the pD was decreased to 2-3 by adding conc. hydrochloric acid (HCl) to the stirred suspension, the compound slowly dissolved. At this pH the carboxylate groups become protonated and lanthanum(III) can be released, in turn leading to a protonation of the nitrogens. The introduced charge increases the solubility in water by improving the dipolar interaction with surrounding water molecules. The ^1H NMR of the solution shows all signals expected for an DO3A-hexylamine moiety attached to a octa(3-(ethylmercapto)propionic acid) silsesquioxane (Figure 34). The release of quadrupolar lanthanum(III) is indicated by the much sharper signals of the DO3A moiety as compared to those in the spectrum of complex **48** (see Figure 30).

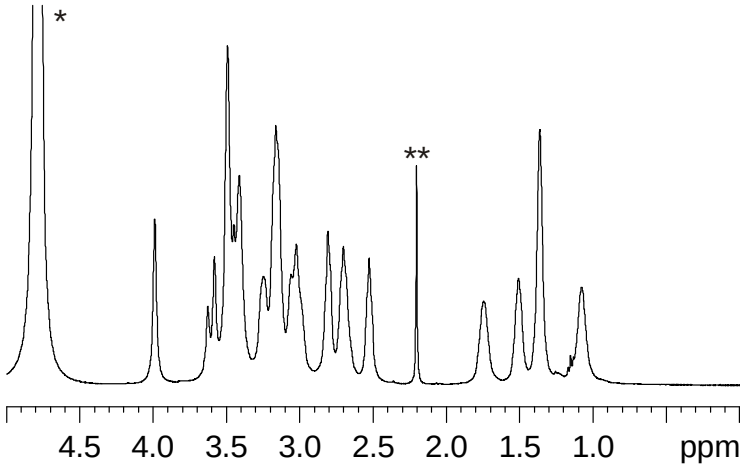

Figure 34. ^1H NMR spectrum of compound **49** in D_2O after decreasing the pD to 2-3. * residual solvent peak, ** residual acetone

The also measured $^{29}Si\{^1H\}$ NMR spectrum shows only one resonance at -67.8 ppm. However, the intensity is poor and therefore the cage might have started to slowly decompose. Nevertheless, the addition of $NaOH_{(aq)}$ up to pH 7 resulted again in a precipitation of the

compound. When the pH was further increased to about pH 12 the precipitate redissolved again. This time the increased solubility is most likely related to the decomposition of the silsesquioxane cage, as the subsequent decrease in pH no longer resulted in a precipitation.

4.2.3.3 Synthesis of DOTA(Bn)$_3$

The second approach to introduce macrocyclic ligands into silsesquioxane systems without using acidic or basic cleaved protecting groups involved the attachment of benzyl protected ligands. Therefore the benzyl protected analogue of DOTA(^{t}Bu)$_3$ (**36**) was synthesised. The synthesis of DOTA(Bn)$_3$ (4,7,10-tricarboxymethyl-benzyl ester 1,4,7,10-tetraaza-cyclododecane-1-acetic acid (**53**)) has already been reported by Anelli *et al.*.[133] Their route involved the monoalkylation of cyclen (**50**) with *tert*-butyl bromoacetate followed by the alkylation of the remaining three nitrogens using benzyl bromoacetate. For this study it was decided to first synthesise tri-benzyl 1,4,7,10-tetraazacyclododecane-1,4,7-triacetate (DO3A(Bn)$_3$ (**51**)), the benzyl protected analogue of DO3A(^{t}Bu)$_3$ (**34**). **51** should allow faster access to various carboxylic acid- or amino-functionalised DO3A(Bn)$_3$-derivatives, once the attachment of gadolinium(III) complexes to silsesquioxanes *via* benzyl protected ligands proved successful. **51** was synthesised by alkylation of three of the cyclen (**50**) nitrogens using 2.8 equivalents benzyl bromoacetate (Scheme 13).

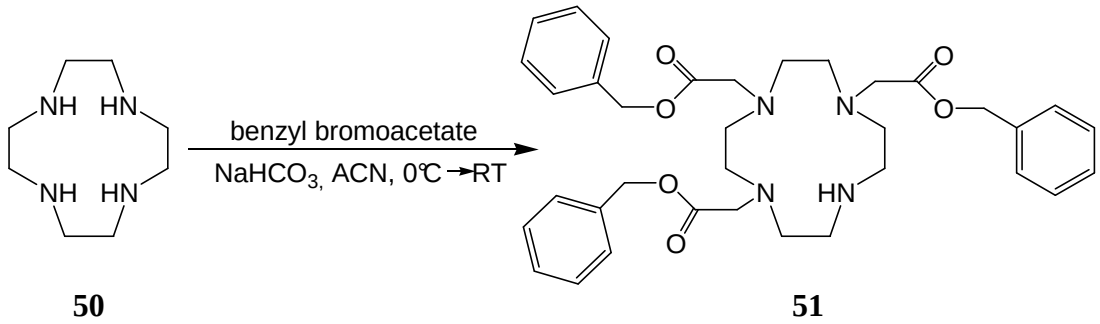

50 **51**

Scheme 13.

The synthesis resulted in a mixture of mono-, di-, tri- and tetra-alkylated cyclen derivatives. Mono- and di-alkylated species could almost completely be removed *via* filtration as their bromide salts are poorly soluble in acetonitrile. However, the separation of **51** from the tetra-alkylated DOTA(Bn)$_4$ could not be achieved by traditional separation techniques. The isolation of **51** was finally accomplished *via* elution from an Amberlite XAD1600 resin column using a water/acetonitrile gradient. Amberlite XAD1600 is a polystyrene resin, to which DOTA(Bn)$_4$, due to its four aromatic groups, has a higher affinity than **51**, which possesses only three aromatic groups. The product was characterised by multidimensional ^{1}H and ^{13}C NMR spectroscopy and ESI-MS. Unfortunately, with only 10 %, the yield remained

poor.

In the next step the forth cyclen nitrogen of **51** was alkylated with *tert*-butyl bromoacetate in order to obtain 4,7,10-tri-benzyl-1-*tert*-butyl-1,4,7,10-tetraazacyclododecane-1,4,7,10-tetraacetate (DOTA(Bn)$_3$^{t}Bu (**52**)) (Scheme 14).

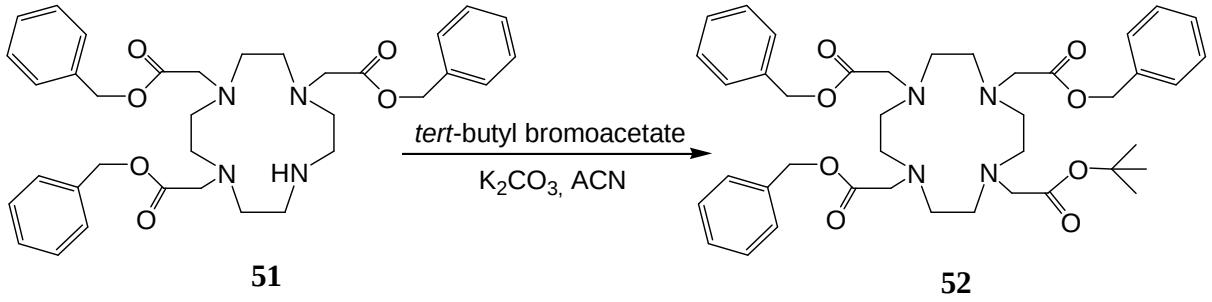

51 **52**

Scheme 14.

The successful synthesis of **52** in 70 % yield could be shown by high resolution mass spectrometry (HR-MS) and by the appearance of a *tert*-butyl hydrogen signal at 1.43 ppm in the ^{1}H NMR spectrum, being in the correct ratio of integrals to the signals in the aromatic region of the spectrum. Finally, deprotection of the *tert*-butyl protected carboxylic acid was achieved by stirring a solution of **52** in TFA:DCM (1:1) for 22 h at room temperature (Scheme 15).

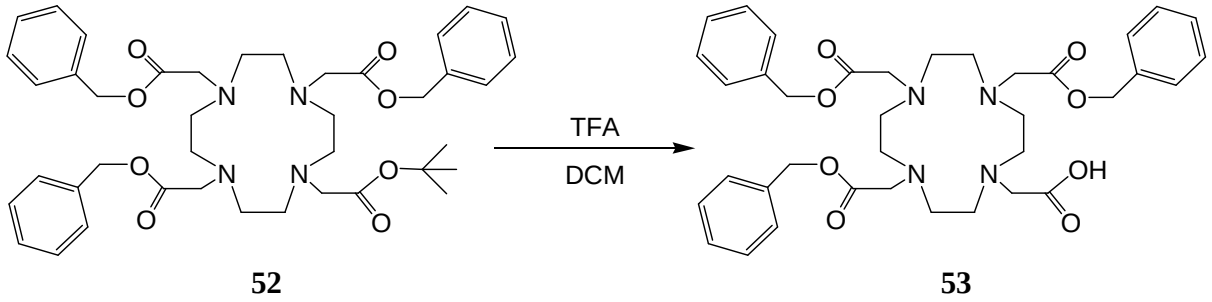

52 **53**

Scheme 15.

The crude product was purified *via* elution from an Amberlite XAD1600 resin column using a water/methanol gradient, however DOTA(Bn)$_3$ (**53**) only eluted at 100 % methanol. **53** was obtained in 43 % yield and was characterised by multidimensional ^{1}H and ^{13}C NMR spectroscopy and ESI-MS.

4.2.3.4 Coupling of DOTA(Bn)$_3$ to octa(3-aminopropyl)silsesquioxane

Analogous to the synthesis described in chapter 4.2.2.2 for the coupling of DOTA(^{t}Bu)$_3$ (**36**), DOTA(Bn)$_3$ (**53**) was attached to octaammonium silsesquioxane **29** by treating **29** with an excess of **53**, TBTU (**38**) and DIPEA in dry DMSO under argon atmosphere and stirring the

mixture for 30 minutes at room temperature (Scheme 16).

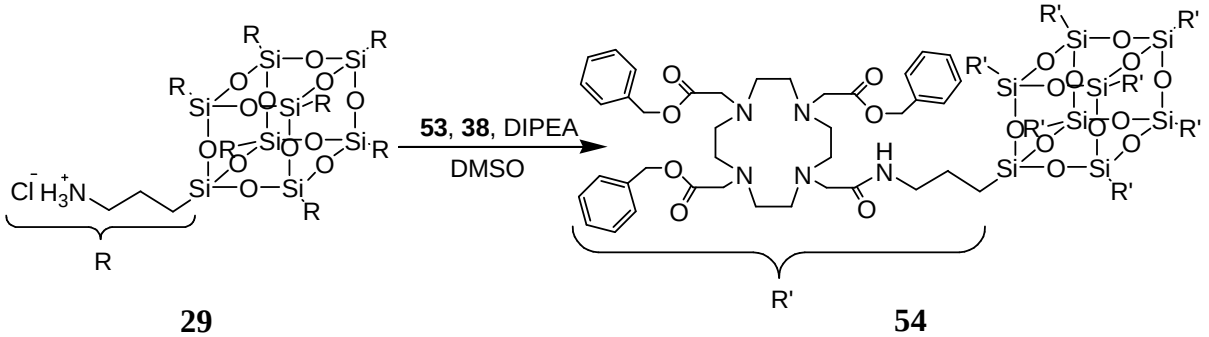

29 **54**

Scheme 16.

Workup afforded a dark yellow solid. The ^{1}H NMR spectrum of a $CDCl_3$ solution of the solid showed the signals of the desired product **54** (Figure 35). However, the spectrum reveals several peaks of residual solvents and TBTU byproducts, and most important the $SiCH_2CH_2$ group shows not only the signal at 1.60 ppm, but also a small signal at 1.79 ppm. The ^{1}H-^{29}Si HSQC NMR spectrum shows that also the signal at 0.59 ppm in the ^{1}H NMR spectrum consists of two resonances, a main peak at 0.58 ppm coupling to a ^{29}Si signal at -67.0 ppm and a small proton signal at 0.63 ppm coupling to a silicon signal at -67.5 ppm.

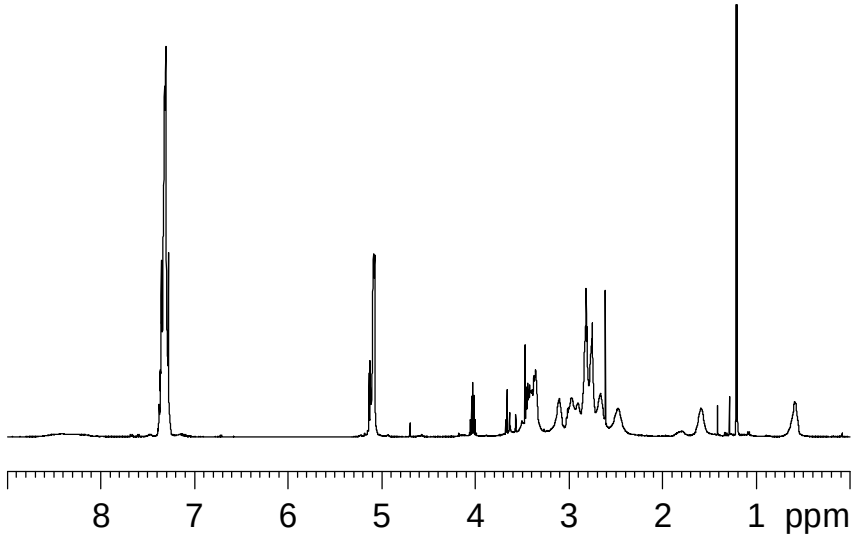

Figure 35. ^{1}H NMR spectrum in $CDCl_3$ of the crude product of the synthesis of **54**.

Since the chemical shifts of the signals further apart from the silsesquioxane core differ stronger, it is more likely that a certain amount of the octaaminopropylsilsesquioxane is not octafunctionalised rather than a degradation of the silsesquioxane cage. The ratio of integration of the signals at 1.60 and 1.79 ppm in the ^{1}H NMR spectrum is about 8:1, indicating mostly incomplete functionalisation. Most likely the excess of ligand was not high enough to achieve full octafunctionalisation in the given time. Nevertheless, it was decided to initially use the obtained product to investigate the possibility of deprotection of these

systems.

4.2.3.5 Cleavage of the benzyl esters

As the obtained dark yellow solid turned out to be insoluble in methanol, the hydrogenolytic cleavage of the benzyl esters was attempted in DMF. The solid was dissolved in dry DMF, Pd/C (10 % Pd) was added and the solvent was degassed. The mixture was stirred under a dihydrogen atmosphere for 2.5 h at room temperature. However, after workup, the residual solid was insoluble in water, but still soluble in $CDCl_3$. As the ^1H NMR spectrum showed no cleavage of the benzyl esters, the reaction was reset in DMF with new catalyst and the mixture was stirred for two days. The ^1H NMR spectrum of the reaction solution (Figure 36) showed only little toluene formation, indicating less than 30 % deprotection. Furthermore, the spectrum revealed the appearance of a new signal at 3.78 ppm, being in the intensity range of the solvent rather than the solutes (integration ratio of 0.5 as compared to the DMF signal at about 8 ppm).

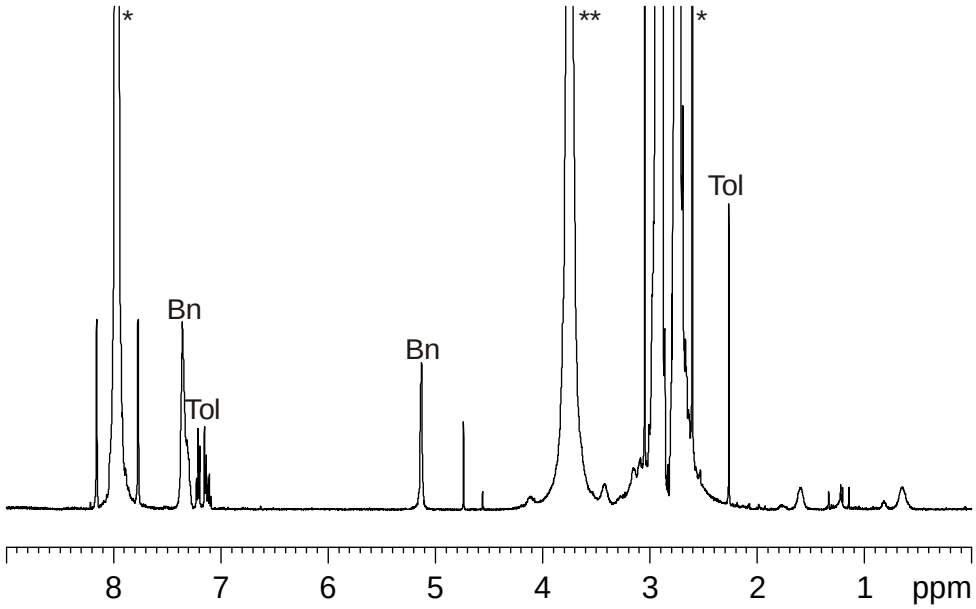

Figure 36. ^1H NMR spectrum of the reaction solution of the attempted deprotection of **54**. The signals of remaining benzyl esters are indicated by "Bn", whereas the resonances of the formed toluene are labelled by "Tol". * DMF. ** most likely dissolved dihydrogen.

The ^1H-^{13}C HSQC NMR spectrum indicates that the hydrogens of this signal are not attached to a carbon and the ^1H-^1H COSY NMR spectrum shows no coupling of the hydrogen nuclei to other hydrogen nuclei. As anhydrous solvent was used, the signal corresponds most likely to dissolved dihydrogen. The small signal appearing at 0.8 ppm might belong to species with a decomposed silsesquioxane cage. As no complete octafunctionalisation was achieved in the previous reaction, free amine groups could destroy the cage as described in chapter 4.2.1.1.

An explanation for the extremely low reaction rates for the deprotection might be the large size of the functionalised silsesquioxane which could prevent a satisfactory interaction with the catalytic centres, leading to slow conversion rates. Even though comparably large amounts of Pd/C were used and the catalyst was renewed, it is also possible that sulphur compounds from residual DMSO poisoned the catalyst, thereby reducing its activity. In order to clarify this, the synthesis of **54** needs to be rerun in DMF using a larger excess of **53**. Then the hydrogenolytic deprotection can be reattempted. However, the results from the simultaneously carried out attachment of La-DO3A-hexylamine (**48**) to octa(3-(ethylmercapto)propionic acid) silsesquioxane (**33**) in chapter 4.2.3.2 pointed out the need of a charge to obtain sufficient water solubility of these highly symmetric systems. For this reason and because the direct introduction of the complexes turned out to be much more convenient, the benzyl protection approach was not pursued further.

4.2.4 Introduction of Charged Macrocyclic Complexes

4.2.4.1 Synthesis of DOTAGA

The easiest way to introduce a charge in those systems is the use of charged complexes. Gd-DOTA (**1**) itself is negatively charged due to the four carboxylate functions complexing the gadolinium(III) ion. However, for the attachment to a silsesquioxane an additional functional group is required. A relatively convenient way is the functionalisation of the methylene group of one of the acetic acids with an additional carboxylic acid. Eisenwiener *et al.* reported the synthesis of DOTAGA(^{t}Bu)$_4$ (1-(1-carboxy- 3-carbo-*tert*-butoxypropyl)-4,7,10-(carbo-*tert*-butoxymethyl)-1,4,7,10-tetraazacyclododecane, **55**) (Figure 37).[134] **55** is an excellent prochelator which can be conjugated to amines and after deprotection and complexation results in a negatively charged monohydrated complex.

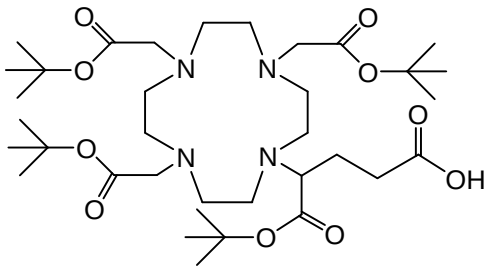

55

Figure 37. Structure of DOTAGA(^{t}Bu)$_4$ (**55**).

Since the complex should be directly attached to the silsesquioxane in this study, the use of orthogonal protecting groups was not required. Therefore a new route for the synthesis of

DOTAGA (1,4,7,10-tetraazacyclododecane-1-glutaric-4,7,10-triacetic acid, **60**) was developed (Scheme 17 and Scheme 18). In the first step glutamic acid (**56**) was converted into 2-bromoglutaric acid (**57**) *via* diazotation analogous to the method described by Holmberg.[135] Following the method by Eisenwiener *et al.*,[134] the crude acid, being about 85 % pure by NMR, was then directly treated with *tert*-butyl trichloroacetimidate (TBTA) in the presence of boron trifuoride ethyl etherate to afford the desired di-*tert*-butyl protected product **58** in about 40 % yield. All steps were characterised by ^{1}H and $^{13}C\{^{1}H\}$ NMR spectroscopy.

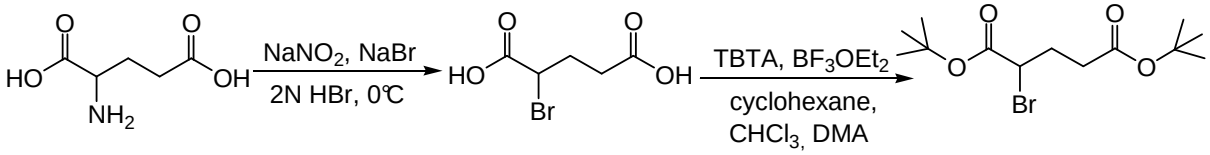

56 **57** **58**

Scheme 17.

The obtained di-*tert*-butyl 2-bromoglutaric acid (**58**) was then used to alkylate the forth ring nitrogen of DO3A(^{t}Bu)$_3$ (**34**) in order to obtain the penta-*tert*-butyl protected DOTAGA(^{t}Bu)$_5$ (**59**). The successful synthesis of **59** in 70 % yield was confirmed by two-dimensional ^{1}H and ^{13}C NMR spectroscopy and HR-MS.

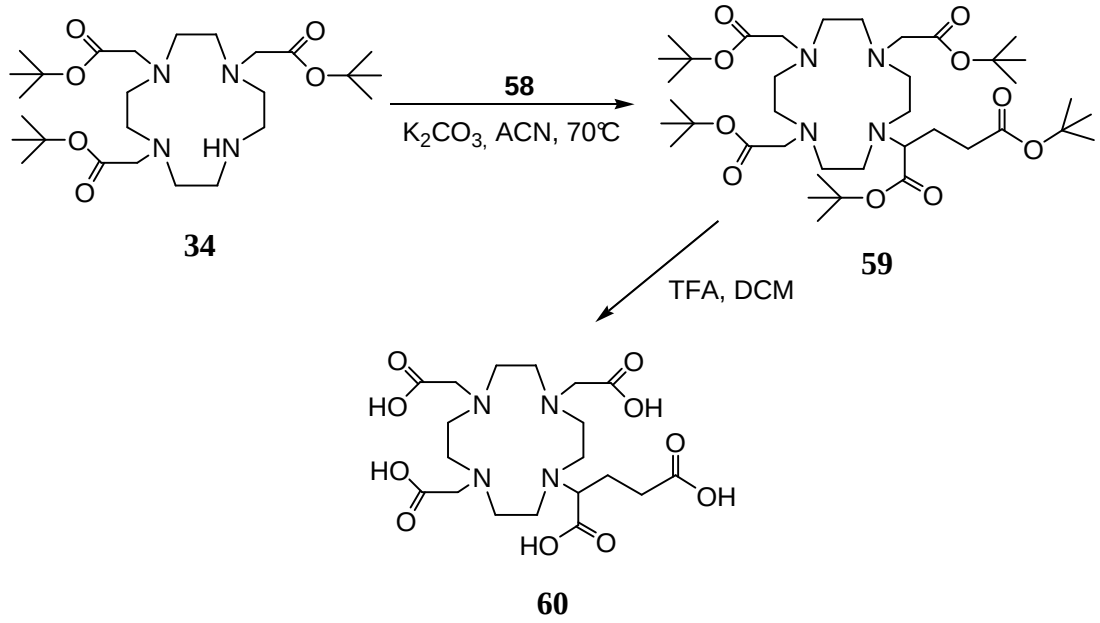

34 **59** **60**

Scheme 18.

Finally, deprotection was accomplished by stirring a solution of **59** in TFA:DCM (3:2) for 23 hours at room temperature. **60** was obtained as an off-white powder, which still contained a small amount of TFA. Rough titrations of the product at about pH 6 with a YCl_3 solution and xylenol orange as the indicator yielded the equivalence point after the addition of about

0.85 equivalents of yttrium(III) referred to the molecular mass of the uncharged structure of **60** as shown in Scheme 18. This corresponds to less than one equivalent TFA per ligand. The yield of complexing species was calculated to be 61 %. As **59**, **60** was characterised by two-dimensional ^{1}H and ^{13}C NMR spectroscopy and HR-MS. Due to their prolonged relaxation times and the coupling to the fluorine atoms the TFA carbons were not visible in the $^{13}C\{^{1}H\}$ NMR spectrum.

Since the protection of **57** as its di-*tert*-butyl ester using the expensive TBTA resulted in only moderate yields and also the deprotection of **59** with TFA was not satisfying, an alternative route for the synthesis of DOTAGA (**60**) was evolved (Scheme 19). Instead of the di-*tert*-butyl ester, the dimethyl ester of **57** was prepared. This could conveniently be accomplished in 75 % yield by treating the crude **57** with catalytic amounts of conc. sulphuric acid in methanol under reflux. The purity of the obtained dimethyl 2-bromoglutaric acid (**61**) was demonstrated by ^{1}H and $^{13}C\{^{1}H\}$ NMR spectroscopy as well as by elemental analysis.

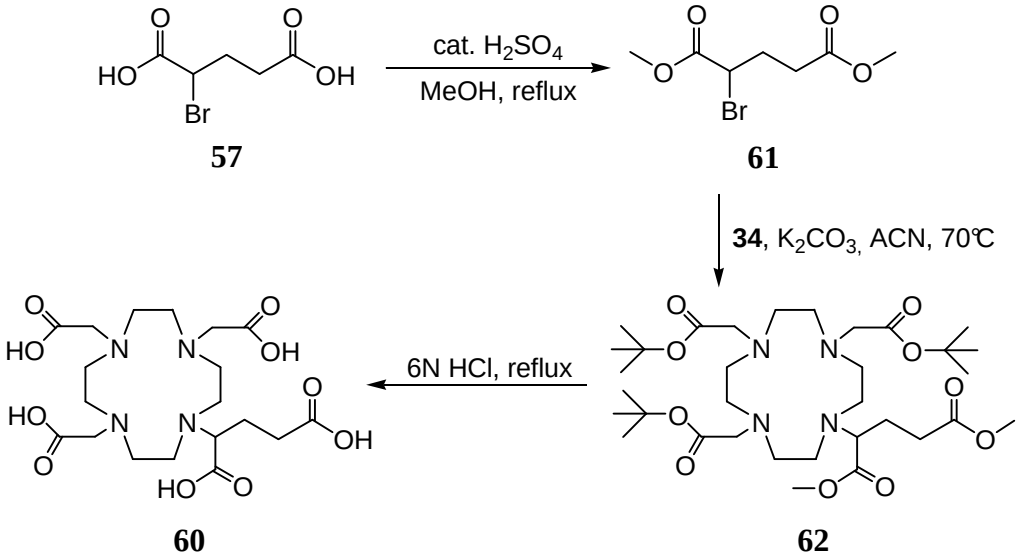

Scheme 19.

In analogy to the synthesis of DOTAGA(^{t}Bu)$_5$ (**59**), DOTAGA(^{t}Bu)$_3$(Me)$_2$ (**62**) was obtained by alkylation of DO3A(^{t}Bu)$_3$ (**34**) with **61** in the presence of a base. The successful synthesis of **62** in 71 % yield was also confirmed by two-dimensional ^{1}H and ^{13}C NMR spectroscopy and HR-MS. Complete deprotection of the ligand was achieved in excellent yield (about 92 %) by refluxing its aqueous 6 N hydrochloric acid solution overnight. Following this route, **60** was isolated as its ammonium chloride salt. Rough titration indicated also in this case the molecular mass of the uncharged structure of **60** to be 85 % of that of the obtained product. This would roughly correspond to DOTAGA·2.5HCl for the obtained product, however, as the product is slightly hygroscopic, some water can also contribute to the increased molecular

mass. Organic impurities are not possible as the ^{1}H and ^{13}C NMR spectra in D_2O contained only signals of the desired product. Furthermore, both NMR spectroscopy and mass spectrometry data were in agreement with that obtained for **60** prepared by the other route.

4.2.4.2 Synthesis of Gadoxane G

Prior to attachment, the lanthanide complexes of **60** needed to be prepared. Therefore an aqueous solution of **60** was treated with aqueous solutions of $LnCl_3$ (Ln = Gd^{3+}, Y^{3+}) while adjusting the pH to 6-7 using hydroxide as base (Scheme 20). Since the complexes are negatively charged, the counter ions have a large influence on the solubility of the systems. To increase the solubility in non-aqueous solvents as required for the following grafting to the silsesquioxane, tetra-*n*-butylammonium hydroxide was used as base. When the complexes were required for analytical studies and not for the attachment to silsesquioxanes, tetra-*n*-butylammonium hydroxide was replaced by sodium hydroxide. Complete complexation was achieved by stirring the solutions for several hours at increased temperature. The solvent of the reaction mixture was then removed under reduced pressure and the residue was kept *in vacuo* for four to six days in order to remove most of the remaining water.

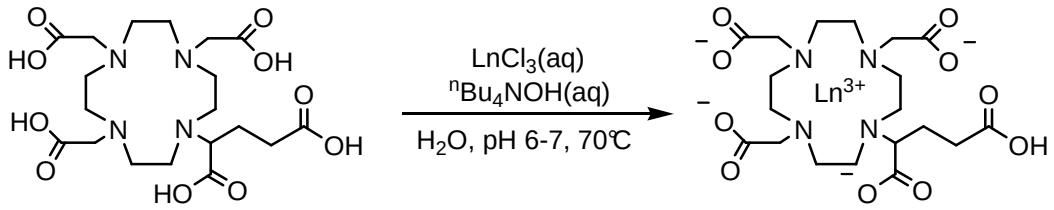

60 **63**

Scheme 20.

The covalent binding of **63** to octa(3-chloroammoniumpropyl)silsesquioxane (**29**) was achieved as for the other systems described above. The silsesquioxane was treated with an excess of the respective complex **63**, TBTU (**38**) and DIPEA in dry DMSO. The tetra-*n*-butylammonium salt of **63** is fairly soluble in DMSO, however the process is relatively slow. Once **63** is dissolved, the coupling to the silsesquioxane can be achieved quantitatively within several minutes. The reaction was quenched after 30 minutes by adding the reaction mixture to a strongly diluted acetic acid/sodium acetate buffer (pH 5.5). This time no precipitation was observed.

Purification of the product was achieved *via* diafiltration using a membrane with a molecular weight cutoff of 3 K. Additionally to the separation of small molecules from larger molecules, diafiltration allows the exchange of counter ions. By using a sodium chloride solution in one step of the filtration process the tetra-*n*-butylammonium counter ion was fully replaced by

sodium to afford Gadoxane G (**GG**) (Figure 38) as its octasodium salt in about 37 % yield. As the obtained white solid can contain residual sodium chloride, the yield was determined by measuring the gadolinium(III) concentration in a known volume using the BMS method (see chapter 5.2.7.2). The yield can be improved by using a smaller cutoff, however, this goes at the expense of purity.

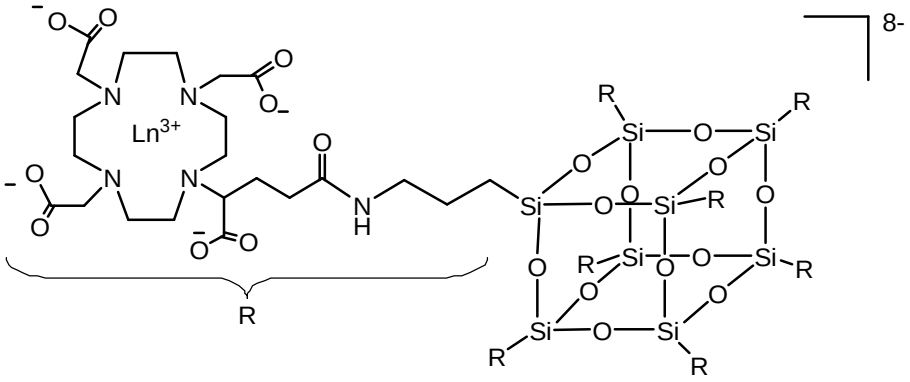

GG

Figure 38. Structure of Gadoxane G (**GG**).

GG was characterised on the basis of its yttrium(III) complex by HR-MS as well as multinuclear (^{1}H, ^{13}C, ^{29}Si) NMR spectroscopy. The absence of non-coordinated lanthanide(III) ions was confirmed by the xylenol test.[136] The HR mass spectrum of the yttrium(III) complex (M = 5228.2 g/mol) is shown in Figure 39.

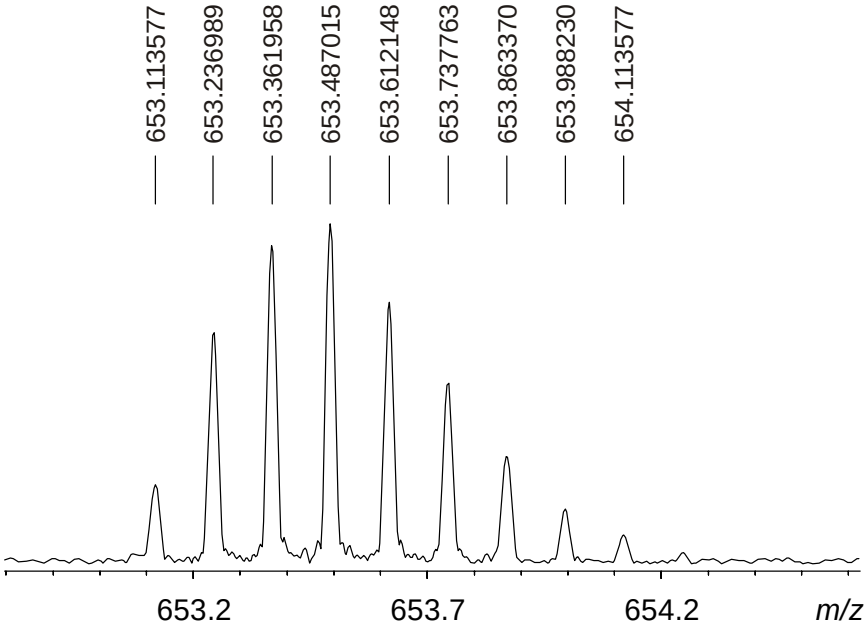

Figure 39. HR-MS of the yttrium(III) complex of Gadoxane G (**GG**) $[M]^{8-}$.

The characteristic isotope pattern of the eight-times negatively charged $[M]^{8-}$ ion was well resolved and the *m/z* was determined to be 653.487015 (theor.: 653.487060). No signals

corresponding to less than eight-times substituted silsesquioxanes, partly hydrolysed or free Y-DOTAGA were detected. This shows that pure **GG** can be synthesised with an intact silsesquioxane core by this method. Furthermore, no hydrolysis products were observed in samples which were stored at -28°C for more than 10 months.

The NMR spectra were measured in D_2O at 25°C and pD 7.0. The ^{1}H NMR spectrum is depicted in Figure 40. A complete assignment of the ^{1}H and ^{13}C NMR resonances to the structure of **GG** was achieved using two dimensional techniques. To reduce the acquisition time the ^{29}Si NMR spectrum was also recorded *via* a 2D ^{1}H-^{29}Si HSQC experiment. It shows only one ^{29}Si signal at -65.3 ppm which is again owed to the cubic symmetry of the undamaged silsesquioxane core.

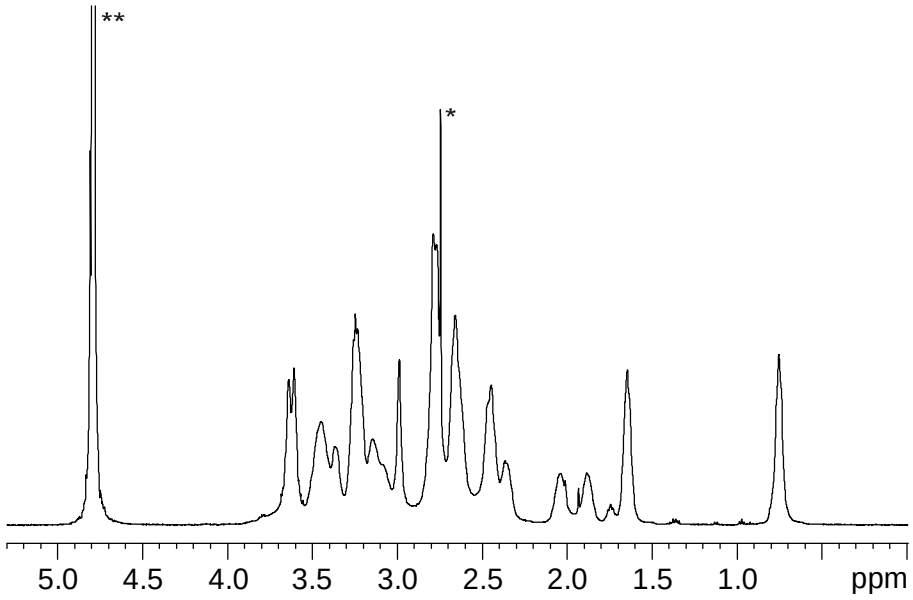

Figure 40. ^{1}H NMR spectrum of the yttrium(III) complex of Gadoxane G (**GG**) in D_2O (pD 7.0). *DMSO, **solvent residual peak.

4.2.4.3 Synthesis of DOTAMA and DOTABA

In order to synthesise derivatives of **GG** which posses a further reduced internal flexibility and therefore show little anisotropic local rotational motion (cf. chapter 4.1.1.1), two novel bifunctional ligands were designed (Figure 41).

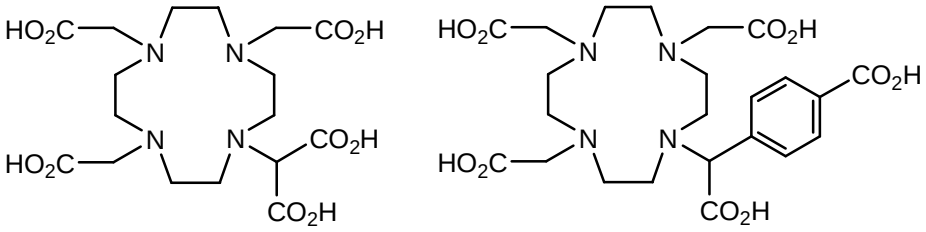

64 **65**

Figure 41. Structures of DOTAMA (**64**) and DOTABA (**65**).

Instead *via* an ethyl spacer as in DOTAGA (**60**) the additional carboxylate group is directly attached to the DOTA moiety in the case of DOTAMA (1,4,7,10-tetraazacyclododecane-1-malonic-4,7,10-triacetic acid, **64**) and *via* a phenyl ring in the case of DOTABA (1,4,7,10-tetraazacyclododecane-1-(4-(carboxymethyl)benzoic)-4,7,10-triacetic acid, **65**).

In analogy to the synthesis of DOTAGA (**60**), the synthetic strategy for both novel ligands implies the alkylation of the secondary nitrogen of DO3A(^{t}Bu)$_3$ (**34**) by an appropriate protected 2-bromodicarboxylic acid.

Dimethyl 2-bromomalonate (**67**), for the synthesis of **64**, was prepared in one step from dimethyl malonate (**66**) *via* radical bromination analogously to the method of Palmer and McWherter[137] (Scheme 21). Repeated distillation under reduced pressure afforded **67** in 45 % yield. Due to its ^{1}H NMR spectrum the final product was 98 % pure with 2 % of unreacted **66**.

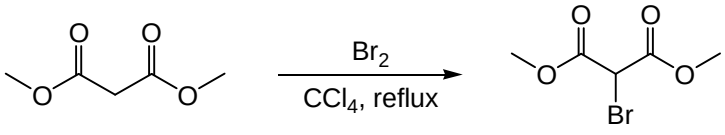

66 **67**

Scheme 21.

For the synthesis of DOTABA (**65**), methyl 4-((methoxycarbonyl)bromomethyl)benzoate (**71**) was synthesised in three steps from the commercially available methyl 4-(cyanomethyl)-benzoate (**68**) (Scheme 22).

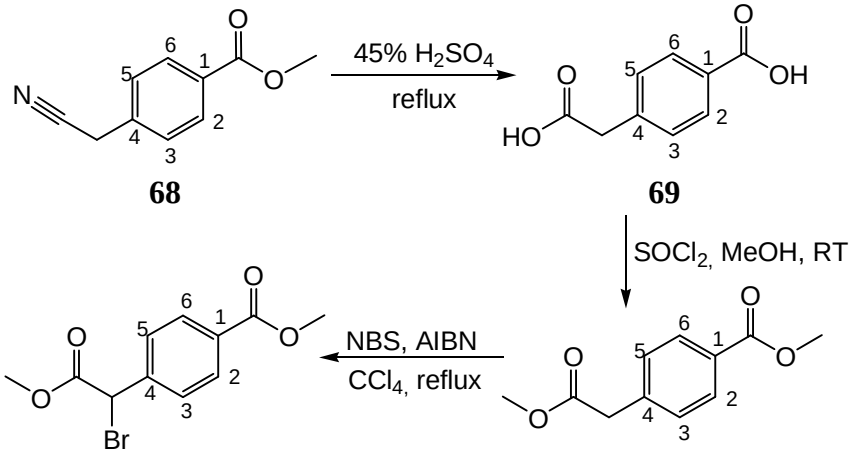

68 **69** **70** **71**

Scheme 22.

Following the procedure of Schaper *et al.*,[138] **68** was hydrolysed to afford 4-(carboxymethyl)benzoic acid (**69**) in 84 % yield. Protection of the acid groups using thionyl chloride in methanol gave the dimethyl ester (**70**) in 95 % yield. The bottle neck of this route

was the bromination of **70**. When **70** was refluxed with *N*-bromosuccinimide (NBS) and catalytical amounts of AIBN in carbon tetrachloride for five hours the conversion was only about 49 % due to ^{1}H NMR spectroscopy. Readdition of AIBN and additional 17 hours heating to reflux were necessary to achieve at least 73 % conversion. Interestingly, much poorer conversion was obtained if the reaction time was directly prolonged to 24 hours. As a complete separation of **71** from unreacted **70** by column chromatography proofed unsuccessful, pure **71** could be obtained in only 48 % yield. All steps were characterised by ^{1}H and ^{13}C{^{1}H} NMR spectroscopy. The purity of **71** was additionally shown by elemental analysis.

DO3A(^{t}Bu)$_3$ (**34)** was then treated with the two obtained dimethyl 2-bromodicarboxylates **67** or **71** in the presence of a base, to afford **72** and **73** as the protected forms of DOTAMA and DOTABA, respectively (Scheme 23). Both alkylations could be carried out in excellent yields of 84 % and 86 % for **72** and **73**, respectively. The yield of the analogous alkylation reactions in the syntheses of DOTAGA (**60**) were with 70 % and 71 % significantly lower. This might be explained by possible eliminations as side reactions in these cases, whereas this is impossible in the synthesis of **72** and **73**. **72** and **73** were both characterised by two-dimensional ^{1}H and ^{13}C NMR spectroscopy and HR-MS. Noteworthy is the hindered rotation of the dimethyl malonate moiety of **72** leading to two distinct signals (52.4 and 52.7 ppm) for the methyl groups in the ^{13}C{^{1}H} NMR spectrum.

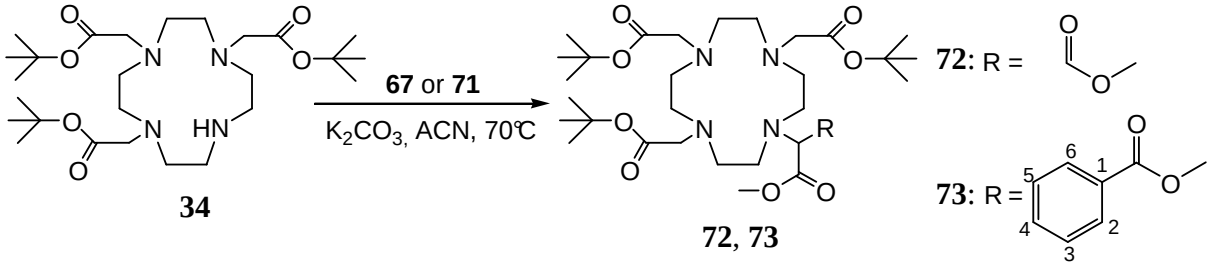

Scheme 23.

The deprotection of **74** was carried out analogously to that of DOTAGA(^{t}Bu)$_3$(Me)$_2$ (**62**) by refluxing its aqueous 6 N hydrochloric acid solution overnight (Scheme 24). The successful synthesis of **74** in 90 % yield was confirmed by two-dimensional ^{1}H and ^{13}C NMR spectroscopy and HR-MS. The ligand was again obtained as its ammonium chloride salt and rough titration of the product at about pH 6 with a YCl_3 solution and xylenol orange as the indicator, showed also in this case the molecular mass of the uncharged structure of **65** to be 85 % of that of the obtained product. This would correspond to about three HCl molecules per ligand. However, also for this ligand the additional inclusion of water molecules is more

likely than a triammonium salt as only about six equivalents of base were necessary in the following complexation reaction to neutralise the solution of the forming complex.

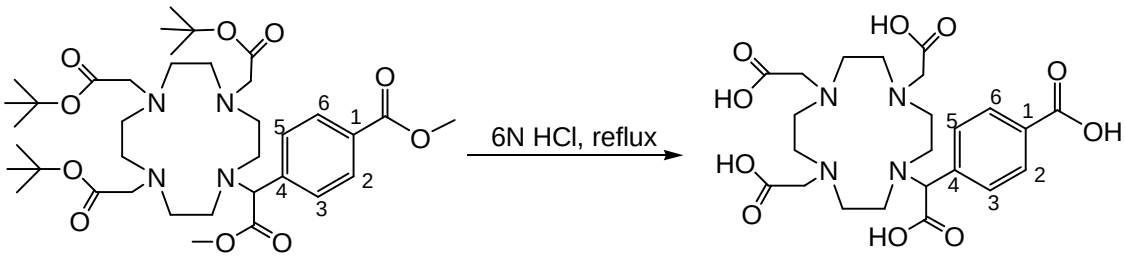

73 **65**

Scheme 24.

In the case of DOTAMA(^{t}Bu)$_3$(Me)$_2$ (**72**) deprotection of the malonic acid moiety under acetic conditions is not possible due to the instability of malonic acid derivatives at low pH. Therefore **72** was deprotected in two steps (Scheme 25). In the first step the *tert*-butyl esters were cleaved by stirring **72** in TFA:DCM (1:1) for 20 hours at room temperature. The cleavage was demonstrated by HR-MS and by the disappearance of the *tert*-butyl signals in the ^{1}H and ^{13}C{^{1}H} NMR spectra. The signals of the methyl groups remain in both spectra, however, now also the ^{13}C{^{1}H} spectrum shows only one resonance for the methyl groups indicating free rotation of the dimethyl malonate moiety after removal of the bulky *tert*-butyl groups.

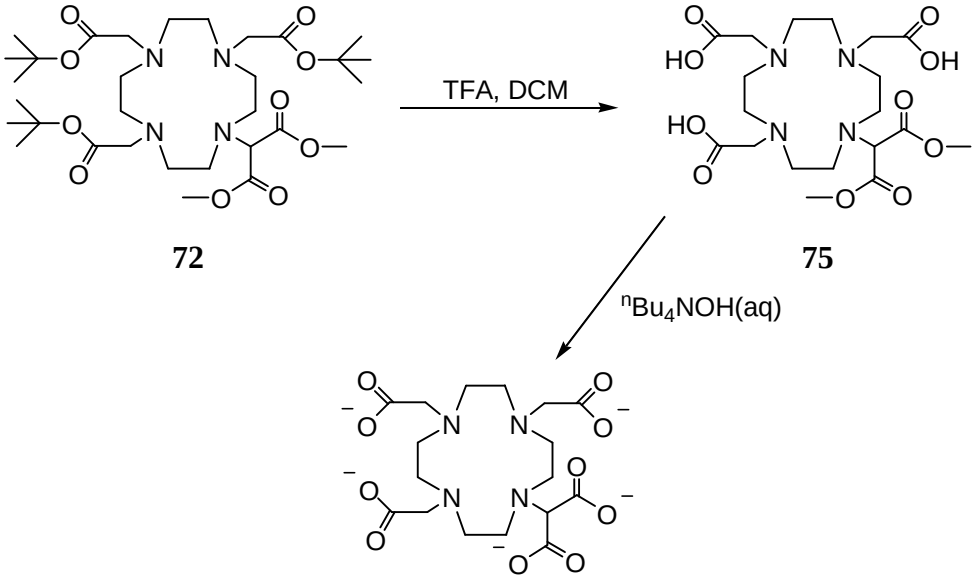

72 **75** **64***

Scheme 25.

The deprotection of the malonic acid moiety was accomplished by stirring **75** in an alkaline aqueous solution for one day. When the obtained deprotected and deprotonated

DOTAMA (**64***) was intended for the attachment of its complexes to a silsesquioxane, tetra-*n*-butylammonium hydroxide was used as base, whereas when it was scheduled for the characterisation of **64*** and its lanthanide complexes lithium hydroxide or sodium hydroxide was used. All three methods resulted in the fully deprotected **64*** as was shown by two-dimensional ^{1}H and ^{13}C NMR spectroscopy.

4.2.4.4 Coupling of DOTAMA complexes to the silsesquioxane

The complex formation of DOTAMA (**64***) and the lanthanide(III) was carried out by treating the respective aqueous solution of **64*** with an aqueous solution of $LnCl_3$ (Ln = Gd^{3+}, Y^{3+}). Upon the addition of the lanthanide(III) chloride solution the pH dropped from about 13 to 7.2±0.1 and a light precipitate was formed, independently of the counter ion. The precipitate is most likely lanthanide(III) hydroxide. After stirring overnight at room temperature, the precipitate had redissolved. Prior to coupling the complexes **76** to the octa(3-chloroammoniumpropyl)silsesquioxane (**29**), the solvent of the reaction mixture was removed under reduced pressure and the residue was kept *in vacuo* for two days in order to remove most of the remaining water. The successful complexation was shown by HR-MS on the basis of the gadolinium(III) complex having sodium as the counter ion.

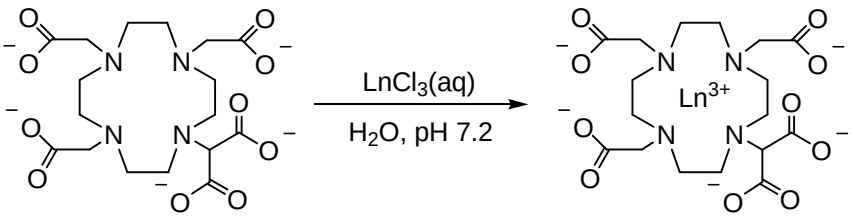

64* **76**

Scheme 26.

In a first attempt to couple **76** as its yttrium(III) complex to the silsesquioxane **29**, the synthesis was performed in the same manner as for the preparation Gadoxane G (**GG**). Once **76** was dissolved in dry DMSO, a DMSO solution of **29** and TBTU (**38**) as well as DIPEA were added under argon atmosphere. The reaction was quenched after 30 minutes by adding the reaction mixture to a strongly diluted acetic acid/sodium acetate buffer (pH 5.5). In order to purify the desired product, diafiltration with a 3 K molecular weight cutoff membrane was performed. Unfortunately after removal of the solvent, no product was obtained. In order to investigate why no product was obtained, the reaction was reattempted using dry DMSO-d6. Interestingly, the ^{1}H-^{1}H COSY NMR spectrum measured after 15 minutes showed the characteristic change in the chemical shift from 2.75 ppm to 3.09 ppm for the

$SiCH_2CH_2CH_2N$ group (see chapter 4.2.2.2 or ref. 127) indicating the completeness of the reaction. Therefore, the reaction was quenched after 40 minutes. However, workup afforded again no product. If a complete octafunctionalisation was really achieved, the product must have decomposed during diafiltration. In the octafunctionalised product (**77**, Figure 42) of this reaction, the hydrophilic lanthanide complexes are closer to the silsesquioxane core than in the case of **GG**. Therefore a hydrolytic cleavage of Si-O-Si bonds might occur significantly faster and thereby preventing the isolation of **77**.

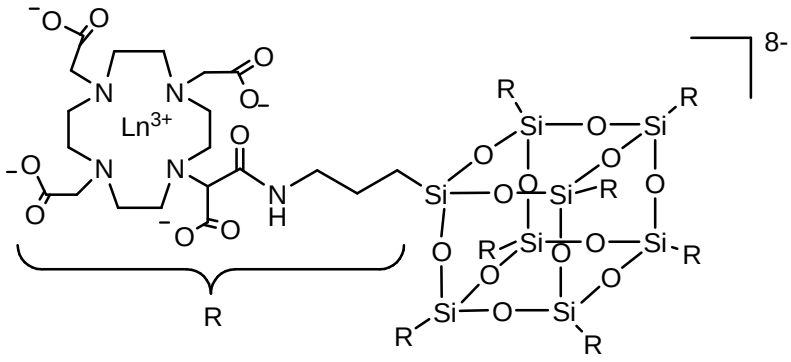

77

Figure 42. Structure of the desired coupling product of Ln-DOTAMA (**76**) and octa(3-chloroammoniumpropyl)silsesquioxane (**29**).

4.2.4.5 Synthesis of Gadoxane B

The lanthanide complexes of DOTABA (**65**) were also prepared by treating aqueous solutions of **65** with aqueous solutions of $LnCl_3$ (Ln = Gd^{3+}, Y^{3+}) while adjusting the pH to 6-7 (Scheme 27). When the complex **78** was intended for the attachment to the silsesquioxane **29**, again tetra-*n*-butylammonium hydroxide was used as base, otherwise sodium hydroxide was used. Complete complexation was achieved by stirring the solutions for several hours at increased temperature.

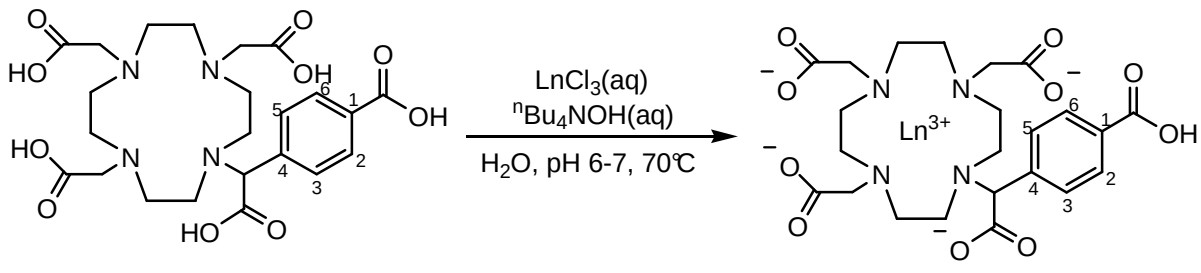

65 **78**

Scheme 27.

The solubility of the $^nBu_4N[Ln(DOTABA)H_2O]$ complex in water turned out to be extremely

low, leading to a white precipitate once the complex has formed. With sodium as the counter ion the solubility of **78** is significantly higher, but still low compared to the complexes of DOTAGA (**60**) and DOTAMA (**64**). Nevertheless, the solvent of the respective reaction mixture was removed under reduced pressure after this time and the residue was kept *in vacuo* for four to six days in order to remove most of the remaining water.

Despite the use of tetra-*n*-butylammonium as the counter ion, **78** is only poorly soluble also in DMSO. The residue was taken up in a significantly larger amount of dry DMSO than in the case of the other two systems, still a suspension remained after stirring for two days. Nevertheless, a DMSO solution of **29** and TBTU (**38**) as well as DIPEA were added. As the reaction had to be carried out in suspension, the reaction time was prolonged to three hours. The reaction was then quenched by adding the reaction mixture to the diluted acetic acid/sodium acetate buffer (pH 5.5). Upon addition the suspension dissolved. This allowed the purification of the product *via* diafiltration (3K membrane). During the filtration process the tetra-*n*-butylammonium counter ion was again fully replaced by sodium ions. In contrast to the coupling of Ln-DOTAMA (**76**), the octafunctionalised Gasdoxane B (**GB**) (Figure 43) could be isolated in about 30 % yield. Again the gadolium(III) concentration was determined by the BMS method (see chapter 5.2.7.2) in order to calculate the yield. The absence of non-coordinated lanthanide(III) ions was confirmed by the xylenol test.[136]

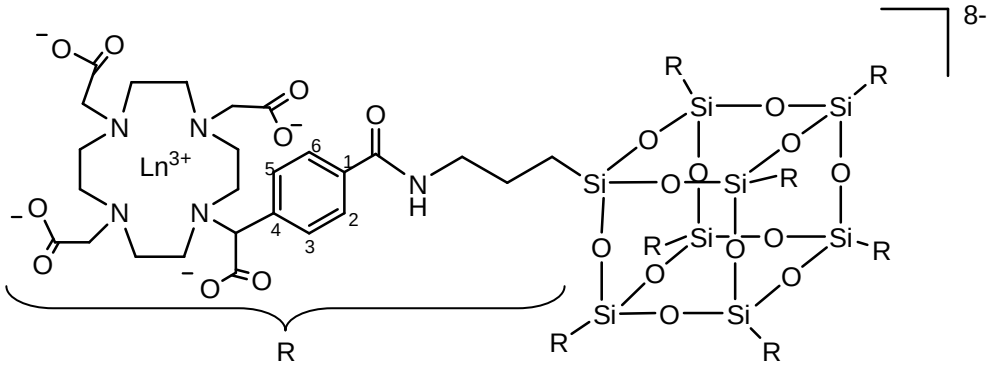

GB

Figure 43. Structure of Gadoxane B (**GB**).

Gadoxane B (**GB)** was characterised by multinuclear (^{1}H, ^{13}C, ^{29}Si) NMR spectroscopy on the basis of its yttrium(III) complex and by HR-MS using the gadolinium(III) complex. The HR mass spectrum of the gadolinium(III) complex (M = 6159.3 g/mol) is shown in Figure 44. The characteristic isotope pattern of the eight-times negatively charged $[M]^{8-}$ ion was well resolved and the *m/z* was determined to be 769.881065 (theor.: 769.880308). No signals corresponding to less than eight-times substituted silsesquioxanes, partly hydrolysed or free

Y-DOTABA were detected, showing that pure **GB** can be synthesised with an intact silsesquioxane core by this method.

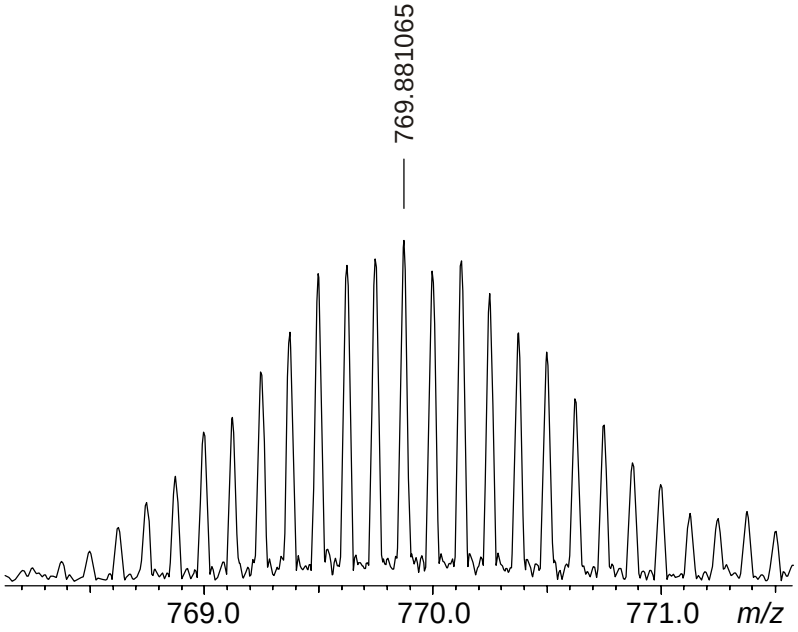

Figure 44. HR-MS of the gadolinium(III) complex of Gadoxane B (**GB**) $[M]^{8-}$.

The NMR spectra were measured in D_2O at 25°C and pD 7.0. The ^{1}H NMR spectrum is depicted in Figure 45. Again two dimensional techniques were used to achieve a complete assignment of the ^{1}H and ^{13}C NMR resonances to the structure of **GB**. Furthermore, the ^{29}Si NMR spectrum shows only one signal at -65.4 ppm due to the cubic symmetry of the undamaged silsesquioxane core.

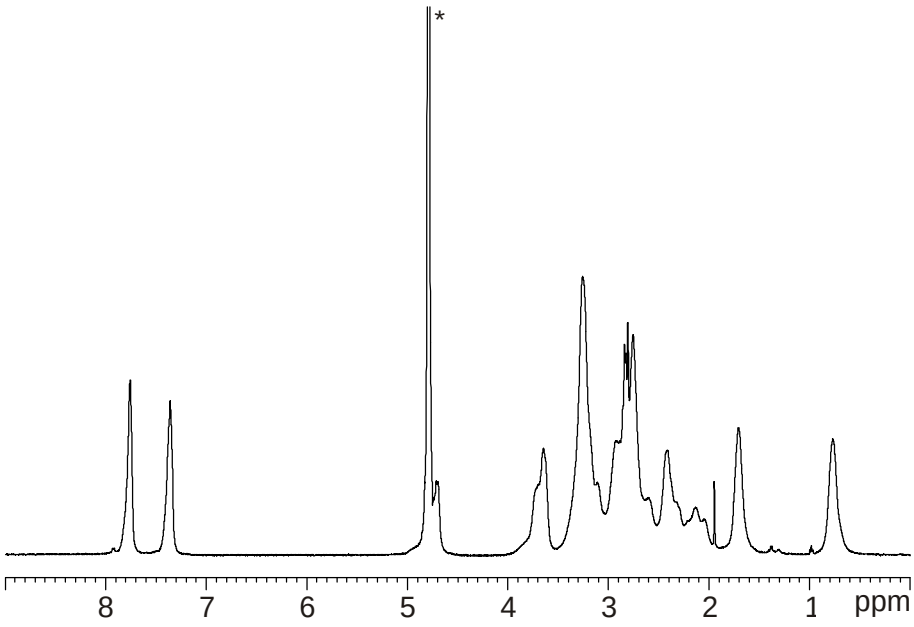

Figure 45. ^{1}H NMR spectrum of the yttrium(III) complex of Gadoxane B (**GB**) in D_2O (pD 7.0). *solvent residual peak.

4.2.5 The Molecular Size of Gadoxane G and B

The importance of the molecular size of a CA was already pointed out in chapter 4.1.1.1 and 4.1.3. The size of the CA is not only related to the rotational correlation time τ_R, it also influences the distribution of the CA within the body and its excretion rate. As described in chapter 3.2.3, PGSE diffusion ^{1}H NMR spectroscopy is a powerful tool in determining the size and also the rotational correlation time of very small to extremely big molecules.[75, 76, 78] Using PGSE NMR spectroscopy, the translational self-diffusion coefficients D of the yttrium(III) complexes of **GG** and **GB** as well as of their corresponding monomeric complexes **63** and **78** were determined at 25°C. For spherical molecules, like the Gadoxanes and in good approximation also the monomers, the Stokes-Einstein equation (equation 3.1 in chapter 3.2.3) is valid and allows the calculation of reliable hydrodynamic radii r_H. From r_H the rotational correlation time τ_{RDiff} can be calculated applying equation 3.2 (chapter 3.2.3) and the hydrodynamic volume V_H is obtained using equation 4.2:

$$V_H = \frac{4}{3}\pi r_H^3 \tag{4.2}$$

As strongly diluted samples (2-3 mM of the Gadoxanes and 15-20 mM for the monomers) were used, r_H, V_H and τ_{RDiff} could be calculated from the diffusion constants assuming $\eta_{\text{solution}} = \eta_{\text{solvent}}$ (Table 6).[139]

Table 6. Translational diffusion coefficient D and resultant hydrodynamic radius r_H, hydrodynamic volume V_H, and rotational correlation time τ_{RDiff} at 25°C of **GG**, **GB**, Y-DOTAGA (**63**) and Y-DOTABA (**78**).

Compound	D [m^2/s]	r_H [nm]	V_H [nm^3]	τ_{RDiff} [ps]
Gadoxane G (**GG**)	(1.373±8)x10^{-10}	1.442±0.008	12.56±0.22	3370±60
Gadoxane B (**GB**)	(1.379±7)x10^{-10}	1.436±0.007	12.40±0.19	3320±50
Y-DOTAGA (**63**)	(3.976±9)x10^{-10}	0.499±0.001	0.52±0.00	139±1
Y-DOTABA (**78**)	(3.625±8)x10^{-10}	0.547±0.001	0.68±0.01	183±1

Evaluation of the diffusion data revealed almost identical hydrodynamic radii for **GG** and **GB** (about 1.44 nm), showing that the different linkers have no net effect on the size of the CAs. By contrast, in the case of the monomers, the replacement of the ethylene spacer by a phenyl ring leads to a significant increase in the hydrodynamic volume V_H of about 30 % (0.52 nm^3 and 0.68 nm^3 for Y-DOTAGA and Y-DOTABA, respectively). With hydrodynamic volumes of 12.56 nm^3 and 12.40 nm^3 the two Gadoxanes are thereby about 20-times larger than their respective monomers. This should result in a significantly increase in relaxivity, especially at

field strength currently used in clinical MRI (see chapter 4.1.3).

Furthermore, the Gadoxanes are still considerably smaller than the small pores (r = 3-5 nm) of the glomerular filter in the kidneys (see chapter 4.1.1.1), which should allow a sufficiently fast clearance of the Gadoxanes from the body.

4.2.6 The Stability of the Silsesquioxane Cage in Aqueous Media

Silsesquioxanes are formed in a condensation reaction, therefore hydrolysis, being the reverse reaction, can be an issue in aqueous media. It has been reported that degradation of the silsesquioxane cage occurs in wet organic solvents in the presence of amine bases,[124] which could be confirmed in this study (see chapter 4.2.2.2). However, as most of the so far reported silsesquioxanes are insoluble in water, not many data are available on their hydrolysis in aqueous media. Feher *et al.*[124] referred the stability of octa(3-chloroammonium-propyl)silsesquioxane (**29**) to be very high in neutral or acidic solutions, though no quantitative data were given. On the other hand, they reported the appearance of a prominent new set of resonances in the ^{29}Si NMR spectrum of an alkaline D_2O solution (pH 9) of **29** ten minutes after preparation. These resonances, which grow at the expense of the resonance for **29**, are believed to belong to a silsesquioxane cage, in which one Si-O-Si bond is cleaved. Attempts to achieve higher conversion then led to complete decomposition of the cage.

4.2.6.1 Time-dependent ^{29}Si NMR measurements

In order to investigate the stability of the silsesquioxane cage of the Gadoxanes towards hydrolysis, initially ^{29}Si NMR spectra of an aqueous solution (pD 7.0) of the yttrium(III) complex of Gadoxane G (**GG**) were measured at 25°C as a function of time. To reduce the acquisition time the ^{29}Si NMR spectra were recorded *via* a 2D ^{1}H-^{29}Si HSQC experiment. The ^{29}Si projections are depicted in Figure 46. The spectrum measured directly after preparation of the solution shows, as already mentioned in chapter 4.2.4.2, only one signal in the typical range of T^3 groups[120] at -65.3 ppm, being owed to the cubic symmetry of the undamaged silsesquioxane core (trace 0 d). The solution was then kept at 25°C for two weeks during which further ^{1}H-^{29}Si HSQC NMR spectra were recorded. The intensity of the resonance at -65.3 ppm slowly decreased during this period of time, clearly indicating the hydrolysis of the silsesquioxane. This leads to various T^n (n = 1-3) species with much lower symmetry which generate numerous magnetically inequivalent ^{29}Si nuclei in poor concentrations circumventing their detection in a reasonable time.

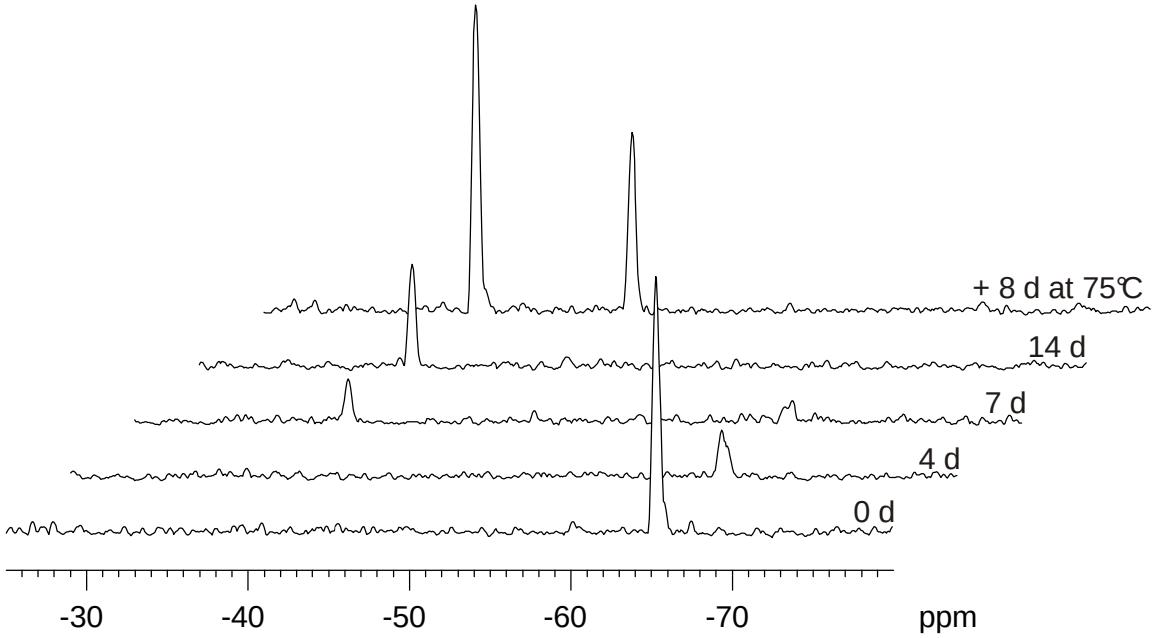

Figure 46. ^{29}Si projections of ^{1}H-^{29}Si HSQC NMR spectra of the yttrium(III) complex of **GG** after 0 d, 4 d, 7 d, 14 d at 25°C (pD 7.0) and after additional 8 days at 75°C.

After seven days a new signal appeared at -38.2 ppm which is in the range of T^0 groups[140] and thus is assigned to the fully hydrolysed species **80** (Scheme 28). After 14 days the intensity of this peak had further increased and a very small signal at -47.9 ppm could also be observed. As this resonance is in the range for T^1 groups, it is assigned to the $(OH)_2RSi\text{-}O\text{-}SiR(OH)_2$ fragment (**81**) (Scheme 28). To achieve complete hydrolysis, after 14 days at 25°C the solution was heated to 75°C. In a spectrum measured after two days the signal due to **81** had not vanished, but on the contrary, the intensities of both **80** and **81** strongly increased. The ratio between them remained unchanged even after the solution was kept at 75°C for additional six days, suggesting an equilibrium between the two species, **80** and **81**.

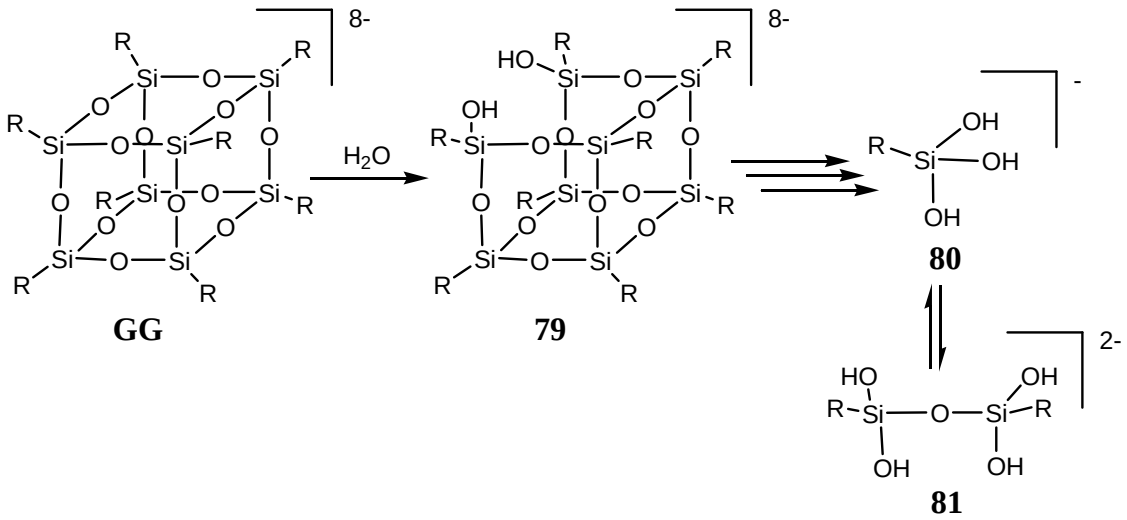

Scheme 28.

4.2.6.2 Time-dependent PGSE diffusion ^{1}H NMR spectroscopy

Simultaneously to the ^{29}Si NMR measurements, the same solution was also used to determine the translational self-diffusion coefficient *D* of Gadoxane G (**GG)** and of its fragments by PGSE diffusion ^{1}H NMR spectroscopy at 25°C (Figure 47). All fragments are measured with the same sensitivity than the undamaged species which makes PGSE NMR ideal for following decomposition processes. However, as the signals of **GG** and its fragments could not be separated in the proton NMR spectra, only an average diffusion coefficient of all species was obtained during decomposition of **GG**.

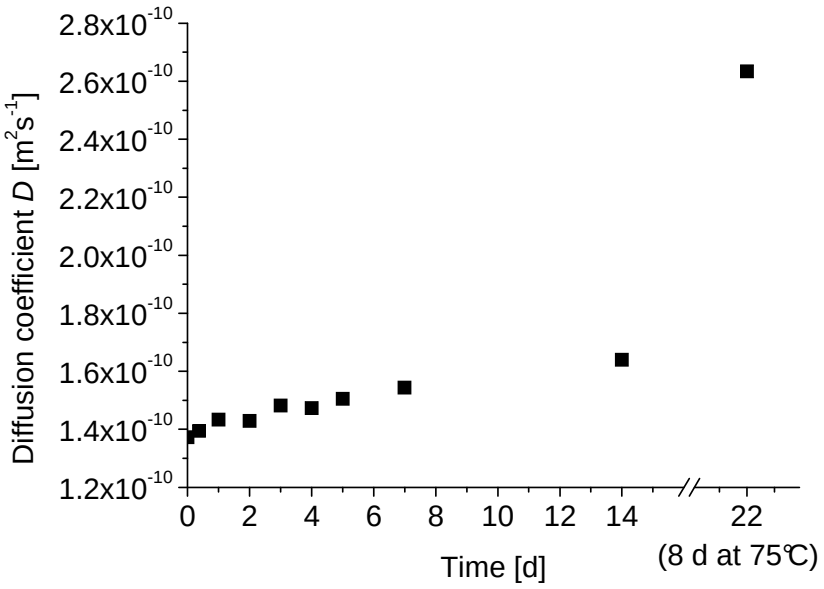

Figure 47. Average translational diffusion coefficient *D* of Gadoxane G (**GG**) and its fragments at 25°C (pD 7.0) as a function of time.

The sample was strongly diluted (the initial concentration of Gadoxane was about 2-3 mM), therefore r_H, V_H and τ_R were again calculated from the diffusion constants assuming $\eta_{solution} = \eta_{solvent}$ (Table 7).[139] For comparison, the data of Y-DOTAGA (**63**) is also included in the table. As already reported in chapter 4.2.5, 1.37×10^{-10} m^2s^{-1} was obtained for the diffusion coefficient of the undamaged **GG** (Time = 0). The average diffusion coefficient of **GG** and its fragments then slowly increased with time (Figure 47 and Table 7). As not all fragments are supposed to be spherical, the Stokes-Einstein equation is in this case not generally valid and therefore the resulting average values of r_H, V_H and τ_R during decomposition (Table 7) can only be considered as approximations. It is still conspicuous that after 14 days the average V_H had only decreased to about half the value of the undamaged Gadoxane. Although the corresponding ^{29}Si NMR spectrum showed no resonances due to T^3 and T^2 groups after that time, this points out that a considerable amount of only partly degraded species still remains

under these conditions. Heating the solution to 75°C for additional eight days then changed *D* significantly, showing that higher temperatures are necessary to obtain mostly small fragments at neutral pH within a reasonable time.

Table 7. Translational diffusion coefficient *D*, hydrodynamic radius r_H, hydrodynamic volume V_H, and rotational correlation time τ_R at 25°C of Gadoxane G (**GG**) (time = 0), Y-DOTAGA (**63**), and the average values during the decomposition of **GG**.

Time [d]	D [m^2/s]	r_H [nm]	V_H [nm^3]	τ_R [ps]
0 (**GG**)	$1.37x10^{-10}$	1.44	12.56	3366
0.375	$1.39x10^{-10}$	1.42	12.00	3216
1	$1.43x10^{-10}$	1.38	11.05	2960
2	$1.43x10^{-10}$	1.39	11.14	2985
3	$1.48x10^{-10}$	1.34	10.01	2682
4	$1.47x10^{-10}$	1.34	10.17	2726
5	$1.51x10^{-10}$	1.32	9.54	2555
7	$1.54x10^{-10}$	1.28	8.83	2367
14	$1.64x10^{-10}$	1.21	7.38	1979
+ 8d at 75°C	$2.63x10^{-10}$	0.75	1.78	477
Y-DOTAGA (**63**)	$3.98x10^{-10}$	0.50	0.52	139

4.2.6.3 Time-dependent ESI-MS measurements

A possibility to follow the single steps of the hydrolysis in more detail is offered by ESI-MS. The gadolinium(III) complex of Gadoxane G (**GG**) was used for this investigation. As the reaction rate increases with temperature, the aqueous solution of **GG** was kept at 37°C and pH 7.0. ESI mass spectra were recorded at the outset, after seven hours, 48 hours and 144 hours (Figure 48). With a molar mass of 5774.95 g/mol the eight-times negatively charged gadolinium complex has a *m/z* of 721.9. Unlike in the high resolution mass spectra, the isotopic pattern of this highly charged compound could not be resolved in the ESI mass spectra. Instead a broad signal appeared in the starting spectrum. Each breaking of a Si-O-Si moiety involves the addition of a water molecule (see Scheme 28 in chapter 4.2.6.1). For an eight-times negatively charged compound this corresponds to an increase in *m/z* of 2.25. The hydrolysis of the first Si-O-Si unit was observed after seven hours by the appearance of the signal at *m/z* = 724.1. After 48 hours the spectrum showed additional signals corresponding to two and three hydrolysed Si-O-Si moieties in the silsesquioxane core, but also the appearance of the isotope pattern of the fully degraded species **80** at *m/z* = 749.3. The signal

corresponding to the undamaged species had almost vanished when the solution was kept for additional 96 hours, whereas the isotope pattern of **80** was now clearly visible. Interestingly no signals corresponding to seven- to two-times negatively charged fragments could be observed by this method.

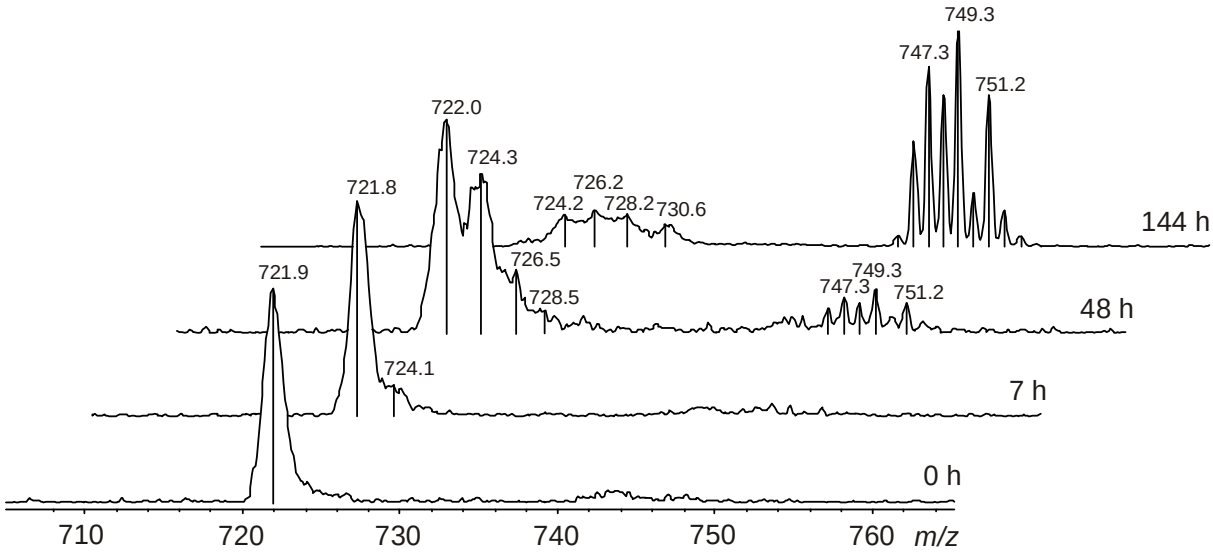

Figure 48. ESI mass spectra of the gadolinium(III) complex of Gadoxane G (**GG**) and its fragments after 0 h, 7 h, 48 h and 144 h at 37°C and pH 7.0.

4.2.6.4 Time-dependent relaxivity measurements

The degradation rate of Gadoxane G (**GG**) under physiological conditions was tested *via* relaxivity measurements. Therefore various concentrated solutions of the gadolinium(III) complex of **GG** in typical cell culture media (20 mM HEPES, pH 7.4-7.6) with and without fetal calf serum (FCS) were incubated at 37°C, for different periods of time. T_1-relaxation times of the solutions were measured at 3 T and room temperature. No significant differences between the serum containing and serum free solutions could be observed. Thus, for the further evaluations the data of both experiments were combined. The respective longitudinal relaxivities r_1 were calculated from the T_1 measurements (Figure 49). Without incubation a longitudinal relaxivity of 10.6 $mM^{-1}s^{-1}$ per gadolinium(III) ion was obtained. Within the first three to four hours of incubation r_1 did not significantly change. This is understandable as the gadolinium(III) ion remains complexed safely and the initial breaking of Si-O-Si bonds should not have much influence on the size or rather the rotational correlation time τ_R. Further hydrolysis then leads to smaller fragments with a reduced average τ_R resulting in a decrease of r_1. Fitting the period of decrease with a first order exponential decay showed a half-life $t_{1/2}$ of about 15±3 hours. A plateau of 6.7 $mM^{-1}s^{-1}$ is reached after about 125 h. This relaxivity still belongs to an equilibrium between the fully hydrolysed **80** and fragment **81** (see Scheme 28 in

chapter 4.2.6.1). As **81** was not observable in the ESI-MS measurements this could not be directly verified. However, when the same measurements were performed in solutions of pH 8.1 to 8.6 (without HEPES and gas exchange) the decay was much faster ($t_{1/2}$ about 55 min), and, even more important, the plateau was significantly lower (5.4 $mM^{-1}s^{-1}$) showing that the increase in pH can further shift the equilibrium towards **80**.

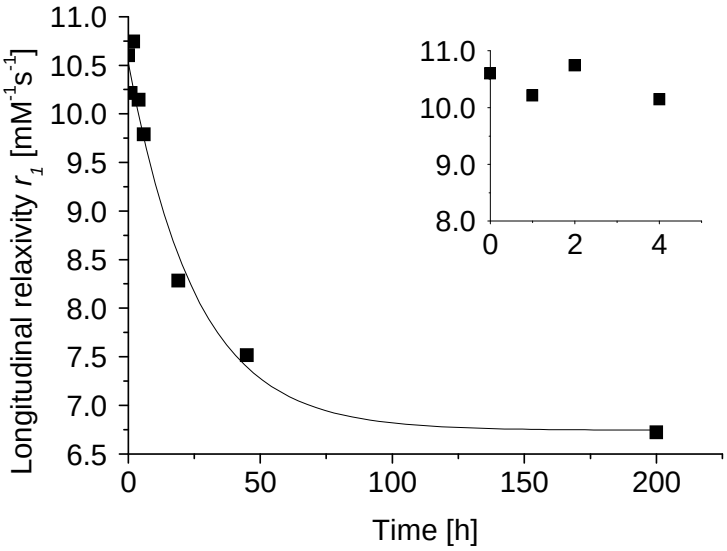

Figure 49. Longitudinal relaxivity r_1 (3 T, r.t.) during the degradation of **GG** under physiological conditions (cell culture media, 20 mM HEPES, pH 7.4-7.6). The inset highlights the first four hours of incubation.

The degradation of the silsesquioxane core of Gadoxane B (**GB**) was also investigated by its effect on the longitudinal relaxivity r_1. Since the water itself (or rather OH^-) is responsible for the degradation of the silsesquioxane (see Scheme 28 in chapter 4.2.6.1) and no influence of serum, but a strong dependence on the pH was observed for **GG**, the measurements were carried out in HEPES buffered water (pH 7.4), where the pH can be adjusted more accurately. The sample was kept at 37°C and the longitudinal relaxation time T_1 was measured at a proton Larmor frequency of 10 MHz after different periods of time. The longitudinal relaxivities were calculated from these data (Figure 50). As was observed for **GG**, r_1 of **GB** also remained constant (14.14±0.08 $mM^{-1}s^{-1}$) within the first three hours and only then started to decrease. The decrease, starting after three hours, could also be fitted with a first order exponential decay. With a half-life $t_{1/2}$ of 11.2±0.2 h the decay rate is comparable to that obtained for **GG** ($t_{1/2}$ = 15±3 h).

This result verifies the degradation of the silsesquioxane core also for **GB**. As mentioned earlier, the initial period of constant relaxivity can be explained by the negligible influence of the breaking of the first Si-O-Si bonds of the silsesquioxane core on the rotational correlation

time. Despite their degradation, the Gadoxanes should therefore allow the performance of MRI measurements with high reproducibility.

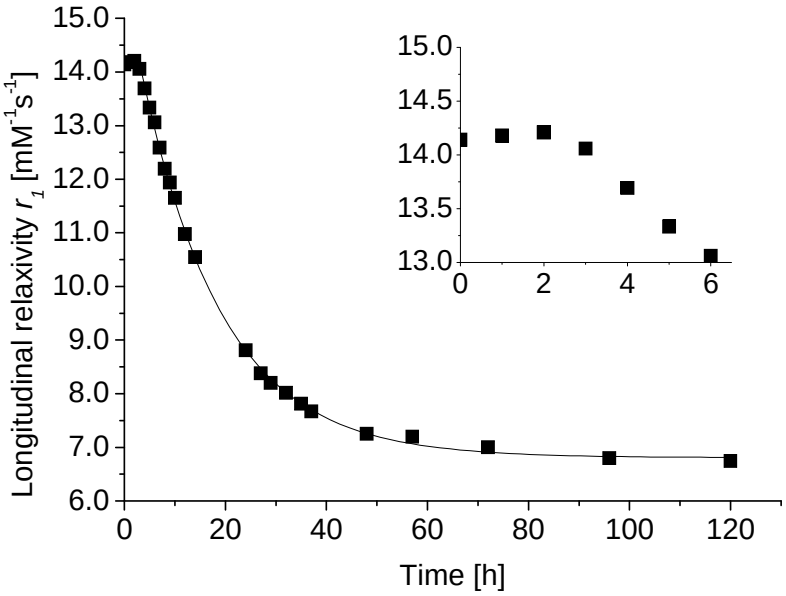

Figure 50. Longitudinal relaxivity r_1 of Gadoxane B (**GB**) under physiological conditions as a function of the time (37°C, pH 7.4, 10 MHz). The inset highlights the first six hours.

4.2.7 Physico-chemical Characterisation of Gadoxane G and B

The diffusion measurements revealed a rotational correlation time τ_{RDiff} of about 3.35 ns for both Gadoxanes (see chapter 4.2.5), which should result in highly efficient CAs. However, τ_{RDiff} reflects the rotational correlation time of the whole molecule, and, as was outlined in chapter 4.1.1.1, the major influence on the relaxivity of a macromolecular CA does not arise from the global rotational movement of the compound, but from the local tumbling of the attached gadolinium(III) complexes. The difference between the global and the local rotational dynamics is in turn based on the internal flexibility of the macromolecule. As mentioned in chapter 4.2.4.3, the phenyl ring in Gadoxane B (**GB**) was thus introduced, to replace the more flexible ethylene spacer in Gadoxane G (**GG**).

In order to quantify the effect of the different rigidity of the linking groups on the rotational motion of the gadolinium(III) complexes in **GG** and **GB**, but also to determine the parameters describing water exchange and electronic relaxation, variable-temperature ^{17}O NMR and ^{1}H NMRD measurements were performed in aqueous solutions of the gadolinium(III) complexes of **GG** and **GB** as well as of their corresponding monomers Gd-DOTAGA (**63**) and Gd-DOTABA (**78**). For both monomers, the ^{17}O reduced transverse relaxation rates, $1/T_{2r}$, increase at lower temperatures, while above ~300 K they decrease with temperature (slow and fast exchange regions, respectively; Figure 51). As already mentioned in chapter 3.2.7, a

detailed discussion of variable-temperature ^{17}O NMR measurements for the physico-chemical characterisation of CA, can be found elsewhere.[1] The equations involved in the ^{17}O NMR study are given in the experimental part (chapter 5.1.8) of this thesis.

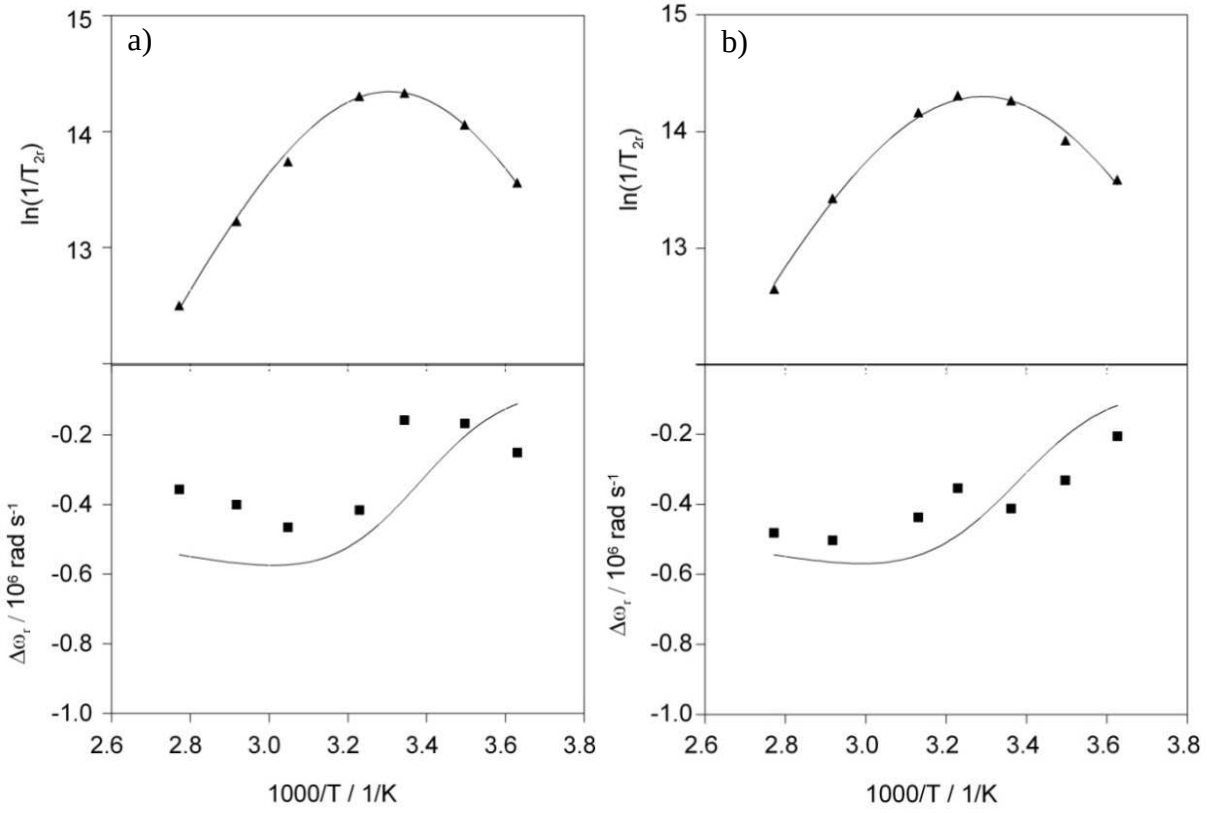

Figure 51. Temperature dependence of reduced transverse relaxation rates, $1/T_{2r}$, and chemical shifts, $\Delta\omega_r$, of (a) Gd-DOTAGA (**63**) and (b) Gd-DOTABA (**78**). The lines represent the least-squares simultaneous fit of all data points.

In the slow exchange region, the reduced transverse relaxation rate $1/T_{2r}$ is given exclusively by the water exchange rate k_{ex}. In the fast exchange regime, $1/T_{2r}$ is defined by the transverse relaxation rate of the bound water oxygen $1/T_{2m}$, which is in turn influenced by k_{ex}, the longitudinal electronic relaxation rate $1/T_{1e}$, and the scalar coupling constant $A/\hbar$. The ^{17}O reduced chemical shifts $\Delta\omega_r$ (Figure 51) are determined by $A/\hbar$, and to a small extent by an outer-sphere contribution C_{OS}. Due to the significantly increased lability of the silsesquioxane core at higher temperatures, the ^{17}O reduced transverse relaxation rates and ^{17}O reduced chemical shifts $\Delta\omega_r$ of the Gadoxanes could only be obtained in a temperature range of 273-320 K (Figure 52). Nevertheless, even in this limited temperature range, both the slow and fast exchange regimes are observable for Gadoxane G and B, evidencing that the water exchange rate k_{ex} on the gadolinium complexes is not significantly changed by the attachment to the silsesquioxane core.

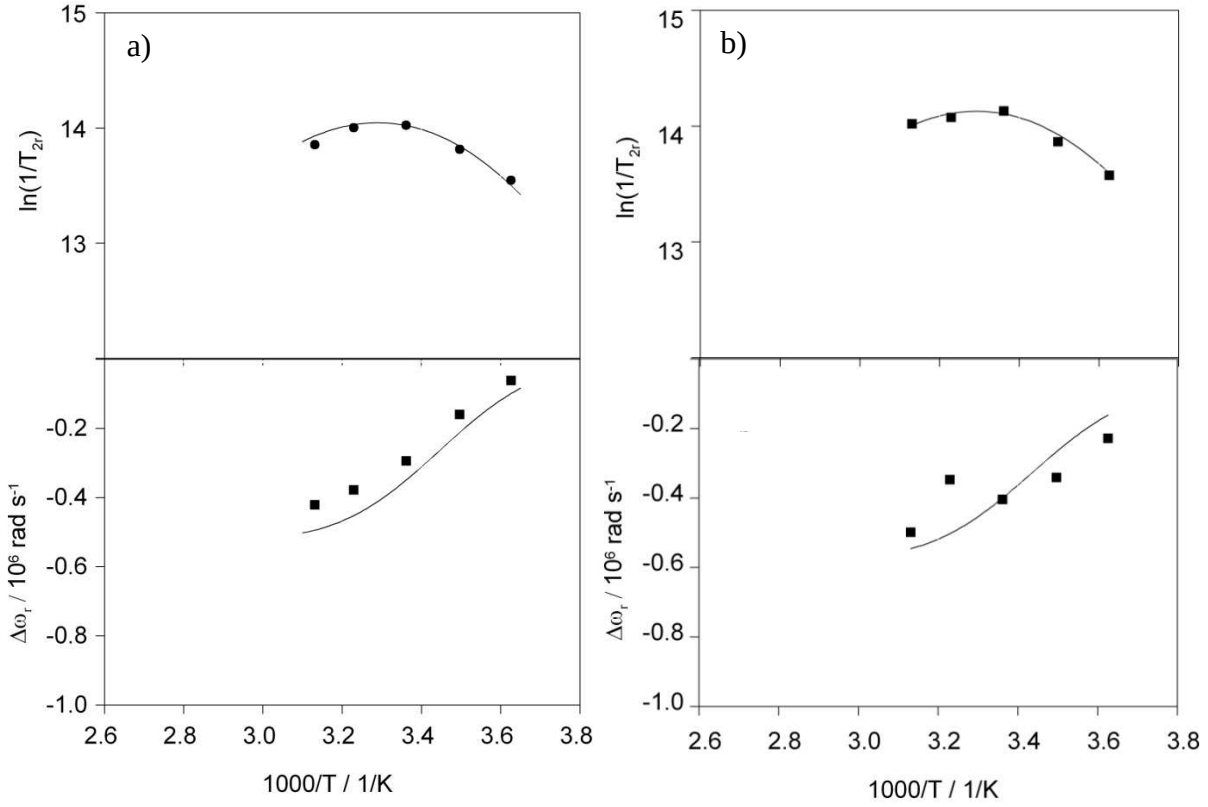

Figure 52. Temperature dependence of reduced transverse relaxation rates, $1/T_{2r}$, and chemical shifts, $\Delta\omega_r$, of (a) Gadoxane G (**GG**) and (b) Gadoxane B (**GB**). The lines represent the least-squares simultaneous fit of all data points.

Since the transverse ^{17}O relaxation is governed by the scalar relaxation mechanism, it contains no information on the rotational motion of the system. In contrast to $1/T_{2r}$, the longitudinal ^{17}O relaxation rates $1/T_{1r}$ are determined by dipole-dipole and quadrupolar relaxation mechanisms, both related to the rotation of the molecules. The dipolar term depends on the Gd^{3+}-water oxygen distance, r_{GdO}, while the quadrupolar term is influenced by the quadrupolar coupling constant, $\chi(1+\eta^2/3)^{1/2}$. The longitudinal relaxation rates have also been measured. However, the differences between the diamagnetic reference and the paramagnetic samples were too small because of the low gadolinium(III) concentration owed to the poor solubility of the complexes, in particular of **78**. Therefore, the reduced longitudinal ^{17}O relaxation rates have not been included in the analysis. The relatively poor quality of the chemical shifts should also be noted. Nevertheless, in accordance to related systems, the shifts confirm the hydration number of one for all four compounds.

In recent years, it has become general practice to fit ^{17}O NMR and NMRD data simultaneously, which is thought to yield physically more meaningful parameters.[88] However, such an approach was not possible in the case of both Gadoxanes, as an acceptable fit of the ^{1}H relaxation profile could not be reconciled with the electronic relaxation parameters

obtained from the ^{17}O NMR studies. This discrepancy is most probably related to an inadequate description of the electron spin relaxation, having a strong influence on both the low-field proton relaxivities and the transverse ^{17}O relaxation rates in the intermediate and fast water exchange regimes. A new appropriate theory that is capable of describing the field dependence (low frequency part of the NMRD curve: <0.02 T; ^{17}O data: 7.05 T) of electron spin relaxation rates by the inclusion of both transient and static zero-field splitting (ZFS) has been reported.[141, 142] However, this theory is only applicable to small molecular weight chelates and not to larger compounds like Gadoxane G and Gadoxane B. Indeed, attempts to simultaneously fit ^{17}O T_2 and NMRD data failed in the case of the "intermediate" sized metallostar compound (cf chapter 3.1.1.3).[55]

Therefore, for all four compounds the transverse ^{17}O relaxation rates, which primarily give access to the water-exchange rate, were fitted together with the ^{17}O chemical shifts using the traditional Solomon–Bloembergen–Morgan equations (see chapter 5.1.8). From these fittings the water exchange rate k_{ex}^{298}, its activation entropy $\Delta S^{\ddagger}$, and enthalpy $\Delta H^{\ddagger}$ as well as the parameters of the electron spin relaxation, namely the correlation time for the modulation of the zero-field-splitting τ_v^{298} and the mean-square zero-field-splitting energy Δ^2 have been adjusted. The values obtained for these parameters are presented in Table 8.

Table 8. Parameters obtained from the independent fit of ^{17}O NMR and ^{1}H NMRD data. For each complex, the left and right semicolumns show the electron spin relaxation parameters calculated from ^{17}O NMR and ^{1}H NMRD, respectively. In the NMRD analysis, parameters of water exchange were fixed to values obtained by ^{17}O NMR.

	Gd-DOTAGA		Gadoxane G		Gd-DOTABA		Gadoxane B	
$\Delta H^{\ddagger}$ (kJ mol^{-1})	49.9±0.5		43.5±0.5		47.5±0.5		42.2±0.5	
$\Delta S^{\ddagger}$ (Jmol^{-1}k^{-1})	+52±2		+30±2		+43±2		+25±2	
k_{ex}^{298} (10^6 s^{-1})	5.9±0.3		5.3±0.5		5.4±0.3		5.5±0.5	
E_{lH} (kJ mol^{-1})	17.2±0.3[a)]		23±0.8		19.7±0.3[a)]		20±0.8	
τ_{lH}^{298} (ps)	93±8[a)]		240±10		117±10[a)]		380±20	
E_{gR} (kJ mol^{-1})			23±0.8				19.3±0.8	
τ_{gR}^{298} (ps)			1500±400				1900±400	
S^2			0.14±0.02				0.21±0.02	
τ_v^{298} (ps)	6.6±0.3	6.5±0.3	3.9±0.4	30±8	9.7±0.7	7.0±0.4	4.5±0.3	31±8
Δ^2 (10^{19} s^{-2})	5.1±0.3	3.9±0.4	5.0±0.4	0.7±0.1	5.0±0.3	3.9±0.4	5.0±0.3	0.6±0.1

[a)] No Lipari-Szabo treatment; only a single τ_{RH}^{298} and E_{RH} is calculated, respectively

The water exchange rates of all four compounds are higher than that reported for Gd-DOTA (**1**) (k_{ex}^{298} = (4.1±0.2)×10^6 s^{-1}).[88] Gd-DOTAGA (**63**) shows the strongest increase in k_{ex}^{298} as compared to **1** (about 40 %). The large activation enthalpies $\Delta H^{\ddagger}$ and the positive activation entropies $\Delta S^{\ddagger}$ suggest a dissociative mechanism for all compounds.[143] In such a dissociative mechanism, the additional negatively charged (at neutral pH) carboxyl group in **63**, being relatively close to the coordination cage, can favour the leaving of the coordinated water molecule, thus resulting in faster exchange. This was previously observed for Gd-DOTASA (**82**, Figure 53) (DOTASA = 1,4,7,10-tetraazacyclododecane-1-succinic-4,7,10-triacetic acid), where the carboxylate group is even closer to the coordination cage (k_{ex}^{298} = (6.3±0.2)×10^6 s^{-1}).[144]

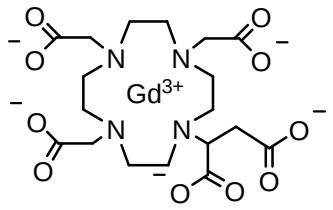

82

Figure 53. Structure of Gd-DOTASA (**82**)

Beside the effect of the negative charge of the carboxylate on the water exchange, the pending group might lead to a structural change and induce some sterical crowding in the inner coordination sphere of the complex with respect to Gd-DOTA (**1**). This might also contribute to the acceleration of the water exchange. This effect is expected to increase with increasing length and rigidity of the linker. It is likely operative for Gd-DOTABA (**78)**, where the additional negative charge is farther away from the inner sphere, and becomes even more important for Gadoxane G and B. Indeed, the Gadoxane compounds do not have an additional negative charge and still present a faster water exchange than **1**.

In a second step, the NMRD profiles of all four compounds (Figure 54 and Figure 55) were analysed to yield primary information on the rotational dynamics. In these fittings the parameters describing the water exchange (k_{ex}^{298}, $\Delta H^{\ddagger}$) were fixed to the values obtained from the fit of the ^{17}O NMR data. In addition, r_{GdH} was set to the common value of 3.10 Å based on recent electron-nuclear double resonance (ENDOR) spectroscopic results,[87, 145] and the distance of closest approach of an outer-sphere water proton to gadolinium(III), a_{GdH}, to 3.5 Å. The diffusion constant D_{GdH}^{298} (23×10^{-10} m^2 s^{-1} (**63** and **78**); 26×10^{-10} m^2 s^{-1} (**GG** and **GB**)) used in the analysis of the proton NMRD data and the corresponding activation energy E_{GdH} (22 kJ mol^{-1} (**63** and **78**); 20 kJ mol^{-1} (**GG** and **GB**)) were adjusted to reasonable values.

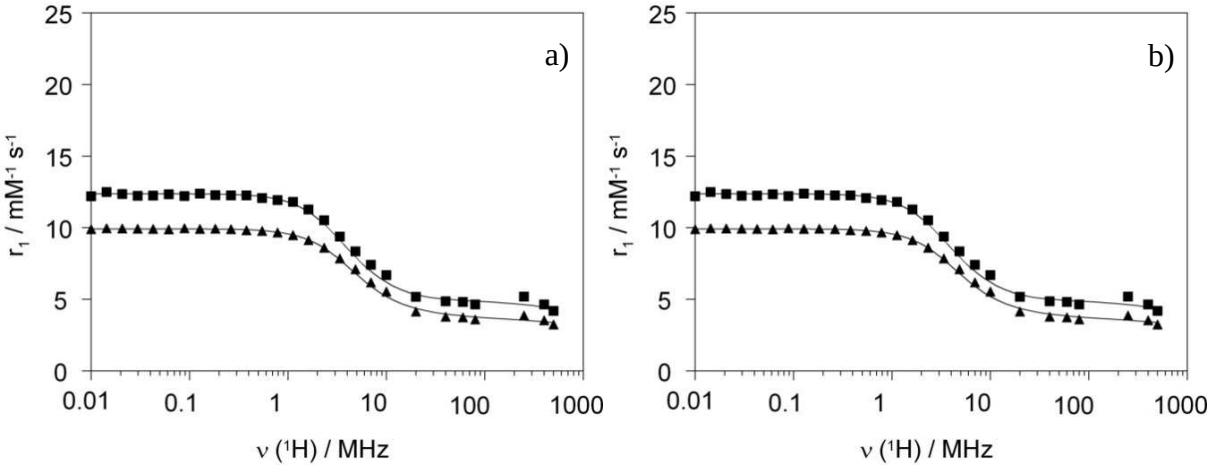

Figure 54. NMRD profile of (a) Gd-DOTAGA and (b) Gd-DOTABA at 25°C (■) and 37°C (▲). The lines represent the least-squares simultaneous fit of all data points.

The ^{1}H NMRD profiles of the monomers (Figure 54) were fitted according to the equations described in chapter 2.3 using a single rotational correlation time τ_{RH}^{298}, corresponding to the rotation of the Gd-H_{water} vector. It should be noted that due to the internal motion of the coordinated water molecules around the Gd-O axis, τ_{RH}^{298} is usually lower than the rotational correlation time of the Gd-O_{water} vector τ_{RO}^{298} (τ_{RH}/τ_{RO} = 0.65±0.2).[146, 147] The obtained values for τ_{RH}^{298} and its activation energy E_{RH}, as well as the parameters of the electron spin relaxation (τ_v^{298}, Δ^2) are depicted in Table 8.

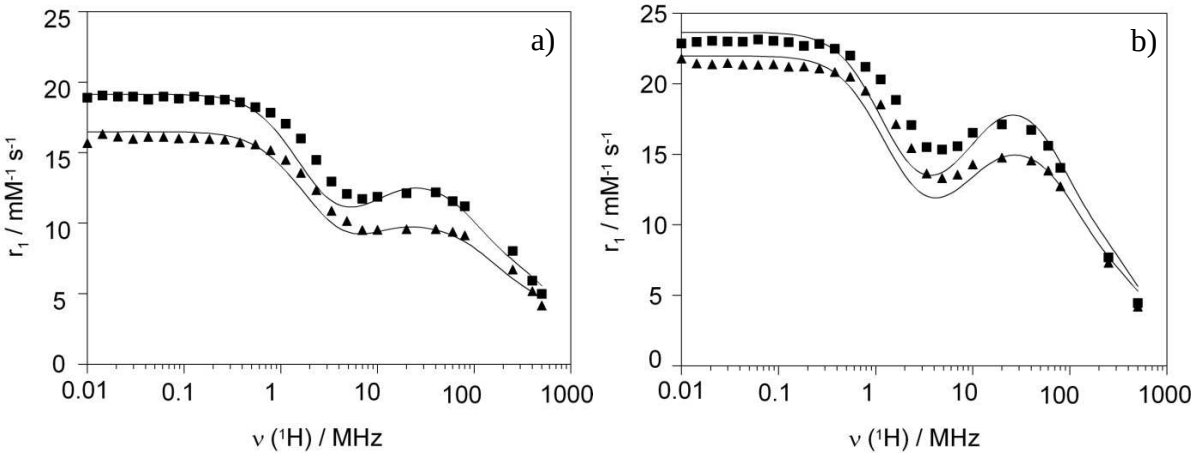

Figure 55. NMRD profiles of (a) Gadoxane G and (b) Gadoxane B at 25°C (■) and 37°C (▲). The lines represent the least-squares simultaneous fit of all data points.

For the two Gadoxanes, a satisfying fit of the experimental high filed NMRD data (> 10 MHz) (Figure 55) could only be obtained by using the Lipari-Szabo model-free approach,[148, 149] previously applied to evaluate NMR relaxation data of numerous macromolecular systems (equations are given in chapter 5.2.7.5). The Lipari-Szabo approach

allows the separation of the two kinds of rotational motions influencing relaxation, the fast local motion being characterised by a correlation time τ_{lR}^{298} and its activation energy E_{lR}, as well as the slower global motion with a correlation time τ_{gR}^{298} (activation energy E_{gR}) (Table 8). A measure for the spatial restriction of the local motion is given by the parameter S^2. For an isotropic internal motion $S^2 = 0$, while for a fully restricted motion $S^2 = 1$ (Table 8).

Table 9 shows proton relaxivity data and rotational correlation times of Gadoxane G and B and the monomeric complexes **63** and **78** together with a series of other DOTA-type gadolinium complexes of various sizes, previously reported in the literature. In the case of Gd-DOTASA (**82**), the rotational correlation time τ_{RH}^{298} is about 60 % larger than that of Gd-DOTA (**1**). As referred to the increased molecular weight, one would only expect an increase in τ_{RH}^{298} of about 10 %. The significantly higher increase was explained by the ability of the negatively charged additional carboxylate to assemble water molecules in the second coordination sphere. They move together with the complex, thereby further increasing the rotational correlation time. The rotational correlation time τ_{RH}^{298} of Gd-DOTAGA (**63**) is also higher than that of **1**, but with only 20 % the increase is significantly smaller than for **82**. Due to the longer alkyl chain the hydrophobicity of the linker might increase, thereby preventing the formation of a large second sphere hydration layer. As was already observed in the diffusion NMR study (4.2.5), the larger linker of Gd-DOTABA (**78**) prolongs the rotational correlation time of **78**. τ_{RH}^{298} of **78** is therefore again in the range of that of **82**. The obtained values for the rotational correlation time of **63** and **78** by the analysis of the NMRD profiles, τ_{RH}^{298}, are smaller than those obtained from the diffusion NMR studies, τ_{RDiff}^{298} (Table 9 and Table 6). As mentioned above, τ_{RH}^{298} corresponds to the rotation of the Gd-H_{water} vector, being faster than that of the Gd-O_{water} vector due to the internal rotation of the water molecule. On the contrary, τ_{RDiff}^{298} should represent the global rotational motion of the whole complex. Indeed, if the τ_{RH}^{298} values of **63** and **78** are multiplied with the above mentioned relation to τ_{RO}^{298}, values of 143±12 ps and 180±15 ps, respectively, are obtained. These values are in excellent agreement with the obtained τ_{RDiff}^{298} values of 139±1 ps and 183±1 ps for **63** and **78**, respectively. As one can assume that the τ_{RO}^{298} of these monomeric complexes match with their global rotational correlation times, these results emphasise that PGSE diffusion ^{1}H NMR spectroscopy is an appropriate method for determining the global rotational correlation time of such almost spherical compounds.

The effect of the longer rotational correlation times of **63** and **78** is reflected in their higher relaxivities as compared to **1**. At 25°C and a proton resonance frequency of 20 MHz the

relaxivity of **63** is 9 % higher and the relaxivity of **78** is even 24 % higher than that of **1**. Since at this field and for such small molecular weight compounds, the relaxivities are exclusively limited by the rotational correlation time, the relaxivity of **78** is comparable to that of **82** despite the faster water exchange rate of the latter.

Table 9. Relaxivity r_1 (at 25°C and 20 MHz) and parameters characterising the rotational tumbling of selected DOTA-type gadolinium complexes.

Complex	τ_{lR}^{298} [ps]	τ_{gR}^{298} [ps]	S^2	τ_{RDiff}^{298} [ps]	r_1 [$mM^{-1}s^{-1}$]
monomers					
Gd-DOTAGA (**63**)	93±8[a)]			139±1	5.18
Gd-DOTABA (**78**)	117±10[a)]			183±1	5.87
Gd-DOTASA (**82**)[144]	125±2[a)]				5.93
Gd-DOTA (**1**)[88]	77±4[a)]				4.74
dendrimers					
Gadoxane G (**GG**)	240±10	1500±400	0.14	3370±60	12.13
Gadoxane B (**GB**)	380±20	1900±400	0.21	3320±50	17.11
Gadomer 17[111]	760	3050	0.50		16.46
micelles					
Gd-DOTASA-C_{12}[95]	920±40[a)]				18.03
Gd-DOTA-C_{12}[96]	430	1600	0.23		17.24

[a)] No Lipari-Szabo treatment; a single τ_{RH}^{298} is calculated.

The attachment of Gd-DOTAGA (**63**) and Gd-DOTABA (**78**) to the octa(amino-propyl)silsesquoxane core results in the expected "high field" peak in the NMRD profiles (Figure 55) of Gadoxane G (**GG**) and Gadoxane B (**GB**) being typical for macromolecular CAs, where the rotation of the gadolinium(III) chelates is substantially slowed down (see chapter 4.1.1.1). However, especially in the case of **GG** the peak is not as distinctive as it could be for a CA of that size. At 25°C and a proton resonance frequency of 20 MHz, **GG** only revealed a relaxivity of 12.13 $mM^{-1}s^{-1}$. This reflects the still high flexibility of the ethylenecarboxyl linker on the Gd-DOTAGA moiety together with the aminopropyl group on the silsesquioxane part, resulting in a short local correlation time τ_{lR}^{298} of only 240 ps. Remarkably, the replacement of the ethyl spacer in the linking group of **GG** by a phenyl ring in **GB** increases τ_{lR}^{298} to 380 ps and, more important, it leads to a significantly higher relaxivity (17.11 $mM^{-1}s^{-1}$ at 25°C and 20 MHz). This points out that DOTABA (**65**) can be in general an extremely useful ligand for attaching stable DOTA-type complexes to

(bio)macromolecules and thereby achieving high relaxivities. The apparent global rotational correlation times of **GG** and **GB** calculated from the NMRD profiles are 2 and 1.5 times shorter, respectively, than those obtained from the diffusion measurements. This difference can be attributed to the still relatively high flexibility of the systems and hence the poor correlation (S^2) between the local and the global motion. With a greater rigidity of the systems the global motion is better represented in the NMRD profiles. This is supported by the better consistency of the two obtained values (τ_{gR}^{298} and τ_{RDiff}^{298}) for the global rotational correlation time of Gadoxane B (**GB**) compared to Gadoxane G (**GG**). As is evident from Table 9, the relaxivity of **GB** is comparable to other DOTA-type macromolecular dendrimers and micelles. The increase in relaxivity of more than 40 % from **GG** to **GB**, however shows the potential for even higher relaxivities by further increasing the rigidity of these systems.
Note, that for **GG** and **GB**, the electron spin relaxation parameters obtained from ^{17}O NMR data are significantly different from those obtained by the evaluation of the ^{1}H NMRD data (Table 8). As this is related to the shortcomings of the electron spin relaxation theory used, the interpretation of these values in terms of physical meaning is not possible.

4.3 Conclusions and Perspectives

In order to obtain moderate sized macromolecular CAs, several approaches to octafunctionalise T_8-silsesquioxane cages with gadolinium(III) complexes were carried out. First of all, an amino functionalised T_8-silsesquioxane (**29**) and a carboxylic acid functionalised T_8-silsesquioxane (**33**) were synthesised. These silsesquioxanes should allow the attachment of various protected macrocyclic ligands bearing an additional amino or carboxylate moiety in high yields by using classical peptide coupling reagents. Initially, the tri-*tert*-butyl protected DOTA ligand **36** was coupled to **29**. An issue in these coupling reactions is the hydrolysis of the silsesquioxane cage under the used basic conditions in the presence of even small amounts of water. Complete octafunctionalisation without destruction of the silsesquioxane cage could be achieved by reducing the reaction time to 30 minutes and avoiding hydrated reagents. This points out the suitability of peptide coupling reagents to synthesise eight-fold functionalised silsesquioxanes without generating complicated mixtures with less functionalised systems. Nevertheless, this initial route turned out to be unsuitable for the synthesis of silsesquioxane-based CAs, as the cleavage of the *tert*-butyl esters of the octafunctionalised **46** could not be fulfilled without decomposition of the silsesquioxane cage. A route where the *tert*-butyl esters were replaced by benzyl esters to avoid the harsh conditions necessary for the cleavage of *tert*-butyl esters, also proved unsuccessful as a

complete deprotection could not be achieved under the used conditions. A much more promising and also much more convenient approach was the direct eight-fold grafting of the hexylamine functionalised DO3A-type complex **48** to **33**. In this case, the carboxylate moieties of the macrocyclic ligand are protected by coordination to the lanthanide(III) itself. This makes a later deprotection and subsequent complexation unnecessary, which reduces the risk of destroying the silsesquioxane cage. Unfortunately, the obtained product **49** turned out to be insoluble in aqueous media at moderate pH, what makes it unsuitable as a MRI CA. However, **49** could be dissolved by reducing the pH to about 2-3. At this pH the carboxylate groups become protonated and the lanthanide(III) ion can be released, in turn leading to a protonation of the nitrogens. Since this suggested the need of a charge to obtain sufficient water solubility of these highly symmetric systems, macrocyclic ligands were synthesised which form charged lanthanide (III) complexes. The first of these systems was DOTAGA (**60**). **60** is a DOTA-type ligand having an additional ethylene carboxylate function on one of the methylene moieties for the coupling to **29**. As the lanthanide (III) complexes (**63**) themselves were attached to **29**, no orthogonal protecting group chemistry was required in the synthesis of **60**. The counter ion of the negatively charged complexes **63** is an important factor for the solubility of **63**. Thus, for the binding of the complexes to **29**, tetra-*n*-butyl ammonium was used as the counter ion to increase the solubility in DMSO. Complete octafunctionalisation could be achieved within 30 minutes using TBTU (**38**) and DIPEA. The obtained product was purified by diafiltration. Diafiltration also allowed the exchange of the tetra-*n*-butyl ammonium counter ion by sodium to yield the water soluble silsesquioxane-based CA, Gadoxane G (**GG**), as its octasodium salt. The yttrium(III) complex of **GG** was synthesised in order to allow its characterisation with multinuclear (^{1}H, ^{13}C, ^{29}Si) NMR spectroscopy and HR-MS. The data showed, that pure **GG** can be synthesised by this method with a fully condensed silsesquioxane cage. Encouraged by this success, two novel ligand systems, DOTAMA (**64**) and DOTABA (**65**), were designed and prepared. In these systems the flexible ethylene spacer by which the additional carboxylate group is attached to the DOTA moiety in DOTAGA (**60**) is replaced by a rigid phenyl ring in the case of **65** and in the case of **64** the carbxylate group is directly attached to one of the methylene groups of the DOTA moiety. This should further reduce the internal flexibility of the system, resulting in higher relaxivities. Unfortunately, a silsesquioxane bearing eight Ln-DOTAMA complexes (**76**) could not be isolated, even though the ^{1}H NMR spectrum of the reaction solution indicated the successful octafunctionalisation of **29**. By contrast, the eight-fold grafting of **29** with Ln-DOTABA (**78**) succeeded after allowing the reaction mixture to stir for three hours.

The longer reaction time was necessary as **78** was poorly soluble in DMSO and DMF, even as its tetra-*n*-butyl ammonium salt. Nevertheless, as in the case of **GG**, the desired Gadoxane B (**GB**) turned out to be water soluble and could be isolated after diafiltration as its octasodium salt. **GB** was also characterised by multinuclear (^{1}H, ^{13}C, ^{29}Si) NMR spectroscopy and HR-MS.

A key issue of the Gadoxanes is the stability of the silsesquioxane cage towards hydrolysis in aqueous media. This point was initially investigated at neutral pH on the basis of **GG** by ^{29}Si NMR and PGSE diffusion ^{1}H NMR spectroscopy as well as by ESI-MS. It could be shown that aqueous solutions of **GG** can be stored at -28°C for at least 10 months without any decomposition. However, already at 25°C and pH 7.0 a slow hydrolysis of the silsesquioxane core was observed, which accelerated by increasing the temperature. Additionally, these experiments showed that having a single resonance in the ^{29}Si NMR spectrum is not necessarily a proof of an intact silsesquioxane core. In fact, several techniques should be used to fully describe the state of the silsesquioxane cage. Relaxivity measurements of **GG** and **GB** were then used to determine the degradation rate of the cage under physiological conditions (pH 7.4, 37°C) in the presence and absence of cell culture media and fetal calf serum. Since the water itself is responsible for the decomposition of the silsesquioxane, no significant effect of the added serum on the degradation rate was observed. Interestingly, the relaxivity of both compounds remained constant within the first three hours, before starting to decrease due to the shorter rotational correlation time of the fragments. The initial period of constant relaxivity can be explained by the negligible influence of the breaking of the first Si-O-Si bonds of the silsesquioxane core on the rotational correlation time. This time frame should be sufficient to perform MRI measurements with high reproducibility. With half-lives $t_{1/2}$ of 15±3 and 11.2±0.2 hours, the decay rates of **GG** and **GB**, respectively, are then already significantly faster than at neutral pH. The influence of the pH on the hydrolysis rate becomes obvious, when the same experiment is carried out at pH 8.1 to 8.6. In this case a half-life $t_{1/2}$ of only 55 minutes was observed for the degradation of **GG**. In terms of toxicity the degradation of the silsesquioxane core is a very crucial aspect. Since silica monomers are nontoxic,[123] the hydrolysis of the core is not supposed to increase the toxicity by itself. However, if silsesquioxanes are used as the dendrimeric core, the stability of the gadolinium(III) complex must not depend on the intactness of the silsesquioxane, since then the risk of gadolinium related diseases increases. On the other hand, if appropriate gadolinium(III) chelators are applied, like DOTAGA (**60**) and DOTABA (**65**) in the case of **GG** and **GB**, the decomposition of the silsesquioxane core has no influence on the stability of

the gadolinium (III) complex. On the contrary, the lability of the silsesquioxane core may allow the development of even larger and still well defined macromolecular CAs for MRI, whose fragments are then readily excreted *via* the kidneys.

However, with a hydrodynamic radius of about 1.44 nm, as obtained by PGSE diffusion ^{1}H NMR spectroscopy, both **GG** and **GB** are still significantly smaller than the small pores of the glomerular filtration system and hence should be excreted relatively fast *via* the kidneys, even before a significant amount of the silsesquioxane cages is fragmented.

PGSE diffusion ^{1}H NMR spectroscopy revealed also rotational correlation times of about 3.35 ns for both, **GG** and **GB**. Even though variable temperature ^{17}O NMR measurements showed that both CAs have also almost identical water exchange rates, the longitudinal relaxivities of **GB** are significantly higher than those of **GG** (54 % at 37°C and 20 MHz) over almost the whole range of magnetic fields. The discrepancy arises from a different local rotational correlation time of the Gd-H_{water} vector of **GG** and **GB,** due to the lower internal flexibility of **GB** towards **GG**, as was intended. Having already relaxivities in the range of other, larger macromolecular CAs, **GB** still possesses a fairly high internal flexibility. This, together with the observed strong effect of replacing an ethylene by a phenyl spacer on the relaxivity, points out the high potential of silsesquioxane-based CAs to become extremely efficient, once the rigidity is further improved and the water exchange rate is optimised.

Furthermore, the introduction of additional functional groups into these systems, e.g. *via* functionalisation of the remaining methylene groups of the complexes, could allow their use in the targeting of biomolecules within the body.

5 Experimental Part

5.1 Calcium(II)-sensitive MRI Contrast Agents

5.1.1 General Remarks

All **LnL^1**-**LnL^4** complexes used in this part of the thesis were kindly provided by Dr. I. Mamedov, Max-Planck-Institute for Biological Cybernetics, Tübingen. pH and pD[150] values of the aqueous solutions were measured using a Schott handylab pH12 pH-meter equipped with a Hamilton Spintrode or a Mettler-Toledo Inlab Micro glass electrode. The absence of the non-coordinated metal ions in the systems was confirmed by the xylenol test.[136] The calcium(II) chloride stock solutions were prepared by dissolving an accurately weighed amount of the chloride salt in the appropriate volume of distilled water. The exact concentration was determined *via* complexometric titration with Titriplex III in a buffered indicator solution (Merck indicator buffer tablet / conc. ammonia).

5.1.2 Relaxivity *vs.* Calcium(II) Concentration

The relaxivity measurements were performed at 9.4 T, 25°C and pH 7.3-7.4 (maintained by HEPES buffer). A solution of calcium(II) chloride of known concentration was added stepwise to the respective complex solution and the longitudinal proton relaxation time T_1 of the water peak was measured after each addition of the analyte. The initial gadolinium(III) concentration was determined by measuring the bulk magnetic susceptibility (BMS) shift of the solution (see chapter 5.2.7.2).[151] The relaxivity r_1 was calculated according to equation 2.4 from chapter 2.3, using the respective gadolinium(III) concentration at each point of the titration.

Table 10. Relaxometric calcium(II) titration of **GdL^1** at 25°C, pH 7.3 and 9.4 T.

$[Gd^{3+}]$ (mM)	$[Ca^{2+}]$ (mM)	$[Ca^{2+}]$/[CA]	T_1 (ms)	r_1 ($mM^{-1}s^{-1}$)
2.490	0.000	0.00	56.869	6.915
2.441	1.225	0.50	58.070	6.904
2.394	2.404	1.00	58.217	7.022
2.349	3.538	1.51	59.219	7.033
2.306	4.630	2.01	61.075	6.943
2.264	5.682	2.51	62.207	6.940
2.223	6.696	3.01	63.405	6.929
2.184	7.675	3.51	64.874	6.890
2.147	8.621	4.02	66.457	6.839
2.110	9.534	4.52	67.901	6.806
2.075	10.417	5.02	69.336	6.774

Table 11. Relaxometric calcium(II) titration of **GdL^2** at 25°C, pH 7.3 and 9.4 T.

$[Gd^{3+}]$ (mM)	$[Ca^{2+}]$ (mM)	$[Ca^{2+}]/[CA]$	T_1 (ms)	r_1 ($mM^{-1}s^{-1}$)
2.500	0.000	0.00	52.783	7.432
2.451	1.225	0.50	54.596	7.324
2.404	2.404	1.00	58.128	7.004
2.358	3.538	1.50	61.672	6.720
2.315	4.630	2.00	65.328	6.455
2.273	5.682	2.50	68.027	6.307
2.232	6.696	3.00	70.769	6.166
2.193	7.675	3.50	72.075	6.160
2.155	8.621	4.00	74.706	6.041
2.119	9.534	4.50	76.659	5.984
2.083	10.417	5.00	80.068	5.819

Table 12. Relaxometric calcium(II) titration of **GdL^3** at 25°C, pH 7.3 and 9.4 T.

$[Gd^{3+}]$ (mM)	$[Ca^{2+}]$ (mM)	$[Ca^{2+}]/[CA]$	T_1 (ms)	r_1 ($mM^{-1}s^{-1}$)
2.520	0.000	0.00	57.987	6.698
2.471	1.225	0.50	62.942	6.283
2.423	2.404	0.99	71.899	5.589
2.377	3.538	1.49	82.757	4.929
2.333	4.630	1.98	87.024	4.768
2.291	5.682	2.48	92.989	4.534
2.250	6.696	2.98	95.433	4.494
2.211	7.675	3.47	98.422	4.431
2.172	8.621	3.97	100.227	4.424
2.136	9.534	4.46	102.642	4.391
2.100	10.417	4.96	104.209	4.395

Table 13. Relaxometric calcium(II) titration of **GdL^4** at 25°C, pH 7.3 and 9.4 T.

$[Gd^{3+}]$ (mM)	$[Ca^{2+}]$ (mM)	$[Ca^{2+}]/[CA]$	T_1 (ms)	r_1 ($mM^{-1}s^{-1}$)
2.540	0.000	0.00	66.734	5.755
2.490	1.225	0.49	72.389	5.400
2.442	2.404	0.98	81.963	4.846
2.396	3.538	1.48	95.151	4.233
2.352	4.630	1.97	105.052	3.892
2.309	5.682	2.46	109.725	3.788
2.268	6.696	2.95	115.238	3.665
2.228	7.675	3.44	118.426	3.626
2.190	8.621	3.94	120.841	3.612
2.153	9.534	4.43	123.108	3.604
2.117	10.417	4.92	127.143	3.543

5.1.3 Relaxivity *vs.* Complex Concentration

Like the calcium(II) dependent relaxivity measurements, the complex concentration dependent measurements were performed at 9.4 T, 25°C and pH 7.3-7.4 (maintained by HEPES buffer). The initial gadolinium(III) concentration of each complex solution was determined by measuring the bulk magnetic susceptibility (BMS) shift of the solution (see chapter 5.1.2). From these solutions, two new solutions per complex were prepared, one without calcium(II) and the other one with three equivalents of $CaCl_2$. The longitudinal proton

relaxation time T_1 of the water peak was measured of these solutions and remeasured after each dilution step. Dilution was carried out by addition of appropriate amounts of dest. H_2O and the gadolinium(III) concentration was calculated including the additional volume. The relaxivity r_1 was calculated according to equation 2.4 from chapter 2.3, using the respective gadolinium(III) concentration.

Table 14. Complex concentration dependent relaxivity of **GdL[1]** at 25°C, pH 7.3 and 9.4 T.

Without calcium(II)			With three equivalence of calcium(II)		
$[Gd^{3+}]$ (mM)	T_1 (ms)	r_1 ($mM^{-1}s^{-1}$)	$[Gd^{3+}]$ (mM)	T_1 (ms)	r_1 ($mM^{-1}s^{-1}$)
18.25	8.032	6.802	18.55	9.584	5.605
14.95	9.786	6.811	14.95	11.476	5.804
12.25	12.027	6.758	12.20	13.656	5.972
10.00	14.637	6.795	10.00	16.234	6.123
7.50	19.327	6.850	7.50	20.998	6.301
5.00	29.398	6.730	5.00	30.518	6.480
2.50	57.117	6.857	2.50	56.766	6.900

Table 15. Complex concentration dependent relaxivity of **GdL[2]** at 25°C, pH 7.3 and 9.4 T.

Without calcium(II)			With three equivalence of calcium(II)		
$[Gd^{3+}]$ (mM)	T_1 (ms)	r_1 ($mM^{-1}s^{-1}$)	$[Gd^{3+}]$ (mM)	T_1 (ms)	r_1 ($mM^{-1}s^{-1}$)
19.58	8.179	6.226	18.13	11.331	4.848
14.86	10.593	6.328	14.83	13.689	4.901
12.21	12.657	6.441	12.20	16.081	5.067
10.01	15.077	6.589	10.00	19.321	5.139
7.51	19.854	6.658	7.50	24.576	5.377
5.00	28.995	6.825	5.00	34.639	5.701
2.50	54.301	7.220	2.50	64.59	6.047

Table 16. Complex concentration dependent relaxivity of **GdL[3]** at 25°C, pH 7.3 and 9.4 T.

Without calcium(II)			With three equivalence of calcium(II)		
$[Gd^{3+}]$ (mM)	T_1 (ms)	r_1 ($mM^{-1}s^{-1}$)	$[Gd^{3+}]$ (mM)	T_1 (ms)	r_1 ($mM^{-1}s^{-1}$)
18.54	12.987	4.133	19.88	11.61	4.314
15.00	15.279	4.339	14.70	15.803	4.280
12.19	17.258	4.723	12.21	18.381	4.426
10.00	19.887	4.992	10.01	21.767	4.553
7.50	24.632	5.364	7.51	29.988	4.392
5.00	33.217	5.948	5.00	41.944	4.695
2.50	58.844	6.651	2.50	83.545	4.641

Table 17. Complex concentration dependent relaxivity of **GdL[4]** at 25°C, pH 7.3 and 9.4 T.

Without calcium(II)			With three equivalence of calcium(II)		
$[Gd^{3+}]$ (mM)	T_1 (ms)	r_1 ($mM^{-1}s^{-1}$)	$[Gd^{3+}]$ (mM)	T_1 (ms)	r_1 ($mM^{-1}s^{-1}$)
17.19	11.891	4.871	17.16	14.659	3.954
14.98	13.615	4.879	14.77	16.911	3.979
12.22	16.374	4.968	12.17	20.891	3.903
9.98	19.375	5.135	9.98	24.796	4.004
7.50	25.185	5.245	7.50	34.485	3.818
5.00	35.635	5.539	5.00	50.853	3.860
2.50	66.662	5.854	2.50	100.918	3.817

5.1.4 PGSE Diffusion ^{1}H NMR Spectroscopy

Appropriate amounts of **YL^{1}** and **YL^{4}** were dissolved in D_2O and in a solution of three equivalents of $CaCl_2$, respectively. The samples were diluted stepwise while keeping the pD at 7.2-7.4. The measurements were performed by using the standard stimulated echo pulse sequence on a Bruker Avance II^{+} 500 MHz spectrometer equipped with a gradient unit and a multinuclear inverse probe with a Z-gradient coil. The temperature was 298 K and the sample was not spun. The shape of the gradient pulses was rectangular, their duration (δ) was between 1.4 and 1.8 ms, depending on the sample and their strength (G) was varied during the experiments. The delay between the midpoints of the gradients (Δ) was set to 200 ms. The spectra were recorded using 32 – 1K scans, 32K points, a relaxation delay of 1.4 – 3.8 s, a spectral width of 7500 Hz and were processed with a line broadening of 2. The intensity of the ^{1}H resonances of the alkyl groups of the side chain was determined in all spectra. The plots of $\ln(I/I_0)$ versus G^2 were fitted using a linear regression algorithm to obtain the D values according to equation 5.1, where I = intensity of the observed spin-echo, I_0 = intensity of the spin-echo without gradients, γ = magnetogyric ratio, δ = length of the gradient pulse, D = diffusion coefficient, Δ = delay between the midpoints of the gradients and G = gradient strength.

$$\ln\frac{I}{I_0} = -(\gamma\delta)^2 D\left(\Delta - \frac{\delta}{3}\right)G^2 \qquad (5.1)$$

5.1.5 ^{31}P{^{1}H} NMR Spectroscopy

Appropriate amounts of **EuL^{1}** and **EuL^{4}** were dissolved in D_2O and the pD was adjusted to about 7.4. The ^{31}P{^{1}H} NMR spectra were recorded on a Bruker DRX 400 MHz and a Bruker Avance II^{+} 500 MHz spectrometer. The temperature was measured using an external thermocouple (PT 100). The signals were externally referenced to 1 % phosphoric acid in D_2O *via* deuterium lock. Calcium(II) was added via an highly concentrated solution of $CaCl_2 \cdot 6H_2O$ in D_2O while maintaining the pD at about 7.4.

5.1.6 Luminescence Spectroscopy

Solutions of **EuL^{1}-EuL^{4}** were prepared in H_2O (pH 7.3, HEPES) at various complex concentrations (5-50 mM) in the presence and absence of three equivalents of $CaCl_2$. The luminescence steady-state emission spectra were performed at 25°C on a QuantaMaster^{TM} 3 PH fluorescence spectrometer from Photon Technology International, Inc., USA.

5.1.7 Luminescence Lifetime Measurements

The decay experiments were performed on H_2O and D_2O **(**25°C, pH 7.3, HEPES) solutions of **EuL^1-EuL^4** at concentrations ranging from 5 to 50 mM. As for the steady state spectra, a QuantaMaster™ 3 PH fluorescence spectrometer from Photon Technology International, Inc., USA was used. The europium(III) ion was directly excited at 395 nm and the emission intensity at 615 nm was recorded with 10 μs resolution. Excitation and emission slits were set to 15 and 5 nm bandpass respectively. Datasets are average of 25 scans and each reported value is the mean of three independent measurements. Obtained curves are fitted to the first order exponential decay with $r^2 = 0.99$. The *q* values were calculated using equation 3.3 described in chapter 3.2.6.

Table 18. Emission lifetimes and estimated *q* values of **EuL^1** at 25°C and pH 7.3.

Without calcium(II)				With three equivalence of calcium(II)			
[**EuL^1**] (mM)	τ_{H2O} (ms)	τ_{D2O} (ms)	*q*	[**EuL^1**] (mM)	τ_{H2O} (ms)	τ_{D2O} (ms)	*q*
50	0.43	1.34	1.6	50	0.73	1.59	0.6
25	0.43	1.36	1.6	25	0.65	1.71	0.8
10	0.43	1.38	1.6	10	0.58	1.76	1.1
5	0.42	1.37	1.7	5	0.54	1.75	1.2

Table 19. Emission lifetimes and estimated *q* values of **EuL^2** at 25°C and pH 7.3.

Without calcium(II)				With three equivalence of calcium(II)			
[**EuL^2**] (mM)	τ_{H2O} (ms)	τ_{D2O} (ms)	*q*	[**EuL^2**] (mM)	τ_{H2O} (ms)	τ_{D2O} (ms)	*q*
50	0.66	1.45	0.7	50	0.77	1.45	0.4
25	0.63	1.46	0.8	25	0.75	1.57	0.5
10	0.60	1.48	0.9	10	0.72	1.64	0.6
5	0.58	1.55	1.0	5	0.68	1.65	0.7

Table 20. Emission lifetimes and estimated *q* values of **EuL^3** at 25°C and pH 7.3.

Without calcium(II)				With three equivalence of calcium(II)			
[**EuL^3**] (mM)	τ_{H2O} (ms)	τ_{D2O} (ms)	*q*	[**EuL^3**] (mM)	τ_{H2O} (ms)	τ_{D2O} (ms)	*q*
50	0.67	1.50	0.7	50	0.86	1.45	0.3
25	0.62	1.60	0.9	25	0.86	1.48	0.3
10	0.55	1.64	1.1	10	0.85	1.53	0.3
5	0.50	1.63	1.4	5	0.84	1.60	0.4

Table 21. Emission lifetimes and estimated *q* values of **EuL^4** at 25°C and pH 7.3.

Without calcium(II)				With three equivalence of calcium(II)			
[**EuL^4**] (mM)	τ_{H2O} (ms)	τ_{D2O} (ms)	*q*	[**EuL^4**] (mM)	τ_{H2O} (ms)	τ_{D2O} (ms)	*q*
50	0.69	1.52	0.6	50	0.88	1.57	0.3
25	0.67	1.59	0.7	25	0.88	1.61	0.3
10	0.66	1.65	0.8	10	0.88	1.70	0.4
5	0.65	1.66	0.8	5	0.89	1.75	0.4

5.1.8 ^{17}O NMR Spectroscopy

The ^{17}O NMR experiments were performed on a Bruker Avance 500 spectrometer (11.75 T, 67.8 MHz). The longitudinal ($1/T_1$) and transverse ($1/T_2$) ^{17}O NMR relaxation rates were measured for complexes **GdL^1-GdL^4** in the temperature range of 275–350 K. The concentration of the samples was about 50 mM and the pH of the solutions was adjusted to 6 using KOH/HCl. To improve the sensitivity in ^{17}O NMR, ^{17}O-enriched water (10 % $H_2{}^{17}O$, CortecNet) was added to the solutions to yield about 1 % ^{17}O enrichment. The exact gadolinium(III) concentration was determined using the BMS method described in chapter 5.1.2. The samples were sealed in glass spheres in order to eliminate the influence of the bulk magnetic susceptibility.[152] The exact temperature was calculated according to previous calibration with ethylene glycol and methanol.[153] The $1/T_1$-data were obtained by the inversion recovery method, while the $1/T_2$-data were measured by the Carr–Purcell–Meiboom–Gill spin-echo technique. Acidified water ($HClO_4$, pH 3.3) was used as external reference. The least-squares fit of the ^{17}O NMR data was performed by using Micromath® Scientist® version 2.0 (Salt Lake City, UT, USA). The reported errors correspond to one standard deviation obtained by the statistical analysis.

The least-squares fits were carried out using the following equations based on the Solomon-Bloembergen-Morgan theory (cf. chapter 2.3).

As outlined in chapter 3.2.7, the reduced relaxation rates, $1/T_{1r}$, $1/T_{2r}$, can be calculated from the measured ^{17}O NMR relaxation rates of the paramagnetic solutions, $1/T_1$, $1/T_2$, and of the reference, $1/T_{1A}$, $1/T_{2A}$, by using equations 5.2 and 5.3, where P_m is the molar fraction of bound water, $1/T_{1m}$, $1/T_{2m}$ are the relaxation rates of the bound water and $\Delta\omega_m$ is the chemical shift difference between bound and bulk water.

$$\left(\frac{1}{T_{1r}}\right) = \frac{1}{P_m}\left(\frac{1}{T_1} - \frac{1}{T_{1A}}\right) = \frac{1}{T_{1m} + \tau_m} \tag{5.2}$$

$$\left(\frac{1}{T_{2r}}\right) = \frac{1}{P_m}\left(\frac{1}{T_2} - \frac{1}{T_{2A}}\right) = \frac{1}{\tau_m}\frac{T_{2m}^{-2} + \tau_m^{-1}T_{2m}^{-1} + \Delta\omega_m^2}{(\tau_m^{-1} + T_{2m}^{-1})^2 + \Delta\omega_m^2} \tag{5.3}$$

$\Delta\omega_m$ is determined by the hyperfine interaction between the gadolinium(III) electron spin and the ^{17}O nucleus. Therefore, the hyperfine or scalar coupling constant $A/\hbar$ can be directly obtained from the chemical shifts measured for the paramagnetic sample, ω_p, referred to the chemical shift of the reference, ω_A, through equations 5.4 and 5.5.

$$\Delta\omega_r = \frac{1}{P_m}(\omega_p - \omega_A) = \frac{\Delta\omega_m}{(1 + \tau_m T_{2m}^{-1})^2 + \tau_m^2\Delta\omega_m^2} \tag{5.4}$$

$$\Delta\omega_m = \frac{g\mu_B S(S+1)B}{3k_B T}\frac{A}{\hbar} \tag{5.5}$$

where $\Delta\omega_r$ is the reduced ^{17}O chemical shift, B represents the magnetic field, S is the electron spin and g is the isotropic Landé g factor.

The ^{17}O longitudinal relaxation rate of the coordinated water molecules, $1/T_{1m}$, is governed by quadrupolar and dipolar mechanisms, $1/T_{1q}$ and $1/T_{1d}$, respectively, with the quadrupolar term being the major contribution. The terms are given in equation 5.6-5.9, where γ_S is the electron and γ_I is the nuclear gyromagnetic ratio (γ_S = 1.76×10^{11} rad s^{-1} T^{-1}, γ_I=-3.626×10^7 rad s^{-1} T^{-1}), r is the effective distance between the electron charge and the ^{17}O nucleus, I is the nuclear spin (5/2 for ^{17}O), χ^2 is the quadrupolar coupling constant and η is an asymmetry parameter:

$$\frac{1}{T_{1m}} = \frac{1}{T_{1q}} + \frac{1}{T_{1d}} \tag{5.6}$$

$$\frac{1}{T_{1q}} = \frac{3\pi^2}{10}\left(\frac{2I+3}{I^2(2I-1)}\right)\chi^2\left(1+\frac{\eta^2}{3}\right)\tau_{RO} \tag{5.7}$$

$$\frac{1}{T_{1d}} = \frac{1}{15}\left(\frac{\mu_0}{4\pi}\right)^2\left(\frac{\hbar^2\gamma_I^2\gamma_S^2}{r_{GdO}^6}\right)S(S+1)\left(6\tau_{d1}+14\frac{\tau_{d1}}{1+\omega_S^2\tau_{d2}^2}\right) \tag{5.8}$$

where:

$$\frac{1}{\tau_{d1,2}} = \frac{1}{\tau_{RO}} + \frac{1}{T_{1,2e}} + \frac{1}{\tau_m} \tag{5.9}$$

The rotational correlation time of the Gd-O$_{water}$ vector, τ_{RO}, is assumed to have a simple exponential temperature dependence with the activation energy E_R as follows:

$$\tau_{RO} = \tau_{RO}^{298} exp\left\{\frac{E_R}{R}\left(\frac{1}{T}-\frac{1}{298.15}\right)\right\} \tag{5.10}$$

Note that due to the internal motion of the coordinated water molecules around the Gd-O axis, the rotational correlation time of the Gd-H$_{water}$ vector, τ_{RH}^{298}, is usually lower than τ_{RO}^{298} (τ_{RH}/τ_{RO} = 0.65±0.2).[146, 147]

Since the oxygen is directly coordinated to gadolinium(III), in the ^{17}O transverse relaxation rate of coordinated water molecules, $1/T_{2m}$, the scalar contribution, $1/T_{2sc}$, is the most important (equation 5.11). In this equation, $1/\tau_{s1}$ is the sum of the exchange rate constant and the electron spin relaxation rate (equation 5.12).

$$\frac{1}{T_{2m}} \cong \frac{1}{T_{2sc}} = \frac{S(S+1)}{3}\left(\frac{A}{\hbar}\right)^2\tau_{s1} \tag{5.11}$$

$$\frac{1}{\tau_{s1}} = \frac{1}{\tau_m} + \frac{1}{T_{1e}} \tag{5.12}$$

The inverse binding time (or exchange rate k_{ex}) of water molecules in the inner sphere is assumed to obey the Eyring equation (equation 5.13), where $\Delta S^{\ddagger}$ and $\Delta H^{\ddagger}$ are the entropy and enthalpy of activation for the exchange, and k_{ex}^{298} is the exchange rate at 298.15 K.

$$\frac{1}{\tau_m} = k_{ex} = \frac{k_B T}{h} exp\left\{\frac{\Delta S^{\neq}}{R} - \frac{\Delta H^{\neq}}{RT}\right\} = \frac{k_{ex}^{298}}{298.15} exp\left\{\frac{\Delta H^{\neq}}{R}\left(\frac{1}{298.15} - \frac{1}{T}\right)\right\} \tag{5.13}$$

The electron spin relaxation rate, $1/T_{1e}$, has been fitted to a simple exponential equation:

$$\frac{1}{T_{1e}} = \frac{1}{T_{1e}^{298}} exp\left\{\frac{E_T}{R}\left(\frac{1}{T} - \frac{1}{298.15}\right)\right\} \tag{5.14}$$

Table 22. Variable temperature reduced longitudinal and transverse ^{17}O relaxation rates and chemical shifts of a **GdL^1** solution with c_{Gd} = 0.0509694 mol/L, B =11.75 T and using q = 1.

T (K)	T_{1A} (ms)	T_{2A} (ms)	ω_A (ppm)	T_1 (ms)	T_2 (ms)	ω (ppm)	ln(1/T_{1r})	ln(1/T_{2r})	$\Delta\omega_r$ (Hz)
278.1	3.990	3.972	1.566	3.080	0.904	-0.532	11.30	13.74	-9.74E+05
283.1	4.652	4.632	1.389	3.537	1.088	-0.849	11.21	13.55	-1.04E+06
293.1	6.092	6.052	0.761	4.754	1.612	-1.435	10.83	13.11	-1.02E+06
300.8	7.663	7.464	0.45	5.804	2.172	-1.624	10.73	12.78	-9.63E+05
308.1	9.436	9.142	0.139	7.032	2.804	-1.721	10.58	12.50	-8.64E+05
318.2	11.633	11.408	-0.312	8.699	3.830	-1.971	10.36	12.15	-7.70E+05
328.1	13.829	13.656	-0.935	10.701	5.112	-2.539	10.04	11.80	-7.45E+05
338.2	16.508	16.424	-1.203	12.767	6.756	-2.612	9.87	11.46	-6.54E+05
348.1	19.548	19.242	-1.697	14.906	8.402	-2.905	9.76	11.20	-5.61E+05

Table 23. Variable temperature reduced longitudinal and transverse ^{17}O relaxation rates and chemical shifts of a **GdL^2** solution with c_{Gd} = 0.0540287 mol/L, B =11.75 T and using q = 1.

T (K)	T_{1A} (ms)	T_{2A} (ms)	ω_A (ppm)	T_1 (ms)	T_2 (ms)	ω (ppm)	ln(1/T_{1r})	ln(1/T_{2r})	$\Delta\omega_r$ (Hz)
278.1	3.924	3.870	2.212	2.819	1.144	0.669	11.44	13.26	-6.14E+05
288.1	5.257	5.162	1.791	3.769	1.342	0.157	11.16	13.15	-6.51E+05
300.8	7.673	7.462	0.871	5.151	1.808	-0.88	11.00	12.88	-6.97E+05
308.1	9.307	8.674	0.626	6.227	2.186	-1.045	10.81	12.68	-6.65E+05
318.2	11.299	11.070	0.34	7.549	2.736	-1.299	10.62	12.46	-6.53E+05
328.1	13.833	13.686	-0.484	9.419	3.588	-2.002	10.36	12.17	-6.05E+05
338.2	16.496	16.424	-0.618	11.309	4.568	-2.039	10.17	11.90	-5.66E+05
348.1	19.418	18.784	-1.1	13.747	5.762	-2.069	9.90	11.63	-3.86E+05

Table 24. Variable temperature reduced longitudinal and transverse ^{17}O relaxation rates and chemical shifts of a **GdL^{3}** solution with c_{Gd} = 0.0632339 mol/L, B =11.75 T and using q = 1.

T (K)	T_{1A} (ms)	T_{2A} (ms)	ω_A (ppm)	T_1 (ms)	T_2 (ms)	ω (ppm)	ln(1/T_{1r})	ln(1/T_{2r})	$\Delta\omega_r$ (Hz)
278.1	3.924	3.870	2.212	2.753	1.134	1.255	11.20	12.95	-2.76E+05
288.1	5.257	5.162	1.791	3.753	1.522	0.858	10.85	12.65	-2.69E+05
300.8	7.673	7.462	0.871	4.814	1.758	-0.307	10.87	12.59	-3.39E+05
308.1	9.307	8.674	0.626	5.740	2.139	-0.502	10.72	12.38	-3.25E+05
318.2	11.299	11.070	0.34	7.184	2.728	-0.618	10.44	12.14	-2.76E+05
328.1	13.833	13.686	-0.484	8.872	3.402	-1.472	10.22	11.91	-2.84E+05
338.2	16.496	16.424	-0.618	10.985	4.238	-1.295	9.93	11.68	-1.95E+05
348.1	19.418	18.784	-1.1	13.202	4.582	-1.63	9.70	11.62	-1.53E+05

Table 25. Variable temperature reduced longitudinal and transverse ^{17}O relaxation rates and chemical shifts of a **GdL^{4}** solution with c_{Gd} = 0.0540287 mol/L, B =11.75 T and using q = 1.

T (K)	T_{1A} (ms)	T_{2A} (ms)	ω_A (ppm)	T_1 (ms)	T_2 (ms)	ω (ppm)	ln(1/T_{1r})	ln(1/T_{2r})	$\Delta\omega_r$ (Hz)
278.1	3.990	3.972	1.566	3.182	1.772	1.121	11.09	12.68	-1.95E+05
283.1	4.652	4.632	1.389	3.699	2.004	0.901	10.95	12.58	-2.14E+05
293.1	6.092	6.052	0.761	4.882	2.502	0.236	10.64	12.39	-2.30E+05
300.8	7.663	7.464	0.45	5.926	2.974	-0.124	10.58	12.25	-2.51E+05
308.1	9.436	9.142	0.139	7.096	3.560	-0.233	10.49	12.08	-1.63E+05
318.2	11.633	11.408	-0.312	8.64	4.110	-0.66	10.33	11.98	-1.52E+05
328.1	13.829	13.656	-0.935	10.226	4.466	-1.362	10.17	11.95	-1.87E+05
338.2	16.508	16.424	-1.203	12.217	4.656	-1.624	9.99	11.97	-1.84E+05
348.1	19.548	19.242	-1.697	14.164	4.564	-2.069	9.90	12.05	-1.63E+05

Table 26. Variable temperature reduced longitudinal and transverse ^{17}O relaxation rates and chemical shifts of a **GdL^{1}** solution in the presence of three equivalents of calcium(II) with c_{Gd} = 0.0540287 mol/L, B =11.75 T and using q = 1.

T (K)	T_{1A} (ms)	T_{2A} (ms)	ω_A (ppm)	T_1 (ms)	T_2 (ms)	ω (ppm)	ln(1/T_{1r})	ln(1/T_{2r})	$\Delta\omega_r$ (Hz)
278.1	2.750	1.154	1.328	3.924	3.870	2.212	11.68	13.40	-4.11E+05
300.8	5.098	2.328	0.181	7.673	7.462	0.871	11.18	12.68	-3.20E+05
318.2	6.589	3.102	-0.16	11.299	11.070	0.34	11.14	12.44	-2.32E+05
338.2	9.398	4.660	-0.831	16.496	16.424	-0.618	10.82	12.03	-9.89E+04

5.2 Silsesquioxane-based MRI Contrast Agents

5.2.1 Materials and General Remarks

(3-Aminopropyl)-triethoxysilane (99%), boron trifluoride ethyl etherate, lanthanum trichloride heptahydrate (99.999 %), yttrium trichloride hexahydrate (99.99 %), xylenol orange and methyl 4-(cyanomethyl)-benzoate (96 %) were purchased from Aldrich. Vinyltrichlorosilane (techn, 97%), azobisisobutyronitrile (AIBN), benzyl bromoacetate (purum, 97%), dimethyl sulfoxide (DMSO), purris. absolut, over molecular sieves), Amberlite IR-120, *tert*-butyltrichloroacetimidate (TBTA) were obtained from Fluka. Mercaptopropionic acid, palladium on charcoal (Pd/C, 10% Pd), *O*-(benzotriazol-1-yl)-N,N,N',N'-tetramethyluronium tetrafluoroborate (TBTU, $\geq$ 98 %), 1-hydroybenzotrialzol hydrate (HOBt), diisopropylethylamine (DIPEA), trifluoroacetic acid (TFA), L-glutamic acid, dimethylacetamide (DMA), N-bromosuccinimide (NBS), carbon tetrachloride, dimethyl malonate, tetra-*n*-butylammonium hydroxide (20 % in water) were purchased from Merck. Acetonitrile (extra dry, over molecular sieves, water <50 ppm) and *tert*-butyl bromoacetate (99%) were bought from Acros Organics. Amberlite XAD 1600 was obtained from Rohm and Haas. 1,4,7,10-tetraazacyclododecane (cyclen, 98%) was purchased from CheMatech. Gadolinium trichloride hydrate (99.99 %) was obtained from Chempur. Dihydrogen (purity 5.0) and argon (purity 5.0) was bought from Air Liquide. DO3A(^{t}Bu)$_3$ and DO3A-hexylamine were kindly provided by Dr. I. Mamedov, Max-Planck-Institute for Biological Cybernetics, Tübingen. All reagents not mentioned were obtained from the chemicals store at the University of Tübingen.

The lanthanide(III) chloride stock solutions were prepared by dissolving an accurately weighted amount of the chloride salt in the appropriate volume of distilled water. The exact concentration was determined *via* complexometric titration with the disodium salt of EDTA in an acetic acid / sodium acetate buffer (pH 5.8) using xylenol orange as indicator.

Reactions under inert conditions were performed in an argon atomosphere applying standard Schlenk techniques. Column chromatography was performed using silicagel 60. The absence of non-coordinated metal ions in the solutions of **GG**, **GB**, Gd-DOTAGA (**63**) and Gd-DOTABA (**78**), used in the analytical studies, was confirmed by the xylenol test.[136]

5.2.2 Diafiltration

Diafiltration was carried out on a Pall Minimate™ Tangential Flow Filtration System using a Pall Minimate™ TFF Capsule with an Omega™ 3K PES ultrafiltration membrane.

5.2.3 pH-metric Measurements

pH and pD[150] values of aqueous solutions were measured using a Schott handylab pH12 pH-meter equipped with a Mettler-Toledo Inlab Micro glass electrode.

5.2.4 Mass Spectrometry

HR mass spectra were recorded on a Bruker Daltonics 4.7 T APEX II FT-ICR instrument equipped with an ESI source. In the positive mode appropriate polyethylene glycol molecules were used for internal calibration and perfluoroheptanoic acid, perfluorooctanoic acid, perfluorodecanoic acid and perfluorododecanoic acid were used in the negative mode.
ESI mass spectra were recorded on a Bruker Daltonics esquire3000plus mass spectrometer (quadrupolar ion-trap) with an ESI interface.

5.2.5 Elemental Analysis

Elemental analysis was performed on an Elementar vario MICRO cube elemental analyser.

5.2.6 Solid-State NMR Spectroscopy

The solid state ^{13}C and ^{29}Si CP/MAS NMR spectra were recorded on a Bruker DSX 200 MHz spectrometer in a 4 mm ZrO_2 rotor and on a Bruker ASX 300 MHz spectrometer in a 7 mm ZrO_2 rotor, respectively. Magic angle spinning was performed at 1 KHz for the ^{29}Si NMR spectrum and at 10 KHz in the case of the ^{13}C NMR spectrum. The ^{13}C NMR spectrum was recorded at 50.33 MHz and the ^{29}Si NMR spectrum was recorded at 59.62 ppm

5.2.7 Solution NMR Spectroscopy

5.2.7.1 NMR spectroscopy for structural analysis

^{1}H and $^{13}C\{^{1}H\}$ NMR spectra were recorded on a Bruker Avance II 400 MHz or a Bruker Avance II^{+} 500 MHz spectrometer at room temperature, unless specified otherwise. ^{1}H and ^{13}C resonances were assigned using standard 2D techniques (^{1}H-^{1}H COSY, ^{1}H-^{13}C HSQC, ^{1}H-^{13}C HMBC).$^{29}Si\{^{1}H\}$ NMR spectra were recorded on a Bruker Avance II^{+} 500 MHz spectrometer at room temperature *via* 2D ^{1}H-^{29}Si HSQC experiments or using a DEPT45 sequence. ^{139}La NMR spectra were recorded on a Bruker Avance II^{+} 500 MHz spectrometer operating at 65°C. The NMR spectra were recorded at the following frequencies: ^{1}H NMR: 400.13 and 500.13 MHz; ^{13}C NMR: 100.61 and 125.76 MHz; ^{29}Si NMR: 99.36 MHz; ^{139}La NMR: 77.66 MHz. Except for ^{1}H NMR spectra measured in D_2O, which were referenced to the residual HDO peak ($\delta = 4.79$), all ^{1}H, $^{13}C\{^{1}H\}$ and $^{29}Si\{^{1}H\}$ NMR spectra were externally referenced to 1% TMS in $CDCl_3$ *via* deuterium lock.[154] ^{139}La NMR spectra were externally

referenced to 10 mM $LaCl_3$ in D_2O *via* deuterium lock.

5.2.7.2 Bulk magnetic susceptibility shift measurements

The gadolinium(III) concentration in water can be determined by measuring the bulk magnetic susceptibility (BMS) shift of the solution, independent of the state of coordination of the gadolinium(III).[151] For the BMS measurements a small amount of *tert*-butanol (5 µL) was added to the respective solution and the chemical shift of its ^{1}H NMR resonance was measured relative to a reference (internal capillary with *tert*-butanol/H_2O). The concentration was then calculated according to equation 5.15:

$$[\mathrm{Gd}]in\ mM = \left(\frac{2.84}{7.94}\right)^2 \frac{3\Delta_\chi T}{4\pi} \tag{5.15}$$

where Δ_χ = BMS chemical shift in ppm and T = absolute temperature.

5.2.7.3 PGSE diffusion ^{1}H NMR spectroscopy

^{1}H PGSE diffusion NMR measurements were performed by using the standard Bruker stimulated echo pulse sequence on a Bruker Avance II$^+$ 500 MHz spectrometer equipped with a gradient unit and a multinuclear inverse probe with a Z-gradient coil. Solutions of the yttrium(III) complexes of **GG**, **GB**, Y-DOTAGA (**63**) and Y-DOTABA (**78**) were prepared in D_2O having a pD of 7.0 ± 0.1. The concentrations were estimated from the BMS measurements of the analogous gadolinium(III) complexes (2-3 mM of the Gadoxanes and 15-20 mM for the monomeric complexes). The temperature during the measurements was 298 K and the sample was not spun. Rectangular gradient pulses with durations (δ) of 1.5 and 1.6 ms for the monomers and 2.4 and 3.0 ms for the Gadoxanes were applied. Their strength (G) was varied during the experiments. The delay between the midpoints of the gradients (Δ) was set to 150 ms for the monomers and 200 ms for the Gadoxanes. Δ was also kept at 200 ms during the degradation of **GG**. The spectra were recorded using 32 to 256 scans, 32K points, a relaxation delay of 1.6-3.5 s, a spectral width of 7500 Hz and were processed with a line broadening of 2 Hz. The intensities of the ^{1}H resonance of the following moieties were determined in each spectrum: CHCH_2 for Y-DOTAGA (**63**), Ar-2-H and Ar-6-H for Y-DOTABA (**78**), CH_2Si for the **GB** as well as for **GG** and its fragments. The plots of ln(I/I_0) *versus* G^2 were fitted using a linear regression algorithm to obtain the D values according to equation 5.16:

$$\ln\frac{I}{I_0} = -(\gamma\delta)^2 D\left(\Delta - \frac{\delta}{3}\right)G^2 \tag{5.16}$$

where I = intensity of the observed spin-echo, I_0 = intensity of the spin-echo without

gradients, γ = magnetogyric ratio, δ = length of the gradient pulse, D = diffusion coefficient, Δ = delay between the midpoints of the gradients and G = gradient strength.

5.2.7.4 Relaxivity measurements

Relaxivity measurements during the degradation of **GG** were performed at room temperature (~21 ˚C) in a 3 T (123 MHz) human MR scanner (MAGNETOM Tim Trio, Siemens Healthcare, Germany), using a 12-channel RF Head coil and slice selective measurements from a slice with a thickness of 1 mm positioned through the samples. The samples (0.8 ml) were freshly prepared for each time point (0-200 h) by making dilutions of **GG** at 0, 12.5, 25, 37.5, and 50 µM gadolinium(III) (1.56, 3.12, 4.69 und 6.25 µM **GG**) in culture medium (Dulbecco´s modified Earle´s medium, ± FCS, ± HEPES) in tubes and incubating them at 37°C and 10% CO_2 with or without gas exchange. The samples were then split into two 0.65 mL tubes prior to the MR relaxivity measurements. The pH of the solutions was estimated after the MR measurements. Solutions containing HEPES buffer had a pH in the range of 7.4-7.6 whereas the samples without HEPES and no gas exchange during the incubation period had pH values between 8.1 and 8.6. T_1 was measured using an inversion-recovery sequence, with an adiabatic inversion pulse followed by a turbo-spin-echo readout. Between 10 and 15 images were taken, with the time between inversion and readout varying from 23 to 3000 ms. With a repetition time of 10 s, 15 echoes were acquired per scan and averaged six times. All experiments scanned 256^2 voxels in a field-of-view of 110 mm in both directions resulting in a voxel volume of 0.43 × 0.43 × 1 mm^3. Data analysis was performed by fitting to relaxation curves with self-written routines under MATLAB 7.1 R14 (The Mathworks Inc., United States). The series of T_1 relaxation data were fitted according to equation 5.17 with varying $t = T_I$:

$$S = S_0\left(1 - e^{\frac{-t}{T_1}}\right) + S_{T_I=0}\left(e^{\frac{-t}{T_1}}\right) \tag{5.17}$$

Nonlinear least-squares fitting of three parameters S_0, $S_{(TI\,=\,0)}$, and T_1 was done for manually selected regions-of-interest with the Trust-Region Reflective Newton algorithm implemented in MATLAB. The quality of the fit was controlled by visual inspection and by calculating the mean errors and residuals. The obtained relaxation times T_{1obs} were used to evaluate the relaxivity r_1 according to equation 2.4 in chapter 2.3. The r_1 values were plotted vs. the incubation time and fitted by a first order exponential decay function to get the degradation kinetics of Gadoxane. In case of the incubation at higher pH a fit assuming a second order decay gives a better result indicating to a very fast initial degradation of the silsequioxane core at pH > 8.

The degradation of the silsesquioxane core of **GB** was studied by measuring the longitudinal relaxation rates ($1/T_{1obs}$) of water protons of an aqueous solution of **GB** ($c(Gd^{3+})$ = 1.99 mM, pH 7.4 (HEPES buffer)) on a Stelar SMARtracer Fast Field Cycling NMR relaxometer at 10 MHz and 37°C after different periods of time. During the first 36 h the sample was kept in the relaxometer, then the sample was kept in a water bath (37°C) between the measurements. The longitudinal relaxation rates were measured using an inversion-recovery sequence. The r_1 values were calculated from the obtained $1/T_{1obs}$ values according to equation 2.4 in chapter 2.3. Then the r_1 values were plotted *versus* the time and fitted by a first order exponential decay function using ORIGIN™ (Microcal, USA). The reported errors correspond to one standard deviation obtained by the statistical analysis.

Table 27. Longitudinal relaxivity r_1 of Gadoxane B (**GB**) under physiological conditions as a function of the time (37°C, pH 7.4, 10 MHz).

Time (h)	T_1 (s)	T_1 (s)	T_1 (s)	Mean T_1 (s)	r_1 ($mM^{-1}s^{-1}$)
0	0.03479	0.03492	0.03503	0.03491	14.14
1	0.03475	0.03488	0.03482	0.03481	14.18
2	0.03503	0.03466	0.03453	0.03474	14.21
3	0.03517	0.03513	0.03503	0.03511	14.06
4	0.03596	0.03623	0.03591	0.03603	13.70
5	0.03693	0.03707	0.03698	0.03699	13.34
6	0.03759	0.03788	0.03779	0.03775	13.06
7	0.03897	0.03922	0.03926	0.03915	12.59
8	0.04050	0.04013	0.04055	0.04039	12.20
9	0.04100	0.04161	0.04116	0.04126	11.94
10	0.04211	0.04236	0.04226	0.04224	11.66
12	0.04454	0.04501	0.04485	0.04480	10.98
14	0.04655	0.04619	0.04705	0.04660	10.55
24	0.05535	0.05555	0.05590	0.05560	8.81
27	0.05831	0.05825	0.05861	0.05839	8.38
29	0.05943	0.05962	0.05987	0.05964	8.20
32	0.06079	0.06118	0.06101	0.06099	8.02
35	0.06231	0.06265	0.06260	0.06252	7.82
37	0.06345	0.06364	0.06401	0.06370	7.67
48	0.06723	0.06724	0.06729	0.06725	7.25
57	0.06775	0.06792	0.06764	0.06777	7.20
72	0.06960	0.06944	0.06984	0.06963	7.00
96	0.07136	0.07167	0.07192	0.07165	6.80
120	0.07205	0.07260	0.07198	0.07221	6.74

Table 28. Longitudinal relaxivity r_1 (3 T, r.t.) during the degradation of **GG** under physiological conditions (cell culture media, 20 mM HEPES, pH 7.4-7.6) with and without fetal calf serum (FCS).

	r_1 ($mM^{-1}s^{-1}$)		
Time (h)	With serum	Without serum	Mean value
0	10.62	10.59	10.60
0.5	10.15	9.79	9.97
1	10.54	9.88	10.21
2	10.74	-	10.74
4	10.49	9.80	10.15
6	9.29	10.29	9.79
19	8.23	8.34	8.28
45	7.52	7.51	7.52
200	6.90	6.54	6.72

5.2.7.5 Variable temperature ^{17}O NMR and ^{1}H NMRD measurements

The transverse and longitudinal ^{17}O relaxation rates ($1/T_{1,2}$) and the chemical shifts were measured in the aqueous solutions of the gadolinium(III) complexes in the temperature range 275–361 K for the monomeric complexes (**63**, **78**) and 275–320 K for the Gadoxanes, on a Bruker Avance II 300 MHz (7.05 T, 40.69 MHz) spectrometer with a 10 mm broad band probe. The gadolinium(III) concentration of the samples was between 9.9 and 16.6 mM and the pH of the solutions was 6.7 (HEPES buffer). To improve the sensitivity in ^{17}O NMR, ^{17}O-enriched water (10 % $H_2{}^{17}O$, CortecNet) was added to the solutions to yield about 3 % ^{17}O enrichment. The exact gadolinium(III) concentration was determined using the BMS method (chapter 5.2.7.2). The temperature was determined by measuring the chemical shift of neat ethylene glycol.[155] An acidified water solution was used as reference ($HClO_4$, pH 3.0). The samples were sealed in glass spheres fitted into 10 mm NMR tubes, to eliminate susceptibility corrections to the chemical shifts.[152] Longitudinal ^{17}O relaxation times (T_1) were measured by the inversion-recovery pulse sequence, and the transverse relaxation times (T_2) were obtained by the Carr-Purcell-Meiboom-Gill spin-echo technique.

Proton NMRD profiles were recorded on a Stelar SMARtracer Fast Field Cycling NMR relaxometer (0.01–10 MHz) and a Bruker WP80 NMR electromagnet (20, 40, 60 and 80 MHz) adapted to variable field measurements and controlled by the SMARtracer PC-NMR console. The temperature was controlled by a VTC91 temperature control unit and maintained by a gas flow. The temperature was determined according to previous calibration with a Pt resistance temperature probe. The relaxivities at 250, 400 and 500 MHz was measured on a Bruker DRX 250 MHz, a Bruker Avance II 400 MHz and a Bruker Avance II$^+$ 500 MHz

spectrometer using an inversion-recovery sequence. The temperature was determined with ethylene glycol.[155] The least-squares fits of the ^{17}O NMR and ^{1}H NMRD data were performed by using Micromath® Scientist® version 2.0 (Salt Lake City, UT, USA). The reported errors correspond to one standard deviation obtained by the statistical analysis.

The equations involved in the analysis of the ^{17}O NMR measurements were already reported in chapter 5.1.8. For the analysis of the ^{1}H NMRD profiles the equations of the modified Solomon-Bloembergen-Morgan theory as given in chapter 2.3 were used. The electronic correlation time for the modulation of the zero-field-splitting interaction, τ_v, in equations 2.13-2.15 and the sum of the diffusion coefficients D_I and D_S of water and the gadolinium(III) complex, D_{IS}, were thereby assumed to have simple exponential dependence *versus* $1/T$ (equations 5.18 and 5.19).

$$\tau_v = \tau_v^{298} exp\left\{\frac{E_v}{R}\left(\frac{1}{T} - \frac{1}{298.15}\right)\right\} \tag{5.18}$$

$$D_{IS} = D_{IS}^{298} exp\left\{\frac{E_{IS}}{R}\left(\frac{1}{298.15} - \frac{1}{T}\right)\right\} \tag{5.19}$$

where E_v and E_{IS} are their respective activation energies.

For the two Gadoxanes, the Lipari-Szabo approach was applied. In this model two statistically independent rotational motions are distinguished: A rapid local motion of the Gd-H_{water} vector with a correlation time τ_{lH} and a slower global motion of the entire molecule with a correlation time τ_{gR}. Supposing the global molecular reorientation is isotropic, equation 2.9 in chapter 2.3 is written as the following:

$$\frac{1}{T_1^{DD}} = \frac{2}{15}\left(\frac{\gamma_I^2 g^2 \mu_B^2}{r_{GdH}^6}\right) S(S+1)\left(\frac{\mu_0}{4\pi}\right)^2 (7J(\omega_S;\tau_{C2}) + 3J(\omega_I;\tau_{C1})) \tag{5.20}$$

where

$$J(\omega_S;\tau_{C2}) = \frac{S^2\tau_{c2g}}{1+\omega_S^2\tau_{c2g}^2} + \frac{(1-S^2)\tau_{c2l}}{1+\omega_S^2\tau_{c2l}^2} \tag{5.21}$$

$$J(\omega_I;\tau_{C1}) = \frac{S^2\tau_{c2}}{1+\omega_I^2\tau_{c1g}^2} + \frac{(1-S^2)\tau_{c2}}{1+\omega_I^2\tau_{c1l}^2} \tag{5.22}$$

with

$$\frac{1}{\tau_{c1,2g}} = \frac{1}{\tau_{gR}} + \frac{1}{T_{1,2e}} + \frac{1}{\tau_m} \tag{5.23}$$

$$\frac{1}{\tau_{c1,2l}} = \frac{1}{\tau_{lH}} + \frac{1}{T_{1,2e}} + \frac{1}{\tau_m} \tag{2.24}$$

The general order parameter S^2 describes the degree of spatial restriction of the local motion. If the local motion is isotropic, $S^2 = 0$; if the rotational dynamics is only governed by the global motion, $S^2 = 1$.

Table 29. Variable temperature reduced longitudinal and transverse ^{17}O relaxation rates and chemical shifts of a Gd-DOTAGA (**63**) solution with c_{Gd} = 0.01655 mol/L, B =7.05 T and using q = 1.

T (K)	T_{1A} (ms)	T_{2A} (ms)	ω_A (ppm)	T_1 (ms)	T_2 (ms)	ω (ppm)	ln(1/T_{1r})	ln(1/T_{2r})	$\Delta\omega_r$ (Hz)
275.5	3.544	3.522	4.292	3.059	1.944	4.000	11.92	13.56	-2.51E+05
286.0	5.109	5.092	6.550	4.312	1.736	6.355	11.71	14.06	-1.67E+05
299.1	7.387	7.416	3.131	6.346	1.578	2.947	11.22	14.33	-1.58E+05
309.7	9.304	9.426	5.416	8.030	1.692	4.931	10.96	14.30	-4.16E+05
328.1	13.969	13.94	1.757	12.263	2.874	1.215	10.42	13.74	-4.65E+05
342.8	17.858	17.318	3.894	15.465	4.486	3.428	10.28	13.23	-4.00E+05
360.8	23.207	22.816	0.333	20.089	8.078	-0.082	10.02	12.50	-3.56E+05

Table 30. Variable temperature reduced longitudinal and transverse ^{17}O relaxation rates and chemical shifts of a Gd-DOTABA (**78**) solution with c_{Gd} = 0.01248 mol/L, B =7.05 T and using q = 1.

T (K)	T_{1A} (ms)	T_{2A} (ms)	ω_A (ppm)	T_1 (ms)	T_2 (ms)	ω (ppm)	ln(1/T_{1r})	ln(1/T_{2r})	$\Delta\omega_r$ (Hz)
275.8	3.457	3.500	7.064	3.205	2.154	6.883	11.52	13.59	-2.06E+05
286.0	5.127	5.032	6.632	4.567	2.228	6.341	11.58	13.92	-3.31E+05
297.5	7.325	7.522	6.056	6.513	2.060	5.694	11.23	14.27	-4.12E+05
309.7	9.515	9.548	5.475	8.320	2.116	5.164	11.12	14.31	-3.54E+05
319.4	11.654	11.592	5.008	10.338	2.474	4.624	10.79	14.16	-4.37E+05
342.8	17.485	17.452	4.035	15.772	4.768	3.593	10.23	13.43	-5.03E+05
360.8	23.495	22.996	3.088	21.443	8.806	2.665	9.81	12.65	-4.81E+05

Table 31. Variable temperature reduced longitudinal and transverse ^{17}O relaxation rates and chemical shifts of a Gadoxane G (**GG**) solution with c_{Gd} = 0.01285 mol/L, B =7.05 T and using q = 1.

T (K)	T_{1A} (ms)	T_{2A} (ms)	ω_A (ppm)	T_1 (ms)	T_2 (ms)	ω (ppm)	ln(1/T_{1r})	ln(1/T_{2r})	$\Delta\omega_r$ (Hz)
275.8	3.575	3.592	6.855	3.091	2.196	6.800	12.15	13.55	-6.08E+04
286.0	5.109	5.092	6.550	4.328	2.338	6.406	11.94	13.82	-1.59E+05
297.5	7.318	7.334	5.895	6.203	2.372	5.629	11.57	14.03	-2.94E+05
309.7	9.304	9.426	5.416	7.959	2.596	5.074	11.27	14.00	-3.78E+05
319.4	11.612	11.500	5.009	9.942	3.050	4.628	11.04	13.86	-4.21E+05

Table 32. Variable temperature reduced longitudinal and transverse ^{17}O relaxation rates and chemical shifts of a Gadoxane B (**GB**) solution with c_{Gd} = 0.00994 mol/L, B =7.05 T and using q = 1.

T (K)	T_{1A} (ms)	T_{2A} (ms)	ω_A (ppm)	T_1 (ms)	T_2 (ms)	ω (ppm)	ln(1/T_{1r})	ln(1/T_{2r})	$\Delta\omega_r$ (Hz)
275.8	3.457	3.500	7.064	2.981	2.344	6.904	12.46	13.58	-2.29E+05
286.0	5.127	5.032	6.632	4.207	2.586	6.393	12.38	13.86	-3.42E+05
297.5	7.325	7.522	6.056	5.960	2.644	5.773	12.07	14.13	-4.04E+05
309.7	9.515	9.548	5.475	7.686	2.970	5.232	11.85	14.08	-3.47E+05
319.4	11.654	11.592	5.008	9.536	3.270	4.659	11.58	14.02	-4.99E+05

Table 33. NMRD data of Gd-DOTAGA (**63**) at 25°C and 37°C. (c_{Gd} = 2.02 mM for $\nu(^1H) \leq 10$ MHz and c_{Gd} = 2.49 mM for $\nu(^1H) > 10$ MHz).

$\nu(^1H)$ (MHz)	r_1 ($mM^{-1}s^{-1}$) at 25°C	r_1 ($mM^{-1}s^{-1}$) at 37°C
500	4.19	3.23
400	4.64	3.52
250	5.18	3.86
80	4.64	3.59
60	4.81	3.73
40	4.86	3.78
20	5.17	4.14
10.001	6.69	5.53
6.951	7.40	6.17
4.833	8.36	7.10
3.360	9.38	7.84
2.336	10.52	8.60
1.623	11.27	9.13
1.129	11.81	9.47
0.785	11.93	9.67
0.546	12.07	9.77
0.379	12.26	9.82
0.264	12.26	9.90
0.183	12.28	9.93
0.128	12.38	9.92
0.089	12.20	9.95
0.062	12.34	9.87
0.043	12.25	9.91
0.030	12.23	9.93
0.021	12.35	9.94
0.014	12.49	9.96

Table 34. NMRD data of Gd-DOTABA (**78**) at 25°C and 37°C. (c_{Gd} = 2.00 mM for $\nu(^1H) \leq 10$ MHz and c_{Gd} = 2.01 mM for $\nu(^1H) > 10$ MHz).

$\nu(^1H)$ (MHz)	r_1 ($mM^{-1}s^{-1}$) at 25°C	r_1 ($mM^{-1}s^{-1}$) at 37°C
500	4.46	3.55
250	5.70	4.15
80	5.39	4.19
60	5.41	4.45
40	5.53	4.34
20	5.87	4.73
10.001	6.95	5.68
6.951	7.48	6.23
4.833	8.62	7.16
3.360	9.72	8.00
2.336	10.90	8.97
1.623	11.88	9.61
1.129	12.47	10.17
0.785	12.82	10.38
0.546	13.02	10.57
0.379	13.19	10.62
0.264	13.22	10.66
0.183	13.29	10.66
0.128	13.25	10.78
0.089	13.34	10.67
0.062	13.30	10.65
0.043	13.35	10.72
0.030	13.30	10.78
0.021	13.37	10.72
0.014	13.18	10.79

Table 35. NMRD data of Gadoxane G (**GG**) at 25°C and 37°C. (c_{Gd} = 2.00 mM for $\nu(^1H) \leq 10$ MHz and c_{Gd} = 1.99 mM for $\nu(^1H) > 10$ MHz).

$\nu(^1H)$ (MHz)	r_1 ($mM^{-1}s^{-1}$) at 25°C	r_1 ($mM^{-1}s^{-1}$) at 37°C
500	4.99	4.17
400	5.93	5.17
250	8.03	6.70
80	11.20	9.13
60	11.55	9.38
40	12.19	9.58
20	12.13	9.58
10.001	11.87	9.52
6.951	11.73	9.51
4.833	12.08	10.14
3.360	12.95	10.87
2.336	14.49	12.34
1.623	16.01	13.56
1.129	17.06	14.48
0.785	17.83	15.17
0.546	18.23	15.58
0.379	18.57	15.73
0.264	18.76	15.93
0.183	18.73	15.96
0.128	18.96	16.03
0.089	18.83	16.00
0.062	18.97	16.12
0.043	18.76	16.12
0.030	18.98	15.98
0.021	18.98	16.13
0.014	19.04	16.32

Table 36. NMRD data of Gadoxane B (**GB**) at 25°C and 37°C. (c_{Gd} = 1.99 mM for $\nu(^1H) \leq 10$ MHz and c_{Gd} = 2.00 mM for $\nu(^1H) > 10$ MHz).

$\nu(^1H)$ (MHz)	r_1 ($mM^{-1}s^{-1}$) at 25°C	r_1 ($mM^{-1}s^{-1}$) at 37°C
500	4.46	4.20
250	7.70	7.31
80	14.04	12.73
60	15.61	13.83
40	16.73	14.56
20	17.11	14.76
10.001	16.53	14.28
6.951	15.58	13.55
4.833	15.35	13.30
3.360	15.51	13.64
2.336	17.07	15.45
1.623	18.85	17.13
1.129	20.31	18.53
0.785	21.19	19.50
0.546	22.01	20.49
0.379	22.48	20.83
0.264	22.83	21.08
0.183	22.69	21.22
0.128	22.95	21.20
0.089	23.05	21.38
0.062	23.13	21.34
0.043	22.98	21.37
0.030	23.01	21.47
0.021	23.05	21.38
0.014	22.97	21.45

5.2.8 Syntheses

5.2.8.1 Synthesis of octa(3-chloroammoniumpropyl)silsesquioxane (29)

29 was synthesised according to the literature[121] procedure in 39 % yield.

5.2.8.2 Synthesis of octa(3-(ethylmercapto)-propionic acid)silsesquioxane (33)

Synthesis of octavinylsilsesquioxane (31)

31 was synthesised from vinyltrichlorosilane according to the literature[125, 126] in 15 % yield.

Synthesis of octa(3-(ethylmercapto)-propionic acid)silsesquioxane (33)

33 was prepared from **31**, mercaptopropionic acid and AIBN as the radical initiator according to the literature[125] in 98 % yield.

5.2.8.3 Synthesis of DOTA(^{t}Bu)$_3$ (36)

Synthesis of DOTA(^{t}Bu)$_3$Bn (35)

Under argon atmosphere DO3A(^{t}Bu)$_3$ (**34**) (500 mg, 0.973 mmol) was dissolved in dry acetonitrile (35 mL) and benzyl bromoacetat (246 mg, 1.071 mmol) was added followed by K_2CO_3 (202 mg, 1.460 mmol). The mixture was stirred for 19 h at 70°C. After cooling to room temperature the solid was filtered off and the solvent removed under reduced pressure. The crude product was purified on a silica gel column (DCM, increasing the ratio of MeOH to 15%) resulting in a yellow oil (564 mg, 87 %).

^{1}H NMR (500.13 MHz, $CDCl_3$): δ = 7.39-7.28 (m, 5H, Ar-H), 5.11, (s, 2H, CH_2Ph) 3.91-1.95 (br m, 24H, NCH_2), 1.46, 1.43 (s, 27H, C(CH_3)$_3$). ^{13}C{^{1}H} NMR (125.76 MHz, $CDCl_3$): δ = 173.7 (*C*OOBn), 173.2, 173.1 (*C*OO^{t}Bu), 135.3 (Ar-*C*), 128.7, 128.6, 128.5 (Ar-*C*H), 82.0, 81.9 (*C*(CH$_3$)$_3$), 66.9 (*C*H$_2$Ph), 55.9, 55.7, 55.2, 51.9, 51.0, 50.6 (N*C*H$_2$), 28.1, 28.0 (C(*C*H$_3$)$_3$).

Synthesis of DOTA(^{t}Bu)$_3$ (36)

Pd/C (10 % Pd, 200 mg) was added to a solution **35** (280 mg, 0.422 mmol) in dry degassed methanol (25 mL). The mixture was stirred vigorously under a dihydrogen atmosphere (balloon) for 3 h. The catalyst was filtered off and the solvent removed under reduced pressure to afford a pale yellow solid (210 mg, 87 %).

^{1}H NMR (500.13 MHz, $CDCl_3$): δ = 3.93-1.95 (br m, 24H, NCH_2), 1.44, 1.43 (s, 27H, C(CH_3)$_3$). ^{13}C NMR (125.76 MHz, $CDCl_3$): δ = 174.5 (*C*OOH), 172.3 (*C*OO^{t}Bu), 82.5, 82.2 (*C*(CH$_3$)$_3$), 56.1, 55.9, 55.6, 53.6-51.8 (br), 49.5-48.0 (br) (N*C*H$_2$), 28.2, 27.9 (C(*C*H$_3$)$_3$).

ESI-MS: $[M+H]^+$ calc. 573.4 , found 573.5.

5.2.8.4 Synthesis of compound 46

Method 1: Under argon atmosphere **29** (50 mg, 4.26×10^{-5} mol) and **36** (295 mg, 5.11×10^{-4} mol) were dissolved in dry DMSO (4 mL). HOBt (77 mg, 5.11×10^{-4} mol) and TBTU (160 mg, 5.11×10^{-4} mol) were added followed by DIPEA (750 µL, 4.38×10^{-3} mol). The mixture was stirred for 20 h at room temperature and then added drop-wise to distilled water (10 mL) at ~ 0°C while a yellow precipitate was formed. The precipitate was filtered off and dissolved in methanol (30 mL). Removal of the solvent under reduced pressure resulted in a pale yellow solid (219 mg). No signal in the ^{29}Si NMR spectrum. Destruction of the silsesquioxane core.

Method 2: Under argon atmosphere **29** (10 mg, 8.51×10^{-6} mol) and **36** (59 mg, 1.02×10^{-4} mol) were dissolved in dry DMSO (500 µL) and TBTU (33 mg, 1.02×10^{-4} mol) was added followed by DIPEA (100 µL, 5.84×10^{-4} mol). The mixture was stirred for 30 min at room temperature and then added drop-wise to distilled water (10 mL) in a centrifuge tube which was kept in an ice bath. The formed precipitate was centrifuged, washed four-times with cold water and dissolved in methanol (1 mL). Removal of the solvent under reduced pressure resulted in a pale yellow solid (43 mg, 95 %).

^{1}H NMR (500.13 MHz, $CDCl_3$): δ= 3.75-1.92 (192H, Cyclen NCH_2, CH_2CO), 3.19 (br, 8H, NCH_2CH$_2$), 1.60 (br, 8H, NCH$_2$CH_2), 0.59 (br, 8H, CH_2Si), 1.43 (s, 216H, C(CH_3)$_3$). ^{13}C{^{1}H} NMR (125.76 MHz, $CDCl_3$): δ= 173.3-170.7 (br, *C*O), 81.2 (br, *C*(CH$_3$)$_3$), 56.4-46.1 (br Cyclen N*C*H$_2$, CH$_2$*C*O), 41.5 (br, N*C*H$_2$CH$_2$), 27.5 (C(*C*H$_3$)$_3$), 22.4 (br, N*C*H$_2$CH$_2$), 9.4 (br, *C*H$_2$Si). ^{29}Si{^{1}H} NMR (99.36 MHz, $CDCl_3$): δ= -66.9.

5.2.8.5 Attempted deprotection of compound 46

Method 1: To a solution of **46** (36 mg, 6.768×10^{-6} mol) dissolved in DCM (0.5 mL) trifluoroacetic acid (0.25 mL) was added drop-wise. After stirring for 8 h at room temperature the volatile matter was removed under reduced pressure. The residue was taken up into a small amount of acetone. The addition of diethyl ether resulted in an off-white precipitate. The precipitate was dried *in vacuo*. ^{1}H NMR of the product in D_2O indicated an almost complete deprotection but a decomposition of the silsesquioxane core, as well.

Method 2: To a solution of **46** (36 mg, 6.768×10^{-6} mol) dissolved in DCM (0.5 mL) conc. formic acid (0.5 mL) was added drop-wise. After stirring at room temperature for 16 h the solvent was evaporated under reduced pressure. To remove the excess of formic acid, DCM and methanol were added and evaporated off, twice. The product remained soluble in DCM.

^{1}H NMR of the product in $CDCl_3$ revealed incomplete deprotection and also the decomposition of the silsesquioxane core.

5.2.8.6 Synthesis of compound 49

DO3A-hexylamine (**47**) (54 mg, 1.214×10^{-4} mol) was dissolved in distilled water (0.36 mL) and a stock solution of $LaCl_3$ (1.1 equiv.) was added. The pH was adjusted to 7 using a 1 M solution of NaOH. The mixture was heated to 60°C for 3 h. After cooling to room temperature, the pH was verified to be 7.0 and the solvent was evaporated and the remaining solid residue was dried *in vacuo* at 50°C over night.

Under argon atmosphere, the residue was then dissolved in dry DMSO (4 mL) and a solution of **33** (60 mg, 4.048×10^{-5} mol), TBTU (156 mg, 4.856×10^{-4} mol), HOBt (76 mg, 4.856×10^{-4} mol) and DIPEA (160 µL, 9.344×10^{-4}) in dry DMSO (2 mL) was added. After stirring at room temperature for 30 min, the reaction mixture was added drop-wise to an acetic acid/sodium acetate buffer (buffer capacity of 10 mmol/L, pH 5.5, 50 mL). The formed precipitate was centrifuged, washed four-times with cold water (10 mL), followed by four-times acetone (10 mL) and one-times diethyl ether (10 mL) and dried *in vacuo* (off-white solid, 170 mg).

^{13}C CP/MAS (50.33 MHz): δ= 183-167 (*C*OO$^-$, *C*ON), 70-58 (*C*H$_2$COO$^-$), 57-42 (*C*H$_2$N), 41-33 (*C*H$_2$NCO, NO*C*CH$_2$CH$_2$S), 32-19 (alkyl *C*H$_2$, *C*H$_2$S*C*H$_2$), 14 (*C*H$_2$Si). ^{29}Si CP/MAS (59.62 MHz): δ= -67.5.

5.2.8.7 Synthesis of DOTA(Bn)$_3$ (53)

Synthesis of DO3A(Bn)$_3$ (51)

Under argon atmosphere cyclen (**50**) (4.31 g, 25 mmol) and $NaHCO_3$ (6.30 g, 75 mmol) were suspended in dry acetonitrile (50 mL). At 0°C *tert*-butyl bromoacetat (10.98 mL, 70 mmol) dissolved in dry acetonitril (200 mL) was added drop-wise over 6 h. The mixture was then allowed to reach room temperature and stirred for 3 day. The formed white precipitate was filtered off and the solvent was removed under reduced pressure. The solid residue was dissolved in a 10 % acetonitrile/water mixture (240 mL) and the pH was adjusted to 3 using HCl_{aq}. The solution was loaded onto a column of Amberlite XAD 1600 (200 mL), equilibrated with 10 % acetonitrile/water and eluted with a stepwise acetonitrile/water gradient. The product in a mixture with the undesired DOTA(Bn)$_4$ eluted at 30 % acetonitrile/water. At higher ratios of acetonitrile DOTA(Bn)$_4$ eluted exclusively. Removal of the solvent under reduce pressure resulted in about 9 g mixture and 5 g pure DOTA(Bn)$_4$. The

mixture was again dissolved in 10 % acetonitrile/water mixture (200 mL) (pH 3) and loaded onto an Amberlite XAD 1600 column. The ratio of acetonitrile was slowly increased starting from 20 %. The pure product eluted at an acetonitrile ratio of 28-29 %. Removal of the solvent under reduced pressure resulted in a white powder (1.5 g, 10 %).

^{1}H NMR (500.13 MHz, $CDCl_3$): δ = 7.37-7.16 (m, 15H, Ar-H), 5.15, (s, 2H, CH_2Ph), 5.00 (d, $^2J_{HH}$ = 11.4 Hz, 2H, C*H*HPh), 4.90 (d, $^2J_{HH}$ = 11.4 Hz, 2H, CH*H*Ph), 4.58 (br, 2H, NCH_2COO), 4.05, 3.72 (br m, 4H, Cyclen CH_2), 3.57, 3.43 (br m, 4H, NCH_2COO), 3.44, 3.30 (br m, 4H, Cyclen CH_2), 3.40, 2.98 (br m, 4H, Cyclen CH_2), 3.37, 2.90 (br m, 4H, Cyclen CH_2). ^{13}C{^{1}H} NMR (125.76 MHz, $CDCl_3$): δ = 171.6, 166.4 (*C*OOBn), 135.1, 134.1, 128.9, 128.8, 128.75, 128.72, 128.6, 128.5 (Ar-C), 68.1, 67.3 (*C*H_2Ph) 54.7, 53.3 (N*C*H_2COO), 52.7, 50.4, 48.2, 42.8 (Cyclen *C*H_2). ESI-MS: $[M+H]^+$ calc. 617.3 , found 617.5.

Synthesis of DOTA(Bn)$_3$^{t}Bu (52)

Under argon atmosphere **51** (600 mg, 0.973 mmol) was dissolved in dry acetonitrile (35 mL) and *tert*-butyl bromoacetat (228 mg, 1.171 mmol) was added followed by K_2CO_3 (202 mg, 1.459 mmol). The mixture was stirred for 23 h at 70°C. After cooling to room temperature the solid was filtered off and the solvent removed under reduced pressure. The crude product was purified on a silica gel column ($CHCl_3$, increasing the ratio of MeOH to 15%) resulting in a sticky yellow solid (497 mg, 70 %).

^{1}H NMR (500.13 MHz, $CDCl_3$): δ = 7.37-7.23 (m, 15H, Ar-H), 5.19-5.0, (br, 6H, CH_2Ph), 3.87-1.95 (br m, 24H, NCH_2), 1.43 (s, 9H, C(CH_3)$_3$). ^{13}C{^{1}H} NMR (125.76 MHz, $CDCl_3$): δ = 173.9, 173.8, 173.3 (*C*OO), 135.3, 135.2 (br), 128.74, 128.71, 128.68, 128.6, 128.5 (Ar-C), 82.3 (*C*$(CH_3)_3$), 67.07, 67.06 (*C*H_2Ph), 56.0, 55.4, 55.3 (N*C*H_2COO), 53.9-46.3 (br, Cyclen *C*H_2), 28.1 (C(*C*H_3)$_3$). HRMS (FTICR): $[M+H]^+$ calc.: 731.40144, found: 731.40083.

Synthesis of DOTA(Bn)$_3$ (53)

52 was dissolved in DCM (10 mL) and trifluoroacetic acid (10 mL) was added carefully. After stirring for 22 h at room temperature the volatile matter was removed under reduced pressure. To remove the excess of trifluoroacetic acid, DCM (10 mL) was twice added and evaporated off. The solid residue was dissolved in 10 % MeOH/water (60 mL) and the pH was brought to 2 using HCl_{aq}. The solution was loaded onto a column of Amberlite XAD 1600[133] (160 mL), equilibrated with 10 % MeOH/water and eluted with a stepwise MeOH/water gradient. The product only eluted at 100 % MeOH. Evaporation of the solvent under reduced pressure resulted in a yellow solid (205 mg, 47 %).

^{1}H NMR (400.13 MHz, $CDCl_3$): δ = 7.36-7.27 (m, 15H, Ar-H), 5.10, (s, 4H, CH_2Ph), 5.09, (s,

2H, C*H*$_2$Ph), 3.68 (s, 2H, C*H*$_2$COOH), 3.57 (s, 2H, C*H*$_2$COOBn), 3.50 (m, 4H, Cyclen C*H*$_2$), 3.42 (s, 4H, C*H*$_2$COOBn), 2.98 (m, 4H, Cyclen C*H*$_2$), 2.73 (m, 4H, Cyclen C*H*$_2$), 2.73 (m, 4H, Cyclen C*H*$_2$). ^{13}C{^{1}H} NMR (100.61 MHz, $CDCl_3$): δ= 171.2, 170.5 (*C*OOBn), 170.5 (*C*OOH), 135.5, 135.3, 128.68, 128.62, 128.52, 128.44, 128.42, 128.32 (Ar-C), 66.6, 66.4 (*C*H$_2$Ph), 56.1 (*C*H$_2$COOH), 55.9, 55.6 (*C*H$_2$COOBn), 53.5, 53.3, 50.5, 48.3 (Cyclen *C*H$_2$). ESI-MS: $[M+Na]^+$ calc. 697.3, found 697.3.

5.2.8.8 Synthesis of compound 54

Under argon atmosphere **29** (10 mg, 8.51×10^{-6} mol) and **53** (64 mg, 9.48×10^{-5} mol) were dissolved dry DMSO (500 µL) and TBTU (33 mg, 1.02×10^{-4} mol) was added followed by DIPEA (100 µL, 5.84×10^{-4} mol). The mixture was stirred for 30 min at room temperature and then added drop-wise to distilled water (12 mL) in a centrifuge tube which was kept in an ice bath. The formed precipitate was centrifuged and washed four-times with cold water. The residue was dissolved in chloroform (0.4 mL) and transferred into a schlenk tube, (rinsed with 0.4 mL chloroform). Removal of the solvent under reduced pressure resulted in a dark yellow solid (44 mg, 86 %). Due to the ^{1}H and ^{29}Si NMR data no complete octafunctionalisation was achieved.

Data of the octafunctionalised species:

^{1}H NMR (400.13 MHz, $CDCl_3$): δ= 7.40-7.23 (m, 120H, Ar-H), 3.67-2.40 (192H, Cyclen NC*H*$_2$, C*H*$_2$CO), 3.11 (br, 8H, NC*H*$_2$CH$_2$), 1.58 (br, 8H, NCH$_2$C*H*$_2$), 0.57 (br, 8H, C*H*$_2$Si). ^{13}C{^{1}H} NMR (100.61 MHz, $CDCl_3$): δ= 171.6-170.7 (br, *C*O), 135.9, 128.7, 128.4 (br, Ar-C), 66.1 (br, C*H*$_2$Ph), 57.1-47.3 (br Cyclen N*C*H$_2$, CH$_2$*C*O), 42.1 (br, N*C*H$_2$CH$_2$), 22.7 (br, N*C*H$_2$CH$_2$), 9.5 (br, *C*H$_2$Si). ^{29}Si NMR (99.36 MHz, $CDCl_3$): δ= -67.0.

5.2.8.9 Attempted deprotection of compound 54

54 (44 mg, ~7.16×10^{-6} mol) was dissolved in dry DMF (1 mL). Pd/C (10 % Pd, 10 mg) was added and the solvent was degassed. The mixture was stirred vigorously under a dihydrogen atmosphere for 2.5 h at room temperature. The catalyst was filtered off, and the solution was added drop-wise to diethyl ether (11 mL) in a centrifuge tube which was kept in an ice bath. The formed precipitate was centrifuged, washed with diethyl ether and dried under reduced pressure. The residual solid was insoluble in water, but still soluble in $CDCl_3$. As the ^{1}H NMR spectrum showed no cleavage of the benzyl esters, the reaction was reset. Therefore the solid residue was dissolved in dry DMF (1 mL) and Pd/C (10 % Pd, 12 mg) was added. After degassing the solvent, the mixture was stirred vigorously under a dihydrogen atmosphere for 2 days at room temperature. The ^{1}H NMR spectrum of the reaction solution showed only little

toluene formation, indicating less than 30 % deprotection.

5.2.8.10 Synthesis of DOTAGA (60)

Route 1:

Synthesis of 2-bromoglutaric acid (57)

To a stirred solution of L-glutamic acid (**56**) (16.50 g, 112 mmol) and sodium bromide (40.00 g, 389 mM) in aqueous 2 N hydrobromic acid (100 mL) cooled to 0°C sodium nitrite (14.00 g, 203 mM) was added gradually over 2 h. About 10 min after the last addition conc. sulphuric acid (6 mL) was added. The mixture was extracted three times with diethyl ether. The combined organic phases were washed with brine and dried over magnesium sulfate. Removal of the solvent under reduced pressure resulted in a yellow oil (11.13 g, 47%, about 85 % pure due to ^{1}H NMR).

^{1}H NMR (400.13 MHz, $CDCl_3$): δ = 9.99 (br s, 2H, COO*H*), 4.42 (dd, $^{3}J_{HH}$ = 7.3 Hz, $^{3}J_{HH}$ = 6.2 Hz, 1H, C*H*Br), 2.73-2.60 (m, 2H, CH_2COOH), 2.49-2.27 (m, 2H, CHBrCH_2). ^{13}C{^{1}H} NMR (100.61 MHz, $CDCl_3$): δ = 178.8 (CH_2*C*OOH), 175.0 (CHBr*C*OOH), 44.1 (*C*HBr), 31.3 (*C*H_2COOH), 29.3 (CHBr*C*H_2).

Synthesis of di-*tert*-butyl 2-bromoglutarate (58)

The crude 2-bromoglutaric acid (**57**) (3.20 g, ~13 mmol) was dissolved in $CHCl_3$ (40 mL) under argon atmosphere. A solution of *tert*-butyltrichloroacetimidate (TBTA) (13.25 g, 60.66 mmol) in cyclohexane (40 mL) was added drop-wise over 15 min. The formed white precipitate was dissolved by the addition of dimethylacetamide (DMA) (12 mL). Boron trifluoride ethyl etherate (600 µL) was added as catalyst and the solution was stirred for three days at room temperature. The mixture was concentrated and the remaining DMA phase was extracted three times with hexane (50 mL). The combined hexane phases were washed three times with brine, dried over magnesium sulfate and the solvent was removed. The crude product was purified on a silica gel column (*n*-hexane:ethyl acetate 15:1) resulting in a colorless oil (1.69 g, 40 %).

^{1}H NMR (400.13 MHz, $CDCl_3$): δ = 4.23 (dd, $^{3}J_{HH}$ = 8.4 Hz, $^{3}J_{HH}$ = 6.0 Hz, 1H, C*H*Br), 2.44-2.36 (m, 2H, CH_2COO^{t}Bu), 2.35-2.13 (m, 2H, CHBrCH_2), 1.48 (s, 9H, COOC(CH_3)$_3$), 1.45 (s, 9H, COOC(CH_3)$_3$). ^{13}C{^{1}H} NMR (100.61 MHz, $CDCl_3$): δ = 171.6 (CH_2*C*OO^{t}Bu), 168.6 (CHBr*C*OO^{t}Bu), 82.8 (COO*C*(CH$_3$)$_3$), 81.0 (COO*C*(CH$_3$)$_3$), 47.0 (*C*HBr), 33.0 (*C*H_2COO^{t}Bu), 30.1 (CHBr*C*H_2), 28.3 (COOC(*C*H$_3$)$_3$), 81.0 (COOC(*C*H$_3$)$_3$).

Synthesis of DOTAGA(^{t}Bu)$_5$ (59)

DO3A(^{t}Bu)$_3$ (**34**) (1200 mg, 2.332 mmol) was dissolved in dry acetonitrile (50 mL) under argon atmosphere and **58** (820 mg, 2.565 mmol) was added followed by K_2CO_3 (483 mg, 3.498 mmol). The mixture was stirred for 16 h at 70°C. After cooling to room temperature the solid was filtered off and the solvent removed under reduced pressure. The crude product was purified on a silica gel column (pure $CHCl_3$, gradually increasing the ratio of MeOH to 10%) resulting in a yellow solid (1.228 mg, 70 %).

^{1}H NMR (500.13 MHz, $CDCl_3$): δ= 3.45 (dd, $^3J_{HH}$ = 9.9 Hz, $^3J_{HH}$ = 1.7 Hz, 1H, NC*H*COO^{t}Bu), 3.38 (d, $^2J_{HH}$ = 17.3 Hz, 1H, NC*H*HCOO^{t}Bu), 2.78 (d, $^2J_{HH}$ = 17.3 Hz, 1H, NCH*H*COO^{t}Bu), 3.36 (d, $^2J_{HH}$ = 17.2 Hz, 1H, NC*H*HCOO^{t}Bu), 2.78 (d, $^2J_{HH}$ = 17.2 Hz, 1H, NCH*H*COO^{t}Bu), 3.34 (d, $^2J_{HH}$ = 17.5 Hz, 1H, NC*H*HCOO^{t}Bu), 2.78 (d, $^2J_{HH}$ = 17.5 Hz, 1H, NCH*H*COO^{t}Bu), 3.22, 2.10 (br m, 2H, Cyclen CH_2), 3.20, 2.13 (br m, 2H, Cyclen CH_2), 3.19, 2.10 (br m, 2H, Cyclen CH_2), 3.03, 2.47 (br m, 2H, Cyclen CH_2), 2.50, 2.31 (br m, 2H, Cyclen CH_2), 2.50, 2.34 (br m, 2H, Cyclen CH_2), 2.49, 2.30 (br m, 2H, Cyclen CH_2), 2.48, 2.26 (br m, 2H, Cyclen CH_2), 2.47, 2.42 (m, 2H, CH_2CH_2COO^{t}Bu), 1.95, 1.66 (m, 2H, CH_2CH_2COO^{t}Bu), 1.44 (s, 9H, C(CH_3)$_3$), 1.413 (s, 9H, C(CH_3)$_3$), 1.409 (s, 18H, C(CH_3)$_3$), 1.39 (s, 9H, C(CH_3)$_3$). ^{13}C{^{1}H} NMR (125.76 MHz, $CDCl_3$): δ= 174.9 (NCH*C*OO^{t}Bu), 173.0 (NCH$_2$*C*OO^{t}Bu), 172.9 (2C, NCH$_2$*C*OO^{t}Bu), 172.2 (CH_2CH_2*C*OO^{t}Bu), 82.3, 81.9, 81.8 (2C), 80.5 (*C*(CH$_3$)$_3$), 59.9 (N*C*HCOO^{t}Bu), 55.9, 55.8, 55.6 (N*C*H$_2$COO^{t}Bu), 52.7 (2C), 52.5, 48.7, 48.6, 48.2, 47.2, 44.3 (Cyclen *C*H$_2$), 33.6 (CH_2*C*H$_2$COO^{t}Bu), 28.1, 27.9, 27.8, (C(*C*H$_3$)$_3$), 19.7 (*C*H$_2$CH$_2$COO^{t}Bu). HRMS (FTICR): $[M+2H]^{2+}$ calc.: 379.26970, found: 379.26962.

Synthesis of DOTAGA (60)

59 (1.200 g, 1.585 mmol) was dissolved in dichloromethane (10 mL) and trifluoroacetic acid (15 mL) was added carefully. After stirring for 23 h at room temperature the volatile matter was removed under reduced pressure. To remove the excess of trifluoroacetic acid, methanol (20 mL) was twice added and evaporated off. The viscous residue was taken up in a minimum amount of methanol and added drop-wise to cold diethyl ether. The formed precipitate was filtered off and the procedure repeated with water-acetone. Again the precipitate was filtered off and dried *in vacuo* to yield the ammonium TFA salt of DOTAGA (containing about 85 % pure DOTAGA) as an off-white powder (541 mg, 61 %).

^{1}H NMR (400.13 MHz, D_2O): δ= 3.99 (dd, $^3J_{HH}$ = 9.0 Hz, $^3J_{HH}$ = 3.8 Hz, 1H, NC*H*COOH), 3.95-2.90 (br, 22H, NCH_2), 2.68 (m, 2H, CH_2CH_2COOH), 2.01 (m, 2H, CH_2CH$_2$COOH). ^{13}C{^{1}H} NMR (100.61 MHz, D_2O): δ= 177.4 (CH_2CH_2*C*OOH), 175.2, 174.0, 170.4 (br, NCH$_2$*C*OOH), 59.6 (br, *C*HCOOH), 55.9, 53.8, 51.0, 48.5, 45.6, 44.3 (br, N*C*H$_2$), 31.4

(CH_2CH_2COOH), 21.7 (CH_2CH_2COOH). HRMS (FTICR): $[M+H]^+$ calc.: 477.21912, found: 477.21900.

Route 2:

Synthesis of dimethyl 2-bromoglutarate (61)

The crude 2-bromoglutaric acid (**57**) (5.00 g, ~20 mmol) was dissolved in a solution of conc. sulphuric acid (700 µL) in methanol (50 mL) and the mixture was heated to reflux for 1 h. The solution was allowed to reach room temperature and concentrated under reduced pressure. Diethyl ether was added and the organic phase was washed with aqueous $NaHCO_3$ (5%) followed by brine and dried over magnesium sulfate. After removal of the solvent under reduced pressure, the crude product was purified on a short silica gel column (n-hexane:ethyl acetate 9:1) resulting in a colorless oil (3.60 g, 75 %).

^{1}H NMR (400.13 MHz, $CDCl_3$): δ= 4.32 (dd, $^3J_{HH}$ = 8.4 Hz, $^3J_{HH}$ = 5.8 Hz, 1H, C*H*Br), 3.72 (s, 3H, CH_2COOCH_3), 3.63 (s, 3H, $CHBrCOOCH_3$), 2.54-2.40 (m, 2H, CH_2COOCH_3), 2.38-2.16 (m, 2H, $CHBrCH_2$). ^{13}C{^{1}H} NMR (100.61 MHz, $CDCl_3$): δ= 172.4 (CH_2COOCH_3), 169.8 ($CHBrCOOCH_3$), 53.0 (CH_2COOCH_3), 51.8 $CHBrCOOCH_3$), 44.6 (*C*HBr), 31.2 (CH_2COOCH_3), 29.7 ($CHBrCH_2$). Anal. calc. for $C_7H_{11}BrO_4$: C, 35.17, H, 4.64, found: C, 35.13, H, 4.38.

Synthesis of DOTAGA(^{t}Bu)$_3$(Me)$_2$ (62)

Under argon atmosphere DO3A(^{t}Bu)$_3$ (**34**) (470 mg, 0.913 mmol) was dissolved in dry acetonitrile (25 mL) and **61** (240 mg, 1.000 mmol) was added followed by K_2CO_3 (242 mg, 1.749 mmol). The mixture was stirred for 16 h at 70°C. After cooling to room temperature the solid was filtered off and the solvent removed under reduced pressure. The crude product was purified on a silica gel column (pure $CHCl_3$, gradually increasing the ratio of MeOH to 15%) resulting in a yellow solid (435 mg, 71 %).

^{1}H NMR (500.13 MHz, $CDCl_3$): δ= 3.59 (s, 3H, $NCHCOOCH_3$), 3.53 (s, 3H, $CH_2CH_2COOCH_3$), 3.48 (dd, $^3J_{HH}$ = 10.3 Hz, $^3J_{HH}$ = 2.4 Hz, 1H, $NCHCOOCH_3$), 3.32 (d, $^2J_{HH}$ = 17.3 Hz, 1H, NC*H*HCOO^{t}Bu), 2.73 (d, $^2J_{HH}$ = 17.3 Hz, 1H, NCH*H*COO^{t}Bu), 3.27 (d, $^2J_{HH}$ = 17.6 Hz, 1H, NC*H*HCOO^{t}Bu), 2.74 (d, $^2J_{HH}$ = 17.6 Hz, 1H, NCH*H*COO^{t}Bu), 3.27 (d, $^2J_{HH}$ = 17.0 Hz, 1H, NC*H*HCOO^{t}Bu), 2.72 (d, $^2J_{HH}$ = 17.0 Hz, 1H, NCH*H*COO^{t}Bu), 3.08, 2.05 (br m, 6H, Cyclen CH_2), 2.96, 2.37 (br m, 2H, Cyclen CH_2), 2.49 (m, 2H, $CH_2CH_2COOCH_3$), 2.43, 2.25 (br m, 4H, Cyclen CH_2), 2.41, 2.25 (br m, 2H, Cyclen CH_2), 1.92, 1.68 (m, 2H, $CH_2CH_2COOCH_3$), 1.34 (s, 9H, $C(CH_3)_3$), 1.33 (s, 9H, $C(CH_3)_3$), 1.31 (s,

9H, C(C*H*$_3$)$_3$). ^{13}C{^{1}H} NMR (125.76 MHz, $CDCl_3$): δ = 175.9 (NCH*C*OOCH$_3$), 173.2 (CH$_2$CH$_2$*C*OOCH$_3$), 173.0, 172.9, 172.7 (NCH$_2$*C*O^{t}Bu), 82.0, 81.90, 81.86 (*C*(CH$_3$)$_3$), 59.2 (*C*HCOOCH$_3$), 55.7, 55.6, 55.4 (N*C*H$_2$COO^{t}Bu), 52.6, 52.5, 52.3, 48.5, 48.4, 48.0, 47.0, 44.6 (Cyclen *C*H$_2$), 52.1 (NCHCOO*C*H$_3$), 51.5 (CH$_2$CH$_2$COO*C*H$_3$), 31.6 (CH$_2$*C*H$_2$COOCH$_3$), 27.73, 27.72, 27.68, (C(*C*H$_3$)$_3$), 19.0 (*C*H$_2$CH$_2$COOCH$_3$). HRMS (FTICR): $[M+Na]^+$ calc.: 695.42017, found: 695.42074.

Synthesis of DOTAGA (60)

62 (435 mg, 0.647 mmol) was dissolved in aqueous 6 N hydrochloric acid (30 mL) and refluxed for 18 h. The solution was allowed to reach room temperature, washed with diethyl ether and the solvent removed under reduced pressure to yield the ammonium chloride salt of DOTAGA (containing 85 % pure DOTAGA) as an off-white powder (333 mg, 92%).

^{1}H NMR (400.13 MHz, D_2O): δ = 3.99 (dd, $^3J_{HH}$ = 9.0 Hz, $^3J_{HH}$ = 3.8 Hz, 1H, NC*H*COOH), 3.95-2.90 (br, 22H, NC*H*$_2$), 2.68 (m, 2H, CH$_2$C*H*$_2$COOH), 2.01 (m, 2H, C*H*$_2$CH$_2$COOH). ^{13}C{^{1}H} NMR (100.61 MHz, D_2O): δ = 177.4 (CH$_2$CH$_2$*C*OOH), 175.2, 174.0, 170.4 (br, NCH$_2$*C*OOH), 59.6 (br, *C*HCOOH), 55.9, 53.8, 51.0, 48.5, 45.6, 44.3 (br, N*C*H$_2$), 31.4 (CH$_2$*C*H$_2$COOH), 21.7 (*C*H$_2$CH$_2$COOH). HRMS (FTICR): $[M+H]^+$ calc.: 477.21912, found: 477.21900.

5.2.8.11 Synthesis of Gadoxane G (GG)

60 (49 mg, 8.74×10^{-5} mol) was dissolved in an aqueous solution of *n*-Bu$_4$NOH (20 %, 548 µL, 4.18×10^{-4} mol), followed by the addition of 1.1 equivalents of a stock solution of $LnCl_3$. The pH was verified to be between 6 and 7. The solution was heated to 70°C for about 3 h. The solvent was removed under reduced pressure and the remaining solid residue was dried for 4 to 6 days *in vacuo*. Under argon atmosphere the residue was taken up in dry DMSO (1 mL) and stirred for 1 day. To the resulting solution **29** dissolved in dry DMSO (10 mg, 8.51×10^{-6} mol in 0.5 mL dry DMSO) was added, followed by DIPEA (0.1 mL, 5.84×10^{-4} mol) and TBTU (33 mg, 1.02×10^{-4} mol). After 30 min of stirring at room temperature the reaction mixture was added drop-wise to an acetic acid/sodium acetate buffer (buffer capacity of 12 mmol/L, pH 5.5, 50 mL). This solution was poured into 50 mL of distilled water in the reservoir of a Pall Minimate™ Tangential Flow Filtration System. Diafiltration was carried out using a membrane with a molecular weight cutoff of 3K. The permeated volume was continuously replaced by an aqueous solution of NaCl (1 %, 400 mL), followed by pure water (400 mL). After the volume replacement was stopped, the diafiltration was continued until the volume had reduced to about 10 mL. The remaining solution was

collected in a schlenk flask (rinsed with 10 mL H_2O). The solvent was removed *in vacuo* at 25°C to afford **GG** as a white solid. Absence of non-coordinated lanthanide ions was confirmed by the xylenol test.[136] The yield calculated from the gadolinium(III) concentration obtained by the BMS method (see chapter 5.2.7.2) was about 37 %.

Characterisation data of the yttrium complex:

^{1}H NMR (500.13 MHz, D_2O,): δ= 3.63 (br d, 16H, C*H*HCOO$^-$), 3.25 (br d, 16H, CH*H*COO$^-$), 3.63 (br d, 8H, C*H*HCOO$^-$), 3.22 (br d, 8H, CH*H*COO$^-$), 3.48, 2.47 (br, 32H, Cyclen CH_2), 3.45, 2.44 (br, 16H, Cyclen CH_2), 3.36 (br, 8H, NC*H*COO$^-$), 3.25, 3.14 (br, 16H, NCH_2CH$_2$), 3.07, 2.81 (br, 16H, Cyclen CH_2), 2.84, 2.73 (br, 16H, Cyclen CH_2), 2.77 (br, 32H, Cyclen CH_2), 2.67 (br, 16H, Cyclen), 2.63, 2.35 (br, 16H, CH_2CON), 2.04, 1.88 (br, 16H, CHCH_2), 1.64 (br, 16H, CH_2CH$_2$Si), 0.75 (br, 16H, CH_2Si). ^{13}C{^{1}H} NMR (125.76 MHz, D_2O): δ= 180.7, 180.5, 180.3 (*C*OO$^-$), 175.4 (*C*ON), 68.4 (N*C*HCOO$^-$), 65.9, 65.8 (br, *C*H$_2$COO$^-$) 56.1, 55.9, 55.6, 55.4, 55.1, 54.7, 54.4, 45.8 (br, Cyclen *C*H$_2$), 41.6 (N*C*H$_2$CH$_2$), 34.8 (*C*H$_2$CON), 22.0 (*C*H$_2$CH$_2$Si), 20.4 (CH*C*H$_2$), 8.4 (*C*H$_2$Si). ^{29}Si{^{1}H} NMR (99.36 MHz, D_2O): δ= -65.3. HRMS (FTICR): $[M]^{8-}$ calc.: 653.48706, found: 653.48702

5.2.8.12 Synthesis of DOTAMA (64)

Synthesis of dimethyl 2-bromomalonate (67)

To a solution of dimethyl malonate (**66**) (13.21 g, 100 mmol) in freshly distilled carbon tetrachloride (15 mL) dry bromine (16.2 g, 101 mmol) was added gradually under stirring. After the first few milliliters of bromine had been added to the solution, an electric bulb was held under the flask until the reaction started. Then the rest of the bromine was added at such a rate as to keep the solution boiling gently. After the last addition the solution was refluxed for 45 min. The mixture was cooled, washed with aqueous K_2CO_3 (5%) and dried over magnesium sulfate. Repeated distillation under reduced pressure afforded the product in 98 % purity (2 % dimethyl malonate) as a colorless liquid (9.60 g, 45 %).

^{1}H NMR (500.13 MHz, $CDCl_3$): δ= 4.85 (s, 1H, C*H*Br), 3.83 (s, 6H, COOCH_3). ^{13}C{^{1}H} NMR (125.76 MHz, $CDCl_3$): δ= 165.1 (*C*OOCH$_3$), 54.1 (COO*C*H$_3$), 41.7 (*C*HBr).

Synthesis of DOTAMA(^{t}Bu)$_3$(Me)$_2$ (72)

Under argon atmosphere DO3A(^{t}Bu)$_3$ (**34**) (600 mg, 1.166 mmol) was added to a solution of **67** (271 mg, 1.282 mmol) in dry acetonitrile (25 mL), followed by K_2CO_3 (242 mg, 1.749 mmol). The mixture was stirred for 16 h at 70°C. After cooling to room temperature the solid was filtered off and the solvent removed under reduced pressure. The crude product was

purified on a silica gel column (pure $CHCl_3$, gradually increasing the ratio of MeOH to 15%) resulting in a yellow solid (631 mg, 84 %).

^{1}H NMR (400.13 MHz, $CDCl_3$): δ= 4.22 (s, 1H, C*H*($COOCH_3$)$_2$), 3.73 (s, 6H, COOC*H*$_3$), 3.43, 2.78 (m, 2H, NC*H*$_2$COO^{t}Bu), 3.38, 2.53 (m, 2H, Cyclen C*H*$_2$), 3.36, 2.10 (m, 2H, Cyclen C*H*$_2$) 3.34, 2.81 (m, 4H, NC*H*$_2$COO^{t}Bu), 3.30, 2.11 (m, 4H, Cyclen C*H*$_2$), 2.87, 2.30 (m, 2H, Cyclen C*H*$_2$), 2.47, 2.31 (m, 2H, Cyclen C*H*$_2$), 2.45, 2.35 (m, 4H, Cyclen C*H*$_2$), 1.41, 1.40 (s, 27H, C(C*H*$_3$)$_3$). ^{13}C{^{1}H} NMR (100.61 MHz, $CDCl_3$): δ= 173.1, 172.9 (NCH$_2$*C*OO^{t}Bu), 171.0, 167.1 (*C*OOCH$_3$), 82.4, 82.0 (*C*(CH$_3$)$_3$), 64.6 (*C*H(COOCH$_3$)$_2$), 55.9, 55.6 (N*C*H$_2$COO^{t}Bu), 52.8, 52.3, 48.8, 48.3, 48.2, 46.0, (Cyclen *C*H$_2$), 52.7, 52.4 (COO*C*H$_3$), 27.9, (C(*C*H$_3$)$_3$). HRMS (FTICR): $[M+Na]^+$ calc.: 667.38887, found: 667.38902.

Synthesis of DOTAMA(Me)$_2$ (75)

72 (265 mg, 0.411 mmol) was dissolved in dichloromethane (5 mL) and trifluoroacetic acid (5 mL) was added carefully. After stirring for 20 h at room temperature the volatile matter was removed under reduced pressure. To remove the excess of trifluoroacetic acid methanol (5 mL) was twice added and evaporated off. The viscous residue was taken up in a minimum amount of methanol and added drop-wise to cold diethyl ether. The precipitate was filtered off and dried under reduced pressure to yield 171 mg (87%) of an off-white powder.

^{1}H NMR (500.13 MHz, D_2O): δ= 5.24 (s, 1H, C*H*($COOCH_3$)$_2$), 4.00 (br, 4H, NC*H*$_2$COOH), 3.83 (s, 6H, COOC*H*$_3$), 3.69 (br, 2H, NC*H*$_2$COOH), 3.60, 3.50 (m, 4H, Cyclen C*H*$_2$), 3.57, 3.47 (m, 4H, Cyclen C*H*$_2$), 3.28, 3.19 (m, 4H, Cyclen C*H*$_2$), 3.13, 3.02 (m, 4H, Cyclen C*H*$_2$). ^{13}C{^{1}H} NMR (125.76 MHz, D_2O): δ= 174.3 (*C*OOH), 169.7 (*C*OOH), 168.8 (*C*OOCH$_3$), 63.3 (*C*H(COOCH$_3$)$_2$), 56.0 (*C*H$_2$COOH), 53.3 (COO*C*H$_3$), 52.8 (*C*H$_2$COOH), 51.6, 71,0, 47.9, 45.5 (Cyclen *C*H$_2$). HRMS (FTICR): $[M+Na]^+$ calc.: 499.20106, found: 499.20143.

Synthesis of DOTAMA (64*)

Method 1: **75** (49 mg, 1.02x10^{-4} mol) was dissolved in an aqueous solution of *n*-Bu$_4$NOH (20 %, 682 µL, 5.20×10^{-4} mol) and H_2O (500 µL) was added. The solution was stirred for 21 h, after which the solvent was removed under reduced pressure.

Method 2: **75** (26 mg, 5.46x10^{-5} mol) was dissolved in an aqueous solution (1 mL) of sodium hydroxide (11.6 mg, 2.89x10^{-4} mol) and the solution was stirred for 26 h, after which the solvent was removed under reduced pressure.

Characterisation data of the sodium salt:

^{1}H NMR (400.13 MHz, D_2O): δ= 3.98 (s, 1H, C*H*(COO^-)$_2$), 3.12 (br, 4H, NC*H*$_2$COO$^-$), 3.07 (s, 2H, NC*H*$_2$COO$^-$) 2.72, 2.71, 2.58, 2.42 (br, 16H, Cyclen C*H*$_2$). ^{13}C{^{1}H} NMR

(100.61 MHz, D_2O): δ = 180.6, 180.0 ($NCH_2\mathit{C}OO^-$), 177.1 ($CH(\mathit{C}OO^-)_2$), 70.7 ($\mathit{C}H(COO^-)_2$), 58.2, 57.9 ($N\mathit{C}H_2COO^-$), 51.3, 50.5, 50.1, 48.2 (Cyclen $\mathit{C}H_2$). HRMS (FTICR) of the gadolinium(III) complex of **64**: $[M]^-$ calc.: 602.074376, found: 602.074098.

5.2.8.13 Attempted synthesis of compound 77

DOTAMA($^nBu_4N)_5$ (**64***) (1.02×10^{-4} mol) was dissolved in distilled water (0.8 mL) and 1.4 equivalents of a stock solution of YCl_3 were added. A light precipitate could be observed. The pH was verified to be 7.2±0.1 The suspenion was stirred at room temperature for 17 h, after which a clear solution (pH 7.0) was obtained. The solvent was removed under reduced pressure and the remaining solid residue was dried for 2 days *in vacuo*. Under argon atmosphere the residue was taken up in dry DMSO (1 mL) and stirred for 2 days. To the resulting almost clear solution TBTU (33 mg, 1.02×10^{-4} mol) and a solution of octa(3-chloroammoniumpropyl)silsesquioxane in dry DMSO (10 mg, 8.51×10^{-6} mol, 0.5 mL dry DMSO) were added, followed by DIPEA (0.1 mL, 5.84×10^{-4} mol). After 30 min of stirring at room temperature the reaction mixture was added drop-wise to an acetic acid/sodium acetate buffer (buffer capacity of 12 mmol/L, pH 5.5, 50 mL). The solution was poured into 50 mL of distilled water in the reservoir of a Pall Minimate™ Tangential Flow Filtration System. Diafiltration was carried out using a membrane with a molecular weight cutoff of 3K. The permeated volume was continuously replaced by an aqueous solution of NaCl (1 %, 400 mL), followed by pure water (400 mL). After the volume replacement was stopped, the diafiltration was continued until the volume had reduced to about 10 mL. The remaining solution was collected in a schlenk flask (rinsed with 10 mL H_2O). The solvent was removed under reduced pressure at 25°C. No product could be obtained.

5.2.8.14 Synthesis of DOTABA (65)

Synthesis of 4-(carboxymethyl)benzoic acid (69)

69 was prepared from methyl 4-(cyanomethyl)-benzoate (**68**) according to the literature[138] in 84 % yield.

Synthesis of methyl 4-((methoxycarbonyl)methyl)benzoate (70)

Under argon atmosphere **69** (1.00 g, 5.55 mmol) was dissolved in dry methanol (20 mL) and cooled to 0°C. A solution of thionyl chloride (1 mL, 13.78 mmol) in dry methanol (20 mL) was added drop-wise over 15 min. The solution was allowed to reach room temperature and stirred for 22 h. Removal of the volatile matters under reduced pressure resulted in a yellow oil (1.10 g, 95 %).

^{1}H NMR (400.13 MHz, $CDCl_3$): δ = 8.00 (m, A-portion of an $[AB]_2$-system, 2H, Ar-2-H, Ar-6-H), 7.37 (m, B-portion of an $[AB]_2$-system, 2H, Ar-3-H, Ar-5-H) 3.67 (s, 2H, C*H*$_2$), 3.90 (s, 3H, ArCOOC*H*$_3$), 3.69 (s, 3H, CH_2COOC*H*$_3$). ^{13}C{^{1}H} NMR (100.61 MHz, $CDCl_3$): δ = 171.1 (CH_2*C*OOCH$_3$), 166.7 (Ar*C*OOCH$_3$), 138.8 (Ar-4-C), 129.8 (Ar-2-C, Ar-6-C), 129.3 (Ar-3-C, Ar-5-C), 128.9 (Ar-1-C), 52.5 (CH_2COO*C*H$_3$), 52.4 ArCOO*C*H$_3$), 41.2 (*C*H$_2$).

Synthesis of methyl 4-((methoxycarbonyl)bromomethyl)benzoate (71)

Under argon atmosphere N-bromosuccinimide (NBS) (0.970 g, 5.450 mmol) and AIBN (50 mg, 0.304 mmol) were added to a solution of **70** (1.075 g, 5.163 mmol) in freshly distilled carbon tetrachloride (20 mL). The mixture was heated to reflux for 5 h, after which ^{1}H-NMR indicated only 49 % conversion. Therefore new AIBN (50 mg, 0.304 mmol) was added and the mixture was refluxed for additional 17 h. The white solid was filtered off and the solvent removed under reduced pressure. The crude product (73 % due to ^{1}H NMR) was purified on a silica gel column (*n*-hexane:ethyl acetate 3:1) resulting in a colorless oil (711 mg, 48 %).

^{1}H NMR (250.13 MHz, $CDCl_3$): δ = 8.04 (m, A-portion of an $[AB]_2$-system, 2H, Ar-2-H, Ar-6-H), 7.63 (m, B-portion of an $[AB]_2$-system, 2H, Ar-3-H, Ar-5-H) 5.39 (s, 1H, C*H*Br), 3.93 (s, 3H, ArCOOC*H*$_3$), 3.81 (s, 3H, CHBrCOOC*H*$_3$). ^{13}C{^{1}H} NMR (62.90 MHz, $CDCl_3$): δ = 168.4 (CHBr*C*OOCH$_3$), 166.3 (Ar*C*OOCH$_3$), 140.5 (Ar-4-C), 130.9 (Ar-1-C), 130.0 (Ar-2-C, Ar-6-C), 128.7 (Ar-3-C, Ar-5-C), 53.6 (CHBrCOO*C*H$_3$), 52.3 ArCOO*C*H$_3$), 45.4 (*C*HBr). Anal. calc. for $C_{11}H_{11}BrO_4$: C, 46.02, H, 3.84, found: C, 46.22, H, 3.54.

Synthesis of DOTABA(^{t}Bu)$_3$(Me)$_2$ (73)

Under argon atmosphere DO3A(^{t}Bu)$_3$ (**34**) (600 mg, 1.166 mmol) was dissolved in dry acetonitrile (25 mL) and **71** (368 mg, 1.282 mmol) was added followed by K_2CO_3 (242 mg, 1.749 mmol). The mixture was stirred for 17 h at 70°C. After cooling to room temperature the solid was filtered off and the solvent removed under reduced pressure. The crude product was purified on a silica gel column (pure $CHCl_3$, gradually increasing the ratio of MeOH to 10%) resulting in an off-white powder (719 mg, 86 %).

^{1}H NMR (500.13 MHz, $CDCl_3$): δ = 8.00 (m, A-portion of an $[AB]_2$-system, 2H, Ar-2-H, Ar-6-H), 7.11 (m, B-portion of an $[AB]_2$-system, 2H, Ar-3-H, Ar-5-H), 4.72 (s, 1H, C*H*COOCH$_3$), 3.89 (s, 3H, ArCOOC*H*$_3$), 3.67 (s, 3H, CHCOOC*H*$_3$), 3.56 (d, $^2J_{HH}$ = 17.4 Hz, 1H, NC*H*HCOO^{t}Bu), 2.87 (d, $^2J_{HH}$ = 17.4 Hz, 1H, NCH*H*COO^{t}Bu), 3.41 (d, $^2J_{HH}$ = 17.5 Hz, 1H, NC*H*HCOO^{t}Bu), 2.94 (d, $^2J_{HH}$ = 17.5 Hz, 1H, NCH*H*COO^{t}Bu), 3.37 (d, $^2J_{HH}$ = 17.3 Hz, 1H, NC*H*HCOO^{t}Bu), 2.83 (d, $^2J_{HH}$ = 17.3 Hz, 1H, NCH*H*COO^{t}Bu), 3.34, 2.22 (m, 2H, Cyclen C*H*$_2$), 3.27, 2.12 (m, 2H, Cyclen C*H*$_2$), 3.24, 2.09 (m, 2H, Cyclen C*H*$_2$), 3.17, 2.25 (m,

2H, Cyclen CH_2), 2.86, 1.71 (m, 2H, Cyclen CH_2), 2.71, 2.52 (m, 2H, Cyclen CH_2), 2.51, 2.35 (m, 2H, Cyclen CH_2), 2.50, 2.36 (m, 2H, Cyclen CH_2), 1.46, 1.43 (overl. s, 27H, C(CH_3)$_3$). ^{13}C{^{1}H} NMR (125.76 MHz, $CDCl_3$): δ = 174.7 (CH*C*OOCH$_3$), 173.9, 173.3, 173.1 (*C*OO^{t}Bu), 166.5 (Ar*C*OOCH$_3$), 136.9 (Ar-4-C), 130.3 (Ar-1-C), 130.1 (Ar-3-C, Ar-5-C), 129.7 (Ar-2-C, Ar-6-C), 82.5, 82.2, 82.1 (*C*(CH$_3$)$_3$), 65.0 (*C*HCOOCH$_3$), 56.1, 55.9, 55.6 (*C*H$_2$COO^{t}Bu) 52.9, 52.6, 52.5, 49.0, 48.5, 48.3, 48.1, 45.1 (Cyclen *C*H$_2$), 52.6 (CHCOO*C*H$_3$), 52.3 (ArCOO*C*H$_3$), 28.1, 28.0, 27.9 (C(*C*H$_3$)$_3$). HRMS (FTICR): $[M+Na]^+$ calc.: 743.42017, found: 743.42024.

Synthesis of DOTABA (65)

73 was dissolved in aqueous 6 N hydrochloric acid (20 mL) and refluxed for 16 h. The solution was allowed to reach room temperature and washed with diethyl ether. Removal of the solvent under reduced pressure afforded the ammonium chloride salt of DOTABA (containing 85 % pure DOTABA) as an off-white powder (291 mg, 90%).

^{1}H NMR (500.13 MHz, D_2O): δ = 8.01(m, A-portion of an [AB]$_2$-system, 2H, Ar-2-H, Ar-6-H), 7.55 (br m, B-portion of an [AB]$_2$-system, 2H, Ar-3-H, Ar-5-H), 5.45 (br s, 1H, C*H*COOH), 4.63-2.38 (br, 22H, CH_2). ^{13}C{^{1}H} NMR (125.76 MHz, D_2O): δ = 174.9, 173.5, 168.9, 167.8 (extr. br) (*C*OOH), 169.6 (Ar*C*OOH), 138.4 (Ar-4-C), not observed (Ar-1-C), 130.5 (Ar-2-C, Ar-6-C), 130.4 (Ar-3-C, Ar-5-C), 63.3 (*C*HCOOH), 54.9, 53.2, 52.0(br), 51.2(br), 50.0-46.1(extr. br), 45.6, 43.3 (*C*H$_2$). HRMS (FTICR): $[M+H]^+$ calc.: 525.21912, found: 525.21938.

5.2.8.15 Synthesis of Gadoxane B (GB)

65 (65 mg, 1.02×10^{-4} mol) was dissolved in distilled water (1 mL) and an aqueous solution of *n*-Bu$_4$NOH (20 %, 802 µL, 6.12×10^{-4} mol) was added, followed by 1.1 equivalents of a stock solution of $LnCl_3$. The pH was verified to be between 6 and 7. The suspension was heated to 70°C for about 3 h. The solvent was removed under reduced pressure and the remaining solid residue was dried for 4 to 6 days *in vacuo*. Under argon atmosphere the residue was taken up in dry DMSO (5 mL) and stirred for 2 days. To the resulting suspension octa(3-chloroammoniumpropyl)silsesquioxane (10 mg, 8.51×10^{-6} mol) was added, followed by DIPEA (0.1 mL, 5.84×10^{-4} mol) and TBTU (33 mg, 1.02×10^{-4} mol). After 3 h of stirring at room temperature the reaction mixture was added drop-wise to an acetic acid/sodium acetate buffer (buffer capacity of 12 mmol/L, pH 5.5, 50 mL), resulting in a clear solution. This solution was poured into 50 mL of distilled water in the reservoir of a Pall Minimate™ Tangential Flow Filtration System. Diafiltration was carried out using a membrane with a

molecular weight cutoff of 3 K. The permeated volume was continuously replaced by an aqueous solution of NaCl (1 %, 400 mL), followed by pure water (400 mL). After the volume replacement was stopped, the diafiltration was continued until the volume had reduced to about 10 mL. The remaining solution was collected in a schlenk flask (rinsed with 10 mL H_2O). The solvent was removed *in vacuo* at 25°C to afford **GB** as a white solid. Absence of non-coordinated lanthanide ions was confirmed by the xylenol test. The yield calculated from the gadolinium(III) concentration obtained by the BMS method (see chapter 5.2.7.2) was about 30 %.

NMR characterisation data of the yttrium complex:

^{1}H NMR (500.13 MHz, D_2O): δ = 7.77 (m, A-portion of an $[AB]_2$-system, 16H, Ar-2-H, Ar-6-H), 7.37 (br m, B-portion of an $[AB]_2$-system, 16H, Ar-3-H, Ar-5-H), 4.70 (br s, 8H, C*H*COO$^-$), 3.79 (br, 8H, C*H*HCOO$^-$), 3.31 (br, 8H, CH*H*COO$^-$), 3.69 (br, 8H, C*H*HCOO$^-$), 3.31 (br, 8H, CH*H*COO$^-$), 3.66 (br, 8H, C*H*HCOO$^-$), 3.28 (br, 8H, CH*H*COO$^-$), 3.29, 2.63 (br, 16H, Cyclen CH_2), 3.29, 2.35 (br, 16H, Cyclen CH_2), 3.29, 2.06 (br, 16H, Cyclen CH_2), 3.22 (br, 16H, NCH_2CH$_2$), 2.94, 2.75 (br, 16H, Cyclen CH_2), 2.94, 2.37 (br, 16H, Cyclen CH_2), 2.83, 2.21 (br, 16H, Cyclen CH_2), 2.81, 2.47 (br, 16H, Cyclen CH_2), 2.79 (br, 16H, Cyclen CH_2), 1.71 (br, 16H, CH_2CH$_2$Si), 0.76 (br, 16H, CH_2Si). ^{13}C{^{1}H} NMR (125.76 MHz, D_2O): δ = 180.8 (br, CH$_2$*C*OO$^-$), 178.3 (br, CH*C*OO$^-$), 168.8 (br, Ar*C*ON), 135.3 (br, Ar-4-C), 133.9 (br, Ar-1-C), 132.7 (br, Ar-3-C, Ar-5-C), 126.8 (br, Ar-2-C, Ar-6-C), 74.1 (br, *C*HCOO$^-$), 66.0 (br, *C*H$_2$COO$^-$), 56.0, 55.9, 55.4, 55.2, 55.0, 54.7, 45.7 (br, Cyclen *C*H$_2$) 41.7 (NCH$_2$CH$_2$), 22.2 (*C*H$_2$CH$_2$Si), 8.4 (*C*H$_2$Si). ^{29}Si{^{1}H} NMR (99.36 MHz, D_2O): δ = -65.4.

HRMS data of the gadolinium complex:

HRMS (FTICR): $[M]^{8-}$ calc.: 769.880308, found: 769.881065.

5.2.8.16 General procedure for the synthesis of complexes 63 and 78

Ligand **60** or **65** was dissolved in distilled water (0.5 mL) and a stock solution of $LnCl_3$ (1.1 equivalents for YCl_3 and 0.9 equivalents for $GdCl_3$) was added. The pH was adjusted to 6-7 using a 1 M solution of NaOH. The mixture was heated to 70°C for 1 h. After cooling to room temperature, the pH was adjusted to 7.0 using a 1 M solution of NaOH, followed by the evaporation of the solvent. The absence of non-coordinated Gd^{3+} ions in the gadolinium(III) complexes was confirmed by the xylenol test.

NMR data of Y-DOTAGA (**63**):

^{1}H NMR (500.13 MHz, D_2O, pD 7.0): δ = 3.63 (br d, 2H, C*H*HCOO$^-$), 3.25 (br d, 2H, CH*H*COO$^-$), 3.63 (br d, 1H, C*H*HCOO$^-$), 3.22 (br d, 1H, CH*H*COO$^-$), 3.48, 2.47 (br, 4H, Cyclen CH_2), 3.45, 2.44 (br, 2H, Cyclen CH_2), 3.38 (br, 1H, NC*H*COO$^-$), 3.07, 2.81 (br, 2H,

Cyclen C*H*$_2$), 2.84, 2.73 (br, 2H, Cyclen C*H*$_2$), 2.77 (br, 4H, Cyclen C*H*$_2$), 2.67 (br, 2H, Cyclen), 2.58, 2.29 (br, 2H, $CH_2CH_2COO^-$), 1.99, 1.86 (br, 2H, CHC*H*$_2$). $^{13}C\{^1H\}$ NMR (125.76 MHz, D_2O, pD 7.0): δ = 181.0 ($CH_2CH_2COO^-$), 180.7 (br, COO^-), 68.6 (N*C*HCOO$^-$), 66.0, 65.7 (br, CH_2COO^-), 56.1, 55.9, 55.6, 55.4, 55.1, 54.7, 54.3, 45.7 (br, Cyclen CH_2), 36.2 ($CH_2CH_2COO^-$), 20.4 (CHCH_2).

NMR data of Y-DOTABA (**78**):

^1H NMR (400.13 MHz, D_2O, pD 7.0): δ = 7.93 (m, A-portion of an $[AB]_2$-system, 2H, Ar-2-H, Ar-6-H), 7.37 (br m, B-portion of an $[AB]_2$-system, 2H, Ar-3-H, Ar-5-H), 4.76 (br s, 1H, C*H*COO$^-$), 3.79 (br d, 1H, C*H*HCOO$^-$), 3.31 (br d, 1H, CH*H*COO$^-$), 3.69 (br d, 1H, C*H*HCOO$^-$), 3.31 (br d, 1H, CH*H*COO$^-$), 3.66 (br d, 1H, C*H*HCOO$^-$), 3.28 (br d, 1H, CH*H*COO$^-$), 3.47, 2.47 (br, 2H, Cyclen C*H*$_2$), 3.46, 2.80 (br, 2H, Cyclen C*H*$_2$), 3.43, 2.43 (br, 2H, Cyclen C*H*$_2$), 3.02, 2.76 (br, 2H, Cyclen C*H*$_2$), 2.99, 2.37 (br, 2H, Cyclen C*H*$_2$), 2.96, 2.39 (br, 2H, Cyclen C*H*$_2$), 2.81, 2.48 (br, 2H, Cyclen C*H*$_2$), 2.79 (br, 2H, Cyclen C*H*$_2$). $^{13}C\{^1H\}$ NMR (100.61 MHz, D_2O, pD 7.0): δ = 180.7 (CH_2COO^-), 179.4 (CHCOO^-), 175.3 (Ar*C*OOH), 136.2 (Ar-4-C), 133.9 (Ar-1-C), 132.0 (Ar-3-C, Ar-5-C), 128.6 (Ar-2-C, Ar-6-C), 74.5 (*C*HCOO$^-$), 65.9 (br, CH_2COO^-), 56.0, 55.9 (2), 55.3, 55.1, 55.0, 54.7, 45.6 (br, Cyclen CH_2).

6 References

1. *The Chemistry of Contrast Agents in Medical Magnetic Resonance Imaging*, (Eds.: É. Tóth, A.E. Merbach), Wiley, Chichester, 2001.
2. *Contrast Agents I - Magnetic Resonance Imaging*, (Editor: W. Krause) Springer-Verlag, Berlin Heidelberg New York, 2002.
3. M. Reiser and W. Semmler, *Magnetresonanztomographie*, Springer-Verlag, Berlin Heidelberg New York, **2002**.
4. M. P. Lowe, *Aust. J. Chem.*, 2002, **55**, 551-556.
5. D. Artemov, *J. Cell. Biochem.*, 2003, **90**, 518-524.
6. P. Caravan, J. J. Ellison, T. J. McMurry and R. B. Lauffer, *Chem. Rev.*, 1999, **99**, 2293-2352.
7. R. B. Lauffer, *Chem. Rev.*, 1987, **87**, 901-927.
8. R. V. Southwood-Jones, W. L. Earl, K. E. Newman and A. E. Merbach, *J. Chem. Phys.*, 1980, **73**, 5909-5918.
9. J.-M. Idée, M. Port, I. Raynal, M. Schaefer, S. Le Greneur and C. Corot, *Fundam. Clin. Pharmacol.*, 2006, **20**, 563-576.
10. N. Bloembergen and L. O. Morgan, *J. Chem. Phys.*, 1961, **34**, 842-850.
11. I. Solomon, *Phys. Rev.*, 1955, **99**, 559-565.
12. I. Solomon and N. Bloembergen, *J. Chem. Phys.*, 1956, **25**, 261-266.
13. J. Kowalewski, L. Nordenskiöld, N. Benetis and P.-O. Westlund, *Prog. Nucl. Magn. Reson. Spectrosc.*, 1985, **17**, 141-185.
14. J.-M. Idée, M. Port, C. Robic, C. Medina, M. Sabatou and C. Corot, *J. Magn. Reson. Imaging*, 2009, **30**, 1249-1258.
15. M. Rohrer, H. Bauer, J. Mintorovitch, M. Requardt and H.-J. Weinmann, *Invest. Radiol.*, 2005, **40**, 715-724.
16. P. Hermann, J. Kotek, V. Kubícek and I. Lukes, *Dalton Trans.*, 2008, **23**, 3027-3047.
17. S. Aime and P. Caravan, *J. Magn. Reson. Imaging*, 2009, **30**, 1259-1267.
18. M. Oudkerk, P. Sijens, E. van Beek and T. Kuijpers, *Invest. Radiol.*, 1995, **30**, 75-78.
19. T. Grobner, *Nephrol. Dial. Transplant.*, 2006, **21**, 1104-1108.
20. M. A. Sieber, H. Pietsch, J. Walter, W. Haider, T. Frenzel and H.-J. Weinmann, *Invest. Radiol.*, 2008, **43**, 65-75.
21. T. Frenzel, P. Lengsfeld, H. Schirmer, J. Hütter and H.-J. Weinmann, *Invest. Radiol.*, 2008, **43**, 817-828.
22. S. Laurent, L. V. Elst and R. N. Muller, *Contrast Med. Mol. Imaging*, 2006, **1**, 128-137.
23. S. Laurent, L. Vander Elst, F. Copoix and R. Muller, *Invest. Radiol.*, 2001, **36**, 115-122.
24. K. Kumar, *J. Alloys Comp.*, 1997, **249**, 163-172.
25. P. Caravan, C. Comuzzi, W. Crooks, T. J. McMurry, G. R. Choppin and S. R. Woulfe, *Inorg. Chem.*, 2001, **40**, 2170-2176.
26. M. F. Tweedle, J. J. Hagan, K. Kumar, S. Mantha and C. A. Chang, *Magn. Reson. Imaging*, 1991, **9**, 409-415.
27. X. Wang, T. Jin, V. Comblin, A. Lopez-Mut, E. Merciny and J. F. Desreux, *Inorg. Chem.*, 1992, **31**, 1095-1099.
28. S. I. Kang, R. S. Ranganathan, J. E. Emswiler, K. Kumar, J. Z. Gougoutas, M. F. Malley and M. F. Tweedle, *Inorg. Chem.*, 1993, **32**, 2912-2918.
29. P. Wedeking, C. H. Sotak, J. Telser, K. Kumar, C. A. Chang and M. F. Tweedle,

Magn. Reson. Imaging, 1992, **10**, 97-108.
30. X. Zhang, C. A. Chang, H. G. Brittain, J. M. Garrison, J. Telser and M. F. Tweedle, *Inorg. Chem.*, 1992, **31**, 5597-5600.
31. É. Tóth, O. M. N. Dhubhghaill, G. Besson, L. Helm and A. Merbach, *Magn. Reson. Chem.*, 1999, **37**, 701-708.
32. J. I. Bruce, R. S. Dickins, L. J. Govenlock, T. Gunnlaugsson, S. Lopinski, M. P. Lowe, D. Parker, R. D. Peacock, J. J. B. Perry, S. Aime and M. Botta, *J. Am. Chem. Soc.*, 2000, **122**, 9674-9684.
33. R. S. Dickins, S. Aime, A. S. Batsanov, A. Beeby, M. Botta, J. I. Bruce, J. A. K. Howard, C. S. Love, D. Parker, R. D. Peacock and H. Puschmann, *J. Am. Chem. Soc.*, 2002, **124**, 12697-12705.
34. W. Kaim and B. Schwederski, *Bioanorganische Chemie*, Teubner Verlag, 2005.
35. N. K. Logothetis, J. Pauls, M. Augath, T. Trinath and A. Oeltermann, *Nature*, 2001, **412**, 150-157.
36. S. Ogawa and T.-M. Lee, *Magn. Res. Med.*, 1990, **16**, 9--18.
37. N. K. Logothetis, H. Guggenberger, S. Peled and J. Pauls, *Nat Neurosci*, 1999, **2**, 555-562.
38. R. S. Menon, S. Ogawa, X. Hu, J. P. Strupp, P. Anderson, gcaron, K. urbil, acaron and mil, *Magn. Res. Med.*, 1995, **33**, 453-459.
39. R. Turner, D. L. Bihan, C. T. W. Moonen, D. Despres and J. Frank, *Magn. Res. Med.*, 1991, **22**, 159-166.
40. G. J. Augustine, M. P. Charlton and S. J. Smith, *Annu. Rev. Neurosci.*, 1987, **10**, 633-693.
41. R. F. Thompson, *Das Gehirn*, Spektrum Akademischer Verlag, 2001.
42. C. Nicholson, G. ten Bruggencate, H. Stockle and R. Steinberg, *J Neurophysiol*, 1978, **41**, 1026-1039.
43. A. Y. Louie, M. M. Huber, E. T. Ahrens, U. Rothbacher, R. Moats, R. E. Jacobs, S. E. Fraser and T. J. Meade, *Nat. Biotech.*, 2000, **18**, 321-325.
44. R. A. Moats, S. E. Fraser and T. J. Meade, *Angew. Chem., Int. Ed.*, 1997, **36**, 726-728.
45. U. Himmelreich, S. Aime, T. Hieronymus, C. Justicia, F. Uggeri, M. Zenke and M. Hoehn, *NeuroImage*, 2006, **32**, 1142-1149.
46. A. L. Nivorozhkin, A. F. Kolodziej, P. Caravan, M. T. Greenfield, R. B. Lauffer and T. J. McMurry, *Angew. Chem., Int. Ed.*, 2001, **40**, 2903-2906.
47. A. Bogdanov Jr, L. Matuszewski, C. Bremer, A. Petrovsky and R. Weissleder, *Mol. Imag.*, 2002, **1**, 16-23.
48. C. F. G. C. Geraldes and S. Laurent, *Contrast Med. Mol. Imaging*, 2009, **4**, 1-23.
49. S. Zhang, K. Wu and A. D. Sherry, *Angew. Chem., Int. Ed.*, 1999, **38**, 3192-3194.
50. N. Raghunand, C. Howison, A. D. Sherry, S. Zhang and R. J. Gillies, *Magn. Reson. Med.*, 2003, **49**, 249-257.
51. I. Mamedov, A. Mishra, G. Angelovski, H. A. Mayer, L.-O. Palsson, D. Parker and N. K. Logothetis, *Dalton Trans.*, 2007, 5260-5267.
52. M. P. Lowe, D. Parker, O. Reany, S. Aime, M. Botta, G. Castellano, E. Gianolio and R. Pagliarin, *J. Am. Chem. Soc.*, 2001, **123**, 7601-7609.
53. S. Aime, S. G. Crich, M. Botta, G. Giovenzana, G. Palmisano and M. Sisti, *Chem. Commun.*, 1999, 1577--1578.
54. S. Aime, M. Botta, M. Fasano and E. Terreno, *Spectrochim. Acta, Part A*, 1993, **49**, 1315-1322.
55. J. B. Livramento, A. Sour, A. Borel, A. E. Merbach and É. Tóth, *Chem.-Eur. J.*, 2006, **12**, 989-1003.
56. J. B. Livramento, C. Weidensteiner, M. I. M. Prata, P. R. Allegrini, C. F. G. C. Geraldes, L. Helm, R. Kneuer, A. E. Merbach, A. C. Santos, P. Schmidt and É. Tóth,

Contrast Med. Mol. Imaging, 2006, **1**, 30-39.
57. K. Hanaoka, K. Kikuchi, Y. Urano and T. Nagano, *J. Chem. Soc., Perkin Trans. 2*, 2001, 1840-1843.
58. K. Hanaoka, K. Kikuchi, Y. Urano, M. Narazaki, T. Yokawa, S. Sakamoto, K. Yamaguchi and T. Nagano, *Chem. Biol.*, 2002, **9**, 1027-1032.
59. W.-h. Li, S. E. Fraser and T. J. Meade, *J. Am. Chem. Soc.*, 1999, **121**, 1413-1414.
60. W.-h. Li, G. Parigi, M. Fragai, C. Luchinat and T. J. Meade, *Inorg. Chem.*, 2002, **41**, 4018-4024.
61. G. Angelovski, P. Fouskova, I. Mamedov, S. Canals, E. Toth and N. K. Logothetis, *ChemBioChem*, 2008, **9**, 1729-1734.
62. K. Dhingra, P. Fousková, G. Angelovski, M. Maier, N. Logothetis and É. Tóth, *JBIC*, 2008, **13**, 35-46.
63. K. Dhingra, M. E. Maier, M. Beyerlein, G. Angelovski and N. K. Logothetis, *Chem. Commun.*, 2008, 3444-3446.
64. A. Mishra, P. Fousková, G. Angelovski, E. Balogh, A. K. Mishra, N. K. Logothetis and É. Tóth, *Inorg. Chem.*, 2008, **47**, 1370-1381.
65. I. Mamedov, University of Tübingen, Dissertation, 2006.
66. L. Helm, *Prog. Nucl. Magn. Reson. Spectrosc.*, 2006, **49**, 45-64.
67. Z. Kotková, G. A. Pereira, K. Djanashvili, J. Kotek, J. Rudovský, P. Hermann, L. V. Elst, R. N. Muller, C. F. G. C. Geraldes, I. Lukescaron and J. A. Peters, *Eur. J. Inorg. Chem.*, 2009, **2009**, 119-136.
68. I. K. Adzamli, M. Blau, M. A. Pfeffer and M. A. Davis, *Magn. Reson. Med.*, 1993, **29**, 505-511.
69. V. Kubicek, J. Rudovsky, J. Kotek, P. Hermann, L. Vander Elst, R. N. Muller, Z. I. Kolar, H. T. Wolterbeek, J. A. Peters and I. Lukes, *J. Am. Chem. Soc.*, 2005, **127**, 16477-16485.
70. P. Buglyó, T. Kiss, M. Dyba, M. Jezowska-Bojczuk, H. Kozlowski and S. Bouhsina, *Polyhedron*, 1997, **16**, 3447-3454.
71. S. J. Westerback and A. E. Martell, *Nature*, 1956, **178**, 321--322.
72. E. Matczak-Jon, B. Kurzak, A. Kamecka, W. Sawka-Dobrowolska and P. Kafarski, *Dalton Trans.*, 1999, 3627-3637.
73. E. Matczak-Jon, B. Kurzak, P. Kafarski and A. Wozna, *J. Inorg. Biochem.*, 2006, **100**, 1155-1166.
74. M. Alajarín, A. Pastor, R.-A. Orenes, E. Martínez-Viviente and P. S. Pregosin, *Chem. Eur. J.*, 2006, **12**, 877-886.
75. Y. Cohen, L. Avram and L. Frish, *Angew. Chem., Int. Ed.*, 2005, **44**, 520-554.
76. A. Macchioni, G. Ciancaleoni, C. Zuccaccia and D. Zuccaccia, *Chem. Soc. Rev.*, 2008, **37**, 479-489.
77. M. Valentini, H. Rüegger and P. S. Pregosin, *Helv. Chim. Acta*, 2001, **84**, 2833-2853.
78. S. Yao, J. J. Babon and R. S. Norton, *Biophys. Chem.*, 2008, **136**, 145-151.
79. P. Atkinson, B. S. Murray and D. Parker, *Org. Biomol. Chem.*, 2006, **4**, 3166-3171.
80. S. Aime, M. Botta, E. Garino, S. G. Crich, G. Giovenzana, R. Pagliarin, G. Palmisano and M. Sisti, *Chem.-Eur. J.*, 2000, **6**, 2609-2617.
81. P. Atkinson, Y. Bretonniere and D. Parker, *Chem. Commun.*, 2004, 438-439.
82. A. Beeby, I. M. Clarkson, R. S. Dickins, S. Faulkner, D. Parker, L. Royle, A. S. de Sousa, J. A. G. Williams and M. Woods, *J. Chem. Soc., Perkin Trans. 2*, 1999, 493-503.
83. R. M. Supkowski and W. D. Horrocks, *Inorg. Chim. Acta*, 2002, **340**, 44-48.
84. F. A. Rojas-Quijano, E. Tircsóné Benyó, G. Tircsó, F. K. Kálmán, Z. Baranyai, S. Aime, A. D. Sherry and Z. Kovács, *Chem.-Eur. J.*, 2009, **15**, 13188-13200.
85. P. Lebduskova, P. Hermann, L. Helm, E. Toth, J. Kotek, K. Binnemans, J. Rudovsky,

I. Lukes and A. E. Merbach, *Dalton Trans.*, 2007, 493-501.
86. P. Lebduskova, A. Sour, L. Helm, E. Toth, J. Kotek, I. Lukes and A. E. Merbach, *Dalton Trans.*, 2006, 3399-3406.
87. A. M. Raitsimring, A. V. Astashkin, D. Baute, D. Goldfarb and P. Caravan, *J. Phys. Chem. A*, 2004, **108**, 7318-7323.
88. D. H. Powell, O. M. N. Dhubhghaill, D. Pubanz, L. Helm, Y. S. Lebedev, W. Schlaepfer and A. E. Merbach, *J. Am. Chem. Soc.*, 1996, **118**, 9333-9346.
89. A. Congreve, D. Parker, E. Gianolio and M. Botta, *Dalton Trans.*, 2004, 1441-1445.
90. J. Engelmann, personal communication, 2009.
91. P. Caravan, *Chem. Soc. Rev.*, 2006, **35**, 512-523.
92. J. Kotek, P. Lebdusková, P. Hermann, L. V. Elst, R. N. Muller, C. F. G. C. Geraldes, T. Maschmeyer, I. Lukes and J. A. Peters, *Chem.-Eur. J.*, 2003, **9**, 5899-5915.
93. M. Port, C. Corot, I. Raynal, J.-M. Idee, A. Dencausse, E. Lancelot, D. Meyer, B. Bonnemain and J. Lautrou, *Invest. Radiol.*, 2001, **36**, 445-454.
94. D. A. Fulton, M. O'Halloran, D. Parker, K. Senanayake, M. Botta and S. Aime, *Chem. Commun.*, 2005, 474-476.
95. J. P. André, É. Tóth, H. Fischer, A. Seelig, H. R. Mäcke and A. E. Merbach, *Chem.-Eur. J.*, 1999, **5**, 2977-2983.
96. G. M. Nicolle, É. Tóth, K.-P. Eisenwiener, H. R. Mäcke and A. Merbach, *JBIC*, 2002, **7**, 757-769.
97. R. B. Lauffer, D. J. Parmelee, S. U. Dunham, H. S. Ouellet, R. P. Dolan, S. Witte, T. J. McMurry and R. C. Walovitch, *Radiology*, 1998, **207**, 529-538.
98. W. Lin, D. R. Abendschein, A. Celik, R. P. Dolan, R. B. Lauffer, R. C. Walovitch and E. M. Haacke, *J. Magn. Reson. Imaging*, 1997, **7**, 963-971.
99. S. Torres, J. A. Martins, J. P. André, C. F. G. C. Geraldes, A. E. Merbach and É. Tóth, *Chem.-Eur. J.*, 2006, **12**, 940-948.
100. M. Spanoghe, D. Lanens, R. Dommisse, A. Van der Linden and F. Alderweireldt, *Magn. Reson. Imaging*, 1992, **10**, 913-917.
101. K. E. Kellar, P. M. Henrichs, R. Hollister, S. H. Koenig, J. Eck and D. Wei, *Magn. Reson. Med.*, 1997, **38**, 712-716.
102. É. Tóth, L. Helm, K. E. Kellar and A. Merbach, *Chem.-Eur. J.*, 1999, **5**, 1202-1211.
103. C. Casali, M. Janier, E. Canet, J. F. Obadia, S. Benderbous, C. Corot and D. Revel, *Acad. Radiol.*, 1998, **5**, S214-S218.
104. L. H. Bryant Jr., M. W. Brechbiel, C. Wu, J. W. M. Bulte, V. Herynek and J. A. Frank, *J. Magn. Reson. Imaging*, 1999, **9**, 348-352.
105. Z. Jaszberenyi, L. Moriggi, P. Schmidt, C. Weidensteiner, R. Kneuer, A. E. Merbach, L. Helm and E. Tóth, *J. Biol. Inorg. Chem.*, 2007, **12**, 406-420.
106. H. Kobayashi, S. Kawamoto, S.-K. Jo, H. L. Bryant, M. W. Brechbiel and R. A. Star, *Bioconjugate Chem.*, 2003, **14**, 388-394.
107. L. D. Margerum, B. K. Campion, M. Koo, N. Shargill, J.-J. Lai, A. Marumoto and P. Christian Sontum, *J. Alloys Comp.*, 1997, **249**, 185-190.
108. É. Tóth, D. Pubanz, S. Vauthey, L. Helm and A. E. Merbach, *Chem.-Eur. J.*, 1996, **2**, 1607-1615.
109. E. Wiener, M. W. Brechbiel, H. Brothers, R. L. Magin, O. A. Gansow, D. A. Tomalia and P. C. Lauterbur, *Magn. Reson. Med.*, 1994, **31**, 1-8.
110. Y. Fu, H.-J. Raatschen, D. E. Nitecki, M. F. Wendland, V. Novikov, L. S. Fournier, C. Cyran, V. Rogut, D. M. Shames and R. C. Brasch, *Biomacromolecules*, 2007, **8**, 1519-1529.
111. G. M. Nicolle, E. Toth, H. Schmitt-Willich, B. Radüchel and A. E. Merbach, *Chem.-Eur. J.*, 2002, **8**, 1040-1048.
112. J. W. Booth and C. J. Lumsden, *Biophys J.*, 1993, **64**, 1727-1734.

113. J. Tencer, I.-M. Frick, B. W. Oquist, P. Alm and B. Rippe, *Kidney Int.*, 1998, **53**, 709-715.
114. D. W. Scott, *J. Am. Chem. Soc.*, 1946, **68**, 356-358.
115. R. H. Baney, M. Itoh, A. Sakakibara and T. Suzuki, *Chem. Rev.*, 1995, **95**, 1409-1430.
116. R. M. Laine, C. Zhang, A. Sellinger and L. Viculis, *Appl. Organomet. Chem.*, 1998, **12**, 715-723.
117. G. Li, L. Wang, H. Ni and C. U. Pittman, *J. Inorg. Organomet. Polym.*, 2001, **11**, 123-154.
118. D. A. Loy and K. J. Shea, *Chem. Rev.*, 1995, **95**, 1431-1442.
119. P. P. Pescarmona and T. Maschmeyer, *Aust. J. Chem.*, 2001, **54**, 583-596.
120. E. Lindner, T. Schneller, F. Auer and H. A. Mayer, *Angew. Chem., Int. Ed.*, 1999, **38**, 2154-2174.
121. F. J. Feher and K. D. Wyndham, *Chem. Commun.*, 1998, 323-324.
122. H. J. Murfee, T. P. S. Thoms, J. Greaves and B. Hong, *Inorg. Chem.*, 2000, **39**, 5209--5217.
123. R. K. Ilner, *The Chemistry of Silica*, Wiley, New York, 1979.
124. F. J. Feher, K. D. Wyndham, S. D. and N. F., *Dalton Trans.*, 1999, 1491-1497.
125. D. Ruiz-Abad, Universität Tübingen, Dissertation, 2008.
126. E. O. Dare, L.-K. Liu and J. Peng, *Dalton Trans.*, 2006, 3668-3672.
127. F. J. Feher, K. D. Wyndham, M. A. Scialdone and Y. Hamuro, *Chem. Commun.*, 1998, 1469-1470.
128. A. Heppeler, S. Froidevaux, H. R. Mäcke, E. Jermann, M. Béhé, P. Powell and M. Hennig, *Chem.-Eur. J.*, 1999, **5**, 1974-1981.
129. R. Knorr, A. Trzeciak, W. Bannwarth and D. Gillessen, *Tetrahedron Lett.*, 1989, **30**, 1927-1930.
130. S. Fuchs, FU Berlin, Dissertation, 2004.
131. F. J. Feher, D. Soulivong and G. T. Lewis, *J. Am. Chem. Soc.*, 1997, **119**, 11323-11324.
132. C. F. G. C. Geraldes and A. D. Sherry, *J. Magn. Reson.*, 1986, **66**, 274--282.
133. P. L. Anelli, L. Lattuada, M. Gabellini and P. Recanati, *Bioconjugate Chem.*, 2001, **12**, 1081-1084.
134. K.-P. Eisenwiener, P. Powell and H. R. Mäcke, *Bioorg. Med. Chem. Lett.*, 2000, **10**, 2133-2135.
135. B. Holmberg, *Chem. Ber.*, 1927, **60**, 2198-2211.
136. A. Barge, G. Cravotto, E. Gianolio and F. Fedeli, *Contrast Med. Mol. Imaging*, 2006, **1**, 184-188.
137. C. S. Palmer and P. W. McWherter, *Org. Synth., Coll.*, 1941, **1**, 245-246.
138. K. Schaper, S. A. M. Mobarekeh and C. Grewer, *Eur. J. Org. Chem.*, 2002, **2002**, 1037-1046.
139. G. N. Lewis and R. T. Macdonald, *J. Am. Chem. Soc.*, 1933, **55**, 4730-4731.
140. Y. Sugahara, T. Inouea and K. Kuroda, *J. Mater. Chem.*, 1997, **7**, 53-59.
141. S. Rast, A. Borel, L. Helm, E. Belorizky, P. H. Fries and A. E. Merbach, *J. Am. Chem. Soc.*, 2001, **123**, 2637-2644.
142. S. Rast, P. H. Fries and E. Belorizky, *J. Chem. Phys.*, 2000, **113**, 8724-8735.
143. K. Micskei, L. Helm, E. Brucher and A. E. Merbach, *Inorg. Chem.*, 1993, **32**, 3844-3850.
144. J. P. André, H. R. Mäcke, É. Tóth and A. E. Merbach, *JBIC*, 1999, **4**, 341-347.
145. S. G. Zech, W.-C. Sun, V. Jacques, P. Caravan, A. V. Astashkin and A. M. Raitsimring, *ChemPhysChem*, 2005, **6**, 2570-2577.
146. F. A. Dunand, A. Borel and A. E. Merbach, *J. Am. Chem. Soc.*, 2002, **124**, 710-716.
147. F. Yerly, K. I. Hardcastle, L. Helm, S. Aime, M. Botta and A. E. Merbach, *Chem.-*

Eur. J., 2002, **8**, 1031-1039.
148. G. Lipari and A. Szabo, *J. Am. Chem. Soc.*, 1982, **104**, 4559-4570.
149. G. Lipari and A. Szabo, *J. Am. Chem. Soc.*, 1982, **104**, 4546-4559.
150. P. K. Glasoe and F. A. Long, *J. Phys. Chem.*, 1960, **64**, 188-190.
151. D. M. Corsi, C. Platas-Iglesias, H. van Bekkum and J. A. Peters, *Magn. Reson. Chem.*, 2001, 723-726.
152. A. D. Hugi, L. Helm and A. E. Merbach, *Helv. Chim. Acta*, 1985, **68**, 508-521.
153. D. S. Raiford, C. L. Fisk and E. D. Becker, *Anal. Chem.*, 1979, **51**, 2050-2051.
154. H. E. Gottlieb, V. Kotlyar and A. Nudelman, *J. Org. Chem.*, 1997, **62**, 7512-7515.
155. C. Ammann, P. Meier and A. Merbach, *J. Magn. Reson.*, 1982, **46**, 319-321.

Summary

The evolvement of magnetic resonance imaging (MRI) to one of the most powerful tools in medical diagnosis is strongly related to the development of paramagnetic contrast agents (CAs). Today, more than 30% of all MRI investigations use a CA. These are mainly gadolinium based extracellular perfusion agents which distribute non-specifically throughout plasma and interstitial spaces. The next generation of CAs is aimed at a more efficient and more specific imaging.

Since calcium(II) plays an important role in regulating a great variety of neuronal processes, there is a strong interest to generate gadolinium(III) complexes which can act as calcium(II)-sensors in functional magnetic resonance imaging (fMRI). In this work the mechanistic aspects of the calcium(II) sensitivity of a series of DO3A-based lanthanide(III) chelates, bearing an alkyl aminobisphosphonate group (alkyl = propyl–hexyl, **L^1**–**L^4**) as the additional coordination site, were investigated.

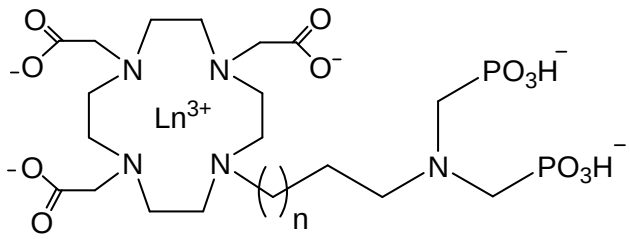

LnL^1-LnL^4, n = 1-4

Instead of increasing, as observed for other calcium(II) sensitive CAs, the longitudinal relaxivity r_1 (the paramagnetic longitudinal proton relaxation rate enhancement referred to one millimolar concentration of Gd^{3+}) of the respective gadolinium(III) complexes of **L^2**–**L^4** decreased after the addition of calcium(II) at low concentrations of the CA (2.5 mM), whereas r_1 of **GdL^1** showed no calcium(II) dependence at this complex concentration.

Concentration-dependent relaxivity and pulsed gradient spin echo (PGSE) diffusion ^{1}H NMR measurements revealed that calcium(II)-induced aggregation is responsible for the observed changes in relaxivity. **GdL^1** has a lower tendency to form aggregates in the presence of calcium than **GdL^2**-**GdL^4**, resulting in a calcium(II) dependent relaxivity change only at high complex concentrations. This can be attributed to a different coordination behavior of the phosphonate groups in **GdL^1** as compared to **GdL^2**-**GdL^4**. ^{31}P NMR and luminescence measurements on the europium(III) analogues indicated the coordination of one phosphonate group to the lanthanide(III) ion for **GdL^1** in the absence and presence of calcium(II), but not

for **GdL^2**-**GdL^4**. In the case of **GdL^1**, only one phosphonate group per lanthanide(III) complex is involved in the calcium(II)-induced aggregation, explaining the lower tendency to form aggregates. In contrast, for **GdL^2**-**GdL^4**, where no coordination of a phosphonate group to the lanthanide(III) ion is observed, both phosphonate groups can be involved in the calcium(II)-induced aggregate formation, resulting in larger and more stable aggregates. In all cases, the water access to the inner and/or the second sphere of the lanthanide(III) complexes is significantly hindered after aggregation, shown by a reduction in the apparent hydration number *q*. The hindered access of water molecules to the paramagnetic centre is therewith the explanation for the observed decrease in relaxivity. Furthermore, variable temperature ^{17}O NMR measurements revealed an extremely high water exchange rate k_{ex}^{298} for these complexes, being in the same order of magnitude as that of the $[Gd(H_2O)_8]^{3+}$ aqua ion.

The second part of the dissertation focuses on macromolecular silsesquioxane based CAs. Macromolecules are considerably useful for constructing highly-sensitive CAs as their high molecular weight increases the rotational correlation time of the molecule and therefore enhances their relaxivity especially at higher field strength as used in today's clinical MR scanners. Furthermore, the grafting of several gadolinium(III) complexes to a macromolecule leads to a higher local concentration of paramagnetic centres. Both factors allow the use of significantly lower CA concentrations, while achieving the same or even better contrast qualities. A high local concentration of gadolinium(III) complexes with high relaxivities is particularly needed for the development of targeted CAs. The main drawback of most of the so far developed large macromolecular CAs is their slow excretion rate from the body, which increases the risk of releasing toxic gadolinium(III) from the chelates. Furthermore, such large macromolecules often have poorly defined structures and therefore random morphologies, which can lead to inconsistent pharmacokinetics.

Functionalised T_8-silsesquioxanes could be ideal building blocks for the development of macromolecular CAs, which overcome these problems. As the dendrimeric core, functionalised T_8-silsesquioxanes could allow the binding of eight gadolinium(III) complexes already in the first generation. This would result in macromolecular CAs which possess a high local gadolinium(III) concentration, while still having a defined globular structure and a molecular size small enough to be excreted from the body within reasonable time.

Hence, several synthetic strategies to functionalise T_8-silsesquioxanes each with eight appropriate gadolinium(III) complexes were investigated in the course of this work. It turned out to be more convenient to directly graft the gadolinium(III) complexes to the silsesquioxane than to introduce a protected ligand, which needs subsequent deprotection and

complexation. These reaction steps increase the risk of destroying the silsesquioxane cage. Furthermore, it could be shown that the introduction of a charge is necessary to achieve sufficient solubility of these highly symmetric systems in aqueous media. Therefore macrocyclic ligands were synthesised which form charged lanthanide(III) complexes and possess an additional functional group for binding to a silsesquioxane. Two of these systems could be successfully attached to a T_8-silsesquioxane to yield Gadoxane G (**GG**) and Gadoxane B (**GB**).

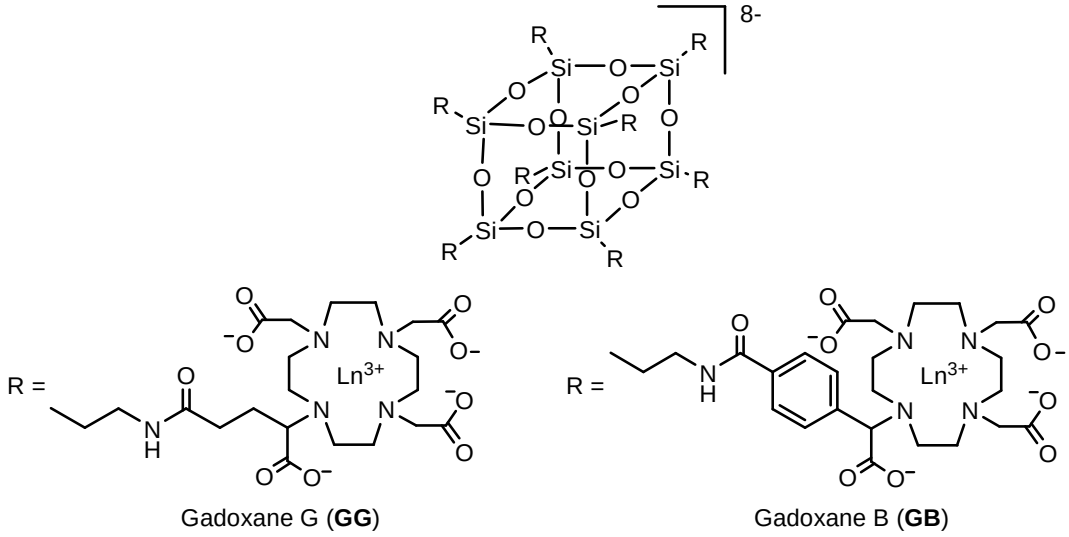

Gadoxane G (**GG**) Gadoxane B (**GB**)

Both Gadoxanes possess eight monohydrated lanthanide(III) (Ln^{3+} = Gd^{3+}, Y^{3+}) complexes, spherically arranged around the silsesquioxane core, but differ in the rigidity of the linking group. The structure and size of the novel CAs was fully characterised by multinuclear (^{1}H, ^{13}C, ^{29}Si) NMR spectroscopy, high resolution mass spectrometry and PGSE diffusion ^{1}H NMR spectroscopy. Relaxivity measurements revealed fairly high longitudinal relaxivities r_1 per gadolinium(III) as compared to commercial CAs like Dotarem™. At a proton resonance frequency of 40 MHz and a temperature of 37°C, r_1 of **GG** is about three-times and r_1 of **GB** is more than four-times higher than r_1 of Dotarem™. Per CA the relaxivity of **GB** is even 35-times higher than that of Dotarem™. The discrepancy in the relaxivities of the Gadoxanes arises from a different local rotational correlation time of the Gd-H_{water} vector of **GG** and **GB,** due to the higher rigidity of the phenyl ring of **GB** as compared to the ethylene spacer of **GG**.

Apart from their distinct increase in relaxivity, the most important feature of these CAs is the lability of the silsesquioxane core in aqueous media. The hydrolysis of the Si-O-Si bonds was investigated by ^{29}Si NMR and PGSE diffusion ^{1}H NMR spectroscopy, ESI-MS as well as by relaxivity measurements. No decomposition was observed when the solutions were stored at -28°C for at least 10 months. At 25°C and pH 7.0, hydrolysis takes place within days to weeks, whereas at 37°C and pH 7.4 the compounds decompose within several hours. Since the

cleavage of the first Si-O-Si moieties has negligible influence on the structure of the CA, the relaxivity and most likely the pharmacokinetics remain unchanged within the first three to four hours, after which a decrease in relaxivity can be observed due to the shortened rotational correlation times of the arising fragments.

Even though both Gadoxanes are small enough to be excreted sufficiently fast *via* the kidneys, the lability of the silsesquioxane core may allow the development of even larger and still well defined macromolecular CAs for MRI, whose fragments are then readily excreted. In addition, the strong effect of the replacement of an ethylene spacer in **GG** by a phenyl ring in **GB** on the relaxivity points out the high potential of silsesquioxane-based CAs to become extremely efficient, once the rigidity is further improved and the water exchange rate is optimised. Moreover, the introduction of additional functional groups into these systems, e.g. *via* functionalisation of the remaining methylene groups of the complexes, could allow their use in the targeting of biomolecules within the body.

Meine akademischen Lehrer:

K. Albert; M. Attfield; D.J. Berrisford; B.L. Booth; F. Bordusa; A.K. Brisdon; T. Chassé; D. Christen; H. Eckstein; H.-J. Egelhaaf; G. Gauglitz; A. Hinchliffe; J. Ihringer; W. Jäger; A. Klein; N. Kuhn; N.P. Lockyer; M.E. Maier; F.S. Mair; A.J. Masters; J.L. Matthews; H.A. Mayer; A.J. Meixner; H.-J. Meyer; G.A. Morris; U. Nagel; C. Ochsenfeld; H. Oberhammer; E. Plies; R.G. Pritchard; V. Schurig; M. Schwarz; E. Schweda; B. Speiser; J. Strähle; U. Weimar; L. Wesemann; K.-P. Zeller; T. Ziegler;

Lebenslauf

Persönliche Daten:

Name:	Jörg Henig
Geboren am/in:	24. Dezember 1982 in Tübingen
Staatsangehörigkeit:	deutsch
Eltern:	Dipl. Ing. Klaus Henig, Andrea Henig (geb. Waiblinger)

Schulausbildung:

1989 – 1993:	Grundschule Innenstadt Tübingen
1993 – 2002:	Wildermuth-Gymnasium Tübingen
Juni 2002	Allgemeine Hochschulreife

Hochschulausbildung:

10/2002 – 8/2004:	Grundstudium Chemie, Universität Tübingen, Vordiplom
9/2004 – 4/2005:	Auslandsemester, The University of Manchester, UK
10/2004 – 3/2007:	Hauptstudium Chemie, Universität Tübingen, Diplom mit Auszeichnung
10/2006 – 3/2007:	Diplomarbeit im Arbeitskreis von Prof. Dr. H. A. Mayer am Institut für Anorganische Chemie, Universität Tübingen
5/2007 – 1/2010	Anfertigung der Doktorarbeit bei Prof. Dr. H. A. Mayer Titel der Arbeit: Calcium(II)-sensitive und Silsesquioxan-basierte Kontrastmittel für die Magnetresonanztomographie // Synthese, Charakterisierung und Mechanistische Untersuchungen